Model updating of microsystems using test data

Zhu, Jun

2008

Zhu, J. (2008). Model updating of microsystems using test data. Doctoral thesis, Nanyang Technological University, Singapore.

https://hdl.handle.net/10356/13416

https://doi.org/10.32657/10356/13416

NANYANG TECHNOLOGICAL UNIVERSITY

MODEL UPDATING OF MICROSYSTEMS USING VIBRATION TEST DATA

MODEL UPATING OF MICROSYSTEMS USING VIBRATION TEST DATA

ZHU JUN

ZHU JUN

SCHOOL OF MECHANICAL & AEROSPACE ENGINEERING

2008

2008

Model Updating of Microsystems Using Vibration Test Data

Zhu Jun

School of Mechanical & Aerospace Engineering

A thesis submitted to the Nanyang Technological University
in fulfilment of the requirement for the degree of
Doctor of Philosophy

2008

Abstract

In modern electronics technology, the rapid advances of microsystems present an imperative requirement in the modeling and the testing of their dynamic characteristics. Due to particular sophistication of microsystems in design and fabrication, finite element (FE) method has limitations to produce accurate mathematical models for microsystems. To obtain a credible analytical model of a microsystem, model updating is employed as an effective approach for improving the FE model using vibration test data. Considering particular testing techniques and damped microstructures of microsystems, this dissertation deals with the research on development of identification of damped structures and suitable updating methods for microsystems. The relationship between structural and viscous damping models in damped systems has been addressed. A complex FRF method has been proposed for generally damped structures. A novel method directly using base excitation test data has been developed successfully for model updating.

The modal identification procedure, where a damping model is arbitrarily chosen for a damped system in the cases of viscous and structural damping, has been studied. It is shown that an exact relationship exists between structural and viscous damping models in a proportionally damped system. The identified damping matrix is not proportional though the equivalent mode shapes remain real. For a non-proportionally damped system, the equivalent mode shapes consist with their counterparts of the original system except differing by a complex scaling factor. It is demonstrated efficiently by numerical studies and an experimental example that the error in estimating modal parameters induced by wrong interpretation of damping model is quite small. In addition, the equivalent damping

matrix is physically meaningful in the case of a system with distributed damping while there is no such equivalent damping matrix if the damping is localized.

The real frequency response function (FRF) based method has been further developed and extended to the case of model updating of generally damped structures. The complex updating formulations using FRF data to identify damping coefficients directly and correct modeling errors, have been established for the cases of proportionally damped structures and general non-proportionally damped structures, respectively. The successful numerical studies based on typical and realistic damped structures reveal the practicality of the proposed method when applied to the identification of damping coefficients, as well as the modification of mass and stiffness modeling errors. The investigation of the effect of FRF data measurement noise on the complex updating process shows that damping coefficients may not be identified with sufficient accuracy in the case of high measurement noise level.

A two-level updating scheme of the Taguchi method has been introduced to identify modeling errors and damping coefficients respectively in different levels for the case of damped structures. Modal data and FRF data are employed for the different objective functions in the two levels, respectively. A numerical example demonstrates that the updating scheme is feasible and efficient when applied to model updating of damped structures even using noisy test data. The reasonably identified results of stiffness modeling errors and damping coefficients show that this method is robust against various noises even in the case of high level noise.

Aiming at model updating of microsystems, a novel method has been developed, which uses vibration test data under base excitation directly for model updating rather than those

conventional FRF data or the derived modal data. The updating formulations, in which response function data under base excitation are employed directly to correct modeling errors, have been established. Various simulated numerical examples have successfully proved the applicability of the proposed method in the case of complete and incomplete measured coordinates. The promising identified results are obtained even for the case of measured response function data with high level of noise. An experimental example based on a mini-cantilever under base excitation illustrates that this method can be applied to model updating of practical structures especially microstructures with confidence.

In order to characterize dynamic behaviors of microsystems, modal testing and finite element analysis have been performed based on an example of Head Actuator Assembly (HAA), a typical microsystem. The various FRFs are measured under voice coil motor and base excitations and significant modes, such as bending and torsion modes, are exhibited during testing. An entire FE model of the HAA is established and the analytical modal data and FRFs are predicted. They are compared and correlated with the experimental ones from modal testing. It is indicated that the experimental and analytical modal data are in good agreement. However, some differences exist between the measured and predicted FRFs in terms of amplitude and shape. Hence, it is concluded that the FE model of the HAA has not been totally validated by experimental data. The proposed updating methods are intended to be applied to the practical updating procedure of the HAA. Subsequently, the actual and comprehensive model updating of microsystems is to be achieved in future work.

Acknowledgements

The author's most sincere gratitude is expressed to his supervisor, Associate Professor Lin Rongming, for his invaluable guidance, advice and constant encouragement over these years, without which this dissertation will never become possible. His knowledge and experience on this area are most valuable to my learning.

Gratitude is also given to my colleagues, Dr. Wang Weijun, Dr. Hou Xiaoyan, Dr. Wang Xiaowei and Mr. Wang Deyang, for their valuable suggestion on academic issues and kind help. I would like to thank all technical staffs in the Centre for Mechanics of Micro Systems (CMMS) for their friendship and support.

I take great pleasure in acknowledging the financial support from Nanyang Technological University, Singapore.

The love and support of my family inspirit me to complete this dissertation. To them this dissertation is gratefully dedicated.

Table of Contents

List of Figures

List of Tables

Nomenclature

Basic Terms, Dimensions and Subscripts

A	Cross-section area
i, j, k, l	Integers
I	Second moment of area
i	$\sqrt{-1}$
x, y, z	Translational degrees of freedom / coordinates
r	Current mode number
s	Number of slave set of degrees of freedom
ω	Frequency of vibration
m	Number of modes
n	Number of measured DOFs / coordinates
N	Total number of DOFs in analytical model
N_p	Dimension of p-value vector
J	Optimization function
W	Weighting function
θ, φ	Phase angle
β, γ	Design variable changes
$\beta_c, \gamma_c, \beta_d, \gamma_d$	Proportional coefficients
$\theta_x, \theta_y, \theta_z$	Rotational degrees of freedom / coordinates

Matrices, Vectors, Scalars

[ ]	Matrix
{ }	Column vector
( )	Single element
$[\,]^T$, $\{\}^T$	Transpose of a matrix, vector
$[\,]^*$, $\{\}^*$	Complex conjugate of a matrix, vector
$[\,]^H$, $\{\}^H$	Complex conjugate transpose of a matrix, vector

$[\ ]^{-1}$	Inverse of a square matrix
$[\ ]^{+}$	Generalized / pseudo inverse of a matrix
$Re(\ )$	Real part of a matrix, vector
$Im(\ )$	Imagine part of a matrix, vector
$[\ _R]$	Reduced matrix
$[I]$	Identity matrix
$[0]$	Null matrix
$[S]$	Sensitivity matrix
$\{\varepsilon\}$	Modal or FRF residual vector
$\{p\}$	P-value vector
$\{\Delta p\}$	P-value change vector

Spatial Model Properties

$[M]$	Mass matrix
$[K]$	Stiffness matrix
$[M^e]$	Element mass matrix
$[K^e]$	Element stiffness matrix
$[M_{ij}]$	Sub-matrix of mass matrix
$[K_{ij}]$	Sub-matrix of stiffness matrix
$[M_{ij}^e]$	Sub-matrix of element mass matrix
$[K_{ij}^e]$	Sub-matrix of element stiffness matrix
$[A]$	Generalized mass matrix
$[B]$	Generalized stiffness matrix
$[C]$	Viscous damping matrix
$[D]$	Structural damping matrix
$[\Delta M]$	Mass correction matrix
$[\Delta K]$	Stiffness correction matrix
$[\Delta D]$	Structural damping correction matrix
$[Z(\omega)]$	Dynamic stiffness (impedance) matrix
$[\Delta Z(\omega)]$	Dynamic stiffness (impedance) error matrix
$\{f(t)\}$	Excitation force vector in time domain
$\{x(t)\}$	Displacement vector in Cartesian coordinates

$\{\dot{x}(t)\}, \{\ddot{x}(t)\}$	The first and second derivatives of $\{x(t)\}$
$[\ _A]$	Analytical model description
$[\ _X]$	Experimental model description
$[\ _U]$	Updated model description

Modal and Frequency Response Properties

ω_r	r-th natural frequency
λ_r	Eigenvalue of r-th mode
ξ_r , ζ_r	Viscous damping ratio of r-th mode
η_r	Structural damping loss factor of r-th mode
s_r	r-th eigenvalue of the viscously damped system
m_r	Element of modal mass matrix
k_r	Element of modal stiffness matrix
c_r	Element of modal damping matrix
A_r	real part of r-th modal constant
B_r	imaginary part of r-th modal constant
$[\Lambda]$	Eigenvalue matrix
$[\Phi]$	Mass-normalized mode shape (eigenvector) matrix
$[\Psi]$	'A' normalized mode shape (eigenvector) matrix
$[S]$	'A' normalized eigenvalue matrix
$[\Theta]$	'A' normalized eigenvector matrix
$\{\phi\}_r$	r-th mode shape vector
$\{\theta\}_r$	r-th eigenvector of the viscously damped system
$(\phi_X)_{ir}$	i-th element of r-th experimental mode shape
Φ_{jr}	j-th element of r-th mass normalized mode shape
Ψ_{jr}	j-th element of r-th 'A' normalized mode shape
$[H(\omega)]$	General frequency response function matrix including receptance, mobility and inertance
$[\alpha(\omega)]$	Receptance matrix
$H_{ij}(\omega_k)$	General frequency response function element, response at DOF i, excitation at DOF j. frequency point k

Standard Abbreviations

COMAC	Coordinate modal assurance criterion
DOF(s)	Degree(s) of freedom
EMA	Experimental modal analysis
FDAC	Frequency domain assurance criterion
FE	Finite element
FEA	Finite element analysis
FEM	Finite element method
FFT	Fast Fourier Transform
FRAC	Frequency response assurance criterion
FRF	Frequency response function
HAA	Head actuator assembly
HDD	Hard disk drive
IES	Inverse eigensensitivity
LDV	Laser Doppler vibrometer
MAC	Modal assurance criterion
MEMS	Micro Electro Mechanical System
MFAC	Modal frequency response function assurance criterion
MSF	Modal scale factor
PZT	Piezoelectric transducer
RBF	Radial basis function
SDOF	Single degree-of-freedom
SN	Signal to Noise
SVD	Singular value decomposition
VCM	Voice coil motor

Chapter 1

Introduction

1.1 Motivation

System integration and miniaturization have become one of the most distinct trends of modern electronics technological development today. In electronics industry, miniaturized mechanical systems or mechanical components called micro-mechanical systems are typically employed. However, as mechanical components become smaller in feature size, structural vibration problems become more acute. In order to improve mechanical design capabilities of micro-mechanical systems, properly representing the dynamic properties of micro-mechanical systems is crucial. For this purpose, accurate and reliable mathematical models of such micro-mechanical systems need to be established. Since microsystems are in principle miniaturized mechanical machines and hence similar to conventional machines, existing conventional analytical modeling techniques can be adopted. Finite element method has been successfully and widely applied to design and analysis of macro structures. Currently, this method is also applied to model the micro-structures at design and application stages of microsystems.

However, due to the sophistication and extra complexity of microsystem in design and fabrication, the predicated results using finite element method usually do not agree well with test data of microsystems. A microsystem includes mechanical elements that are built on such a small scale that FEM may not perform quite successful simulation of microstructure. As feature size becomes so tiny, surface and interface effects can have great importance, compared with inertial effects and elastic forces. On the other hand, properties of materials may change when feature sizes of mechanical elements are scaled downwards.

These lead to difficulties of accurate predictions for microstructure using FEM. Damping associated with microsystem has been shown dominant in dynamic properties of microstructure. Its mechanism cannot be readily described especially for air damping whereas FEM usually assumes simple proportional damping case for structures.

Particular process techniques of microsystem have also presented some limitations concerning accurate FEM simulation of microstructures. The residual thermal stress and residual deformation induced during micro fabrication process exist in microstructure while they are difficult to be quantified in FE modeling. The designed geometry of microstructures may not be perfect because of lithography based processing techniques. For example, the section of real microbeam may not be strictly rectangular due to etching. However, the unknown imperfect geometry of microstructures is hard to be examined for FE modeling. All these issues have a notable impact on the accuracy of numerical modeling of microstructures using FEM since a tiny error of input parameter in FE modeling can produce large deviations from the actual structural model of microstructure.

Because of the above major issues concerning FE modeling, gaining accurate and deep insight into the underlying dynamics of microstructure can be difficult from FEM simulation results alone. Fortunately, a few solutions have been suggested or employed to characterize dynamic model of microsystem for design and application. Developing new numerical approaches is an area of major research focus. A few novel characterization methods have been reported only for limited application of microsystems from time to time. Meanwhile, some reasonable damping models have been proposed to efficiently characterize energy dissipation mechanisms of microsystems.

On the other hand, to establish an accurate and reliable FE model of a structure, validating or updating FE model using test data has always been an active research area. Alongside with the rapid development of microsystem, there is a growing need for accurate modeling and simulation techniques. Since FEM simulation usually does not achieve exact results for microsystem, more attention should be paid to modeling of microsystem, with an ultimate objective to achieve effective mathematical models for accurate prediction. FE model updating, which has been successfully applied to conventional macro structures, can also be considered for modeling of microsystem. As specific testing techniques have been developed and applied in experimental modal analysis for microsystems (Ozdoganlar *et al.* 2003; Lin and Wang, 2006), more confidence can be placed in test data. Based on actual and credible test data, various techniques can be carefully chosen to update FE models. Such modified models shall not only preserve the detailed dynamics from FEM simulations, but represent actual experimental information of microsystem in testing environments. The predicted results from these updated models may approach the maximum correlation with experimental measurement data of microsystems. It is observed that these results have more reliability than those from the original deficient FE model when they are used for detailed design and analysis. Therefore, updating FE models of microsystems using test data is an efficient way to provide full and credible mathematical models for further application of microsystems.

1.2 Background

Structural vibration problems nowadays present a major limitation in engineering production and design especially for microsystems. To ensure that a designed structural system satisfies the prescribed safety, performance and reliability criteria, it is essential that a complete mathematical model, which can accurately represent the dynamic characteristics

of a structure, be established. In engineering practice, there are two main approaches to model a structure, analytical approach and experimental approach, which are typically represented by Finite Element Analysis (FEA) and Experimental Modal Analysis (EMA), respectively. In fact, finite element analysis method has become a more and more powerful tool in industry design and production. However, it is well known that the predictions of finite element method are often in conflict with test results in which more confidence can be placed. Many efforts have been directed to validate FE models. The area referred as model updating is concerned with the correction of FE model by correlating it with test data from experiment. As it will become a robust analysis technology in industrial practice, model updating has been developing rapidly during the last three decades.

Finite Element Analysis

Most practical problems in engineering are either difficult or impossible to solve in their closed forms by conventional analytical methods. Nowadays, finite element method has become well established as a universally accepted analysis method for structural designs. This method originated from the field of structural analysis and was quickly developed in the aerospace industry in the 50’s and 60’s. Currently, it has been widely used in structural design, simulation and analysis due to its powerful ability to model large and complex structures in engineering. There are a lot of literatures available on the subject of finite element method. A comprehensive introduction to this subject has been provided by Zienkiewicz (1971) and Hughes (1987).

Finite element method involves spatially discretizing the geometry of a structure into small elements called finite elements. Based on such discretization, matrices representing the mass and stiffness of a continuous structure are constructed, sometimes including the

damping matrix. The resulting mathematical model is a simple set of differential equations which includes mass and stiffness matrices. Generally speaking, the mathematical formulation of finite element modeling can be posed as a variation problem with an elemental Rayleigh-Ritz treatment and shape function discretization. Upon these approximations, different and complicated structural dynamic problems can be modeled and solved by the introduction of a large number of finite elements, which may have different types. With the large improvement of computational capacity, dynamic finite element analysis of large structures has been adopted widely, including eigenproblem analysis and response analysis of structures.

However, due to modeling errors and uncertain factors, results from finite element analysis do not generally agree well with those of the actual structure. Surveys have shown that dynamic finite element analysis is not always as reliable as one would have expected. And it was found that if a same structure was analyzed by different parties independently, the modeling results could differ considerably (Ewins and Imregun, 1988). Therefore, before FE models can be used in practice with confidence, it should be verified, corrected (if necessary) and validated.

Vibration Testing

Apart from the aforementioned analytical approach, experimental study of structural dynamics is a major way to understand and control many structural vibration phenomena encountered in engineering practice (Ewins, 2000b). As a mature experimental dynamics test technique, vibration testing has been widely used in the characterization of structural systems with the development of instruments and powerful analysis techniques. An experimental model can be established by performing vibration test and its subsequent

analysis. The analysis is known as Experimental Modal Analysis. And the established model by this means is referred as Experimental Analysis Model. Ewins (2000b) gave further details of the theory and practice of vibration modal testing.

Modal testing technique has become quite matured to date after rapid development in past decades. In vibration testing, a structure or a component is driven into vibration with a known excitation force and both the input force and the corresponding response are measured. Then, the input-output relationship of a structure is analyzed in either time domain or frequency domain. Modal testing is usually performed in frequency domain, promoted by the Fast Fourier Transform (FFT) and digital technology. Basically, modal testing consists of two steps: data acquisition and data analysis for the extraction of modal parameters. To acquire output data, exciting the test structure becomes necessary. There are two main excitation methods: single-point excitations and multi-point excitations. After measurements have been carried out, a modal analysis or modal identification is performed to extract the modal parameters, which govern the dynamic performances of a structural system. If the testing procedure is properly conducted, we will have confidence in getting reliable modal parameters of the structure, including natural frequencies, mode shapes and damping ratios.

However, modal testing approach does have some limitations that prevent us from getting the true model of structures in some cases. The measurement is inevitably incomplete and band-limited. Also, measured data are usually contaminated by a certain level of noise. In a word, to achieve a perfect mathematical model of the structure by testing alone is very hard and not practical. Moreover, ill conditioning problem when identifying spatial model of structure and availability of identification algorithms are also factors that prevent the

derived model from being used as the complete model at design stage. Generally speaking, what we gain from modal testing is a relatively reliable but incomplete model.

Model Updating

In most cases, both finite element analysis and modal testing cannot produce a complete and accurate model of the structure for the solution of practical vibration problems due to their respective inherent limitations. We have confidence in two points: first, FE model is not far away from representing the true dynamic behavior of the actual structure, or FEA provides a better frame of true model of the structure; and second, vibration test can be conducted properly so that the results of experimental test can be trusted. Based upon these two points, a group of techniques including comparing and correlating of the analytical and experimental models, reconciling and validating the analytical model, have been developed. The approach that improves the analytical FE model using experimental test data is defined as *Model Updating*.

The objective of model updating in structural dynamics is to generate improved mathematical models, which may then be applied to obtain reliable predications in further analysis. Since this technology combines and exploits all the advantages of the analytical and experimental modeling methods, model updating is able to provide an accurate model of macro structures as well as microsystems, which have great significance to the solution of engineering vibration problems. In mathematical sense, model updating is an inverse problem. During the last thirty years, model updating has been an active research filed. Many techniques have been proposed and there also accumulated a large volume of literature. A book recently published by Mottershead and Friswell (1995) presents a comprehensive description of the current achievements in this area. In chapter 2 of this

dissertation, a systematic and critical review of various aspects of model updating will be given as well as vibration testing techniques for microsystems.

1.3 Objective

Though the methodology of model updating has become more and more mature, most of updating techniques developed for macro structures or systems may not be suited to be applied to updating structural models of microsystems directly and readily. There exist two main issues in vibration tests of microsystems: damping mechanisms and testing techniques. As damping has been shown to be a critical factor in dynamic performances of microsystems (Lin and Wang, 2006), it may not and should not be ignored in model updating procedure for microsystems. In addition, the availability of test data acquired by special testing techniques of microsystems has presented a requirement for the appropriate updating methods. The major difficulty in model updating of microsystems is identification of the particular nature of microstructures. In order to achieve a better performance of model updating for microsystems, attentions in this dissertation should be paid to two basic issues in model updating: (i) identification of damping, and (ii) updating formulation. Identification of damping is to introduce damping model to the FE model and determine the appropriate parameters for this damping model. The updating formulation is related to the way how to establish the new formulation, which is suitable for model updating of microsystmes using particular vibration test data. Hence, the overall objective of this dissertation is:

(i) to extend the existing methods to update FE models of generally damped structures;

(ii) to develop new and efficient methods, which are robust for model updating of microsystems;

(iii) to conduct the characterization of dynamic properties of a microsystem and prepare data acquirement for later possible model updating procedure of this microsystem.

1.4 Outline of Dissertation

The dissertation covers the research work on the development of model updating of microsystems and it is organized as follows. Following the introduction in this chapter, an overview of the relevant research efforts in model updating and vibration test techniques of microsystems is presented in chapter 2. In chapter 3, the relationship between viscous and structural damping models are investigated through the theoretical derivation in the case of proportionally and non-proportionally damped systems, respectively. The significance of the correct interpretation of damping models is demonstrated by the simulated numerical examples and an experimental example. Chapter 4 further develops the FRF based method to identify damping matrices of structural systems, as well as mass and stiffness matrices. The complex updating formulations using FRF data to identify damping coefficients have been established for the cases of proportional damping and non-proportional damping. The applicability of the complex FRF method is investigated through numerical case studies. In chapter 5, a two-level updating scheme of the Taguchi method is proposed to identify modeling errors and damping coefficients of damped structures in different levels, respectively. A numerical simulation demonstrates the feasibility and efficiency of this method when applied to model updating of damped structures even using noise-contaminated test data. Chapter 6 presents a novel method which employs test data under base excitation directly for model updating. The updating formulations using response function data under base excitation to identify modeling errors, are established. The applicability of the proposed method as well as the effect of measurement noise on the updated results is studied in detail based on various simulated numerical examples. In

chapter 7, modal testing and finite element modal analysis of a microsystem based on the HAA are performed, respectively. The measurement of the dynamic characteristics of the HAA is addressed. Then, the modal parameters and FRFs of the HAA are predicted using FEA. In addition, the predicted results are preliminarily compared and correlated to vibration testing data in order to validate the FE model. In last chapter, the achievements of this dissertation are summarized and some directions for future research work are proposed.

Chapter 2

Literature Review of Model Updating Techniques

2.1 Introduction

Model updating is a rapidly developing technology. Many review papers on model updating have appeared since 1980's. Caesar (1987) compared sensitivity, Lagrange multiplier and matrix mixing techniques. Natke (1989) addressed weighted least square approaches for updating analytical model in the frequency domain. Other literature surveys were published by Imregun and Visser (1991), Mottershead and Friswell (1993, 1995), and Ewins (2000a). All of these surveys provide a comprehensive comparison of various methods but are short of efforts to address model updating of microsystems.

Since most of the earlier review papers in model updating have been discussed, this chapter will aim to provide a particular review on the state-of-the-art of model updating which focuses on the practical applicability of various updating methods for microsystems. In addition, current state of vibration testing, damping mechanisms and model updating of microsystems has also been briefly summarized.

2.2 Philosophy of Model Updating

In engineering practice, a sufficiently accurate analytical model representing the characteristics of the structure is required. During the construction of an analytical model using finite element method, it is usual to make simplifying assumptions. Moreover, boundary conditions and connections between components (such as bolted joints and welds) are seldom modelled with certainty. Therefore, it is believed in general that FE models are

not able to accurately describe the dynamic properties of structural systems in case the structural systems are extremely complex. The purpose of model updating is to modify the numerical model in order to obtain better agreement between numerical results and test data. Then the updated model can be subsequently used with confidence for further predictive analysis such as stress analysis and dynamic response analysis.

Vibration testing should be conducted with sufficient care since errors also exist in experimental measurements. The dynamic properties of structures may be affected by the masses and stiffness of the equipment used to excite or measure the vibrations. The practical difficulties of vibration testing in measured data processing, such as aliasing, spectral leakage and linearization of non-linear effects, will result in inaccurate measured data. Further processing, such as modal analysis, also introduces additional errors. On the other hand, the measured coordinates are limited since some coordinates are physically inaccessible such as rotational and internal ones. And the identified modes are usually incomplete due to the limitation of the frequency range and the modal analysis techniques.

In a word, it is impossible for direct experimental test approach to provide a physically meaningful model. However, finite element method is capable of producing a full and meaningful model for real structure. Model updating, which combines the analytical FE model with test data, shows the lights in the way of accurately modeling the dynamics of structural systems especially microsystems.

Incompleteness

The “incompleteness” problem, which means a deficit of modal information, occurs when measured and analytical vibration mode shapes are compared. Usually vibration test has

fewer modes than those of the analytical model. On the other hand, mode shapes of analytical model contain much more elements than are available from test. Incompleteness usually appears due to the fewer measured coordinates or because of the limited frequency ranges involved in experimental tests. The problems caused by incompleteness can be significant in large structures, because measurement of a large number of coordinates is practically expensive. It is well known that incompleteness results in problems of ill-conditioning and non-uniqueness in model updating.

To overcome incompleteness problem, the missing data in experiments can be replaced by their counterparts from analytical model. In that case, either the measured mode shapes should be expanded or the analytical model should be reduced. The techniques for eigenvector expansion and model reduction will be discussed in later sections.

Error Localization

The phenomenon known as error localization, is to locate the most inaccurate model parameters prior to updating when problems of noise and incompleteness are present in test data. The purpose of localization is to determine which DOFs in the model that have serious parameterization errors. After the localization has been made, updating can be performed more effectively by reducing the number of parameters to be corrected.

Sidhu and Ewins (1984) presented a localization method based upon a truncated binomial expansion of the flexibility and the inverse of mass matrices. Zhang and Lallement (1987) extended this method using iteration procedure where the incomplete eigenvectors are recomposed until convergence was obtained. The updated mass and stiffness terms are only used for localization purposes, due to the lacking of connectivity of the original FE model.

Lieven and Ewins (1990a) used Singular Value Decomposition (SVD) approach to produce pseudo-inverse matrices of incomplete stiffness and mass, and localized the mass and stiffness errors from the difference between the experimental and analytical pseudo-inverses.

Regularization

Regularization has become a central issue in model updating, because measurement noise contamination and other experimental uncertainty factors will result in ill-conditioned system equations during model updating. Generally speaking, regularization is a process used to improve the condition and reliability of the solution of equations by introducing extra information or constraints on the solution we seek to obtain. Parameterization techniques, together with other assumptions on the forms and locations of modeling errors also can be considered as regularization techniques. Natke (1991) gave a review of the existing regularization techniques. Ahmadian *et al.* (1998) compared various regularization methods and addressed the problem of selecting a side constraint and determining the regularization parameter in model updating.

2.3 Techniques for Comparison and Correlation

Before updating an analytical model, comparison and correlation of the data sets of analytical and experimental models are necessary. These steps help to have an insight into whether both data sets are in reasonable agreement so that updating is at all feasible. In most cases the experimental data set is incomplete because measurements are taken only at limited locations in selected DOFs. And only a few modes can be identified in the measured frequency range. In essence, these techniques are similar in seeking to obtain useful information about modeling errors from the comparison or correlation of two models.

Most of these techniques are developed in the modal domain. In this way comparison and correlation between modal models can be readily taken due to the availability of modal data.

2.3.1 Comparison Using Modal Data

The Modal Scale Factor (MSF) is a quantitative way of comparing mode shapes of analytical and experimental model, which is defined as (Ewins, 2000b),

$$MSF(\phi_A, \phi_X) = \frac{\{\phi_A\}^T \{\phi_X\}^*}{\{\phi_X\}^T \{\phi_X\}^*}. \tag{2.1}$$

The modal assurance criterion (MAC) (Ewins, 2000b) is widely used to pair and compare mode shapes derived from analytical models with those obtained from experiment. The definition of MAC is expressed as,

$$MAC(\phi_A, \phi_X) = \frac{\left|\{\phi_X\}^T \{\phi_A\}\right|^2}{(\{\phi_X\}^T \{\phi_X\})(\{\phi_A\}^T \{\phi_A\})}. \tag{2.2}$$

A MAC value close to 1 suggests that the two modes are well correlated. The experimental and analytical mode shapes must contain the same number of DOFs, although their scaling does not have to be the same.

The coordinate modal assurance criterion (COMAC) (Ewins, 2000b) is developed on the original idea of MAC. In this case the correlation of analytical and experimental mode shapes for a given coordinate is obtained. The COMAC at each coordinate is defined as,

$$COMAC(i) = \frac{\sum_{r=1}^{L} \left|(\phi_{Xi})_r (\phi_{Ai})_r\right|^2}{\sum_{r=1}^{L} (\phi_{Xi})_r^2 \sum_{r=1}^{L} (\phi_{Ai})_r^2}. \tag{2.3}$$

where L is the total number of well-correlated modes as indicated by the MAC. Again a COMAC value close to 1 indicates a good coordinate correlation.

2.3.2 Comparison Using FRF Data

FRF correlation techniques have developed since 1990's. Compared with traditional comparison techniques, one of the most attractive features of FRF correlation is the availability of FRF data which are supposed to have higher quality than modal data. Frequency Domain Assurance Criterion (FDAC) proposed by Pascual *et al.* (1997) to measure the closeness between measured and analytical FRF is defined as,

$$FDAC(\omega_A, \omega_X)_r = \frac{\left|\{H_A(\omega_A)\}_r^T \{H_X(\omega_X)\}_r^*\right|^2}{(\{H_A(\omega_A)\}_r^T \{H_A(\omega_A)\}_r^*)(\{H_X(\omega_X)\}_r^T \{H_X(\omega_X)_r^*\})}. \quad (2.4)$$

Alongside with the development of FRF correlation, Frequency Response Assurance Criterion (FRAC), the counterpart of COMAC in frequency domain, has also been proposed (Heylen and Avitabile, 1998),

$$FRAC(j,k) = \frac{\left|\{{}_A H_{jk}(\omega)\}^T \{{}_X H_{jk}(\omega)\}^*\right|^2}{(\{{}_X H_{jk}(\omega)\}^T \{{}_X H_{jk}(\omega)\}^*)(\{{}_A H_{jk}(\omega)\}^T \{{}_A H_{jk}(\omega)\}^*)}. \quad (2.5)$$

Fotsch and Ewins (2000) presented a new correlation technique named as Modal FRF Assurance Criterion (MFAC). MFAC is the hybrid correlation indication of mode shapes and frequency responses,

$$MFAC(\{\phi_A\}_r, \{H_X(\omega_X)\}) = \frac{\left|\{\phi_A\}_r^T \{H_X(\omega_X)\}^*\right|^2}{(\{H_X(\omega_X)\}^T \{H_X(\omega_X)\}^*)(\{\phi_A\}_r^T \{\phi_A\}_r)}. \quad (2.6)$$

2.4 Expansion Technique

A lot of updating methods based on modal data require that the measured mode shapes are complete. However, rotational and internal DOFs specified in FE model are hardly measured in practical experiment due to access and measurement difficulties. The task of estimating the unmeasured terms of mode shape vector can be performed by using the corresponding terms of the FE model, which is assumed to represent the structure in test to some accuracy. Hence the eigenvector expansion technique becomes an essential part of all the model updating techniques, which require complete coordinates to be measured. O'Callahan *et al.* (1986) presented an assumption that the measured mode shapes were linear combinations of all the finite element eigenvectors. Lieven and Ewins (1990b) proposed another expansion method using analytical modes combined with the MAC matrix. Jung and Ewins (1991) considered an inverse Guyan technique and extended the method to deal with measured complex modes.

The inverse reduction method (Kidder, 1973) is the most widely used mode expansion technique. This method makes use of the analytical mass and stiffness matrices, and is expressed as follows,

$$\left\{\begin{bmatrix}[K_{11}][K_{12}]\\ [K_{21}][K_{22}]\end{bmatrix}_A - \omega_x^2\begin{bmatrix}[M_{11}][M_{12}]\\ [M_{21}][M_{22}]\end{bmatrix}_A\right\}\begin{Bmatrix}\{\phi_1\}_X\\ \{\phi_2\}_X\end{Bmatrix} = \begin{Bmatrix}\{0\}\\ \{0\}\end{Bmatrix}, \tag{2.7}$$

where $\{\phi_1\}_X$ is the measured part of the mode shape while $\{\phi_2\}_X$ is the unmeasured part. By rearranging the lower matrix equation, the expression of $\{\phi_2\}_X$ is obtained,

$$\{\phi_2\}_X = -([K_{22A}] - \omega_X^2[M_{22A}])^{-1}([K_{21A}] - \omega_X^2[M_{21A}])\{\phi_1\}_X . \tag{2.8}$$

Another expression for $\{\phi_2\}_X$ can also be gained by rearranging the upper matrix equation. For acquiring the expanded mode shape, both equations should be used to form a transformation matrix. However, this technique requires accurate analytical mass and stiffness matrices, which may not be achieved for large systems. Also, errors in the

analytical system matrices will affect the quality of the expansion of measured mode shapes directly.

2.5 Reduction Technique

Usually FE models of real structures are in high order. To overcome the requirement of measuring all DOFs, a reduction of the number of DOFs in the FE model becomes necessary. Variations of a matrix condensation technique were presented (Guyan, 1965; and Paz, 1984) for reduction of the analytical model. All of these techniques focus on choosing master DOFs and expressing the initial mass and stiffness matrices in terms of these chosen master DOFs. The dynamic condensation, where the correct stiffness properties are retained while the inertia properties are approximated, is one main approach and another is the static condensation, where the situation is reversed. For example, Guyan (1965) proposed static condensation, where the equations that do not include external force terms are used to eliminate spatial variables. Paz (1984) proposed a dynamic condensation method that is limited to solving the analytical eigenproblem. Another various condensation technique was Improved Reduced System (O'Callahan, 1989), in which a transformation matrix between the analytical and measured DOFs is defined.

Guyan reduction is the most popular reduction technique. The system equation of motion is considered as follows,

$$\left[\begin{bmatrix}[K_{mm}] & [K_{ms}]\\ [K_{sm}] & [K_{ss}]\end{bmatrix}-\omega^2\begin{bmatrix}[M_{mm}] & [M_{ms}]\\ [M_{sm}] & [M_{ss}]\end{bmatrix}\right]\begin{Bmatrix}\{x_m\}\\ \{x_s\}\end{Bmatrix}=\begin{Bmatrix}\{f_m\}\\ \{f_s\}\end{Bmatrix}. \tag{2.9}$$

From this equation exact relationship between master and slave DOFs can be obtained at certain frequencies. If there are no external forces applied on the slave DOFs, and the

inertia terms are assumed to be negligible, following equation can be obtained,

$$\begin{bmatrix} [K_{mm}] & [K_{ms}] \\ [K_{sm}] & [K_{ss}] \end{bmatrix} \begin{Bmatrix} \{x_m\} \\ \{x_s\} \end{Bmatrix} = \begin{Bmatrix} \{f_m\} \\ \{0\} \end{Bmatrix}. \tag{2.10}$$

Using the lower set of equations leads to,

$$\begin{Bmatrix} x_m \\ x_s \end{Bmatrix} = \begin{bmatrix} [I_{m\times m}] \\ -[K_{ss}]^{-1}[K_{sm}] \end{bmatrix} \{x_m\} = [T_s]\{x_m\}. \tag{2.11}$$

After the transformation matrix $[T_s]$ is established, the reduced system matrix $[M_R]$ and $[K_R]$ are obtained as,

$$[M_R] = [T_s]^T [M_A][T_s], \quad [K_R] = [T_s]^T [K_A][T_s]. \tag{2.12}$$

Guyan Reduction is proved to be effective in low frequency range, and its effectiveness depends heavily on the selection of master DOFs.

It should be noted that the reduction techniques were formulated to obtain the eigensolution of large matrix equations. Hence, when model reduction is used in model updating procedure, some problems will emerge. First, all reduction techniques yield condensed system matrices without the preservation of the connectivity of the original model. Second, the reduction introduces extra inaccuracies since the reduced model is only an approximation of the full model.

2.6 Main Model Updating Methods

The purpose of model updating is to provide a physically meaningful numerical model by combining both FE model and test data such that the updated model will reproduce the set of measured data closely. In previous review papers, different categorizations are presented

according data type, basic principle, and so on. In this work, current existing methods are classified into three groups: (i) Direct updating methods, (ii) Sensitivity based iterative methods, and (iii) Intelligent methods. In the next sections, some representative model updating methods for macro structure are presented in a unified and consistent notation. In addition, a brief and broad description of these methods will be given.

2.7 Direct Updating Method

Direct Methods were very popular in the late 1970s and early 1980s when numerical computational power was quite limited. Due to this limitation on computing, almost all the direct methods were formulated in modal domain. All these methods can guarantee the agreement of the updated analytical model with the experimental modal information through the correction of elements in the system matrices. Since there is no iteration involved in updating process, the convergence is assured and the CPU computational time is usually less than that required by the iterative methods. However, there are also disadvantages: (i) accurate modal analysis is needed; (ii) mode shape expansion techniques are required because of the incomplete experimental modal data; (iii) the updated system matrices are unable to preserve the physical connectivity of in the original model; (vi) the positive definiteness of the updated system matrices are not guaranteed.

According to the different ways in which corrections are made, the methods can be grouped into four categories: Lagrange Multiplier Methods, Matrix Mixing Methods, Error Matrix Methods and Eigenstructure Assignment Methods.

2.7.1 Lagrange Multiplier Methods

The Lagrange Multiplier methods were introduced by Baruch (1982) and Berman (1983) in early 1980s. These methods usually assume one set of parameter from the mass, the stiffness or the measured modes are correct. Then an objective function, with constraints imposed through Lagrange multipliers, is minimized to achieve the other two sets of updated parameters separately.

Berman and Nagy (1983) used this approach to update the mass matrix by minimizing,

$$\varepsilon = \left\| [M_A]^{-1/2} ([M_U] - [M_A])[M_A]^{-1/2} \right\|. \tag{2.13}$$

Using Lagrange multipliers λ_{ij} to enforce orthogonality condition, the objective function to be minimized is obtained as follows,

$$J_M = \left\| [M_A]^{-1/2} ([M_U] - [M_A])[M_A]^{-1/2} \right\| + \sum_{i=1}^{m} \sum_{j=1}^{m} \lambda_{ij} ([\Phi]^T [M_U][\Phi] - [I])_{ij} . \tag{2.14}$$

The minimization procedure results in an updated mass matrix,

$$[M_U] = [M_A] + [\Delta M], \tag{2.15}$$

where

$$\begin{aligned} [\Delta M] = {} & [M_A][\Phi_X]([\Phi_X]^T [M_A][\Phi_X]) \\ & ([I] - [\Phi_X]^T [M_A][\Phi_X])([\Phi_X]^T [M_A][\Phi_X])[\Phi_X]^T [M_A] \end{aligned} . \tag{2.16}$$

Following the computation of $[M_U]$ from equation (2.17), an updated stiffness matrix can then be determined by minimizing another cost function,

$$\varepsilon = \left\| [M_U]^{-1/2} ([K_U] - [K_A])[M_U]^{-1/2} \right\|, \tag{2.17}$$

with the following constraint equations,

$$[K_U][\Phi_X] = [M_U][\Phi_X][\Lambda], \ [\Phi_X]^T [K_U][\Phi_X] = [\Lambda], \text{ and } [K_U] = [K_U]^T . \tag{2.18}$$

Here the Lagrange multipliers are also used to enforce the equation of motion, orthogonality and symmetry of system matrices. The updated stiffness matrix can be written as,

$$[K_U] = [K_A] + [\Delta K] + [\Delta K]^T, \tag{2.19}$$

where

$$[\Delta K] = [M_U][\Phi_X]([\Phi_X]^T[K_A][\Phi_X] + [\Lambda])[\Phi_X]^T[M_U]/2 - [K_A][\Phi_X][\Phi_X]^T[M_U]. \tag{2.20}$$

Caesar (1986) improved this approach by introducing three additional constraints from rigid-body considerations, such as centre of gravity, total mass and moment of inertia. Wei (1989) further developed the method to simultaneously update the mass and stiffness matrices using measured modal data.

2.7.2 Matrix Mixing Methods

The development of matrix mixing methods was introduced by Caesar (1987) and Link *et al.* (1987). Generally the number *m* of measured pairs of eigendata is usually smaller than the order *N* of the required model. Based upon the incomplete measured modes, system matrices can be assembled. This approach combines the experimental mode shapes with the analytical ones to obtain a complete eigenvector set. Thus,

$$[M_U]^{-1} = \sum_{i=1}^{m} \{\phi_X\}_i \{\phi_X\}_i^T + \sum_{i=m+1}^{N} \{\phi_A\}_i \{\phi_A\}_i^T, \tag{2.21}$$

$$[K_U]^{-1} = \sum_{i=1}^{m} \frac{\{\phi_X\}_i \{\phi_X\}_i^T}{\omega_{Xi}^2} + \sum_{i=m+1}^{N} \frac{\{\phi_A\}_i \{\phi_A\}_i^T}{\omega_{Ai}^2}. \tag{2.22}$$

Here the number of elements in the mode shapes from experimental and analytical models is assumed to be the same. If the number of elements in experimental mode shapes available is less than that of the analytical ones, the updated system matrices should be calculated using the following formula,

$$[M_U] = [[M_A]^{-1} + \sum_{i=1}^{m} \{\phi_X\}_i \{\phi_X\}_i^T - \sum_{i=1}^{m} \{\phi_A\}_i \{\phi_A\}_i^T]^{-1}, \tag{2.23}$$

$$[K_U] = [[K_A]^{-1} + \sum_{i=1}^{m} \{\phi_X\}_i \{\phi_X\}_i^T / \omega_{Xi}^2 - \sum_{i=1}^{m} \{\phi_A\}_i \{\phi_A\}_i^T / \omega_{Ai}^2]^{-1}. \tag{2.24}$$

The matrix mixing methods usually generate fully populated mass and stiffness matrices which have little relation or no physical connectivity. To *et al.* (1990) obtained the updated mass and stiffness matrices by applying modal orthogonality of measured mode shapes. In order to preserve the physical meaning of updated system matrices, this method can be extended by adding orthogonality relations to the eigendynamic system equation.

2.7.3 Error Matrix Methods

Error matrix methods estimate the error in the mass and stiffness matrices, on the assumption that this error is small in Euclidean sense as compared with the system matrices themselves. The error matrices between the experimental and analytical models are defined as follows,

$$[\Delta M] = [M_X] - [M_A], \text{ and } [\Delta K] = [K_X] - [K_A]. \tag{2.25}$$

Sidhu and Ewins (1984) defined an expression of the stiffness error matrix by expanding the flexibility matrix $[K_X]^{-1}$ in terms of the error matrix, which is as follows,

$$[K_X]^{-1} = [K_A]^{-1} - [K_A]^{-1}[\Delta K][K_A]^{-1} + o([\Delta K]^2). \tag{2.26}$$

Ignoring the second and higher order terms of the error matrix and rearranging (2.26), an estimate of the error matrix, $[\Delta K]$, is produced,

$$[\Delta K] = [K_A]([K_A]^{-1} - [K_X]^{-1})[K_A]. \tag{2.27}$$

Estimating the two pseudo-flexibility matrices using analytical and measured modal data yields,

$$[\Delta K] \cong [K_A]([\Phi_A][\Lambda_A]^{-1}[\Phi_A]^T - [\Phi_X][\Lambda_X]^{-1}[\Phi_X]^T)[K_A], \tag{2.28}$$

$$[\Delta M] \cong [M_A]([\Phi_A][\Phi_A]^T - [\Phi_X][\Phi_X]^T)[M_A]. \quad (2.29)$$

Since the measured modal data are incomplete, analytical modal data are used to fill in the unmeasured parts.

Zhang and Lallement (1987) considered the inclusion of some of the second order terms in the expansion of the flexibility matrix. Lieven and Ewins (1990a) presented the modified version of the error matrix methods,

$$[\Delta K] \cong ([\Phi_X][\Lambda_X]^{-1}[\Phi_X]^T)^{-1} - ([\Phi_A][\Lambda_A]^{-1}[\Phi_A]^T)^{-1}. \quad (2.30)$$

And they used SVD technique to calculate the inverse of the rank deficient flexibility matrix. Lieven and Ewins (1992) discussed the effect of incompleteness and noise on the quality of the results obtained from the error matrix method.

2.7.4 Eigenstructure Assignment Methods

The eigenstructure assignment method for model updating was first adopted by Minas and Inman (1988). In this approach, state feedback is used to describe the right side of the dynamic equation of motion as follows,

$$[M_A]\{\ddot{X}\} + [C_A]\{\dot{X}\} + [K_A]\{X\} = [B_0]\{U\}, \quad (2.31)$$

$$\{Y\} = [D_1]\{X\} + [D_2]\{\dot{X}\}, \text{ and } \{U\} = [G]\{Y\}, \quad (2.32)$$

where $\{U\}$ is the input force vector and $[B_0]$ is an input distribution matrix. $[D_1]$ and $[D_2]$ are the matrices relating the outputs and states. And here $\{Y\}$ is an arbitrary output and $[G]$ is the feedback matrix. Then the problem becomes to determine the feedback matrix such that the eigendata of the closed loop system are identical to the measured modal data. If the mass matrix remains unchanged, above procedure results in an updated stiffness matrix and damping matrix as,

$$[K_U]=[K_A]+[B_0][G][D_1],\ [C_U]=[C_A]+[B_0][G][D_2], \tag{2.33}$$

where matrices $[B_0]$ can be chosen arbitrarily. $[D_1]$ and $[D_2]$ should be chosen such that $[D_2][\Phi_X][\Lambda_X]+[D_1][\Phi_X]$ is invertible. In general, the correction matrices $[B_0][G][D_1]$ and $[B_0][G][D_2]$ may not be symmetric. Zimmerman and Widengren (1990) proposed a generalized algebraic Riccati equation in eigenstructure assignment method to calculate symmetrically the updated stiffness and damping matrices directly. Inman and Minas (1990) proposed an iterative scheme to ensure symmetry of the updated matrices. Shulz and Inman (1994) used the eigenstructure assignment method with some constraints that could connect the updated matrices with physical properties of a system.

2.8 Sensitivity Based Iterative Methods

Iterative updating methods have become popular since 1990s because these methods seek to improve the correlation between experimental and analytical models via a penalty function. Generally the penalty function to be minimized is nonlinear. Therefore, linearization of the function and iterative procedure are needed. However, possible convergence problem will sometimes arise during iterations. In most cases, iterative methods have three main advantages. First, a wide range of parameters to be updated simultaneously can be chosen and second, the updated system matrices are physically meaningful. Third, the measured data, such as modal data and FRF data, can be reproduced accurately. On the other hand, there are two major problems concerning the implementation of iterative methods: (i) the modal data or FRF data of experimental and analytical models must be paired; (ii) if damping is considered in an analytical model, the complex modal theory should be used and the updating algorithm will become complex too.

2.8.1 Sensitivity Methods Based on Modal Data

Sensitivity based methods have been proven to be very promising due to their ability to reproduce the correct measured modal data. Almost all the sensitivity based methods involve sensitivity analysis, which is the study of changes in measured system modal parameters with respect to physical parameter variation. And a sensitivity matrix $[S]$ is computed by considering the partial derivatives of modal parameters with respective to physical parameter change via a truncated Taylor's series. This truncated series result in linear approximation,

$$\{\varepsilon\} = [S]\{\Delta p\}, \tag{2.34}$$

where the term $\{\Delta p\}$ is the unknown parameter change in structural elements, and $\{\varepsilon\}$ is the modal data change vector, which is defined as,

$$\{\varepsilon\} = \{\{\Delta\lambda_1 \cdots \Delta\lambda_m\}, \{\Delta\phi_1\}^T, \{\Delta\phi_2\}^T, \cdots, \{\Delta\phi_m\}^T\}^T. \tag{2.35}$$

The sensitivity matrix $[S]$ contains the first derivatives of the eigenvalues and eigenvectors with respect to physical parameters. Ojalvo (1987) proposed an efficient method to calculate mode shape derivatives. Lallement and Zhang (1988) discussed some of the difficulties related to sensitivity analysis.

To obtain the unknown vector $\{\Delta p\}$, above matrix equation (2.34) is solved. And then new updated analytical system matrices are calculated using the updated parameters. For possible convergence of the solution, an iterative procedure is needed. In an iterative scheme, a new eigensolution of the updated analytical model needs to be performed at every iteration. And the process is repeated until convergence is reached. Thus a final updated analytical model is obtained and it can be subsequently used for other applications. It should be noted that the formulation of the sensitivity matrix is based on a Taylor expansion and hence requires iterations to be carried out.

Usually, sensitivity based methods may choose a wide range of parameters to be updated. Different sets of parameters may make the updating problem either well-conditioned or ill-conditioned (Friswell and Penny, 1992). The unknown parameters to be identified may be mass and stiffness matrix elements, substructure parameters (Lallement and Piranda, 1990) or macro elements (Jung, 1990). Jung and Ewins (1992) investigated the effect of the choice of macro-elements or substructures on the model error localization.

In general, the number of parameters to be identified and the number of equations are not equal when equation (2.34) is to be solved. When the number of equations exceeds the number of parameters, the equation set is said to have become over-determined. Ojalvo *et al.* (1989) considered a least squares or weighted least squares technique for solving such an over-determined equation set. The updated parameters are calculated as,

$$\{\Delta p\} = ([S]^T[S])^{-1}[S]^T\{\varepsilon\}, \tag{2.36}$$

$$\{\Delta p\} = ([S]^T[W_\varepsilon]^{-1}[S])^{-1}[S]^T[W_\varepsilon]^{-1}\{\varepsilon\}, \tag{2.37}$$

using least squares and weighted least squares respectively. The matrix $[W_\varepsilon]$ is a positive definite weighting matrix that is included to estimate variance of the measured data. Ojalvo *et al.* (1989) used a balance technique to properly scale the parameters and measurements in order to improve the numerical condition of the matrix inversion. Piranda *et al.* (1991) considered the practical implementation of these methods, including the criteria for convergence and automatic mode pairing.

The sensitivity methods usually require the solution of a set of linear simultaneous equations. Friswell and Penny (1992) thought that increasing the weight given to the initially estimated parameters or choosing a different set of parameters would generally

improve the numerical condition of the equation set, although there might exist undesirable occasions. It seems that SVD technique is the best method for solving these sets of equations numerically.

Many researchers have tried other different penalty functions used in the sensitivity methods. For example, Heylen (1987) combined the sensitivity equations (2.34) with orthogonality equations to form a set of simultaneous equations for parameter updating. Berger *et al.* (1990) minimized the residual forces obtained by introducing the measured data into the equations of motion. Nash (1990) considered the minimization of a weighted residue sum of eigenvalues and eigenvectors. Based on the measured modal data, Nobari *et al.* (1992) optimized the error of motion equation, which had been transformed to modal domain using the available low frequency modes.

Jung (1992) investigated in detail the inverse eigensensitivity method (IES), the basic principle of which is to update FE models based on the modal sensitivity and the minimization of the difference between the analytical and experimental modal properties. The design parameters of the model are corrected iteratively using pseudo-inverse of the sensitivity matrix, which is calculated using analytical modal data. However, this classical IES method does have some drawbacks such as the assumption of small error magnitudes and slow speed of convergence. Lin *et al.* (1995) developed an improved IES method, which overcomes the existing problems of the classical IES method. The improved method employs both analytical and experimental modal data to calculate the required eigensensitivity coefficients, and more accurate updated results can be obtained.

2.8.2 FRF Based Methods

The FRF based methods use the measured FRF data directly to optimize a penalty function. This penalty function can be defined in terms of two different types of error function. The two error functions are based on the equations of motion in frequency domain. Consider the equation of motion for viscous damping,

$$(-\omega^2[M] + j\omega[C] + [K])\{x(\omega)\} = \{f(\omega)\}. \tag{2.38}$$

The above equation can be expressed in terms of the dynamic stiffness matrix as,

$$[Z(\omega)]\{x(\omega)\} = \{f(\omega)\}. \tag{2.39}$$

The equation error approach minimizes the errors of input force, which is the difference between the experimental force and its analytical counterpart given by (2.39),

$$\{\varepsilon_{EE}\} = \{f_X(\omega)\} - [Z_A(\omega)]\{x_A(\omega)\}. \tag{2.40}$$

More detailed discussions about this method can be found in (Natke, 1988; Fritzen and Zhu, 1991). Rad (1997) considered this method by applying a unit load at the j^{th} experimental degree of freedom and obtained a new expression as,

$$\{\varepsilon_{EE}\} = \{I(\omega)\}_j - [Z_A(\omega)]\{H_X(\omega)\}_j. \tag{2.41}$$

And a more detailed description of this method including the noise sensitivity reduction, frequency point selection, and the choice of damping, was also given.

The equation error approach can achieve a rapid convergence since the error is a linear function of the spatial parameters. Nevertheless, there are disadvantages that it requires measured data to be complete and that the estimated parameters are biased due to the presence of measurement noise. However, model reduction technique may be used to overcome the first problem and unbiased estimates may be obtained by using instrumental variable approach (Wang, 1988).

The output error method is to minimize the output error, which is defined as the difference between the measured and estimated response given by,

$$\{\varepsilon_{oE}\} = [Z_A(\omega)]^{-1}\{f_A(\omega)\} - \{x_X(\omega)\}. \tag{2.42}$$

In this approach, the minimization of a non-linear function is required, which is prone to associate convergence problems and may require significant computational efforts. However, estimated parameter are unbiased if the measured data are contaminated with random noise with zero mean. Also, the reduction of the analytical model is not required.

Sestieri and Ambrogio (1989) directly minimized the penalty function as a non-linear function of the parameters. Sharp and Brooks (1988) calculated the sensitivity of the FRFs with respect to the parameters using the eigenvalue and eigenvector sensitivity. Santos and Arruda (1990) tried to minimize the output error using component mode synthesis to update a complex structure.

Lin and Ewins (1990, 1994) presented a direct response function method (RFM) in which the difference between the measured and analytical receptances is written as a linear function of the parameters. They suggested using the terms of the analytical receptance matrix for the missing of measured coordinates. When measured data are incomplete, the method could be considered as a weighted equation error method. Visser and Imregun (1991) considered the incompleteness of experimental model and the uniqueness of improved model in this method. Imregun *et al.* (1995a, 1995b) investigated the effectiveness of the technique in the case of noisy and incomplete experimental data. The importance of excitation direction, the implication of coordinate mismatch using simulated cases and the numerical stability of the method, as well as its applicability to practical measured FRF data based on an experimental case were reported. Although the updated

results with adequate engineering accuracy were obtained, the updated model may become non-uniqueness. Lin and Lim (1997) proved the mathematical relationship between improved inverse eigensensitivity and FRF methods and discussed computational considerations regarding the practical application of the two methods. Kwon and Lin (2004) proposed a frequency selection method for efficient FRF based method so that the frequency points used for updating can be chosen optimally and automatically based on the concept of measurement dependency index.

2.9 Intelligent Model Updating Methods

Current iterative model updating methods rely on minimization techniques, which require larger amount of computation and also require compatibility between experimental and analytical data. Ill-conditioning, local minimization and nonlinearity problems in model updating procedures have prompted researchers to explore new techniques used in other research areas. Several novel methods have been tried and applied to the practice of model updating, including: Neural Networks (Attala, 1996 and 1998; Marwala and Hunt, 1998), Simulated Annealing and Genetic Algorithm (Levin and Lieven, 1998a), Taguchi method (Kwon and Lin, 2005). All these methods are considered as nonlinear optimization methods. These techniques mentioned share similar features such as robustness, self-training (intelligent) and global minimum, which are very attractive in model updating applications. Whereas, these methods also have some disadvantages. Neural Networks requires training cases. The optimization process using Genetic Algorithm is slow in nature due to its stochastic approach. Nevertheless, the introduction of these methods brings us new ideas on how to tackle the problems encountered when dealing with practical updating applications.

2.9.1 Neural Networks

Neural Networks are widely adopted in the area of pattern recognition and adaptive control. The major advantages of Neural Networks are nonlinear mapping, generalization capacity and strong adaptability. And it has been proven to be effective in the seeking of global minimums in problems of nonlinear optimization. These features seem to be very attractive for problems of model updating. The main advantage of Neural Networks is that it can quickly achieve accurate updated results once it has been trained. However, the updated results are depended on the training cases.

Atalla and Inman (1998) first applied neural network to model updating. They adopted a Radial Basis Function (RBF) to approximate the mapping between frequency response data and model parameters. Networks trained by analytical FRFs are used to generate the parameters to be updated when experimental FRFs are used as inputs. However, the computational cost is intensive to train the neural networks. Another drawback is the lack of mathematical tools to assure the convergence and accuracy of the updated parameters. Attala (1996) presented a full description of the neural networks based method including choice of input data, nonlinear systems, and computational cost. Levin and Lieven (1998b) also addressed this method using RBF networks in their updating procedure in the presence of experimental noise and obtained promising results. A further advantage of this updating method is its ability to work with a limited number of experimentally measured DOFs and modes. Chang *et al.* (2002) investigated the use of orthogonal array for training sample selection in neural networks for model updating. Lu and Tu (2004) presented a two-level neural network scheme for model updating in which both structural parameters and damping ratios were updated.

2.9.2 Genetic Algorithm

Genetic algorithm is a widely applied optimization method that has been developed based on the analog with natural evolution. This algorithm has some advantages in finding a global minimum for optimization problems. However, the execution of Genetic Algorithm is very slow since the method employs stochastic search for optimal parameters. Friswell *et al.* (1998) combined the genetic algorithm and eigensitivity method to identify the locations and magnitudes of damage variables from measured vibration data. The algorithm is robust even to systematic errors in measured data. Levin and Lieven (1998a) presented a genetic algorithm in model updating, which is capable of seeking the global minimum among many local minima. The algorithm has shown its robustness when applied to updating a simple plate structural model. However, the obtained results show a significant dependence on the choice of updating parameters, and considerable computational efforts are required.

Simulated Annealing is another optimization algorithm analogy to the natural phenomenon of the annealing process in thermodynamics. This technique is capable of searching the lowest energy state among all possible energy states, which are introduced by a variety of neighborhood functions such as line adjustment and fixed radius adjustment. It can avoid local minimum effectively, which is a major obstacle in other updating methods. Although this technique is efficient when applied to simple case study (Levin and Lieven, 1998a), the choice of the set of updating parameters is of primary importance when considering execution time and accuracy required.

2.9.3 Taguchi Method

Taguchi method has been widely used for robust design and quality engineering in industry. This optimization method has advantages that it can be computationally efficient. Because orthogonal arrays are used to screen main effects of parameters rather than the stochastic

approach. In addition, the search process is more straightforward since it maximizes the signal to noise (SN) ratio at each iteration. However, to achieve accurate updated results, proper orthogonal arrays should be employed. Kwon and Lin (2005) applied this novel approach in model updating by optimizing the objective function, which is defined by the difference between measured and analytical vibration data. The simulation examples for model updating in the presence of random and systematic errors demonstrate the effectiveness of the proposed method. It is also shown that the updated results are robust against various noises since parameters are updated such that the SN ratio is maximized.

2.10 Vibration Tests of Microsystems

Almost all above model updating method are developed for macro mechanical systems or macro structures. The rapid development of microsystems has presented requirement to accurately characterize their dynamic behaviors. Although both experimental methods and numerical methods can be employed for that purpose, to fully and accurately describe a dynamic structural microsystem, an improved analytical model with experimental validation is needed. Hence, model updating has become another vital means for modeling dynamic structures of microsystems. As measured information is required in model updating, experimental analysis should be adopted for microsystems in order to obtain test data before analytical models can be updated. Similar to vibrations of conventional mechanical systems, experimental studies of structural vibrations of microsystems have been a major way to understand many structural vibration phenomena encountered in microsystems. In design and application of microsystems, it becomes necessary to achieve major objectives such as: determining the nature and extent of vibration response levels in operation, and validating theoretical models and predictions.

As a typical experimental test technique, modal testing has become indispensable to the development of modern mechanical systems as well as microsystems. Compared with conventional mechanical structures, microstructures possess much higher natural frequencies and smaller vibration amplitudes. Due to limited bandwidth of excitation sources and relatively large transducer size, conventional modal testing methods cannot be directly applied to microstructures. Hence, many new techniques have been currently developed, which are capable of performing modal testing on microstructures, and some of them have been summarized in previous work (Ozdoganlar *et al.*, 2003). Lin and Wang (2006) presented a comprehensive review, which summarizes most methods developed so far for modal testing of microsystems in details. In their work, modal testing techniques are classified into two categories: excitation methods and measurement techniques. In the following, testing techniques, which are suitable for microsystems, will be introduced.

2.10.1 Excitation Methods

To excite structures into vibrations, various devices are available and several of them are widely used. A qualified excitation device should be capable of exciting all the modes of interest in a specified frequency range, which requires that the excitation device needs to have very high excitation frequency bandwidth. Moreover, the attachment of such excitation device should not modify the test structure in any substantial way and the excitation force exerted should ideally approach to a tiny point force as possible. Generally, conventional direct excitation methods, such as impact hammer and shaker, cannot be readily applied to excite microsystems. Indirect and non-contacting excitation methods are required for modal testing of microsystems. Over the last decade, some tools and methods have been developed for the vibration characterization of microsystems.

Electrostatic excitation. The excitation can be conducted by electrostatic forces, which are applied either by built-in electrodes or by integrating electrodes into a microstructure if it is made of dielectric materials (Zhang *et al.*, 1998; Ozdoganlar *et al.*, 2003). However, the effect of these additional electrodes on the dynamics of the microstructure must be considered in the latter case. This method has disadvantages that electrostatic forces are nonlinear functions of structural motions and that there is coupling between electrostatic and structural fields.

Smart material excitation. In order to excite microstructures, attached or embedded smart materials such as piezoelectric elements and shape memory alloys can be employed (Swei *et al*., 2001; Lin and Wang, 2006). However, this technique adds complexities to the fabrication methods since smart material elements need to be integrated into or attached to the structure. In addition, dynamic characteristics of microstructures can be significantly altered by the inclusion of extra materials.

Magnetic excitation. An electromagnetic exciter was developed by Wilson and Bogy (1996) to investigate the dynamic characteristics of a suspension assembly. In this method a ferromagnetic target must be attached to the nonferrous suspension test structure so that it can be excited. The experimental system setup was capable of obtaining FRFs of the test structure and then modal parameters were identified accurately. The disadvantages of this method are the attachment of a ferromagnetic target onto a test structure and its limited excitation bandwidth.

Electric discharge. Chou and Wang (2001) presented a modal testing system based on the principle of base excitation. A test structure was mounted on a rigid platform that can move

with only one translational degree of freedom. An electric discharge generated a spark and struck the rigid platform. The moving platform then shook the test structure mounted on its top surface to provide a very wide frequency band of base excitation.

Air hammer. Frees and Miu (1990) introduced an 'air-hammer' excitation for vibration testing of a hard disk drive head suspension system. The air hammer system can direct the blast of air onto the bottom surface of the suspension with a controlled force of the impulse. Air hammer has the advantage that it can excite microstructures without any attachment to them, but its applications are limited since the force exerted cannot be measured or precisely controlled.

Although many excitation techniques based on different principles have been developed for modal testing of microsystems, there exist limitations in most of these techniques since none of them is truly external. In addition, most of these methods cannot be applied to obtain FRFs since it is impossible or difficult to measure the input forces accurately in most cases. One promising alternative is base excitation which has the capability of exciting a microstructure using external elements without altering its vibration characteristics (Chen *et al.*, 1995; Chou and Wang, 2001). In this case, a micro piezoelectric shaker made of bulk PZT materials, is employed to excite a microstructure (Lin and Wang, 2006), to which traditional shakers cannot be applied due to their limited frequency ranges. Once the experimental device is developed, which is capable of exciting microstructures to vibrate, modal testing of microstructures can be performed based on the principle of base excitation since motion-over-motion FRFs can be derived by taking the base motions as references. Above all, this base excitation technique can be applied to model updating of microstructures where the excitation input are required.

2.10.2 Measurement Techniques

Laser Doppler Vibrometry. In early 1990's, Laser Doppler Vibrometer (LDV), which is a valuable technique for vibration testing of conventional structures, was developed and was applied to microsystems (Lawrence *et al.*, 2003). LDV technology is ideally suitable for characterizing dynamic behaviors of microsystems. Because measurement using LDV is non-contact and hence there is no mass loading effect on test microsystems. Furthermore, LDV systems can measure vibrations of microstructures for a high frequency range. Nowadays, it has been extensively used for modal testing applications of microstructures.

An LDV can achieve a spatial resolution in sub-micron range to accurately position the laser spot anywhere within the visible microscope image when coupled with a microscope (Rembe *et al.*, 2001). This has great significance for microstructures as the velocity measured using LDV is an average over the spot area and the actual motion of a tiny microstructure can only be measured with a small enough spot size. Microscope scanning laser vibrometer is capable of delivering distributions of the total deflections within a narrow frequency bandwidth, i.e., are frequency-resolved which facilitates the detection of resonance frequencies.

However, microscope scanning vibrometer has a limitation that it cannot characterizing in-plane vibrations of microstructures since Doppler shift is derived from a velocity vector normal to the plane of the moving surface. By introducing additional stroboscopic video microscopy for in-plane motion analysis, three dimensional dynamic characterization of microstructures can be achieved. Combined with base excitation, an LDV is the most promising measurement technique which can be used to obtain motion-over-motion FRFs

for FE model updating of microsystems.

Optical Microscope. The Computer Microvision System (CMS), which can achieve 3-D imaging, is non-interferometry based method developed by Davis and Freeman (1998). In a CMS, periodic motions of a microstructure that are imaged with a microscope on a charge-coupled device camera (CCD) are frozen using a high-speed strobed light source. By processing the measured data with digital-image-processing algorithms, the CMS can recover in-plane motions from the captured imagines. Moreover, by employing an additional focus system, the CMS can also extract the out-of-plane motions.

Photomicrography. High-speed photomicrography is a special technique developed for the visualization of fast moving objects on a microscope scale. Under a CCD-camera microscope, resonant frequencies of a microstructure can be measured by sweeping driving frequency until largest displacement envelopes are observed. As a standard tool for characterization of ink-jet printheads, cinemicrography (Rembe *et al.*, 2001) has also been applied to a few other microsystems, which allows measurement of displacement time history of moving microstructures. However, this technique fails to characterize microstructures with non-periodic or non-reproducible transient behaviors.

2.11 Damping Mechanisms in Microsystems

In order to achieve accurate measurement of microsystems, damping cannot be ignored during vibration testing since it plays a crucial role in energy dissipation associated with microsystems. It has significant effects on dynamic characteristics of microsystems. For instance, for a micro-accelerometer, the overall damping of the device has a critical value to achieve maximum bandwidth. For a resonant sensor, damping needs to be minimized to

enhance quality factor to achieve higher resolution. The general energy dissipation mechanisms existing in typical microsystems include intrinsic losses of the material, anchor/clamping losses due to micro-slips at support and losses to surrounding fluid (Tilmans *et al*., 1992).

Anchor/clamping losses. Anchor/clamping losses mean vibration energy losses to substrate when oscillating elements are fixed to stationary substrate. They can be reduced by insulating the vibrating elements from the substrate. Wang *et al*. (1999) proposed the torsional-mode support springs to effectively isolate a free-free resonating beam from its anchors via impedance transformations, which leads to a minimum anchor loss. Thilmans *et al*. (1992) suggested another way of reducing anchor loss, which is to employ balanced structural configuration to cancel out moments and shear forces.

Thermoelastic damping. Intrinsic damping, which is related to material and geometrical properties of structures, increases substantially as feature size of microsystems decreases. It has been indicated that thermoelastic damping can be a dominant source of intrinsic damping in microsystems. Based on rigorous linear thermoelasticity theory, Lifshitz *et al*. (2000) studied the mechanism of thermoelastic damping in micro-scale devices and predicted quality factors of various microbeams using their model. Nayfeh and Younis (2004) presented an analytical formula to estimate quality factor of a microplate of general shape and boundary conditions due to thermelastic damping.

Air damping. Viscous damping induced by fluid surrounding a vibrating microstructure, is the most significant one among the various damping sources in microsystems. Lin and Wang (2006) illustrated the mechanism of air damping in a typical microsystem device

which employs parallel-plate capacitor. In that device, air fills the tiny gap between the two parallel plates. If the upper plate moves or bends downward, the pressure between the air gap increases and the air is squeezed out of gap. On the other hand, if the plate moves or bends upward, the situation reverses. In general, damping force created by such squeezed air film is observed in many micro-devices. Besides this squeeze film damping, sliding film damping, caused by the lateral oscillating motion of parallel plates is also an important source of system damping.

Squeeze Film Damping. Before the development of microstructures, squeezed film effect was studied using an analytical method based on linearized Reynolds equation by Blech (1983). The air film damping for rectangular geometry had been solved analytically as a function of frequency. Since most microsystem devices are packaged inside housing with rarefied air, air damping in rarefied air needs to be studied for microsystem. Though squeezed film effect can be conventionally described using Reynolds equation, the use of Reynolds equation for the squeezed film damping in microsystem is questionable as many MEMS devices are designed to be operated under very low pressure with very small gap distances (Lin and Wang, 2006). To date, two approaches have been suggested to address modeling of rarefied air: effective coefficient of viscosity and free molecular model.

The first method proposed that linearized Reynolds equation remains valid in the case of rarefied air, but the viscosity coefficient should be replaced by an effective coefficient of viscosity dependent on Knudsen number (Lin and Wang, 2006). Veijola *et al*. (1995) studied the damped dynamic behavior of a capacitive accelerometer, where the damping coefficient was calculated based on Blech model. They accounted for the slip-flow condition by using an effective coefficient of viscosity. Good agreement between

simulation results and experimental data was achieved. Li and Huges (2000) also presented an empirical equation for the effective coefficient of viscosity. The concept of effective coefficient of viscosity would become questionable when air pressure become much lower than atmospheric pressure since in this case, air can hardly be considered as viscous fluid.

Considering air flow in low vacuum, Zook *et al*. (1992) calculated quality factors of microbeams packaged under low pressure using Christian model, which is a free molecular model for damping without viscosity coefficient (Chritian, 1966). The comparison of computed and measured results showed that the predicted damping tended to be underestimated. Li *et al*. (1999) further improved Christian model by using a new air molecular velocity distribution function and the predicted results using their model were closes to experimental data. Different from Christian model, Bao *et al*. (2002) presented a new model for air damping of microstructures, where an energy transfer mechanism was utilized to describe damping effect.

Sliding Film Damping. Sliding film damping induced by shear is the dominant source of energy loss in laterally driven microstructures. Viscous damping in an air film sliding has been studied by Tang (1990) based on Couette flow. The theoretically predicted damping values were found to be much higher than measured counterparts. Cho *et al*. (1994) employed a Stokes-type damper to investigate shear damping for laterally oscillating microstructures. The results suggested that Stokes-type fluid motion could model viscous damping more accurately than Couette flow. Compared with experimental data, the theoretical damping values had a discrepancy of about 20%. By means of analytical and experimental methods, Zhang and Tang (1995) studied the various mechanisms of air damping in laterally oscillating microstructures. Their study showed that a better agreement

between measured and theoretical results could be achieved by including edge and finite-size effects into Couette and Stokes-type flows.

2.12 Model Updating of Microsystems

Though lots of research efforts have been directed to micro structural dynamics in the last couple of decades with the revolution of microsystem technology, model updating of microsystem, which combines conventional updating techniques and modal testing of microsystem, remains a brand-new area. A little research work in this area has begun its step to realize the efficient description of dynamic models of microsytems. Initially, effort has been placed on the accurate estimation or modeling of microsystems (MEMS). M'Closkey *et al*. (2000) estimated the multiple-input-multiple-output transfer function of a MEMS vibrational gyroscope with a recursive least squares algorithm then created an approximate rigid plate model that reveals the physical orientation of some modes of the gyroscope from this input/output relation. Furlong *et al*. (2005) performed modeling of a MEMS inertial sensor by associating finite element analysis with quantitative optoelectronic holographic microscopy.

Currently, research focus has been attracted to improve existing mathematical models of microsystems. However, only a few achievements about model updating of microstructure have been presented. Link and Zimmerman (2007) proposed a Genetic Algorithm approach for updating the parameters of systems governed by multiphysics equations. They also discussed the issues of sensitivity, mode tracking, and eigenvector function fitting in this approach. The approach was experimentally validated on model updating of the finite element structural model and the electrostatic model of a MEMS micromirror. Chen *et al*. (2006) presented an FE model updating procedure to identify material and geometrical

parameters for microstructures. This updating scheme utilized an optimization sequence that formulated the frequency differences as an error vector to be minimized based on the measured modal data and the predicted ones from FEA. The optimization problem was subsequently solved to give a set of updated material and geometrical parameters. The identification procedure was applied to two examples based on a micro-cantilever and an atomic force microscope probe. Furthermore, the updated FE model was validated by a small frequency difference between the experimental and predicted higher frequency modes.

2.13 Summary

In this chapter, a broad review of the state-of-the-art of model updating has been provided as well as current state of model updating of microsystems. In addition, vibration testing techniques and various damping mechanisms for microsystems have been reviewed. Most of the updating methods developed so for are found to be not quite reliable and still far from being mature. Moreover, there are no existing robust approaches capable of handling the various industrial problems, though many have presented successful results, which seem to be very much case-dependent. Especially for model updating of microsystems, efficient updating methods are required to resolve the issues presented by new testing techniques and damped microstructures.

Generally, direct updating methods cannot obtain adequately accurate results and the updated models fail to preserve any physical meaning. It seems that sensitivity based methods and FRF based methods are the most promising updating techniques, which are able to produce highly accurate updated results through iteration. However, these methods use the pseudo-inverse of sensitivity matrix, which may result in non-unique solutions due

to under-determined or ill-conditioned sensitivity matrix. Some novel approaches, such as Neural Networks, Genetic Algorithm and Taguchi method, are attractive in model updating. These techniques are robust when dealing with some issues in updating procedure, such as noise, global minimum and nonlinearity. However, in Neural Networks method the updated results are dependent on the training cases. The execution of Genetic Algorithm is very computationally exhaustive because of the stochastic search procedure. As for Taguchi method, the proper orthogonal arrays should be employed to achieve accurate results. Due to the practical limitations, these methods need further improvements for application in model updating of industrial cases.

As the feature size of microsystems is tiny, non-contact excitations and vibration measurements are required. It seems that LDV technology combined with base excitation is a promising vibration test technique, which is capable of providing suitable experimental data for model updating of microsystems. Air damping has been proved to be dominant among various damping sources of microsystems and two reasonable models of air damping have been proposed in the literature. Due to particular vibration test techniques, model updating methods of microsystems should be developed to meet the requirements resulting from experimental data. Furthermore, the identification of damped microsystems needs to be taken into account during the practical updating procedure.

Chapter 3

On the Relationship between Viscous and Structural Damping Models

This chapter is devoted to investigate the relationship between viscous and structural damping models. In order to show whether the arbitrary choice of damping model is reasonable, the relationships are derived based on two normalization procedures and the modal parameter identification procedure in the cases of proportional damping and non-proportional damping.

3.1 Introduction

In experimental modal analysis, the estimation or identification of damping models of damped mechanical systems is always the central topic since understanding of damping mechanisms is to date still quite primitive. By far the most common damping model employed in practice is the so-called ‘proportional damping’ (Rayleigh, 1897). Caughey and O’Kelly (1965) presented a general expression for proportional damping matrix in terms of mass and stiffness matrices so that a proportionally damped system can be decoupled by real normal modes. However, most practical structural systems possess general non-proportional damping and this kind of systems cannot be decoupled in the modal coordinates due to the non-diagonal nature of the modal damping matrix. Hence, the system exhibits complex mode behaviors instead of real modes. To overcome the difficulties induced by the existence of complex modes in the identification of a mechanical system, real normal modes are usually required in experimental modal analysis. Lin and

Ibrahim (1984) and Chen *et al.* (1996) proposed methods to obtain the best real normal modes from identified complex modes. The extracted normal modes were then used to construct a proportional damping model together with modal damping matrix.

Though the identification of a non-proportionally damped system still remains an issue in experimental modal analysis, a few effective methods have been developed to identify non-proportional damping matrix from experimentally measured complex modes in case of lightly damped systems. Woodhouse (1998) discussed linear damping models: the familiar dissipation-matrix model and the general linear model and presented simple expressions for complex modal data and transfer functions. Following this idea, Adhikari and Woodhouse (2001) presented a first order perturbation method to obtain a non-proportional viscous damping matrix from complex modal data in the case of sufficiently light damping. The physical damping matrix can be constructed using the inverse transformation of the decoupled modal damping matrix. Kasai and Link (2000) considered a method to determine symmetric non-proportional modal damping matrix using real normal modes based on a generalized modal model of a system.

To date, most proposed methods to identify or estimate system damping whatever it is proportional or non-proportional are based on viscous damping model, whose mechanism is well understood. In fact, for simplicity in engineering calculation and analysis, both viscous damping and structural damping models are generally adopted to describe damping properties in linear vibratory mechanical systems (Ewins, 2000b; Maia and Silva, 1997).

Although other damping models have been proposed from time to time, it has become common practice in modal analysis that either a structural or viscous damping model can be readily used in the interpretation of measured vibration data. However, no verification has been made as to show whether or not this kind of arbitrary interpretation is physically reasonable. Due to the uncertainty of the type of damping model in practical complex structural systems, an inappropriate damping model is perhaps employed for a system during modal analysis. For instance, viscous damping is assumed for a structural system which has structural damping in modal analysis. Or structural damping model is adopted while the system is viscously damped. Hence, it is important to demonstrate theoretically whether this arbitrary choice of damping model will cause large errors in the estimation of modal parameters. Because these parameters are regarded as accurate ones once estimated and they are to be used with confidence to establish the system's mass and stiffness matrices or modify these matrices of the analytical FE model. A large number of studies have ignored this topic on choosing an appropriate damping model for a damped system. The primary research work on the issue was conducted by Balmés (1997). He proposed an identification procedure to extract the normal modes from the experimental complex modes and meanwhile, investigated the relation between normal modes (structural damping case) and complex modes (viscous damping case) in details. It was found that the normal modes are clearly associated with the complex modes in terms of modal damping model and eigenvectors in the case of a proportionally damped system. In fact, for mechanical systems with same mass and stiffness matrices and different damping properties (such as viscous damping or structural damping), there may exist a relationship between the modal models

of these two systems since they have similar frequency response function models, which may also represent systems' dynamic characteristics in nature. The relationship may help us to understand the difference between the same systems with various damping models and choose a suitable damping model for a mechanical system when modal analysis is performed.

In the following section, the relationship between viscous and structural damping models is addressed in proportional damping case and general non-proportional damping case. Numerical simulation is presented to show the importance of the interpretation of damping model (data from viscous damping model have been interpreted as structural one or vice versa) for the estimation of modal parameters. To demonstrate the validity of the damping relationship for practical structural systems, a practical experimental example is also given.

3.2 Mass Normalization and 'A' Normalization

The modal model of a system consists of an eigenvalue matrix $[\omega_r^2]$ and an eigenvector matrix $[\Psi]$, where the eigenvalue matrix is unique while the eigenvector matrix is not. The non-unique eigenvectors or mode shapes are subject to an arbitrary scaling factor which does not affect the shape of the vibration mode, but only its amplitude. The procedure of scaling the eigenvectors is called 'normalization', which is largely governed by the numerical procedures followed by the eigensolution of a dynamic system. In experimental modal analysis, there exist two standard mode shape normalization procedures based on the two different damping models. One is called 'Mass Normalization' (normalized to the

system's mass matrix [*M*]) which is for the case of structural damping and the other is called 'A Normalization' (normalized to the system's generalized mass matrix [*A*]) which is used for viscous damping (Lin, 1990). In order to investigate the relationship between viscous and structural damping models, the various eigensolutions of the systems in the case of two different damping models, which correspond to the two normalization procedures respectively, need to be introduced first.

For a multi-degree-of-freedom (MDOF) system with general viscous damping, the generalized eigenvalue problem of the system can be written as,

$$([A]s_r + [B])\{\theta\}_r = \{0\}; \quad r = 1, 2n, \tag{3.1}$$

where s_r and $\{\theta\}_r$ are the 2*n* eigenvalues and eigenvectors of the system. [*A*] and [*B*] are system's generalized mass and stiffness matrices which have the forms respectively as,

$$[A] = \begin{bmatrix} [C] & [M] \\ [M] & [0] \end{bmatrix} \text{ and } [B] = \begin{bmatrix} [K] & [0] \\ [0] & -[M] \end{bmatrix}. \tag{3.2}$$

By solving equation (3.1), the eigenvalues and the so-called 'A normalized' eigenvectors, which are normalized to the generalized mass matrix [*A*], can be obtained in terms of matrix form as, respectively,

$$[S] = \begin{bmatrix} [\Lambda] & [0] \\ [0] & [\Lambda]^* \end{bmatrix} \text{ and } [\Theta] = \begin{bmatrix} [\Psi] & [\Psi]^* \\ [\Psi][\Lambda] & [\Psi]^*[\Lambda]^* \end{bmatrix}. \tag{3.3}$$

Here, $[\Lambda]$ is the diagonal matrix of complex eigenvalues, which can be expressed as,

$$[\Lambda] = [s_r], \quad s_r = \omega_r(-\xi_r + i\sqrt{1-\xi_r^2}), (r = 1, 2, \cdots, n). \tag{3.4}$$

From (3.3), it is obvious that the eigenproperties of the viscously damped system will be in general complex and always occur in complex conjugate pairs. Hence, the orthogonality

properties of the eigensolution are stated as,

$$[\Theta]^T[A][\Theta] = [I] \quad \text{and} \quad [\Theta]^T[B][\Theta] = [S]. \tag{3.5}$$

The eigenvalue problem for an MDOF system in the case of structural damping can be expressed as,

$$(-\lambda_r^2[M] + [K] + i[D])\{\phi\}_r = \{0\}; \quad r = 1, n. \tag{3.6}$$

Solving above eigenproblem leads to the solution containing complex eigenvalues λ_r^2 and eigenvectors $\{\phi\}_r$. The eigensolution of equation (3.6) is standard when compared with that of equation (3.1) and since $[A] \equiv [M]$ and $[B] \equiv [K] + i[D]$ in this case, the eigenvectors for the structural damping case are therefore mass-normalized (normalized to the mass matrix [*M*] of the system). The eigensolution possesses the orthogonality properties, which are defined by the equations,

$$[\Phi]^T[M][\Phi] = [I] \quad \text{and} \quad [\Phi]^T[K + iD][\Phi] = [\lambda_r^2], \tag{3.7}$$

where $[\Phi]$ is the mass-normalized eigenvector matrix and $[\lambda_r^2]$ is the diagonal matrix of complex eigenvalues.

The eigenvalues of the damped system from equations (3.1) and (3.6) are obviously different and hence the study is focused on the eigenvectors of the damped system for various damping models. Since different normalization procedures are used in the eigenproblems for the case of viscous and structural damping models, respectively, the corresponding mode shapes (eigenvectors) are visually quite different even for the case of a proportionally damped system. The differences in amplitudes as well as phase angles of the

corresponding eigenvectors often cause confusion to analysts. And it is therefore necessary to establish the relationship between the 'A-normalized' and mass-normalized eigenvectors. In fact, the mode shapes for the case of viscous and structural damping models differ simply by a complex scaling factor if the damping of the system is proportional, which will be shown by later derivation. According to modal testing theory (Ewins, 2000b), if the damping is proportional, no matter what type of damping model is used, the mode shapes are expected to be exactly the same as those of the corresponding undamped system. So what is the relationship between these two sets of mode shapes when the damping is proportional? In other words, what is the scaling factor for each mode between the two proportionally damped systems? In the case of proportional damping, suppose the Mass Normalized mode shape matrix $[\Phi]_{n\times n}$ and the 'A' Normalized mode shape matrix $[\Psi]_{n\times n}$ have the relationship as $[\Psi]_{n\times n}=[\Phi]_{n\times n}[N]_{n\times n}$, where $[N]_{n\times n}$ is a diagonal matrix of complex coefficients. Then the relationship between the mode shape matrices in case of different damping models is to determine the coefficient matrix $[N]$, which can be derived as follows. For a general viscously-damped system, the orthogonality properties of the modal model can be expressed as, if the complex conjugate of the eigenvalues and eigenvectors are not considered,

$$\begin{bmatrix}[\Psi]\\ [\Psi][\Lambda]\end{bmatrix}^{T}_{n\times 2n}\begin{bmatrix}[C] & [M]\\ [M] & [0]\end{bmatrix}_{2n\times 2n}\begin{bmatrix}[\Psi]\\ [\Psi][\Lambda]\end{bmatrix}_{2n\times n}=[I]_{n\times n}. \tag{3.8}$$

Expanding the left side of equation (3.8), we have the following equation,

$$[\Psi]^{T}[C][\Psi]+[\Lambda]^{T}[\Psi]^{T}[M][\Psi]+[\Psi]^{T}[M][\Psi][\Lambda]=[I]. \tag{3.9}$$

Substituting $[\Psi]=[\Phi][N]$ into (3.9), we can have,

$$[N]^{T}[\Phi]^{T}[C][\Phi][N]+[\Lambda]^{T}[N]^{T}[\Phi]^{T}[M][\Phi][N]+[N]^{T}[\Phi]^{T}[M][\Phi][N][\Lambda]=[I]. \tag{3.10}$$

The orthogonality of the proportionally damped system is as follows,

$$[\Phi]^T[M][\Phi]=[I],\ \text{and}\ [\Phi]^T[C][\Phi]=[2\xi_r\omega_r], \tag{3.11}$$

where $[2\xi_r\omega_r]$ is a diagonal matrix. Then, based on (3.11), equation (3.10) can be simplified to become the following equation,

$$[N]^T[2\xi_r\omega_r][N]+[\Lambda]^T[N]^T[N]+[N]^T[N][\Lambda]=[I]. \tag{3.12}$$

Since $[2\xi_r\omega_r]$, $[\Lambda]$ and $[N]$ are diagonal matrices, we can rewrite above equation as,

$$(2[\xi_r\omega_r]+2[\Lambda])[N]^2=[I]. \tag{3.13}$$

Upon substituting (3.4) into (3.13) and solving it, we derive the expression for $[N]$ as,

$$[N]^2=[(1/(2i\omega_r\sqrt{1-\xi_r^2}))]. \tag{3.14}$$

As $[N]$ is a diagonal matrix of coefficients, from equation (3.14), the diagonal elements in the matrix can be determined easily as,

$$\mathrm{N}_r=e^{-i\pi/4}\Big/\sqrt{2\omega_r\sqrt{1-\xi_r^2}}\quad(r=1,\cdots,n). \tag{3.15}$$

From equation (3.15), it is clear that for a proportionally damped system, the 'A' Normalized eigenvector of the r^{th} mode is simply the corresponding Mass Normalized eigenvector scaled by a factor of $1\Big/\sqrt{2\omega_r\sqrt{1-\xi_r^2}}$ and a phase angle rotation of $\pi/4$. Therefore, the modal models of a proportionally-damped system should be considered to be similar for different damping models since there is only a complex scaling factor between each mode shape for two mode shape matrices.

3.3 The Relationship between Viscous and Structural Damping Models

As mentioned above, when the damping of a system is proportional, the mode shapes are the same as those of the corresponding undamped system no matter the system is viscously

damped or structurally damped. As for other modal parameters, the undamped natural frequencies are the same because these two systems have the same mass matrix and stiffness matrix. And damping loss factor η_r for structural case and damping ratio ξ_r for viscous case have a simple relationship as $\eta_r = 2\xi_r$, which can be derived from similar frequency response function models of viscous case and structural case. Furthermore, if a proportional viscously-damped (or structurally-damped) system is given, by performing modal analysis on it's FRF model, the system's mass matrix $[M]$, stiffness matrix $[K]$ and damping matrix $[D]$ (or $[C]$) are derived based on structural (or viscous) damping assumption. Then, the system's matrices $[M]$ and $[K]$ are exactly the same as those of the original system and the equivalent damping matrix $[D]$ (or $[C]$) is different from the original damping matrix. Although the thus-identified damping matrix is not proportional in the sense that it cannot be expressed simply as a linear combination of $[M]$ and $[K]$, with this damping matrix, the system's mode shapes are still real. However, for a non-proportionally damped system, the relationship between these two sets of modal parameters is no longer so simple and cannot be readily derived. Because in this case, the real normal modes cannot be preserved due to the coupled nature of non-proportional damping. In order to establish such relationship, receptance FRF in the case of viscous damping is first presented, which can be written as (Ewins, 2000b),

$$\alpha(\omega) = \sum_{r=1}^{n} \frac{(A_r + i(\omega/\omega_r)B_r)}{(\omega_r^2 - \omega^2 + 2i\omega\omega_r\xi_r)}. \tag{3.16}$$

Here, some approximation has to be made in order to carry out the SDOF modal analysis. That is, in the vicinity of the r^{th} resonance, an FRF is dominated by the r^{th} mode so that the receptance expression for the viscous damping case is approximately written as,

$$\alpha(\omega) \approx \frac{(A_r + i(\omega/\omega_r)B_r)}{(\omega_r^2 - \omega^2 + 2i\omega\omega_r\xi_r)}, \tag{3.17}$$

where A_r and B_r are the real and imaginary parts of modal constant, respectively. Since the ratio between sweeping frequency and natural frequency is close to 1 at the r^{th} resonance region (i.e., $\omega/\omega_r \cong 1$), above equation can be further approximated as,

$$\alpha(\omega)\big|_{\omega\cong\omega_r} = \frac{(A_r + iB_r)}{(\omega_r^2 - \omega^2 + 2i\omega_r^2\xi_r)}. \tag{3.18}$$

During practical modal analysis procedure, the difference between modal parameters of a viscously damped system obtained using equation (3.18) and equation (3.17) is really quite small. It is usually within the analysis error if the damping ratio is less than about 4%. The receptance FRF for the structural damping case has the same form as equation (3.18), provided that $\eta_r = 2\xi_r$, which can be written as,

$$\alpha(\omega) = \frac{(A_r + iB_r)}{(\omega_r^2 - \omega^2 + i\omega_r^2\eta_r)}. \tag{3.19}$$

Equations (3.18) and (3.19) are equations from which the relationship between these two eigenvector matrices in different damping cases can be established based on the assumption that these two systems have the same frequency response model around resonance. Also equations (3.18) and (3.19) show that during the stage of modal parameters identification, either equation (3.18) or (3.19) can be chosen for modal analysis no matter FRF to be analysed comes from viscous damping case or structural damping case.

To investigate the relation of these two damping models for non-proportional case, the modal identification procedure, where the damping model is arbitrarily chosen for a damped system, should be illustrated briefly. Generally, the curve-fitting identification

method, which includes Circle-fit method and Line-fit method, is widely used in order to extract modal parameters from measured FRFs. These two methods are established for the case of structurally damped systems. The theory and typical procedures of the methods can be referred to (Ewins, 2000b). Based on these identification methods, the whole process of modal parameter identification for a damped system (if one damping model is interpreted as another model) can be illustrated as follows (for two cases):

1. From viscous damping model to structural damping model (i.e. deriving a structurally damped system to have the same response model around resonances as the original viscously damped one):

(a) Measure the FRFs of the system with viscous damping (one row or column of receptance matrix).

(b) Analyze these FRFs to obtain modal parameters (ω_r, η_r or ξ_r, A_r and B_r) based on the receptance form of equation (3.19) using modal analysis method.

(c) Interpret these modal parameters as those from structural damping model to obtain mode shape matrix.

(d) Use this mode shape matrix to derive the system's mass, stiffness and equivalent structural damping matrices.

2. From structural damping model to viscous damping model, similar procedure of modal parameter identification can be followed. The only different step is step (c), where the modal parameters are interpreted as those from viscous damping model to obtain mode shape matrix.

The theory of relationship between various eigenvector matrices behind this practice is shown as follows. Suppose all the elements of the modal constant vector, A_{jr} and B_{jr} $(j=1,\cdots,n)$, for the r^{th} mode have been derived using modal analysis. Then if a structural damping model is employed to interpret them, the mode shape for the r^{th} mode has the form $\Phi_{jr}=(A_{jr}+iB_{jr})\Big/\sqrt{A_{rr}+iB_{rr}}$, $(j=1,\cdots,n)$, where A_{rr} and B_{rr} are real and imaginary parts of the diagonal elements of the modal constant matrix respectively. If, on the other hand, a viscous damping model is chosen to interpret them, the mode shape for the r^{th} mode is $\Psi_{jr}=G_{jr}\Big/\sqrt{G_{rr}}$, $(j=1,\cdots,n)$ and G_{jr} is related to A_{jr} and B_{jr} by the following equation,

$$G_{jr}=\frac{B_{jr}}{2\omega_r}+\frac{i(-A_{jr}+\xi_r B_{jr})}{2\omega_r\sqrt{1-\xi_r^2}}. \tag{3.20}$$

If we write $A_{jr}+iB_{jr}=A_m e^{i\theta}$ and $G_{jr}=G_m e^{i\varphi}$, then from equation (3.20), the following relationship can be derived,

$$A_m=G_m(2\omega_r\sqrt{1+\xi_r^2\cos 2\varphi-\xi_r\sqrt{1-\xi_r^2}\sin 2\varphi}), \tag{3.21}$$

$$\text{and}\quad ctg\theta=\xi_r-\sqrt{1-\xi_r^2}\,tg\varphi. \tag{3.22}$$

From equation (3.21), since the maximum value for $\xi_r^2\cos 2\varphi-\xi_r\sqrt{1-\xi_r^2}\sin 2\varphi$ is $\sqrt{(\xi_r^2)^2+(\xi_r\sqrt{1-\xi_r^2})^2}=\xi_r$ and the value of ξ_r is usually small (<0.05), A_m is effectively equal to $2\omega_r G_m$ (the percentage error for this estimation, if we take the Talor series expansion of $\sqrt{1+\xi_r}$, is at the level of ξ_r^2). Suppose that the r^{th} mode shapes for the case of structural and viscous damping models can be rewritten as, respectively,

$$\Phi_{jr}=A_m^{jr}e^{i\theta_{jr}}\Big/\sqrt{A_m^{rr}e^{i\theta_{rr}}}=A_m^{jr}e^{i(\theta_{jr}-\theta_{rr}/2)}\Big/\sqrt{A_m^{rr}}, \tag{3.23}$$

$$\Psi_{jr}=G_m^{jr}e^{i\varphi_{jr}}\Big/\sqrt{G_m^{rr}e^{i\varphi_{rr}}}=G_m^{jr}e^{i(\varphi_{jr}-\varphi_{rr}/2)}\Big/\sqrt{G_m^{rr}}. \tag{3.24}$$

then it can be found that the moduli of the r^{th} mode shape for the viscous case is the corresponding moduli of the r^{th} mode shape for the structural case scaled by a constant

which is equal to $1/\sqrt{2\omega_r}$. As for equation (3.22), although it is difficult to prove it mathematically, the maximum error for the estimation of $\theta = \varphi - \pi/2$ or $\theta = \varphi + \pi/2$ is less than $4°$ if the damping ratio is less than 5% (this can be illustrated by examples given in the following section). Base on the above approximate relationship $\theta = \varphi - \pi/2$ (or $\theta = \varphi + 3\pi/2$), from equations (3.23) and (3.24), it can be derived that the r^{th} mode shape for the viscous damping case is the r^{th} mode shape for the structural damping case rotated by a constant phase angle which is $-45°$ or $135°$ (or $-225°$) since the phase difference between two mode shapes is equal to $\theta_{jr} - \varphi_{jr} - (\theta_{rr} - \varphi_{rr})/2$. This will be illustrated in following numerical cases. Combining these two features, it is clear that these two sets of mode shapes are roughly the same and this is what we expect because they are from the same system in the sense that the systems have the same response model.

3.4 The Derivation of System Matrices

Once modal parameters have been identified from the measured FRFs using modal analysis methods, the system's spatial model including mass, stiffness and damping matrices can be constructed using these parameters. In this section, a program has been written to simulate the modal analysis process for the verification of what has been put forward above. Given system's matrices [*M*], [*K*] and [*C*] or [*D*] for a damped system, the first step is to solve the eigenproblem to obtain eigenvalues and eigenvectors of the system. Based on the calculated eigenvalues and eigenvectors, the simulated FRFs are obtained. Then, in the simulated modal analysis process, the modal constants are calculated and used to derive the equivalent eigenvector matrix of its counterpart system (structural damping case if [*C*]

was used and viscous damping case if $[D]$ was used). And subsequently this equivalent mode shape (eigenvector) matrix is used to calculate system's mass, stiffness and damping matrices. In the last paragraph, it was shown how the equivalent mode shape matrix could be derived and here we suppose that this mode shape matrix has already been obtained. Based on the calculated mode shape matrix, the system's matrices can be determined as follows for two cases:

1. From viscous damping model to structural damping model case.

The system's mass and stiffness matrices can be calculated as, respectively,

$$[M] = ([\Phi]^T)^{-1}[\Phi]^{-1}, \tag{3.25}$$

$$[K] + i[D] = ([\Phi]^T)^{-1}[\omega_r^2(1 + i\eta_r)][\Phi]^{-1}. \tag{3.26}$$

The damping matrix [*D*] can be obtained by taking the imaginary part of the right side of equation (3.26).

2. From structural damping model to viscous damping model case.

Based on the eigenvalue and eigenvector matrices of the viscously damped system in equation (3.3), the generalized mass and stiffness matrices are determined as,

$$[A] = ([\Theta]^T)^{-1}[\Theta]^{-1}, \tag{3.27}$$

$$[B] = ([\Theta]^T)^{-1}[S][\Theta]^{-1}. \tag{3.28}$$

In this case, the calculated generalized stiffness matrix has the form,

$$[B] = \begin{bmatrix} -[K] & [0] \\ [0] & [M] \end{bmatrix}. \tag{3.29}$$

From the expressions of the generalized mass matrix $[A]$ in (3.2) and the generalized stiffness matrix $[B]$ in (3.29), the system's mass matrix $[M]$, stiffness matrix $[K]$ and damping matrix $[C]$ can be obtained by taking the partition matrices of $[A]$ and $[B]$,

respectively.

3.5 Discussion of Numerical Case Studies

In order to demonstrate the relationship between viscous and structural damping models derived previously, seven numerical cases have been presented. In each case, a typical mechanical system consisting of mass-spring elements is presented, whose mass, stiffness and damping matrices are specified. Following the identification process in section 3.3, the equivalent eigenvalue and eigenvector matrices of the system are calculated based on the deliberate wrong interpretation of damping model. Consequently, the equivalent system's matrices are derived based on the identified modal data.

Case No.1

A 3-DOFs mass-spring system with proportional structural damping is shown in Fig 3.1. Following parameters are used for this system: m_1=0.5kg, m_2=1.0kg, m_3=1.5kg; k_1=k_2=k_3=k_4=k_5=k_6=1000.0N/m; d_j=0.05k_j, $j=1,\cdots,6$. In this structurally damped system, the damping model, which is distributed, is interpreted as a viscous damping model.

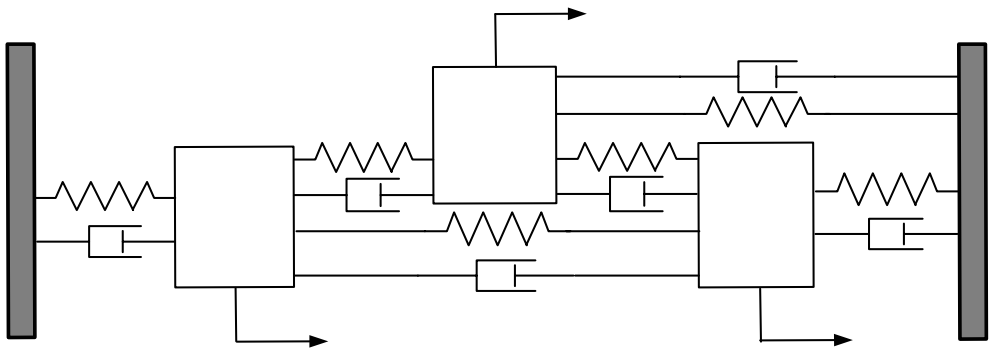

Fig. 3.1 A 3-DOFs mass-spring model

The original system's mass, stiffness and damping matrices in structural damping case are obtained from the parameters as:

$$[M]=\begin{bmatrix}0.5 & 0.0 & 0.0\\ 0.0 & 1.0 & 0.0\\ 0.0 & 0.0 & 1.5\end{bmatrix},\ [K]=\begin{bmatrix}3000 & -1000 & -1000\\ -1000 & 3000 & -1000\\ -1000 & -1000 & 3000\end{bmatrix},$$

$$\text{and}\ \ [D]=\begin{bmatrix}150 & -50 & -50\\ -50 & 150 & -50\\ -50 & -50 & 150\end{bmatrix}.$$

The mode shape matrix of this original system is given by the eigensolution of the system as:

$$[\Phi]=\begin{bmatrix}0.464 & 0.218 & 1.318\\ 0.536 & 0.782 & 0.318\\ 0.635 & 0.493 & 0.142\end{bmatrix}.$$

Following the modal identification process in section 3.3, the eigenvalue and eigenvector matrices can be obtained and then the generalized mass matrix $[A]$ and stiffness matrix $[B]$ are calculated:

$$[A]=\begin{bmatrix}1.895 & -0.419 & -0.467 & 0.500 & 0.000 & 0.000\\ -0.419 & 2.628 & -0.610 & 0.000 & 1.000 & 0.000\\ -0.467 & -0.610 & 3.169 & 0.000 & 0.000 & 1.500\\ 0.500 & 0.000 & 0.000 & 0.000 & 0.000 & 0.000\\ 0.000 & 1.000 & 0.000 & 0.000 & 0.000 & 0.000\\ 0.000 & 0.000 & 1.500 & 0.000 & 0.000 & 0.000\end{bmatrix},$$

$$\text{and}\ \ [B]=\begin{bmatrix}-2999.1 & 1000 & 1000 & 0.0 & 0.0 & 0.0\\ 1000 & -3000 & 1000 & 0.0 & 0.0 & 0.0\\ 1000 & 1000 & -2999.1 & 0.0 & 0.0 & 0.0\\ 0.0 & 0.0 & 0.0 & 0.5 & 0.0 & 0.0\\ 0.0 & 0.0 & 0.0 & 0.0 & 1.0 & 0.0\\ 0.0 & 0.0 & 0.0 & 0.0 & 0.0 & 1.5\end{bmatrix}.$$

From the partition matrices of the above matrices [*A*] and [*B*], the equivalent mass, stiffness and damping matrices can be obtained, respectively. As it can be seen, the derived mass and

stiffness matrices are the same as those from the original system while the damping matrix is different from that of the structurally damped system. The equivalent mode shape matrix is calculated as:

$$[\Psi] = \begin{bmatrix} 0.059(-45°) & 0.020(-45°) & 0.103(-45°) \\ 0.068(-45°) & 0.072(-45°) & 0.025(135°) \\ 0.081(-45°) & 0.046(135°) & 0.011(135°) \end{bmatrix}.$$

Pre- and post- multiplying the damping matrix by the eigenvector matrix has the following condition,

$$[\Psi]^H[C][\Psi] = [\Psi]^H \begin{bmatrix} 1.895 & -0.419 & -0.467 \\ -0.419 & 2.627 & -0.610 \\ -0.467 & -0.610 & 3.168 \end{bmatrix} [\Psi] = \begin{bmatrix} 0.025 & 0 & 0 \\ 0 & 0.025 & 0 \\ 0 & 0 & 0.025 \end{bmatrix}.$$

From the above orthogonal properties of the damping matrix, it can be proved the obtained equivalent damping matrix from [*A*] is physically meaningful.

Case No.2

In a similar 3-DOFs mass-spring system with different system parameters, which is non-proportionally and structurally damped, the damping model is interpreted as a viscous damping model. The system's mass and stiffness matrices are the same as those in Case No.1. And the localized structural damping matrix is:

$$[D] = \begin{bmatrix} 300 & 0 & 0 \\ 0 & 0 & 0 \\ 0 & 0 & 0 \end{bmatrix}.$$

The mode shape matrix of this original system can be obtained by solving the eigenproblem of the system and given by:

$$[\Phi]=\begin{bmatrix} 1.321(0.87°) & 0.463(-5.54°) & 0.217(172.6°) \\ 0.316(173.3°) & 0.537(0.02°) & 0.784(178.9°) \\ 0.142(176.9°) & 0.636(0.96°) & 0.492(-1.34°) \end{bmatrix}.$$

The generalized matrices $[A]$ and $[B]$ are calculated:

$$[A]=\begin{bmatrix} 3.499 & -0.225 & 0.143 & 0.502 & 0.003 & 0.001 \\ -0.222 & 0.797 & 0.825 & 0.001 & 0.998 & -0.001 \\ 0.143 & 0.825 & 1.339 & -0.000 & -0.000 & 1.501 \\ 0.502 & 0.001 & -0.000 & 0.000 & 0.000 & 0.000 \\ 0.003 & 0.998 & -0.000 & 0.000 & -0.000 & -0.000 \\ 0.001 & -0.001 & 1.501 & 0.000 & -0.000 & -0.000 \end{bmatrix},$$

$$\text{and } [B]=\begin{bmatrix} -3013 & 990 & 1000 & -0.857 & -1.956 & -2.251 \\ 990 & -2992 & 1003 & -0.223 & 0.781 & 0.808 \\ 1000 & 1003 & -3002 & 0.144 & 0.817 & 1.329 \\ -0.857 & -0.223 & 0.144 & 0.500 & 0.000 & -0.001 \\ -1.956 & 0.781 & 0.817 & 0.000 & 0.997 & -0.002 \\ -2.251 & 0.808 & 1.329 & -0.001 & -0.002 & 1.500 \end{bmatrix}.$$

The calculated equivalent eigenvector matrix is:

$$[\Psi]=\begin{bmatrix} 0.103(-44.1°) & 0.059(-50.5°) & 0.020(-52.4°) \\ 0.025(128.3°) & 0.068(-45.0°) & 0.073(-43.9°) \\ 0.011(131.9°) & 0.081(-44.1°) & 0.046(133.7°) \end{bmatrix}.$$

In this case, the equivalent mass and stiffness matrices are almost the same as those of the original system in structural damping case, respectively. Compare the eigenvector matrices of the original and the identified systems, it can be found that the moduli of the r^{th}, (r =1,2,3) mode shape for viscous damping case are that for structural damping case scaled by a constant (the constants are 0.127, 0.093 and 0.078 for the three modes, respectively), which is equal to $1/\sqrt{2\omega_r}$, (r =1,2,3). Moreover, it is shown that the r^{th} mode shape for viscous damping case is that for structural damping case rotated by a constant phase angle which is -45° or 135° (or -225°). These features agree well with the relationship we have established between viscous damping and structural damping models in non-proportional

case in section 3.3.

Moreover, the equivalent damping matrix has no physical meanings since it is not a positive-definite or semi-positive definite matrix. This can be verified by the following condition,

$$[\Psi]^H[C][\Psi] =$$

$$[\Psi]^H \begin{bmatrix} 3.499 & -0.225 & 0.143 \\ -0.222 & 0.797 & 0.825 \\ 0.143 & 0.825 & 1.339 \end{bmatrix} [\Psi] = \begin{bmatrix} 0.033 & 0.004 & 0.016+0.003\mathrm{i} \\ 0.004 & 0.002 & 0.004+0.001\mathrm{i} \\ 0.016-0.003\mathrm{i} & 0.004-0.001\mathrm{i} & 0.039 \end{bmatrix}.$$

Case No.3

In this case, a larger mass-spring system, which has 8 DOFs, is considered. It is also non-proportionally and structurally damped. The damping model is interpreted as a viscous damping model. The system's mass, stiffness and localized damping matrices are:

$$[M] = \begin{bmatrix} 1.0 & 0.0 & 0.0 & 0.0 & 0.0 & 0.0 & 0.0 & 0.0 \\ 0.0 & 1.0 & 0.0 & 0.0 & 0.0 & 0.0 & 0.0 & 0.0 \\ 0.0 & 0.0 & 1.0 & 0.0 & 0.0 & 0.0 & 0.0 & 0.0 \\ 0.0 & 0.0 & 0.0 & 1.0 & 0.0 & 0.0 & 0.0 & 0.0 \\ 0.0 & 0.0 & 0.0 & 0.0 & 1.0 & 0.0 & 0.0 & 0.0 \\ 0.0 & 0.0 & 0.0 & 0.0 & 0.0 & 1.0 & 0.0 & 0.0 \\ 0.0 & 0.0 & 0.0 & 0.0 & 0.0 & 0.0 & 1.0 & 0.0 \\ 0.0 & 0.0 & 0.0 & 0.0 & 0.0 & 0.0 & 0.0 & 1.0 \end{bmatrix},$$

$$[K] = \begin{bmatrix} 2.0 & -1.0 & 0.0 & 0.0 & 0.0 & 0.0 & 0.0 & 0.0 \\ -1.0 & 2.0 & -1.0 & 0.0 & 0.0 & 0.0 & 0.0 & 0.0 \\ 0.0 & -1.0 & 2.0 & -1.0 & 0.0 & 0.0 & 0.0 & 0.0 \\ 0.0 & 0.0 & -1.0 & 2.0 & -1.0 & 0.0 & 0.0 & 0.0 \\ 0.0 & 0.0 & 0.0 & -1.0 & 2.0 & -1.0 & 0.0 & 0.0 \\ 0.0 & 0.0 & 0.0 & 0.0 & -1.0 & 2.0 & -1.0 & 0.0 \\ 0.0 & 0.0 & 0.0 & 0.0 & 0.0 & -1.0 & 2.0 & -1.0 \\ 0.0 & 0.0 & 0.0 & 0.0 & 0.0 & 0.0 & -1.0 & 2.0 \end{bmatrix},$$

$$\text{and} \quad [D]=\begin{bmatrix} 0.3 & 0.0 & 0.0 & 0.0 & 0.0 & 0.0 & 0.0 & 0.0 \\ 0.0 & 0.0 & 0.0 & 0.0 & 0.0 & 0.0 & 0.0 & 0.0 \\ 0.0 & 0.0 & 0.0 & 0.0 & 0.0 & 0.0 & 0.0 & 0.0 \\ 0.0 & 0.0 & 0.0 & 0.0 & 0.0 & 0.0 & 0.0 & 0.0 \\ 0.0 & 0.0 & 0.0 & 0.0 & 0.0 & 0.0 & 0.0 & 0.0 \\ 0.0 & 0.0 & 0.0 & 0.0 & 0.0 & 0.0 & 0.0 & 0.0 \\ 0.0 & 0.0 & 0.0 & 0.0 & 0.0 & 0.0 & 0.0 & 0.0 \\ 0.0 & 0.0 & 0.0 & 0.0 & 0.0 & 0.0 & 0.0 & 0.0 \end{bmatrix}.$$

The mode shape matrix of the original system is:

$$[\Phi]=\begin{bmatrix} 0.157(-13°) & 0.301(169°) & 0.414(-7°) & 0.478(177°) & 0.478(-177°) & 0.158(-167°) & 0.301(11°) & 0.414(-173°) \\ 0.299(-4°) & 0.467(179°) & 0.425(7°) & 0.199(-148°) & 0.199(32°) & 0.299(4°) & 0.467(-179°) & 0.425(-7°) \\ 0.407(-1°) & 0.419(-175°) & 0.082(82°) & 0.415(-6°) & 0.415(6°) & 0.407(-179°) & 0.419(-5°) & 0.082(97°) \\ 0.465(0°) & 0.178(-164°) & 0.408(176°) & 0.315(11°) & 0.315(169°) & 0.465(-0°) & 0.178(164°) & 0.408(-176°) \\ 0.467(1°) & 0.159(-13°) & 0.415(-176°) & 0.306(171°) & 0.306(-171°) & 0.467(179°) & 0.159(-167°) & 0.415(-4°) \\ 0.412(2°) & 0.407(-1°) & 0.041(97°) & 0.410(-177°) & 0.410(-3°) & 0.412(-2°) & 0.407(1°) & 0.041(97°) \\ 0.306(2°) & 0.466(1°) & 0.406(-1°) & 0.162(-10°) & 0.162(10°) & 0.306(178°) & 0.466(179°) & 0.406(-179°) \\ 0.163(3°) & 0.305(2°) & 0.409(1°) & 0.463(1°) & 0.463(179°) & 0.163(-3°) & 0.305(-2°) & 0.409(-1°) \end{bmatrix}$$

The calculated mass, stiffness and viscous damping matrices are:

$$[M]=\begin{bmatrix} 0.988 & -0.004 & -0.004 & -0.003 & -0.002 & -0.001 & -0.001 & -0.000 \\ -0.004 & 0.998 & -0.003 & -0.002 & -0.001 & -0.001 & -0.000 & -0.000 \\ -0.004 & -0.003 & 0.998 & -0.002 & -0.001 & -0.001 & -0.000 & -0.000 \\ -0.003 & -0.002 & -0.002 & 0.999 & -0.001 & -0.001 & -0.000 & -0.000 \\ -0.002 & -0.001 & -0.001 & -0.001 & 1.000 & -0.001 & -0.001 & -0.000 \\ -0.001 & -0.001 & -0.001 & -0.001 & -0.001 & 1.000 & -0.001 & -0.001 \\ -0.001 & -0.000 & -0.000 & -0.000 & -0.001 & -0.001 & 1.000 & -0.001 \\ -0.000 & -0.000 & -0.000 & -0.000 & -0.000 & -0.001 & -0.001 & 1.0 \end{bmatrix},$$

$$[K]=\begin{bmatrix} 2.03 & -1.00 & 0.00 & 0.00 & 0.00 & 0.00 & 0.00 & 0.00 \\ -1.00 & 2.00 & -1.00 & -0.00 & 0.00 & 0.00 & 0.00 & 0.00 \\ 0.00 & -1.00 & 2.00 & -1.00 & -0.00 & 0.00 & 0.00 & 0.00 \\ 0.00 & -0.00 & -1.00 & 2.00 & -1.00 & -0.00 & 0.00 & 0.00 \\ 0.00 & 0.00 & -0.00 & -1.00 & 2.00 & -1.00 & -0.00 & 0.00 \\ 0.00 & 0.00 & 0.00 & -0.00 & -1.00 & 2.00 & -1.00 & -0.00 \\ 0.00 & 0.00 & 0.00 & 0.00 & -0.00 & -1.00 & 2.00 & -1.00 \\ 0.00 & 0.00 & 0.00 & 0.00 & 0.000 & -0.00 & -1.00 & 2.00 \end{bmatrix},$$

and

$$[C]=\begin{bmatrix} 0.137 & 0.024 & 0.002 & 0.002 & 0.002 & 0.001 & 0.000 & 0.000 \\ 0.024 & 0.019 & 0.006 & -0.003 & -0.000 & 0.000 & 0.000 & 0.000 \\ 0.002 & 0.006 & 0.015 & 0.004 & -0.004 & -0.001 & 0.000 & 0.000 \\ 0.002 & -0.003 & 0.004 & 0.014 & 0.003 & -0.005 & -0.001 & -0.000 \\ 0.001 & -0.000 & -0.004 & 0.003 & 0.014 & 0.003 & -0.005 & -0.001 \\ 0.001 & 0.000 & -0.001 & -0.005 & 0.003 & 0.014 & 0.003 & -0.005 \\ 0.000 & 0.000 & 0.000 & -0.001 & -0.005 & 0.003 & 0.014 & 0.004 \\ 0.000 & 0.000 & 0.000 & -0.000 & -0.001 & -0.005 & 0.004 & 0.019 \end{bmatrix}.$$

The equivalent mode shape matrix is:

$$[\Psi]=\begin{bmatrix} 0.190(-58°) & 0.258(-56°) & 0.294(-52°) & 0.298(-48°) & 0.273(-42°) & 0.079(-32°) & 0.155(-34°) & 0.222(-38°) \\ 0.359(-49°) & 0.399(-46°) & 0.299(-38°) & 0.123(-13°) & 0.115(104°) & 0.151(139°) & 0.241(136°) & 0.229(128°) \\ 0.487(-46°) & 0.357(-40°) & 0.058(39°) & 0.254(129°) & 0.237(141°) & 0.205(-44°) & 0.216(-50°) & 0.044(-127°) \\ 0.557(-45°) & 0.150(-29°) & 0.289(131°) & 0.195(146°) & 0.180(-56°) & 0.234(135°) & 0.092(119°) & 0.219(-41°) \\ 0.559(-44°) & 0.136(122°) & 0.292(139°) & 0.191(-54°) & 0.174(-36°) & 0.235(-46°) & 0.082(148°) & 0.223(131°) \\ 0.492(-43°) & 0.347(134°) & 0.029(-141°) & 0.255(-42°) & 0.235(132°) & 0.208(133°) & 0.210(-44°) & 0.022(-127°) \\ 0.366(-43°) & 0.397(136°) & 0.287(-46°) & 0.101(-125°) & 0.092(145°) & 0.154(-47°) & 0.240(134°) & 0.218(-44°) \\ 0.195(-43°) & 0.260(137°) & 0.288(-44°) & 0.288(136°) & 0.264(46°) & 0.082(132°) & 0.157(-47°) & 0.220(136°) \end{bmatrix}.$$

Case No.4

In a proportionally damped 3-DOFs system, a distributed viscous damping model is interpreted as a structural damping model. The system's stiffness matrix is the same as in Case No.1, and the mass and viscous damping matrices are:

$$[M]=\begin{bmatrix} 1.0 & 0.0 & 0.0 \\ 0.0 & 0.95 & 0.0 \\ 0.0 & 0.0 & 1.05 \end{bmatrix}, \text{ and } [C]=\begin{bmatrix} 4.8 & -1.6 & -1.6 \\ -1.6 & 4.8 & -1.6 \\ -1.6 & -1.6 & 4.8 \end{bmatrix}.$$

The original system's mode shape matrix is:

$$[\Psi]=\begin{bmatrix} 0.073(-45°) & 0.054(-45°) & 0.049(-45°) \\ 0.071(-45°) & 0.019(-45°) & 0.073(135°) \\ 0.074(-45°) & 0.067(135°) & 0.018(-45°) \end{bmatrix}.$$

The calculated mass, stiffness, and structural damping matrices are:

$$[M]=\begin{bmatrix}1.00 & 0.00 & 0.00\\ 0.00 & 0.95 & 0.00\\ 0.00 & 0.00 & 1.05\end{bmatrix},\ [K]=\begin{bmatrix}3000 & -1000 & -1000\\ -1000 & 3000 & -1000\\ -1000 & -1000 & 3000\end{bmatrix},$$

$$\text{and}\ [D]=\begin{bmatrix}287 & -120 & -116\\ -120 & 293 & -118\\ -116 & -118 & 281\end{bmatrix}.$$

The equivalent mode shape matrix is obtained as:

$$[\Phi]=\begin{bmatrix}0.577 & 0.602 & 0.552\\ 0.567 & 0.215 & -0.827\\ 0.586 & -0.752 & 0.207\end{bmatrix}.$$

In this case, the equivalent mass and stiffness matrices are the same as those of the original system. In addition, the equivalent damping matrix [*D*] is demonstrated to be physically meaningful.

Case No.5

In a 3-DOFs system with non-proportional viscous damping, the damping model is interpreted as a structural damping model. The system's mass and stiffness matrices are the same as those in Case No.4. The original localized viscous damping and mode shape matrices are as follows:

$$[C]=\begin{bmatrix}9.6 & 0.0 & 0.0\\ 0.0 & 0.0 & 0.0\\ 0.0 & 0.0 & 0.0\end{bmatrix},$$

$$[\Psi]=\begin{bmatrix}0.077(-42°) & 0.023(39°) & 0.073(-49°)\\ 0.042(96°) & 0.074(143°) & 0.072(-43°)\\ 0.045(152°) & 0.059(-57°) & 0.074(-43°)\end{bmatrix}.$$

The calculated mass, stiffness and structural damping matrices are:

$$[M]=\begin{bmatrix}0.996 & -0.019 & 0.013\\ -0.019 & 0.963 & 0.006\\ 0.013 & 0.006 & 1.033\end{bmatrix},\quad [K]=\begin{bmatrix}2996 & -1070 & -944\\ -1070 & 3052 & -978\\ -944 & -978 & 2930\end{bmatrix},$$

$$\text{and}\ \ [D]=\begin{bmatrix}391 & -63 & -88\\ -63 & 33 & 51\\ -88 & 51 & 79\end{bmatrix}.$$

The equivalent mode shape matrix is identified as:

$$[\Phi]=\begin{bmatrix}0.862(3°) & 0.264(84°) & 0.580(-4°)\\ 0.465(140°) & 0.837(187°) & 0.571(2°)\\ 0.505(-164°) & 0.669(-13°) & 0.590(2°)\end{bmatrix}.$$

The relationship between the original and the identified mode shape matrices can also be validated by comparing the original and identified eigenvector matrices.

Case No.6

The 8-DOFs system, which is non-proportionally and viscously damped, is considered again in this case. The system's mass and stiffness matrices are the same as those in Case No.3. To identify the modal data of this system, a structural damping model is assumed. The system has damping at two localized locations so that the damping matrix is localized as:

$$[C]=\begin{bmatrix}0.3 & 0.0 & 0.0 & 0.0 & 0.0 & 0.0 & 0.0 & 0.0\\ 0.0 & 0.0 & 0.0 & 0.0 & 0.0 & 0.0 & 0.0 & 0.0\\ 0.0 & 0.0 & 0.0 & 0.0 & 0.0 & 0.0 & 0.0 & 0.0\\ 0.0 & 0.0 & 0.0 & 0.0 & 0.0 & 0.0 & 0.0 & 0.0\\ 0.0 & 0.0 & 0.0 & 0.0 & 0.0 & 0.0 & 0.0 & 0.0\\ 0.0 & 0.0 & 0.0 & 0.0 & 0.0 & 0.0 & 0.0 & 0.0\\ 0.0 & 0.0 & 0.0 & 0.0 & 0.0 & 0.0 & 0.0 & 0.0\\ 0.0 & 0.0 & 0.0 & 0.0 & 0.0 & 0.0 & 0.0 & 0.3\end{bmatrix}.$$

The mode shape matrix of the original system is:

$$[\Psi]=\begin{bmatrix}
0.193(-49°) & 0.260(-51°) & 0.294(-51°) & 0.300(-47°) & 0.276(-41°) & 0.224(-34°) & 0.154(28°) & 0.077(-24°)\\
0.364(-46°) & 0.399(-45°) & 0.294(-39°) & 0.118(-14°) & 0.119(102°) & 0.232(126°) & 0.243(135°) & 0.150(139°)\\
0.490(-45°) & 0.351(-43°) & 0.029(42°) & 0.255(131°) & 0.230(139°) & 0.038(-124°) & 0.219(-51°) & 0.208(-46°)\\
0.558(-44°) & 0.139(-42°) & 0.288(135°) & 0.187(138°) & 0.172(-49°) & 0.216(-46°) & 0.087(127°) & 0.239(132°)\\
0.558(-44°) & 0.139(138°) & 0.288(135°) & 0.187(-42°) & 0.172(-49°) & 0.216(134°) & 0.087(127°) & 0.239(-48°)\\
0.490(-45°) & 0.351(137°) & 0.029(42°) & 0.255(-49°) & 0.230(139°) & 0.038(56°) & 0.219(-51°) & 0.208(134°)\\
0.364(-46°) & 0.399(135°) & 0.294(-39°) & 0.118(166°) & 0.119(102°) & 0.232(-54°) & 0.243(134°) & 0.150(-41°)\\
0.194(-49°) & 0.260(129°) & 0.294(-51°) & 0.300(133°) & 0.276(-41°) & 0.223(146°) & 0.154(-28°) & 0.077(-156°)
\end{bmatrix}$$

The calculated mass, stiffness and viscous damping matrices are:

$$[M]=\begin{bmatrix}
0.994 & -0.006 & -0.000 & -0.002 & -0.000 & 0.000 & -0.000 & -0.000\\
-0.006 & 0.999 & 0.003 & 0.000 & -0.002 & -0.000 & 0.000 & -0.000\\
-0.001 & 0.003 & 0.998 & 0.002 & 0.001 & -0.002 & -0.000 & 0.000\\
-0.003 & 0.000 & 0.002 & 0.999 & 0.002 & 0.001 & -0.002 & -0.000\\
-0.000 & -0.002 & 0.001 & 0.002 & 0.999 & 0.002 & 0.000 & -0.003\\
0.000 & -0.000 & -0.002 & 0.001 & 0.002 & 0.998 & 0.003 & -0.001\\
-0.000 & 0.000 & -0.000 & -0.002 & 0.000 & 0.003 & 0.999 & -0.006\\
-0.000 & -0.000 & 0.000 & -0.000 & -0.003 & -0.001 & -0.006 & 0.994
\end{bmatrix},$$

$$[K]=\begin{bmatrix}
1.995 & -1.007 & 0.002 & -0.003 & 0.002 & 0.001 & -0.000 & -0.000\\
-1.007 & 2.000 & -0.994 & 0.001 & -0.005 & 0.002 & 0.001 & -0.000\\
0.002 & -0.994 & 1.992 & -0.995 & 0.002 & -0.006 & 0.002 & 0.001\\
-0.003 & 0.001 & -0.995 & 1.993 & -0.995 & 0.002 & -0.005 & 0.002\\
0.002 & -0.005 & 0.002 & -0.995 & 1.993 & -0.995 & 0.001 & -0.003\\
0.001 & 0.002 & -0.006 & 0.002 & -0.995 & 1.992 & -0.994 & 0.002\\
-0.000 & 0.001 & 0.002 & -0.005 & 0.001 & -0.994 & 2.000 & -1.007\\
-0.000 & -0.000 & 0.001 & 0.002 & -0.003 & 0.002 & -1.007 & 1.995
\end{bmatrix},$$

and

$$[D]=\begin{bmatrix}
0.263 & -0.039 & -0.037 & -0.001 & -0.000 & -0.002 & -0.001 & -0.000\\
-0.039 & 0.042 & 0.000 & -0.021 & 0.005 & 0.002 & -0.000 & -0.000\\
-0.037 & 0.000 & 0.041 & -0.005 & -0.023 & 0.005 & 0.002 & -0.002\\
-0.001 & -0.021 & -0.005 & 0.042 & -0.005 & -0.023 & 0.005 & -0.000\\
-0.000 & 0.005 & -0.023 & -0.005 & 0.041 & -0.005 & -0.021 & -0.001\\
-0.002 & 0.002 & 0.005 & -0.023 & -0.005 & 0.041 & 0.000 & -0.037\\
-0.001 & -0.000 & 0.002 & 0.005 & -0.021 & 0.000 & 0.042 & -0.039\\
-0.000 & -0.000 & -0.002 & -0.000 & -0.001 & -0.037 & -0.039 & 0.263
\end{bmatrix}.$$

The equivalent mode shape matrix is:

$$[\Psi]=\begin{bmatrix}
0.161(-4°) & 0.304(-6°) & 0.415(-6°) & 0.480(-2°) & 0.483(4°) & 0.417(10°) & 0.298(17°) & 0.153(21°)\\
0.303(-1°) & 0.467(0°) & 0.419(6°) & 0.194(30°) & 0.203(146°) & 0.430(171°) & 0.469(180°) & 0.298(-176°)\\
0.409(0°) & 0.412(2°) & 0.042(84°) & 0.407(176°) & 0.404(-176°) & 0.069(-79°) & 0.423(-6°) & 0.412(-1°)\\
0.465(1°) & 0.163(3°) & 0.408(-180°) & 0.301(-176°) & 0.299(-4°) & 0.401(0°) & 0.169(172°) & 0.474(177°)\\
0.465(1°) & 0.163(-177°) & 0.408(-180°) & 0.301(3°) & 0.299(-4°) & 0.401(180°) & 0.169(172°) & 0.474(-3°)\\
0.409(0°) & 0.412(-178°) & 0.042(84°) & 0.407(-4°) & 0.404(-176°) & 0.069(100°) & 0.423(-6°) & 0.412(179°)\\
0.303(-1°) & 0.467(-180°) & 0.419(6°) & 0.194(-150°) & 0.203(146°) & 0.430(-9°) & 0.469(180°) & 0.298(4°)\\
0.161(-4°) & 0.304(174°) & 0.415(-6°) & 0.480(178°) & 0.483(4°) & 0.417(-170°) & 0.298(17°) & 0.153(-159°)
\end{bmatrix}.$$

Based on the above numerical case studies, all the identified results of damping, mass and stiffness matrices for these cases are summarized in Table 3.1 as well as mode shapes vectors. As can be seen, Case No. 1 and Case No. 4 are the cases in which the damping matrices (structural and viscous) are proportional. Therefore, an exact relationship between structural and viscous damping models exists in these two cases since no assumption has been made for the proportional damping case. The equivalent damping matrix is no longer proportional (cannot be expressed as a linear combination of $[M]$ and $[K]$) while the system still has real modes. Moreover, the identified damping models are physically meaningful in the case of distributed damping properties. Case No. 2 is the case where a non-proportionally damped system has well separated modes. In this case, the estimation errors between the original mass and stiffness matrices and the calculated ones are very small, but the calculated damping matrix is no longer physically meaningful since damping properties are localized. Case No. 5 is closely coupled system with localized damping. In this case, the mode shapes of the original system and its equivalent counterparts are effectively the same except differing by a complex scaling factor. Moreover, as in Case No. 2, the equivalent damping matrices are not physically meaningful. The errors between the original system's mass, stiffness and the calculated ones are also quite small (<5%). In

order to demonstrate whether the theory is valid for large systems, Case No. 3 and Case No. 6, where an 8-DOFs system with non-proportional damping is presented, were also studied. The difference between these two cases is that Case No. 6 has localized damping properties at two separated locations. Numerical results which were observed from Case No. 2 were similarly obtained for Case No. 3. So were the calculated results from Case No. 6 as compared with those from Case No. 5. However, the calculated equivalent damping matrices in the two cases would not possess physical meanings any more. All these shows the above derived theory can be extended to various larger systems without compromising the validity of the conclusions established.

Table 3.1 The identified results of system matrices of simulated cases

Case No.	Original system	Identified system (Relationship between damping models)		
		Damping	Mass and stiffness	Mode shapes
1	Proportional structural damping is distributed.	Viscous damping is non-proportional.	same as the original ones.	same as the original ones.
2	Non-proportional structural damping is localized.	Viscous damping has no physical meanings.	almost same as the original ones.	Differ from the original ones by a complex scaling factor.
3	Non-proportional structural damping is localized. Lager system	Viscous damping has no physical meanings.	almost same as the original ones.	Differ from the original ones by a complex scaling factor.
4	Proportional viscous damping is distributed.	Structural damping is non-proportional.	same as the original ones.	same as the original ones.
5	Non-proportional viscous damping is localized.	Structural damping has no physical meanings.	almost same as the original ones.	Differ from the original ones by a complex scaling factor.
6	Non-proportional viscous damping is localized. Lager system	Structural damping has no physical meanings.	almost same as the original ones.	Differ from the original ones by a complex scaling factor.

The above various simulated case studies have verified that the mode shapes obtained from arbitrary interpretation of modal data are accurate enough to be used to modify analytical

FE model. Moreover, the identified spatial model including mass and stiffness matrices is consistent with those of the original system. However, if the damping information of a system is sought and the damping of the system is localized, then the correct interpretation of damping model becomes very important. The reason is that in this case there is no physically meaningful equivalent damping matrix existing.

3.6 Experimental Case Study

To highlight the significance of interpreting damping model for a damped mechanical system, a sample experimental case study was conducted. This case study is based on the experimental modal testing of a beam. The sketch of the experiment set up is shown as Fig. 3.2, in which a test aluminum beam is suspended free-free. The lateral responses (in *y* direction) were measured by an accelerometer at the nine measurement points on the beam with the hammer excitation at the sixth location in *y* direction. And then the FRF data were gathered from the FFT analyzer and transferred into the computer. Subsequently, modal analysis procedure was performed using modal analysis software to extract modal parameters, such as nature frequencies, mode shapes and damping loss factors.

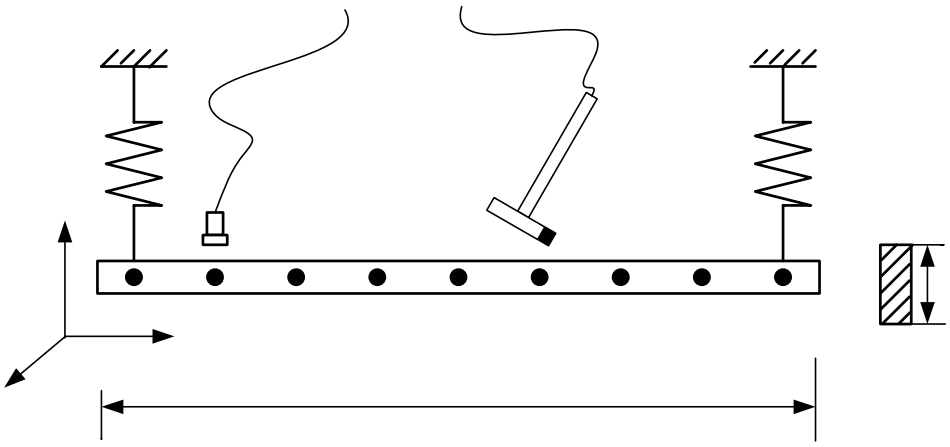

Fig. 3.2 Sketch of a free-free beam under test

A typical measured FRFs, where five resonant peaks are observed, is shown in Fig. 3.3 and the identified modal data for the first five modes are list in Table 3.2 except the mode shapes. The mode shape matrix of this damped structure is obtained as:

$$[\Phi] = \begin{bmatrix} 1.009(86.4°) & 0.792(13.6°) & 0.799(102°) & 0.906(178°) & 0.635(-89.3°) \\ 0.388(93.1°) & 0.036(-171°) & 0.247(-28.3°) & 0.540(-6.4°) & 0.626(82.9°) \\ 0.105(-90.3°) & 0.599(-173°) & 0.588(-83.8°) & 0.180(6.4°) & 0.229(-111°) \\ 0.577(-83.5°) & 0.542(175°) & 0.115(98.9°) & 0.590(-179°) & 0.438(-107°) \\ 0.804(-77.6°) & 0.004(169°) & 0.392(146°) & 0.006(3.9°) & 0.699(97.0°) \\ 0.396(-88.7°) & 0.485(-1.3°) & 0.129(88.8°) & 0.631(3.9°) & 0.420(-82.5°) \\ 0.135(-90.5°) & 0.629(4.5°) & 0.512(-77.7°) & 0.140(-170°) & 0.363(-86.2°) \\ 0.369(91.8°) & 0.059(1.5°) & 0.225(-97.9°) & 0.545(176°) & 0.581(75.6°) \\ 0.988(82.2°) & 0.807(177°) & 0.603(89.6°) & 0.699(30.3°) & 0.654(-94.0°) \end{bmatrix}.$$

It can be observed from the identified mode shape matrix that the structural system is close to a proportionally damped system though some phase angles seem not to agree well due to errors of modal parameter estimation.

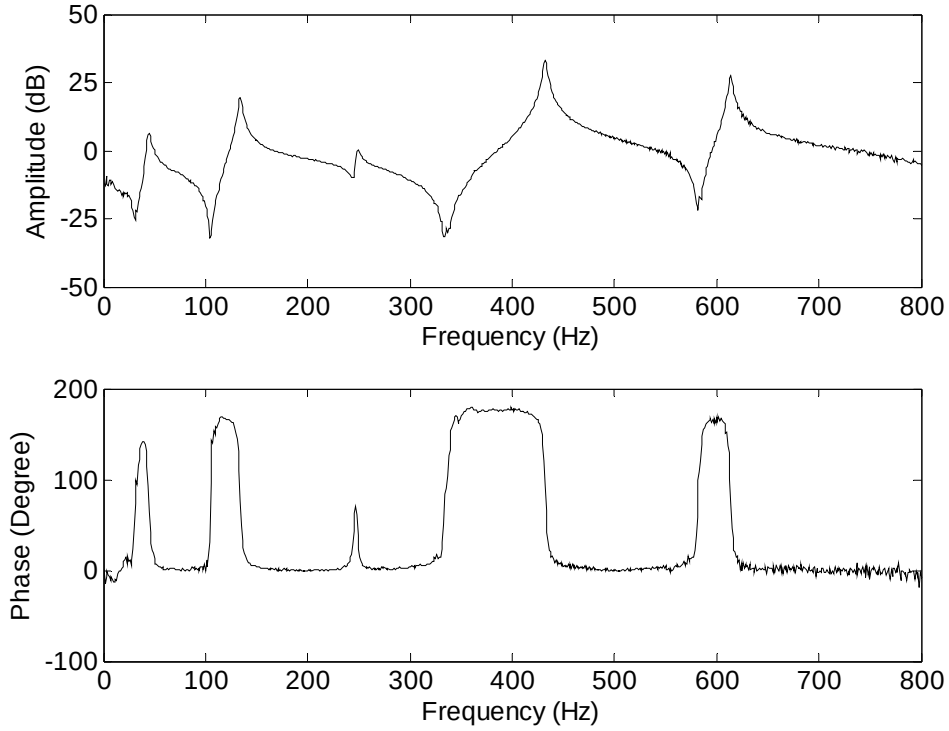

Fig. 3.3 The typical FRF measured at the 4th measurement point

In this case, the modal parameters were estimated based on the response function model, in which structural damping is assumed. In fact, structural damping model can be assumed confidently for this beam since the beam is uniformly made of aluminum and only hysteresis properties of material in the structure needs to be considered for the damping model. Based on the identified modal data in Table 3.2 and the above mode shape matrix, the complex stiffness matrix of the structural system can be calculated using equation (3.26). Hence, by taking the imaginary part of the complex matrix, the structural damping matrix of the beam structure is established as:

$$[D] = \begin{bmatrix} 1.924e5 & 5.069e6 & -2.177e7 & -1.565e7 & -1.270e7 \\ -4.400e6 & 6.348e5 & -4.564e7 & -3.247e7 & -2.476e7 \\ 2.218e7 & 4.628e7 & 5.175e5 & 4.305e6 & -2.651e6 \\ 1.584e7 & 3.281e7 & -3.548e6 & 4.186e5 & -2.823e6 \\ 1.277e7 & 2.487e7 & 3.152e6 & 3.348e6 & 1.881e5 \end{bmatrix}.$$

Here, it should be noted that the damping model is a 5×5 matrix since the identified modes are incomplete compared with measured locations (or coordinates) in this experiment.

Table 3.2 The identified natural frequencies and damping loss factors of the beam (structural damping)

Mode No. (r)	1	2	3	4	5
Natural frequency f_r (Hz)	44.5	134.0	247.4	432.8	612.7
Natural frequency ω_r (rad/sec)	279.6	842.0	1554.5	2719.4	3849.7
Damping loss factor (η_r)	0.0967	0.0287	0.0171	0.0092	0.0070
Damping ratio (ξ_r) (viscous damping)	0.0484	0.0143	0.0086	0.0046	0.0035

Provided that viscous damping model is adopted for the structural system, a little different modal data may be identified according to the modal analysis procedure from structural

damping model to viscous damping model as discussed in section 3.3. The identified undamped natural frequencies in this case are the same as those in the case of structural damping. Moreover, the damping ratios for viscous damping shown in Table 3.2 have the values as $\xi_r = \eta_r / 2, (r = 1, 2, \cdots, 5)$. The calculated equivalent mode shape matrix in the case of viscous damping is as follows:

$$[\Psi] = \begin{bmatrix} 0.047(-139°) & 0.019(-31.3°) & 0.015(56.9°) & 0.012(133°) & 0.007(45.7°) \\ 0.016(-132°) & 0.001(144°) & 0.004(-72.9°) & 0.007(-51.4°) & 0.007(-142°) \\ 0.004(44.7°) & 0.015(142°) & 0.011(-129°) & 0.002(-38.6°) & 0.003(23.3°) \\ 0.024(51.5°) & 0.013(130°) & 0.002(54.0°) & 0.008(136°) & 0.005(27.4°) \\ 0.034(57.6°) & 0.000(124°) & 0.007(101°) & 0.000(-41.1°) & 0.008(-128°) \\ 0.017(46.2°) & 0.012(-46.3°) & 0.002(43.8°) & 0.009(-41.1°) & 0.005(52.5°) \\ 0.006(44.5°) & 0.015(-40.5°) & 0.009(-123°) & 0.002(145°) & 0.004(48.8°) \\ 0.016(-133°) & 0.001(-43.5°) & 0.004(-143°) & 0.007(131°) & 0.007(-149°) \\ 0.042(-143°) & 0.020(132°) & 0.011(44.6°) & 0.009(-14.7°) & 0.007(41.0°) \end{bmatrix}.$$

It can be found that these eigenvectors are effectively the same as those identified in the case of structural damping except differing by a complex scaling factor, the matrix of which can be written after calculation as,

$$[N] = \begin{bmatrix} 0.046(133°) & 0 & 0 & 0 & 0 \\ 0 & 0.024(-46°) & 0 & 0 & 0 \\ 0 & 0 & 0.017(-43°) & 0 & 0 \\ 0 & 0 & 0 & 0.013(138°) & 0 \\ 0 & 0 & 0 & 0 & 0.012(132°) \end{bmatrix}.$$

From the complex matrix [*N*], it is observed that the modulus of the diagonal element for the r^{th} (r =1,2,…,5) mode shape is equal to $1/\sqrt{2\omega_r}$, (r =1,2,…,5). In addition, the r^{th} mode shape for viscous damping case is that for structural damping case rotated by a constant phase angle which is close to -45° or 135°. Based on the identified modal data for viscous damping case, the viscous damping matrices is produced as,

$$[C]=\begin{bmatrix} 9.828e5 & 2.285e6 & 7.152e5 & 7.406e5 & -0.524e5 \\ 2.285e6 & 5.315e6 & 1.664e6 & 1.725e6 & -1.209e5 \\ 7.152e5 & 1.664e6 & 5.185e5 & 5.384e5 & -0.3938e5 \\ 7.406e5 & 1.727e6 & 5.384e5 & 5.618e5 & -0.389e5 \\ -0.524e5 & -1.209e5 & -0.393e5 & -0.389e5 & 0.024e5 \end{bmatrix}.$$

In addition, the calculated damping matrix for viscous case has no physical meanings. As can be seen, these results from the experimental test have sufficiently demonstrated the relationship between viscous damping and structural damping models in non-proportional case, which has been derived previously.

3.7 Concluding Remarks

In this chapter, to address the effect of a reasonable damping model on estimated modal parameters, the relation of the modal models for viscous and structural damping cases has been investigated in detail. The relationship between the two damping models has been presented based on the normalization procedures and the corresponding modal analysis procedures. In the case of a proportionally damped system, there exists an exact relationship between structural and viscous damping models as $\eta_r = 2\xi_r$. The derived mass and stiffness matrices are the same as those of the original system. The identified damping matrix makes the system eigenvectors real though the damping itself is not proportional. As for a non-proportionally damped system, the equivalent mode shapes and their counterparts of the original system are almost the same except differing by a complex scaling factor, and the errors between the original mass, stiffness matrices and the calculated ones are quit small. Numerical cases have shown sufficiently that the error in the estimation of modal parameters caused by the wrong interpretation of damping model is

really quite small since the original and the calculated systems with different damping models share the same response model. Moreover, the equivalent damping matrix is physically meaningful in the case of the system with distributed damping. Whereas, if the damping is localized, the correct interpretation becomes very important since no physically meaningful equivalent damping matrix exists in this case. The experimental example based on a simple vibration test has further demonstrated the validity of the investigation on the relationship between the two damping models.

Chapter 4

Model Updating of Damped Structures Using FRF Data

This chapter further develops the FRF method to identify damped structural systems. In order to overcome the problem of complexity of measured FRF and modal data, complex updating formulations using FRF data to identify damping coefficients as well as mass and stiffness modeling errors have been established.

4.1 Introduction

To date, most model updating methods are able to obtain sufficiently accurate models using various updating algorithms (Friswell and Mottershead, 1995). However, few of these are found to be quite effective in updating the mass and stiffness matrices of damped structures since majority of these methods are developed without considering structural damping. Therefore, model updating of damped structures remains an issue in most developed model updating methods. In fact, damping property, which has significant contribution to vibration of structures, cannot be ignored in practical modeling. Identification of damped structures is usually hard to be achieved because the modeling of damping is very complex and its mechanism is still somewhat unknown (Zbigniew, 1998). Meanwhile, damping forces are small as compared with other interactions present in a mechanical system. Hence, damping is generally ignored in most finite element analysis, or an assumption of proportional damping is usually made. This assumption and the initial estimation of damping in FEA are usually doubtable. In fact, damping characteristics of mechanical

systems should only be properly determined or updated through experimental vibration testing. Therefore, in model updating of a damped structure the main difficulty is how to identify the damping matrix of the system and simultaneously update the erroneous mass and stiffness matrices.

Currently existing direct or iterative identification methods for the determination of system damping matrix have been reviewed in (Pilkey, 1998). However, all these methods are usually based on the assumption that accurate estimation of mass and stiffness matrices and modal parameters are available. In fact, these requirements are hard to achieve in practice. Hence, the identified damping matrices based on these methods are usually unreliable. As a result, these identified damping models need to be further validated or updated.

Some other model updating methods have been proposed for damping matrix identification in recent years. Based on Lagrange multiplier method, Friswell *et al*. (1998) presented a direct updating method for damping matrix using measured modal data. The method requires the correct mass matrix and then the damping and the stiffness matrices are updated simultaneously. Reix *et al.* (1996) considered updating the damping matrix using FRF sensitivity. However, the updating procedure consists of two stages, which requires that the mass and stiffness matrices should be updated first. Rad (1997) presented an FRF based updating method to update structural damping matrix using experimental FRF data directly. This method demands the availability of initial damping ratios, which are obviously difficult to be properly estimated in an FE modeling. Lu and Tu (2004) presented

a two-level neural network scheme for updating damping matrix using FRF data, in which the mass and stiffness parameters need to be updated first and the damping ratios are updated subsequently in the second-level. This scheme is effective in the case that the structural system to be updated is lightly damped. As can be seen, all these updating methods have serious limitations when applied to the identification of damping matrix since some prior requirements should be satisfied before updating process can take place.

To demonstrate the difficulties of some of the major updating methods when applied to measured modal and FRF data of damped structures, numerical case studies have been designed and carried out. First, eigensensitivity based methods are examined.

Eigensensitivity based updating formulations have become popular nowadays. However, these methods will encounter difficulties when they are employed to update damped structures. Because in most cases, the damping a structure possesses is non-proportional, and hence the measured modal data are in theory complex. During the process of modal analysis to identify complex modal data, large analysis errors may have been introduced. Generally, accurate updated results cannot be obtained in the case of non-proportionally damped structures if Eigensensitivity based method employs only real modal data when formulating the eigensensitivity matrix. To demonstrate this point, the inverse eigensensitivity method (IEM) was chosen as a representative to update the analytical model of a generally damped structure. Here in this numerical simulation, a GARTEUR structure (Lin and Ewins, 1994) with general structural damping shown in Fig. 4.1 is

considered. The FE model of the structure consists of 78 2-D beam elements. Each beam segment is a superposition of an axial bar element and a bending beam element. Each node of the beam element has three DOFs (two translations and one rotation). Following material properties are used during FE modeling: Young's modulus is assumed to be $E=0.75\times10^{11}N/m^2$ and density to be $\rho=2800kg/m^3$. For the bar element, the cross-sectional areas are $S_h=0.004m^2$ (horizontal), $S_v=0.006m^2$ (vertical), and $S_d=0.003m^2$ (diagonal). For the bending beam elements, the second moment of area is assumed to be $I=0.0756m^4$ for all the elements. To generate the 'experimental' data, stiffness modeling errors are introduced in the elements of the analytical model of the structure as shown in Table 4.1. Suppose that element structural damping matrix in the 'experimental' model is proportional to element stiffness matrix with a damping coefficient. And the values of element damping coefficients γ_i are all assumed to be 0.006 except those at the joint positions, which are shown in Table 4.1.

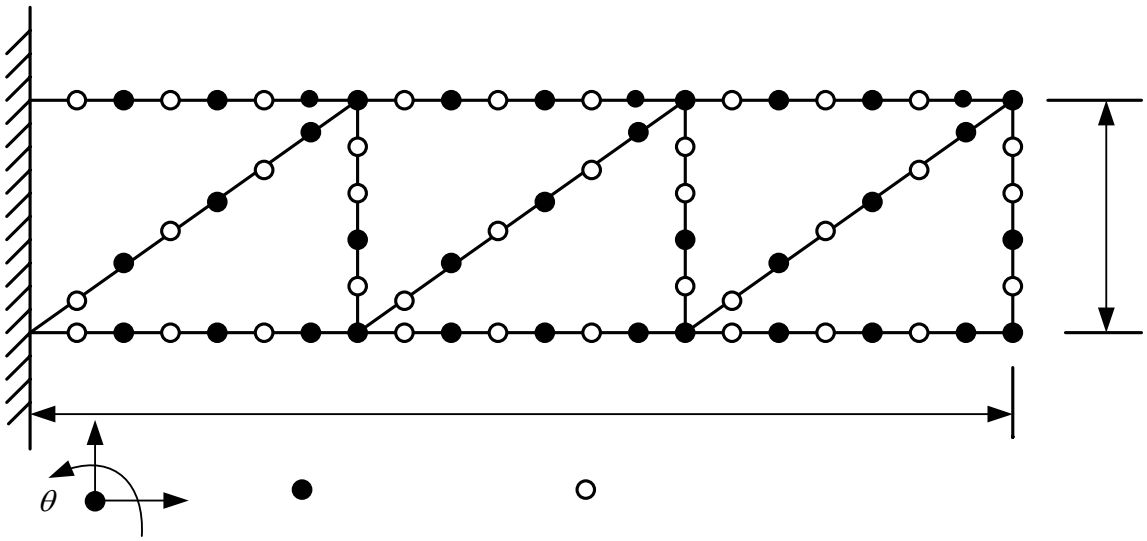

Fig. 4.1 The **GARTEUR** structure

Table 4.1 Location of stiffness modeling errors and damping coefficients (Case 1)

Element No.	1	2	28	29	43	44	45	46	47	48	49	50
Stiffness Error (%)	-90	-90	100	100	100	100	10	-90	-90	-90	-90	-90
Element No.	1	2	7	14	21	26	33	40	45	46	47	
Damping Coefficients	0.05	0.04	0.05	0.05	0.05	0.04	0.05	0.05	0.04	0.05	0.05	

Due to the non-proportional structural damping, the measured FRF data are complex and so are the identified natural frequencies and mode shapes. Here, in order to simulate the real modal data required by the method, the 'identified' complex modes from modal analysis need to be converted to their real counterparts. There are two ways to convert complex modes to real modes. One is to take the real parts of the complex modes as the corresponding real modes. The other is to take the modulus of the complex modes as the modulus of the real modes, while the signs of the elements of the converted real modes are the signs of the cosines of the phase angles associated with the complex values of these elements. After the conversion, the real modal data can then be readily employed to calculate eigensensitivities and the updating procedure of IEM (Lin *et al*., 1995) can be performed. During the updating procedure, the first 5 simulated 'experimental' modes including natural frequencies and mode shapes were used for calculating eignsensitivities and iterations were performed. And the assumed incomplete 'measurement' points of the GARTEUR structure are shown in Fig. 4.1. The iteration results of element modeling errors are shown in Fig. 4.2. As can be seen, stiffness modeling errors are not identified correctly even after 15 iterations. The failure to identify modeling errors correctly is due to the fact

that the IEM does not consider damping in the formulation of its updating procedure and this has affected significantly the updated results. In addition, the errors which are introduced in the conversion process from complex modes to real modes, have added to the deterioration of the accuracy of the identified results.

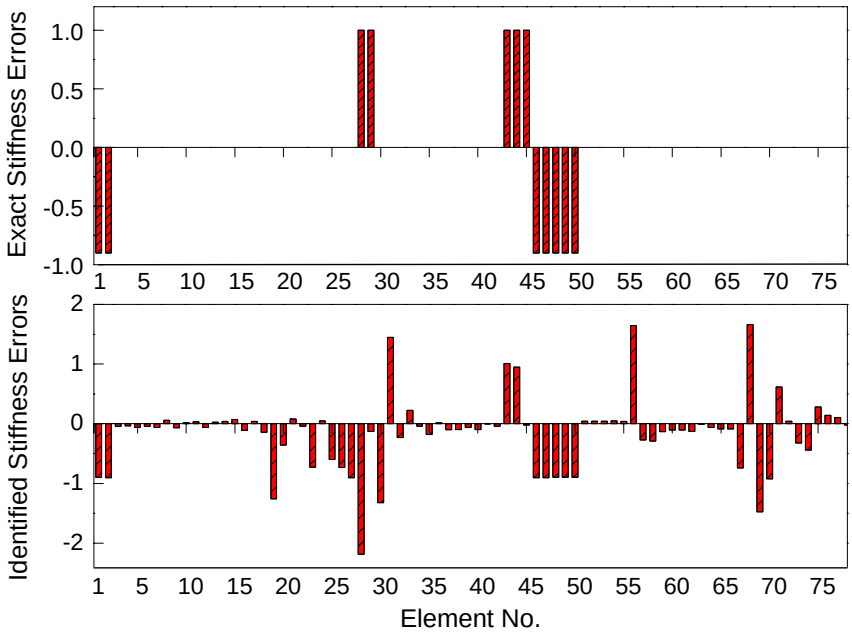

Fig. 4.2 Comparison of the exact and identified stiffness modeling errors (IEM)

The FRF sensitivity based updating formulations are the most promising model updating methods. When applied to the identification of damping matrix, these methods have the advantage that the measured FRFs always contain the information of damping as well as mass and stiffness of a system. Some published work used numerically generated real FRFs without damping as the actual measured FRFs for model updating. However, such procedure may not be rigorous in model updating of damped structures and it always introduces additional numerical errors. In engineering practice, analytical models without damping should be updated using experimentally derived FRFs, which are always complex in nature.

The FRF updating formulation (Lin and Ewins, 1994) was first established in real domain, which did not consider damping in the experimental model. If such real FRF based method employs practically measured complex FRF data from a damped structure to update its model, it can be expected that the updated results may become erroneous. To demonstrate this shortfall of the real FRF based method, the same GARTEUR structure with structural damping and stiffness modeling errors, is considered again for model updating using FRF data. The stiffness modeling errors and the damping coefficients are the same as those listed in Table 4.1. The 'measured' FRF data from the damped 'experimental' structure are always complex while the method requires real FRF data. The real parts of the complex FRF data may be chosen as the 'experimental' FRF data and are used for updating for frequency points off resonances. The alternative is to take the modulus of the complex FRFs as the modulus of the real ones. The signs of the converted real FRFs are the signs of cosines of the phase angles associated with these FRF data. FRF data from 20 different frequency points of the 'experimental' model with excitation being applied in the *v* direction at node 27 are chosen to construct the FRF sensitivity matrix. The updating procedure is the same as that discussed in (Lin and Ewins, 1994). Fig. 4.3 shows the updated results of stiffness modeling errors after 15 iterations, from which it can be seen that the stiffness modeling errors are not correctly identified. Since damping has not been considered in the real FRF based updating method, such loss of actual damping information has led to the failure of such model updating procedure.

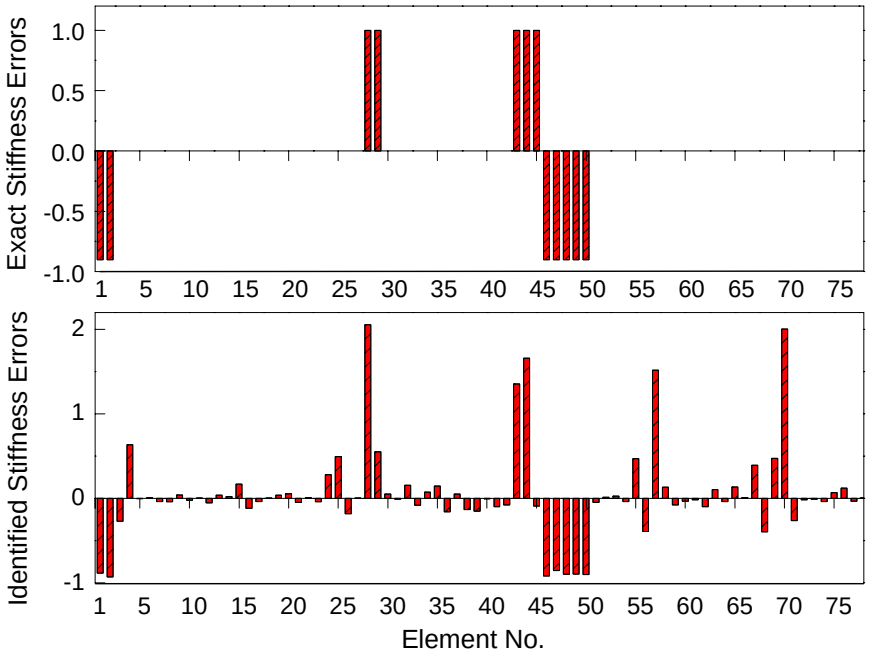

Fig. 4.3 Comparison of the exact and identified stiffness modeling errors (FRF)

From above two case studies, it can perhaps be concluded that the conventional methods developed without consideration of damping are not likely to be effective in the model updating of damped structures. Because damping is not included in those updating formulations and as a result, damping information present in the measured data is eliminated. Subsequently, such loss of damping information significantly affects the updated results and may even lead to a total invalidation of model updating methods when they are used to update damped structures. Therefore, to properly update damped structures, damping information has to be taken into account in updating formulations and new methods which can simultaneously update mass and stiffness modeling errors and identify damping coefficients need to be developed.

4.2 Model Updating of Damped Structures Using FRF Data

The FRF method developed by Lin and Ewins (1990, 1994) is one of the most frequently-used FRF based updating techniques. This method employs both analytical and experimental FRFs to calculate FRF sensitivity and therefore accurate updated results can be obtained more efficiently through iteration. However, Lin and Ewins have not extended the method to the model updating of damped structures, in which identification of damping matrix should be involved. Since the FRF method has been successfully used in model updating of undamped structures, it is feasible and necessary to further develop this method so that it can be applied to update damped structures. In the following section, this method will be further extended to identify or update damping matrix as well as mass and stiffness matrices using measured complex FRF data.

4.2.1 Identification of Proportional Damping

In model updating of damped structures, one important task is to identify structural damping matrix when the analytical model also contains modeling errors. Frequently, damping is conveniently ignored as it places extra constraints on model updating techniques and often leads to numerical instabilities. Since the actual damping mechanisms of practical structures are more complicated, some simple damping types are first chosen to be investigated in the identification of damping through model updating. Generally, linear damping can be divided into proportional damping and non-proportional damping. The eigensolution techniques adopted to analyze these two types of damping are different. In the case of proportional damping, structural dynamics equilibrium equations can be decoupled, resulting in mode shapes which are the same as those of the corresponding

undamped structure. Such proportional damping model is easier to analyze in many aspects. On the other hand, for a system with non-proportional damping, its equations cannot be decoupled and the mode shapes become generally complex. In this section, identification method for the case of proportional damping is first presented, while a more general case of non-proportional damping will be discussed subsequently.

Proportional Viscous Damping

The system equation of a multiple DOF structure with both viscous damping and structural damping can be expressed in time domain as,

$$[M]\{\ddot{x}(t)\}+[C]\{\dot{x}(t)\}+i[D]\{x(t)\}+[K]\{x(t)\}=\{F\}e^{i\omega t}, \tag{4.1}$$

where $[C]$ and $[D]$ are the viscous and structural damping matrices, respectively. For a proportional viscous damping model of a structure, which is normally referred as Rayleigh's damping model, its damping matrix $[C]$ can be expressed as a linear combination of the system stiffness matrix and mass matrix, as shown in the following equation,

$$[C]=\beta_c[K]+\gamma_c[M], \tag{4.2}$$

where β_c and γ_c are proportionality coefficients. Substituting damping matrix into equation (4.1), the general equation of motion has the form (only considering viscous damping),

$$[M]\{\ddot{x}\}+\left[\gamma_c[M]+\beta_c[K]\right]\{\dot{x}\}+[K]\{x\}=\{f\}. \tag{4.3}$$

In this case the system equations of motion can be decoupled by a transformation matrix that is just the eigenvector matrix of the corresponding undamped system. After the

transformation (Ewins, 2000b), the r^{th} individual uncoupled equation becomes in the case of free vibration,

$$\ddot{q}_r + 2\zeta_r \omega_r \dot{q}_r + \omega_r^2 q_r = 0\,, \tag{4.4}$$

where $\omega_r^2 = \frac{k_r}{m_r}$, and $\zeta_r = \frac{1}{2}(\frac{\gamma_c}{\omega_r} + \beta_c \omega_r)$, $(r = 1, 2, ..., N)$.

To implement FRF updating formulations with damping, FRF sensitivity with respect to those proportional damping constants γ_c and β_c should first be derived. The expression for individual receptance element obtained using mass-normalized mode shapes [Φ] becomes,

$$\alpha_{jk}(\omega) = \sum_{r=1}^{N} \frac{(\phi_j)_r (\phi_k)_r}{\omega_r^2 - \omega^2 + 2i\omega\omega_r\zeta_r}\,. \tag{4.5}$$

Since in theory the natural frequencies ω_r and the undamped mass-normalised mode shapes $\{\phi\}_r$ are not functions of γ_c and β_c, we can derive following receptance sensitivity by differentiating equation (4.5) with respect to γ_c,

$$\frac{\partial \alpha_{jk}(\omega)}{\partial \gamma_c} = \sum_{r=1}^{N} \frac{\partial \alpha_{jk}(\omega)}{\partial \zeta_r} \frac{\partial \zeta_r}{\partial \gamma_c} = \sum_{r=1}^{N} \left(\frac{\omega((\phi_j)_r (\phi_k)_r)}{i\left(\omega_r^2 - \omega^2 + 2i\omega\omega_r\zeta_r\right)^2} \right). \tag{4.6}$$

Similarly, we can have,

$$\frac{\partial \alpha_{jk}(\omega)}{\partial \beta_c} = \sum_{r=1}^{N} \frac{\partial \alpha_{jk}(\omega)}{\partial \zeta_r} \frac{\partial \zeta_r}{\partial \beta_c} = \sum_{r=1}^{N} \left(\frac{(\omega\omega_r^2)((\phi_j)_r (\phi_k)_r)}{i\left(\omega_r^2 - \omega^2 + 2i\omega\omega_r\zeta_r\right)^2} \right). \tag{4.7}$$

From equations (4.6) and (4.7), FRF sensitivities with respect to the damping constants γ_c and β_c are obtained. Suppose that the difference between the experimental and analytical receptance can be written to a first order, as,

$$\Delta(\alpha)_{jk} = (\alpha_X)_{jk} - (\alpha_A)_{jk} = \frac{\partial(\alpha_A)_{jk}(\omega)}{\partial \gamma_c} \Delta\gamma_c + \frac{\partial(\alpha_A)_{jk}(\omega)}{\partial \beta_c} \Delta\beta_c\,. \tag{4.8}$$

Usually FRF data available from measurement are abundant, so accurate estimations of γ_c and β_c can be obtained based on above formulation by considering various receptances measured at different frequencies. Also iterations are needed in the updating process since an approximation is made during derivation of equation (4.8) which is just a first order approximation. After the damping coefficients γ_c and β_c are obtained, the viscous damping matrix of the system can be determined. If the analytical FE model to be updated contains both mass and stiffness modeling errors, these erroneous mass and stiffness matrices should be corrected first before the viscous damping matrix can be identified. It should be noted that the above formulation for the identification of damping is based on the assumption that the difference of FRF data between analytical and experimental models is of second order as compared with the FRFs themselves. Therefore, the availability of some initial estimates of the damping coefficients to be identified is preferred.

Proportional Structural Damping

In a proportional structural damping model, the damping matrix $[D]$ can in general be expressed by following equation,

$$[D] = \gamma_d [M] + \beta_d [K]. \tag{4.9}$$

Based on the assumption of such damping model, individual receptance element of the structure can be described as,

$$\alpha_{jk}(\omega) = \sum_{r=1}^{N} \frac{(\phi_j)_r (\phi_k)_r}{\omega_r^2 - \omega^2 + i\omega_r^2 \eta_r}, \quad \eta_r = (\beta_d + \frac{\gamma_d}{\omega_r^2}), \quad (r = 1, 2, ..., N), \tag{4.10}$$

where η_r is defined as the damping loss factor of the r^{th} mode. Using the relationship in (4.10), we obtain the derivatives,

$$\frac{\partial \alpha_{jk}(\omega)}{\partial \gamma_d} = \sum_{r=1}^{N} \frac{\partial \alpha_{jk}(\omega)}{\partial \eta_r} \frac{\partial \eta_r}{\partial \gamma_d} = \sum_{r=1}^{N} \left(\frac{((\phi_j)_r (\phi_k)_r)}{i\left(\omega_r^2 - \omega^2 + i\omega_r^2 \eta_r\right)^2} \right), \tag{4.11}$$

$$\frac{\partial \alpha_{jk}(\omega)}{\partial \beta_d} = \sum_{r=1}^{N} \frac{\partial \alpha_{jk}(\omega)}{\partial \eta_r} \frac{\partial \eta_r}{\partial \beta_d} = \sum_{r=1}^{N} \left(\frac{(\omega_r^2)((\phi_j)_r (\phi_k)_r)}{i\left(\omega_r^2 - \omega^2 + i\omega_r^2 \eta_r\right)^2} \right). \tag{4.12}$$

Based on above equations, γ_d and β_d can be identified using experimental and analytical values of FRF data using least squares procedure. Subsequently, a proportional structural damping matrix of the system is established.

General proportional damping

Now a dynamic system with only general proportional viscous damping (for convenience of analysis) is considered. The equation of motion of this system is the same as equation (4.3) only with the damping matrix $[C]$ having a more general form. In this case, the proportionally damped system still possesses real modes which are the same as the real modes of the corresponding undamped system. And the real modes can be used to decouple the equations of motion of the proportionally damped system. However, certain conditions on the form of proportional damping matrix are required and have been discussed in detail by Caughey (1960). The sufficient damping condition for the existence of real modes in a damped system is that the damping matrix of the system can be expressed as,

$$[C] = \sum_{s=1}^{N} \beta_s [M]([M]^{-1}[K])^{s-1}, \tag{4.13}$$

where N is the dimension of the system and $\beta_s (s = 1, \cdots N)$ are real constants. In the case when $\beta_s = 0\ (s = 3, \cdots, N)$, equation (4.13) becomes the familiar Rayleigh damping as equation (4.2). The sufficiency of equation (4.13) can be shown, by pre-multiplying both sides of the equation by $[\Phi]^T$ and post-multiplying by $[\Phi]$,

$$[\Phi]^T[C][\Phi] = \sum_{s=1}^{N} \beta_s [\omega_r^2]^{s-1} = [c_r], \tag{4.14}$$

where $[\omega_r^2]$ and $[c_r]$ are diagonal matrices. From equation (4.14), since the damping matrix is diagonalised by the real modes of the corresponding conservative system, these real modes are also the real modes of the damped system.

Since the damping matrix $[C]$ of a proportionally damped structure satisfy the condition of equation (4.13)**,** the system equations of motion can naturally be decoupled by pre-multiplying both sides of equation by $[\Phi]^T$ and post-multiplying by $[\Phi]$. And then the r^{th} individual uncoupled equation is derived as (free vibration),

$$\ddot{q}_r + c_r \dot{q}_r + \omega_r^2 q_r = 0, \tag{4.15}$$

where $\omega_r^2 = \dfrac{k_r}{m_r}$ and $c_r = \sum_{s=1}^{N} \beta_s (\omega_r^2)^{s-1} \quad (r = 1, 2, ..., N)$.

Then these characteristics carry over the forced response analysis and lead to the expression for individual receptance FRF as,

$$\alpha_{jk}(\omega) = \sum_{r=1}^{N} \frac{(\phi_j)_r (\phi_k)_r}{\omega_r^2 - \omega^2 + i\omega c_r}. \tag{4.16}$$

As the cases of proportional viscous damping and structural damping given above, FRF sensitivity with respect to the coefficients $\beta_s (s = 1, \cdots N)$ needs to be derived subsequently. Since the undamped natural frequencies and mass-normalised mode shapes are theoretically not functions of $\beta_s (s = 1, \cdots N)$, the receptance sensitivity can be derived by differentiating equation (4.16) with respect to coefficients $\beta_s (s = 1, \cdots N)$,

$$\frac{\partial \alpha_{jk}(\omega)}{\partial \beta_s} = \sum_{r=1}^{N} \frac{\partial \alpha_{jk}(\omega)}{\partial c_r} \frac{\partial c_r}{\partial \beta_s} = \sum_{r=1}^{N} \left(\frac{\omega((\phi_j)_r (\phi_k)_r)}{i\left(\omega_r^2 - \omega^2 + i\omega c_r\right)^2} \right) (\omega_r^2)^{s-1}, (s = 1, \cdots, N). \tag{4.17}$$

Following the updating procedure given in the case of proportional viscous damping model, accurate estimations of $\beta_s (s = 1, \cdots N)$ can be obtained by considering various receptances measured at different frequencies. Due to the approximations made during the derivation of the equation, iterations are also required in the updating process. After the coefficients $\beta_s (s = 1, \cdots N)$ are obtained, the proportional damping matrix of the system can be identified. Since the updating process of proportional damping is quite straightforward and easy to conduct, no case study is warranted. In the following section, a more general case of non-proportionally damped structures will be studied in more detail, instead.

4.2.2 Model Updating of Generally Damped Structures

For most engineering structures, damping is non-proportional. Unlike undamped structures and structures with proportional damping, both eigenvalues and eigenvectors of non-proportionally damped structures are complex. To identify damping models of non-proportionally damped structures, it is more appropriate to adopt measured FRF data to update the analytical model as well as damping matrix of the structure directly.

FRF Sensitivity with respect to Elements of Damping Matrix

In the development of FRF updating method (Lin and Ewins, 1994), the formula governing the FRF difference between the analytical and experimental models is given as follows,

$$\{\Delta\alpha\}_j = -[\alpha_A][\Delta Z]\{\alpha_X\}_j . \tag{4.18}$$

The impedance error matrix $[\Delta Z]$ can be expressed as, after being expanded in Taylor Series and neglecting the second and high order terms,

$$[\Delta Z] = \sum_{k=1}^{N_p} \frac{\partial [Z_A]}{\partial p_k} \Delta p_k \,, \tag{4.19}$$

where p_k denotes the k^{th} design parameter to be updated and N_p is the total number of design parameters. Upon substitution of (4.19) into (4.18), we have,

$$\sum_{k=1}^{N_p} \left\{ [\alpha_A] \left[\frac{\partial [Z_A]}{\partial p_k} \right] \{\alpha_X\}_j \right\} \Delta p_k = -\{\Delta\alpha\}_j \,. \tag{4.20}$$

Generally, equation (4.20) is formulated based on FRF data at one measurement frequency. When FRF data for a sufficient number of frequency points are used, it can be turned into a set of over-determined algebraic equations. And the set of equations can be simplified as,

$$[S]\{\Delta p\} = \{\Delta\alpha\}, \tag{4.21}$$

where, $$\{\Delta\alpha\} = \begin{Bmatrix} \{\alpha_X(\omega_1)\}_j - \{\alpha_A(\omega_1)\}_j \\ \vdots \\ \{\alpha_X(\omega_n)\}_j - \{\alpha_A(\omega_n)\}_j \end{Bmatrix}, \text{ and}$$

$$[S] = \begin{bmatrix} -[\alpha_A(\omega_1)] \left[\frac{\partial [Z_A(\omega_1)]}{\partial p_1} \right] \{\alpha_X(\omega_1)\}_j, \cdots, -[\alpha_A(\omega_1)] \left[\frac{\partial [Z_A(\omega_1)]}{\partial p_{N_p}} \right] \{\alpha_X(\omega_1)\}_j \\ \vdots \\ -[\alpha_A(\omega_n)] \left[\frac{\partial [Z_A(\omega_n)]}{\partial p_1} \right] \{\alpha_X(\omega_n)\}_j, \cdots, -[\alpha_A(\omega_n)] \left[\frac{\partial [Z_A(\omega_n)]}{\partial p_{N_p}} \right] \{\alpha_X(\omega_n)\}_j \end{bmatrix}. \tag{4.22}$$

Here $[S]$ is the FRF sensitivity matrix. In order to identify the damping matrix it is necessary to deduce sensitivity of the dynamic stiffness matrix with respect to the design parameters of the damping matrix. If an assumed damping model is established, then the deduction of the FRF sensitivity with respect to the design parameters of the damping matrix can be made respectively for the cases of viscous damping and structural damping.

In the case of structural damping, the dynamic stiffness matrix of the structure can be expressed in frequency domain as,

$$[Z(\omega)] = [K] + i[D] - \omega^2[M]. \tag{4.23}$$

Here an assumption is also made that the damping matrix $[D]$ is a combination of the element damping matrices. Then a p-value formulation of the damping matrix to be identified can be established as the following since an original analytical FE model usually contains no damping,

$$[D_X] = [\Delta D] = \sum_{k=1}^{N_d} \Delta p_d^k [D_k^e], \tag{4.24}$$

where Δp_d^k is the design parameter change with respect to the k^{th} element damping matrix and $[D_k^e]$ is the element damping matrix. Since the mass and stiffness matrices are not functions of the design parameter p_d^k, the partial derivative of the dynamic stiffness matrix with respect to p_d^k becomes,

$$\frac{\partial [Z]}{\partial p_d^k} = i\frac{\partial [D]}{\partial p_d^k} = i\frac{[\Delta D]}{\Delta p_d^k} = i[D_k^e]. \tag{4.25}$$

Substituting (4.25) into the elements of the sensitivity matrix (4.22), we can obtain complex FRF sensitivity with respect to p_d^k,

$$\frac{\partial \{\alpha(\omega)\}_j}{\partial p_d^k} = -i[\alpha_A(\omega)][D_k^e]\{\alpha_X(\omega)\}_j. \tag{4.26}$$

Thus we have so far established the foundation of FRF updating formulation of damping coefficients at p-value level. For viscous damping, similar expression of FRF sensitivity with respect to damping coefficients can be obtained. The sensitivities derived in this way have the advantage that these sensitivities are formulated using the results of both analytical and experimental observations and can be used to improve the performance of the updating process, as discussed in (Lin, 1995). What is different from the conventional model updating formulation using FRF data is that the problem is now formulated in a complex

domain once damping is assumed and the identification of damping is involved. And usually in this case, the updated parameters will appear in complex form in the first place.

However, unlike the overall stiffness and mass matrices, the damping matrix [*C*] cannot be constructed from the element damping matrix since understanding of damping mechanisms is still quite primitive. In the present work, it is not intended to perform an in-depth study on the most appropriate damping model for a given system; but rather, the focus is placed on the identification of the damping values under a pre-selected damping model.

4.3 Numerical Case Studies

In order to verify the validity and the feasibility of proposed complex FRF based model updating method, numerical case studies for the case of structural damping have been conducted on the GARTEUR structure shown in Fig. 4.1. In order to generate the 'measured' FRF data with structural damping, it is assumed for simplicity that the individual element damping matrix of the 'experimental' model has the same form as that of the element stiffness matrix in the FE model,

$$[D_j^e] = \gamma_j [K_j^e], \tag{4.27}$$

where $[K_j^e]$ is the j^{th} element stiffness matrix and γ_j is the damping proportionality coefficient associated with the j^{th} element. In fact, the proposed method can work for general cases where element structural damping matrices have been given. The new complex stiffness matrix will then have the form with the damping matrix included,

$$[KD_X] = [K_X] + i[D_X] = \sum_{j=1}^{N} (1 + i\gamma_j)[K_j^e]. \tag{4.28}$$

Since there is no damping assumed in the original FE model, the initial values of γ_j are 0 for all the elements. Then, the new complex stiffness error matrix of the system becomes,

$$[\Delta K] = \sum_{j=1}^{N} (\beta_j + i\gamma_j)[K_j^e], \tag{4.29}$$

where β_j is the design parameter change associated with the j^{th} element. Based on (4.29), we can obtain the derivatives of the new complex stiffness matrix with respect to the design parameters. Upon substituting the derivatives into (4.22), we can then derive the FRF sensitivity matrix for the case of damped structures. And the derived sensitivity matrix in this case becomes complex. Then based upon the equation sets (4.21), we can solve the algebraic equations and obtain the vector complex p-value change. Thus the complex p-value vector identified has the form as,

$$\{p_X\} = \{p_A\} + \{\Delta p\} = \text{Re}(\{p_X\}) + \text{Im}(\{p_X\})i. \tag{4.30}$$

After separating the real and imaginary parts of the complex p-value vector, we can obtain the updated stiffness parameters and the identified damping coefficients, respectively. Finally, an updated model of the structure can be set up using the identified parameters.

In case measured coordinates are incomplete, the linear algebraic equations (4.21) constitute a first order approximation. And the p-value change vector $\{\Delta p\}$, which can be solved using linear least squares methods, is only a first-order approximation. Hence, in order to obtain the accurate solution, an iteration scheme is needed in the updating process. During the iteration process, the Euclidean norm of p-value change, $\|\{\Delta p\}\|$ is chosen as a

criterion in order to determine whether the convergent p-values are achieved. Usually, convergence of the p-value change for damping is believed to be reached when the value of $\|\{\Delta p\}\|$ is less than 10^{-6}.

Case 1 (Stiffness Errors and Damping Coefficients)

Following above updating process of damped structures, the GARTEUR structure with structural damping has been investigated. There is no damping assumed for the analytical FE model of the structure. To generate the 'experimental' FRF data, stiffness modeling errors were introduced as shown in Table 4.1. And the values of element damping coefficients γ_i in the 'experimental' model are all assumed to be 0.006 except those at the joint positions, which are much higher as shown in Table 4.1. The 'measured' FRF data are incomplete in coordinates to simulate the practical inaccessibility of internal and rotational DOFs. One incomplete receptance vector of the 'experimental' model is supposed to have been measured at 250 measurement frequency points in a frequency range of 0-500Hz, with excitation being applied in the *v* direction at node 27. Since incomplete 'experimental' FRF data are used for updating, iteration process is required to achieve accurate identified results and in each iteration, FRF data from 20 different frequency points are chosen to construct the FRF sensitivity matrix and the difference vector of analytical and 'experimental' FRFs. The iteration results are shown in Fig. 4.4 and Fig. 4.5, from which it can be seen that both the stiffness modeling errors and the damping coefficients are identified accurately after 30 iterations. However, the proposed complex FRF updating procedure converges slowly compared with that of the corresponding FRF method developed for undamped structures.

The comparisons of FRF curves of the analytical, 'experimental' and updated models are shown in Fig. 4.6. It is shown that the regenerated FRF data from the updated model overlay perfectly over those of the 'experimental' model. After the damping coefficients have been correctly identified, the peaks of the updated FRF curves become damped at resonances because of the presence of structural damping.

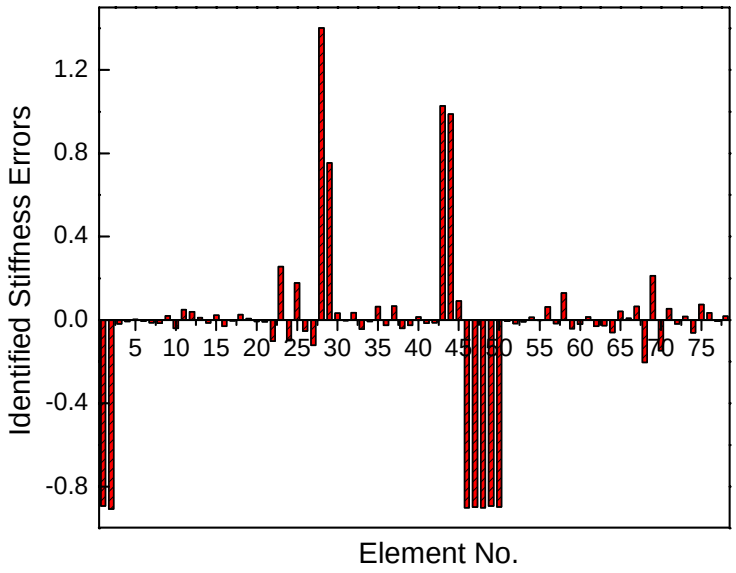

(a) 1st iteration

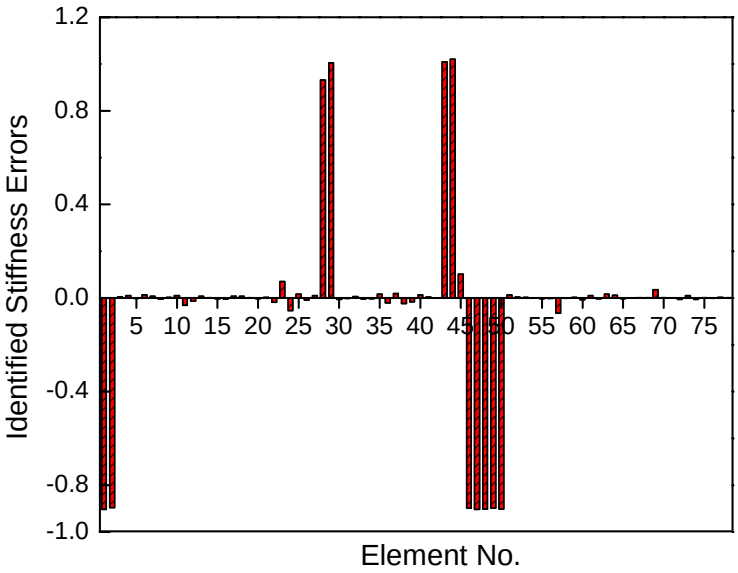

(b) 8th iteration

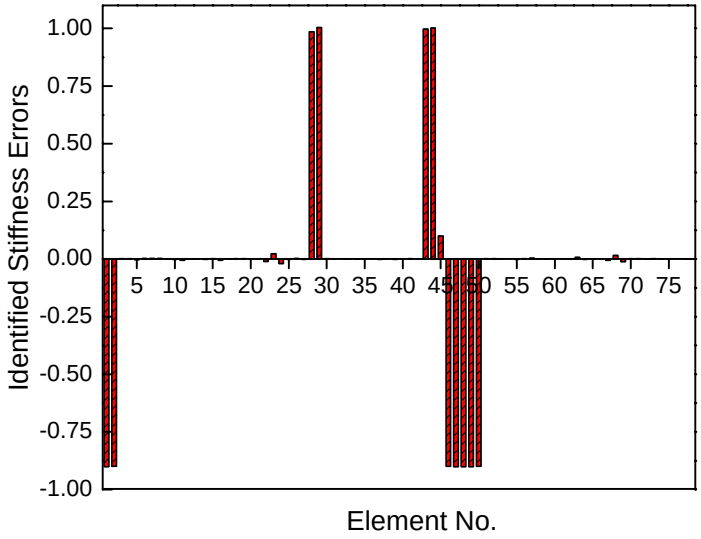

(c) 15th iteration

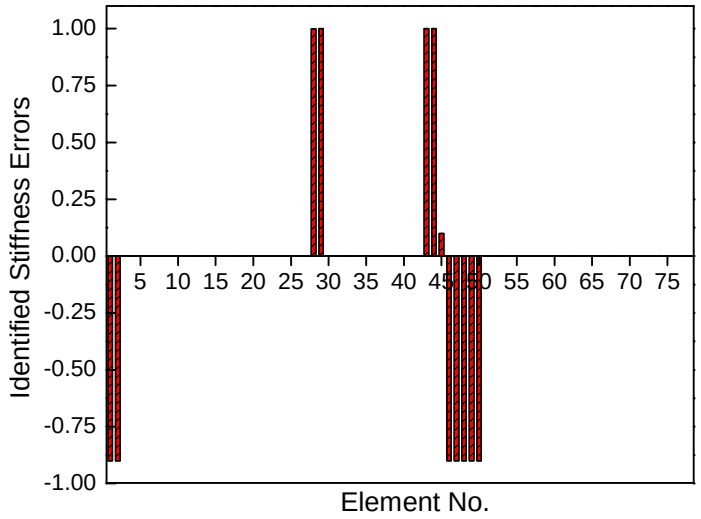

(d) 30th iteration

Fig. 4.4 Iteration results of identified stiffness errors (Case 1)

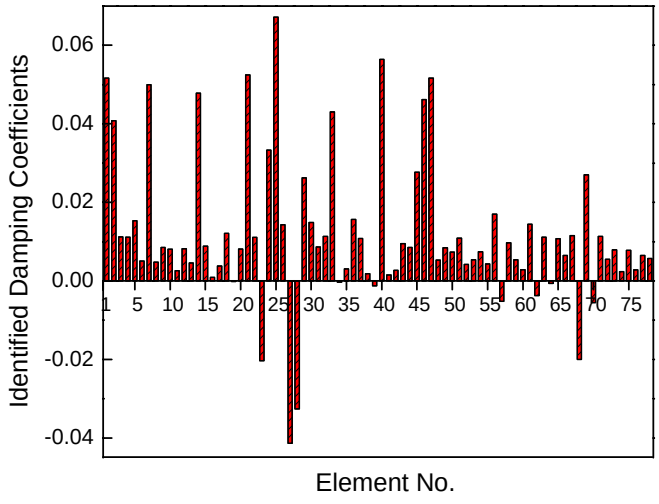

(a) 1st iteration

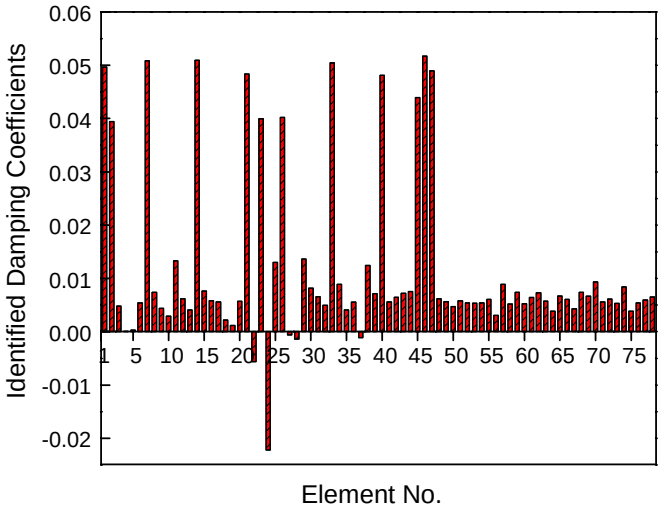

(b) 8th iteration

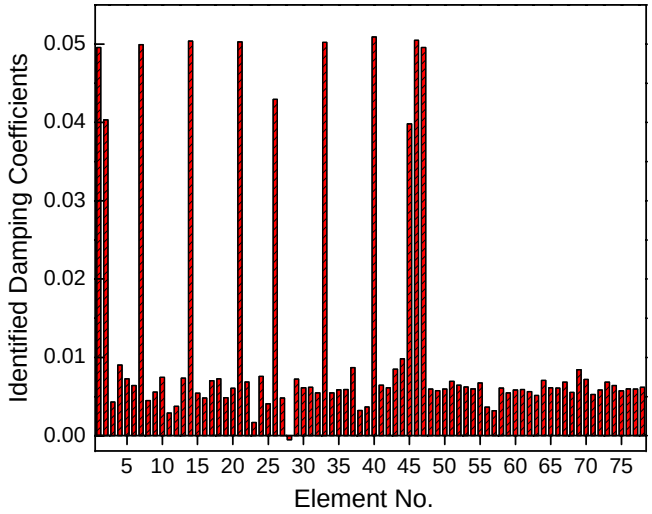

(c) 15th iteration

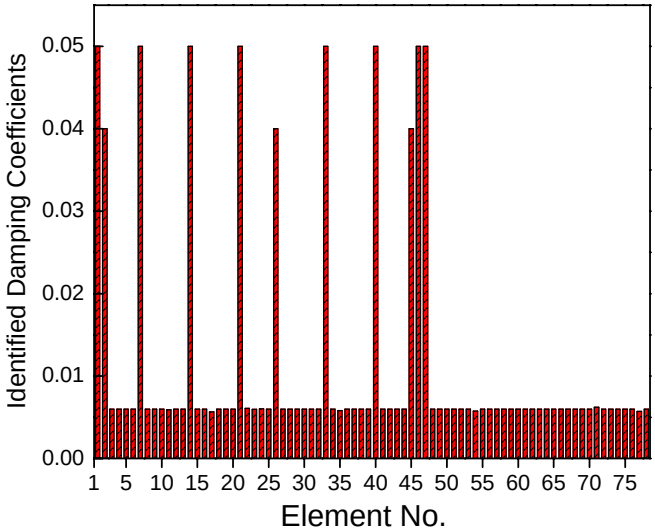

(d) 30th iteration

Fig. 4.5 Iteration results of identified damping coefficients (Case 1)

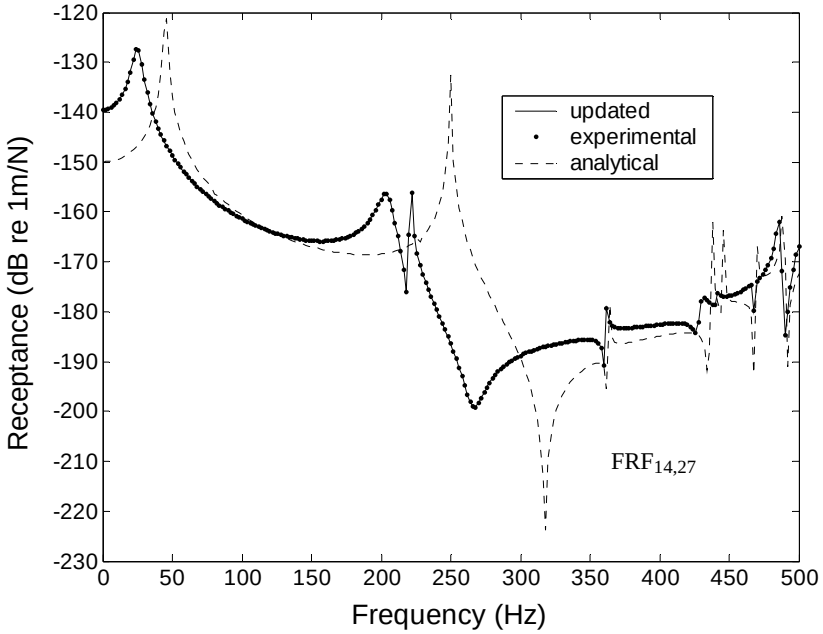

Fig. 4.6 Comparisons of the analytical, the 'experimental' and the updated FRF curves (Case 1)

Case 2 (Stiffness and Mass Errors and Damping Coefficients)

If a structure to be updated has both stiffness and mass modeling errors and at the same time has damping coefficients to be identified, the situation becomes a bit complicated but the proposed method can be applied to do just that. In this case study, successful application of the proposed method to simultaneously updating mass and stiffness matrices and to deriving damping coefficients will be shown. For the 'experimental' model of the structure, we assume that the individual element damping matrix takes the form as that of equation (4.27). The new complex element stiffness matrix is supposed to have the form as expressed by equation (4.28). Since mass modeling errors are also considered in this case, the impedance error matrix of the structure becomes,

$$[\Delta Z]=[\Delta K]-\omega^2[\Delta M]+i[D]=\sum_{j=1}^{N}(\beta_i+i\gamma_j)[K_j^e]-\omega^2\sum_{j=1}^{N}\chi_j[M_j^e], \tag{4.31}$$

where $[M_j^e]$ is the j^{th} element mass matrix and β_j and χ_j are the design parameter changes associated with the j^{th} element. Similarly, upon substituting the derivatives of the dynamic stiffness matrix with respect to the design parameters derived from (4.31) into (4.22), we can derive the complex FRF sensitivity matrix with damping elements, as what we did in Case 1. Here it should be noted that the p-value change vector involves two parts. One is the complex p-value change vector associated with stiffness and damping corrections and the other is the real p-value change vector associated with mass corrections. Since the p-value change vector involves both complex and real parts, the complex algebraic equation sets (4.21) should be first separated into real and imaginary parts before they are solved. Then the real and imaginary parts of the equations sets are combined together and following equation sets are obtained,

$$\begin{Bmatrix}\mathrm{Re}([S])\cdot\mathrm{Re}(\{\Delta p\})-\mathrm{Im}([S])\cdot\mathrm{Im}(\{\Delta p\})\\ \mathrm{Re}([S])\cdot\mathrm{Im}(\{\Delta p\})+\mathrm{Im}([S])\cdot\mathrm{Re}(\{\Delta p\})\end{Bmatrix}=\begin{Bmatrix}\mathrm{Re}(\{\Delta\alpha\})\\ \mathrm{Im}(\{\Delta\alpha\})\end{Bmatrix}. \tag{4.32}$$

Rearranging above equation sets, we have,

$$\begin{bmatrix}\mathrm{Re}([S]) & -\mathrm{Im}([S])\\ \mathrm{Im}([S]) & \mathrm{Re}([S])\end{bmatrix}\begin{Bmatrix}\mathrm{Re}(\{\Delta p\})\\ \mathrm{Im}(\{\Delta p\}\end{Bmatrix}=\begin{Bmatrix}\mathrm{Re}(\{\Delta\alpha\})\\ \mathrm{Im}(\{\Delta\alpha\})\end{Bmatrix}, \tag{4.33}$$

where,

$$\mathrm{Re}(\{\Delta p\})=\begin{Bmatrix}\{\beta\}\\ \{\chi\}\end{Bmatrix},\quad\text{and}\quad\mathrm{Im}(\{\Delta p\})=\begin{Bmatrix}\{\gamma\}\\ \{0\}\end{Bmatrix}.$$

Since the zero vector $\{0\}$ of the imaginary part of $\{\Delta p\}$ has no meanings in equations (4.33), it should be eliminated before the equation sets is solved. Deleting the zero vector from the unknown vector in equations (4.33) and the columns of the coefficient matrix in

equations (4.33), which are corresponding to the zero vector, we can obtain the reduced form of equations (4.33) as equations (4.34),

$$\begin{bmatrix} \mathrm{Re}([S]) & (-\mathrm{Im}([S]))_\gamma \\ \mathrm{Im}([S]) & (\mathrm{Re}([S]))_\gamma \end{bmatrix} \begin{Bmatrix} \{\beta\} \\ \{\chi\} \\ \{\gamma\} \end{Bmatrix} = \begin{Bmatrix} \mathrm{Re}(\{\Delta\alpha\}) \\ \mathrm{Im}(\{\Delta\alpha\}) \end{Bmatrix}, \tag{4.34}$$

where $(-\mathrm{Im}([S]))_\gamma$ and $(\mathrm{Re}([S]))_\gamma$ are the corresponding columns of $-\mathrm{Im}([S])$ and $\mathrm{Re}([S])$ with respect to $\{\gamma\}$, respectively. After the reduced equation sets (4.34) are solved, the design parameter changes will be obtained. Adding the design parameter changes to the analytical design parameters subsequently, one can obtain the updated mass and stiffness parameters, as well as damping coefficients.

To demonstrate the practicality of the proposed method when applied to the case of damped structures where both mass and stiffness modeling errors exist, the same GARTEUR structure with structural damping was considered. The analytical FE model is again considered as having no damping. In order to simulate the practical structure more realistically, the 'experimental' model in this case is generated using a much refined finite element mesh as shown in Fig. 4.7. And this model consists of 384 nodes and 390 elements, which is five times that of the coarse analytical FE model and may be considered to be close to the practical structure. To generate the 'experimental' FRF data from the refined model, both stiffness and mass modeling errors were introduced by changing the cross-section area and the second moment of area of some elements as shown in Table 4.2. The values for the damping coefficients used γ_i in the 'experimental' model shown in Fig. 4.7 are all assumed to be zero except those at the joint positions, which are set high values

as shown in Table 4.2. Using the proposed complex FRF updating formulation, the stiffness and mass modeling errors and damping coefficients are identified through iterations as shown in Figs. 4.8-4.10. As can be seen, the mass modeling errors are corrected accurately and the updated results of stiffness errors are also good. However, only the identified results of the main damping coefficients have reasonable accuracy while the redundant errors also occur at other coefficients whose values should be zero in fact. As mentioned before, it is because the identified damping coefficients are more apt to be affected by the bias errors of FRF data compared with stiffness and mass modeling errors. Fig. 4.11 shows the comparisons of FRF curves of the analytical, the 'experimental' and the updated models. It can be seen that after the modeling errors have been updated correctly and the damping coefficients have been well identified, the regenerated FRF curve of the updated model becomes almost identical to that of the 'experimental' model except some slight variations at resonant and anti-resonant regions.

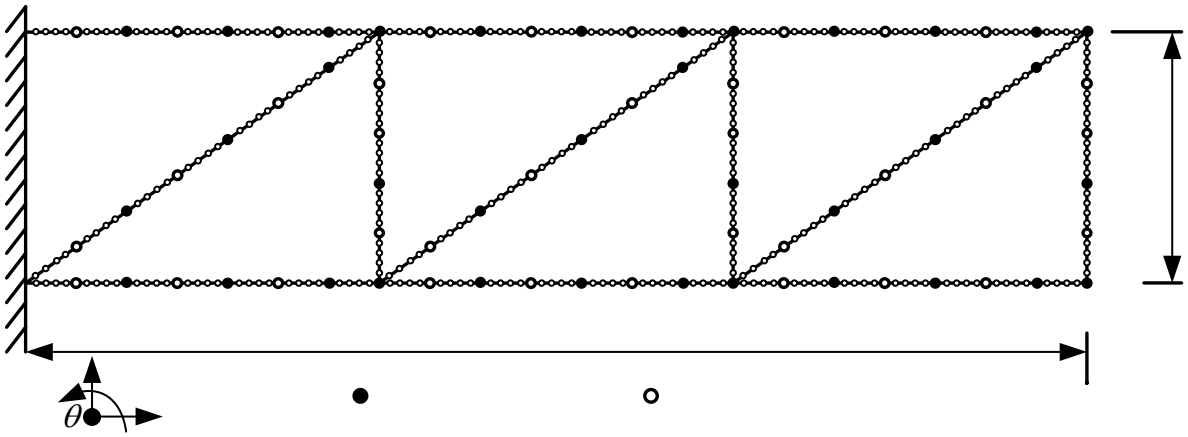

Fig. 4.7 The 'experimental' model of the **GARTEUR** structure with a refined mesh

Table 4.2 Location of introduced modeling errors and damping coefficients in the 'experimental' model (Case 2)

Element No.	1-5	6-10	136-140	141-145	211-215	216-220	221-225	226-230	231-235	236-240	241-245	246-250
Stiffness Error (%)	-50	-50	60	60	60	60	10	-50	-50	-50	-50	-50
Element No.	165-170			326-330			356-360			361-365		
Mass Error (%)	100			100			100			100		
Element No.	31-35	66-70	101-105	161-165	196-200	231-235	236-240	266-270	296-300	326-330	356-360	386-390
Damping Coefficient	0.08	0.08	0.08	0.08	0.08	0.08	0.08	0.08	0.08	0.08	0.08	0.08

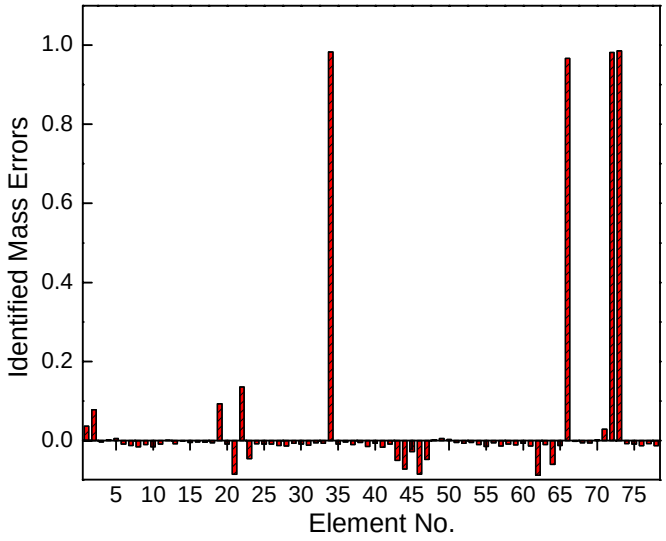

(a) 1st iteration

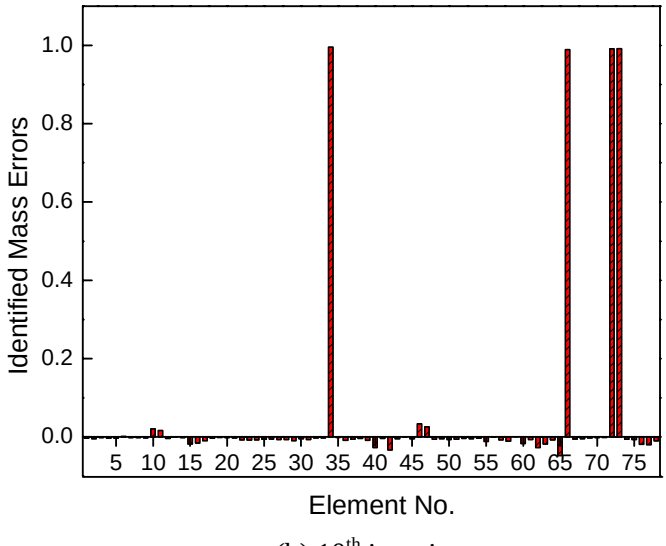

(b) 10th iteration

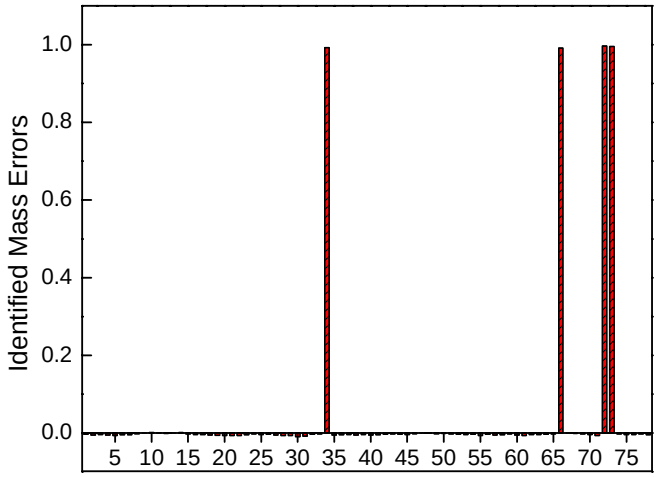

(c) 40th iteration

Fig. 4.8 Iteration results of identified mass errors (Case 2)

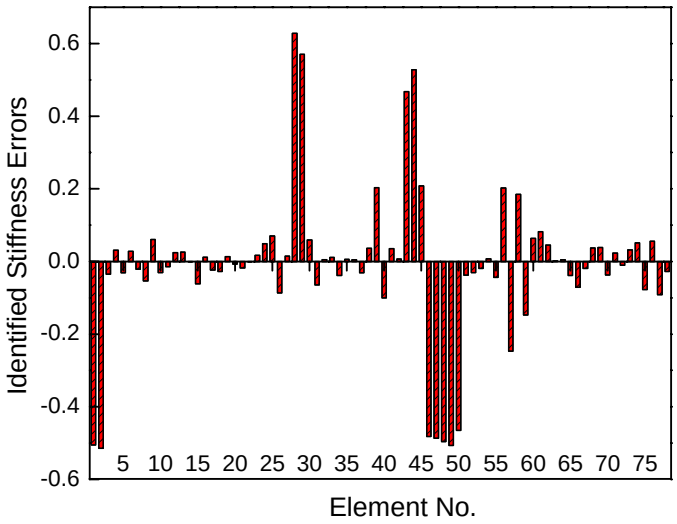

(a) 1st iteration

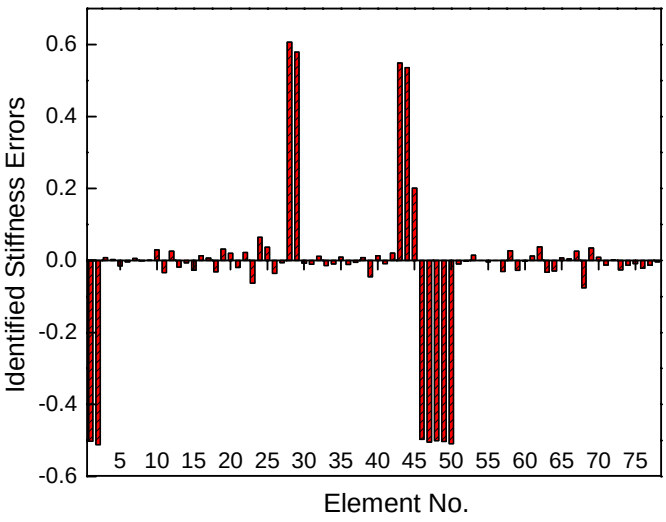

(b) 10th iteration

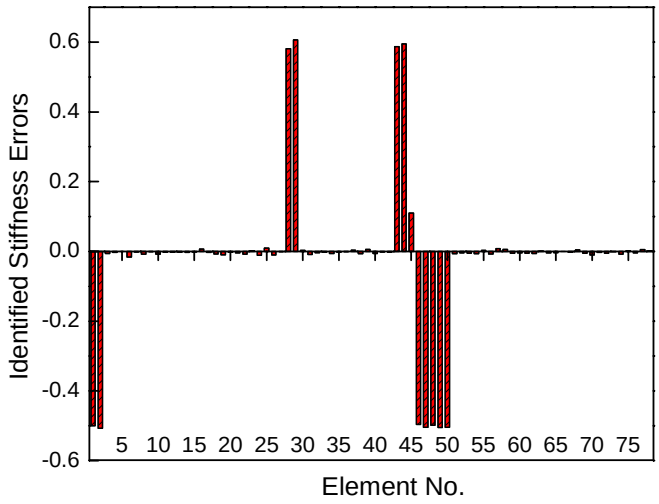

(c) 40th iteration

Fig. 4.9 Iteration results of identified stiffness errors (Case 2)

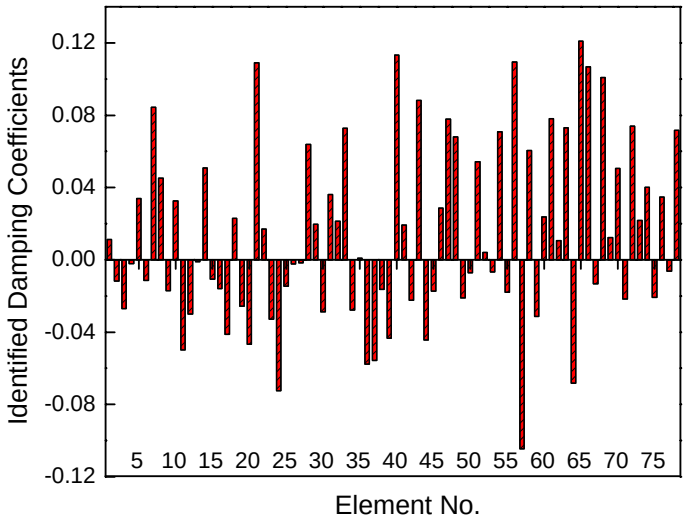

(a) 1st iteration

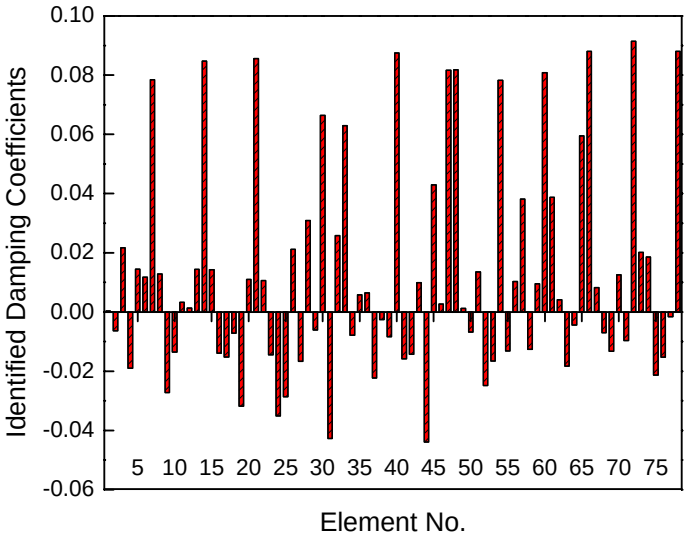

(b) 10th iteration

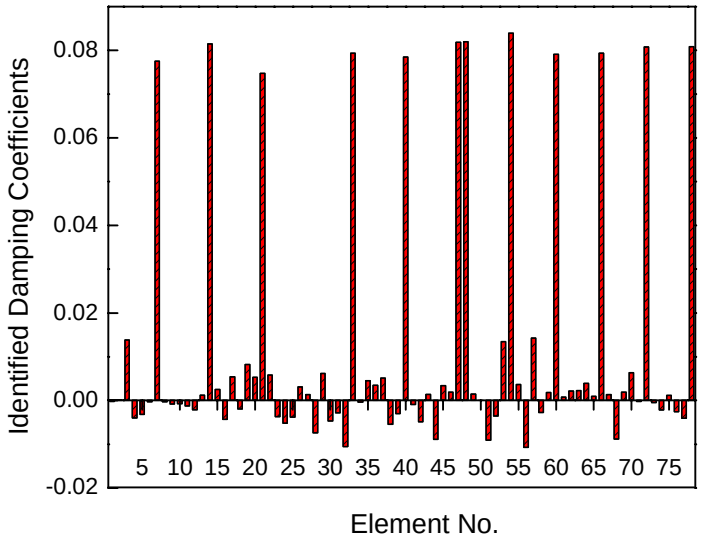

(c) 40th iteration

Fig. 4.10 Iteration results of identified damping coefficients (Case 2)

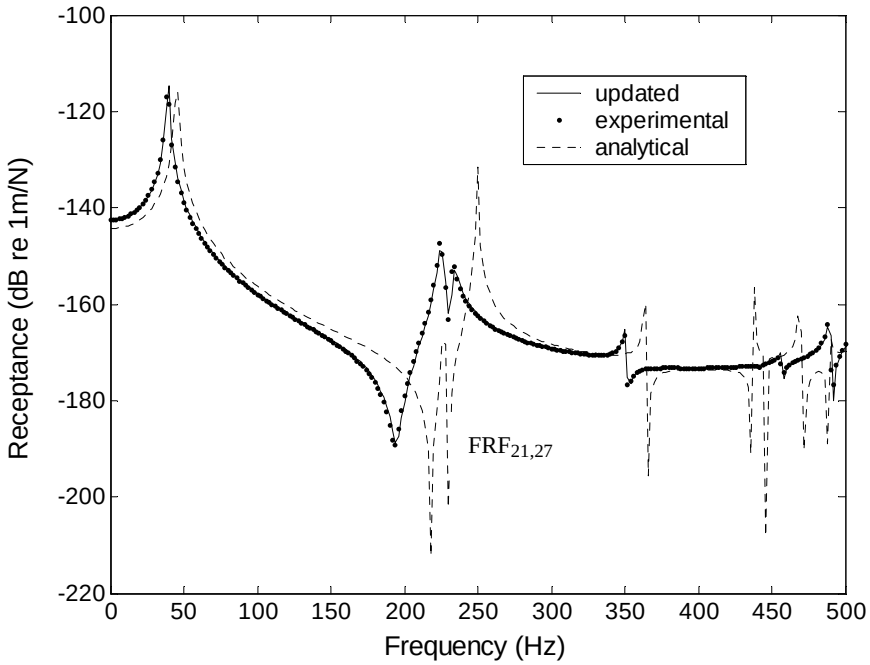

Fig. 4.11 Comparisons of the analytical, the 'experimental' and the updated FRF curves (Case 2)

Case 3 (Viscously Damped Structures)

Since model updating formulations of generally structurally damped structures have been established successfully in the previous sections, it is required and feasible to investigate

updating procedure of generally viscously damped structures. Suppose that there exist modeling errors in the FE model of a structure, which is viscously damped. Then viscous damping model needs to be identified as well as stiffness and mass matrices. Provided that the damping matrix $[C]$ is a linear combination of the element damping matrices, then a p-value formulation of the damping matrix to be identified can be written as, considering no damping included in an original FE model,

$$[C_X] = [\Delta C] = \sum_{k=1}^{N_c} \Delta p_c^k [C_k^e]. \tag{4.35}$$

According to the FRF updating formulation in case of structural damping in section 4.2.2, the expression of complex FRF sensitivity with respect to viscous damping coefficients should be derived first. Similar to the derivation of FRF sensitivity with respect to structural damping coefficients, the expression of FRF sensitivity with respect to viscous damping coefficients can be obtained as follows,

$$\frac{\partial \{\alpha(\omega)\}_j}{\partial p_c^k} = -i\omega [\alpha_A(\omega)][C_k^e]\{\alpha_X(\omega)\}_j, \tag{4.36}$$

where p_c^k is the design parameter with respect to the k^{th} element damping matrix and $[C_k^e]$ is the element viscous damping matrix. From equation (4.36), it is found that FRF sensitivity with respect to p_c^k is also complex as in the case of structural damping. So far, the foundation of FRF updating formulation of viscous damping coefficients at p-value level has been established in a complex domain.

To generate the 'measured' FRF data with viscous damping, it is supposed for simplicity that the individual element damping matrix of the 'experimental' model is proportional to

the element stiffness matrix in the FE model,

$$[C_j^e] = \kappa_j [K_j^e], \tag{4.37}$$

where κ_j is the proportionality coefficient associated with the j^{th} element. In fact, any specified forms of element viscous damping matrices can be chosen in this case as the proposed method is generally formulated. Similar to equation (4.31), the impedance error matrix of the structure is written as,

$$[\Delta Z] = [\Delta K] - \omega^2 [\Delta M] + i\omega [C] = \sum_{j=1}^{N} \beta_i [K_j^e] - \omega^2 \sum_{j=1}^{N} \chi_j [M_j^e] + i\omega \sum_{j=1}^{N} \kappa_j [K_j^e]. \tag{4.38}$$

Upon substituting the derivatives of the impedance matrix with respect to the design parameters derived from (4.38) into (4.22), the complex FRF sensitivity matrix with damping elements can be derived. Since the complex stiffness error matrix does not exist in (4.38), the p-value change vector would be just real in this case. The solution procedure would be a little different from that of the complex updating formulation due to the complex stiffness matrix in the case of structural damping. The p-value change vector involves three parts: The first two parts are the p-value change vectors associated with stiffness and mass corrections, respectively and the third one is the p-value change vector associated with damping coefficients. Although the p-value change vector is real in this case, the complex algebraic equation sets (4.21) should also be separated into real and imaginary parts first and then solved in a similar procedure as that of equations (4.32 and 4.33). Consequently, following equation sets are obtained,

$$\begin{bmatrix} \mathrm{Re}([S]) \\ \mathrm{Im}([S]) \end{bmatrix} \{\Delta p\} = \begin{Bmatrix} \mathrm{Re}(\{\Delta\alpha\}) \\ \mathrm{Im}(\{\Delta\alpha\}) \end{Bmatrix}, \tag{4.39}$$

where, $$\{\Delta p\} = \begin{Bmatrix} \{\beta\} \\ \{\chi\} \\ \{\kappa\} \end{Bmatrix}.$$

Based on the solution of the equation sets (4.39), the design parameter changes of stiffness and mass will be obtained, respectively, as well as damping coefficients. Adding the design parameter changes to the original design parameters subsequently, the stiffness and mass matrices can be constructed and at the same time viscous damping matrix is established using the damping coefficients. Such process is repeated iteratively until convergent solutions of p-values are reached.

For demonstration of its application, the proposed complex FRF method is applied to a truss structure consisting of composite beams shown in Fig. 4.12. Suppose that the top beam of this structure is constructed by adding a viscoelastic damping treatment to an existing beam. And some viscoelastic damping material (such as rubber) is added as a layer which is sandwiched in between another two layers of metal. It is assumed that the metal layers provide the appropriate stiffness and the sandwiched viscoelastic layer provides the damping required. The material parameters of this beam are as followings: Young's modulus of elasticity E=70.0×10^9N/m^2; cross sectional area A=b×h=0.02×0.006m^2; lengths of beam L_1=1.0m and L_2=0.5m; material density ρ =2700.0kg/m^3. The analytical FE model of the truss structure consisting of 20 beam elements is considered to be updated here. Each element is a superposition of a bar element and a bending beam element and hence each node has three DOFs (two translations and one rotation). This initial analytical model is assumed to have no damping. To simulate experimental data, it is assumed that the

'experimental' model has mass and stiffness variations because of 50% reduction of cross-section area, A, in the 4^{th}, 5^{th}, 9^{th} elements and 50% reduction of second moment of area, I, in the 6^{th}, 8^{th}, 10^{th}, 17^{th} elements, respectively. The viscous damping coefficients of the 6^{th}-15^{th} elements of the top beam are assumed to be 0.06 whereas those of other elements are zero.

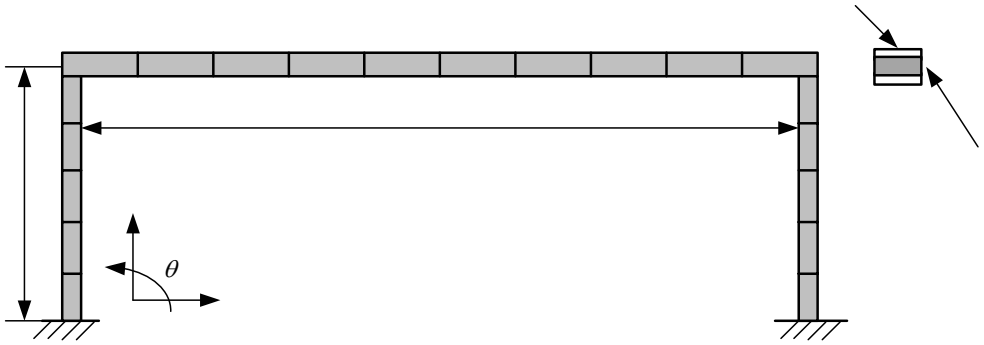

Fig. 4.12 A truss structure with viscous damping

Considering incompleteness of the measured coordinates in practical testing, only the translational DOFs u and v of one element are assumed to have been measured in this case. Therefore, during the establishment of equation sets (4.21), those unmeasured rotational DOFs are replaced by their analytical counterparts. Due to the approximations introduced in the calculation of the sensitivity matrix and the FRF difference vector, iteration procedures are required. The simulated 'experimental' FRF data at five frequency points in the frequency range from 20 to 150Hz were selected for updating. The solution path was also examined by selecting different sets of frequency points from the same range. Figs. 4.13 and 4.14 show the updating procedure of the stiffness and mass modeling errors as well as damping coefficients. It is observed that both modeling errors and damping coefficients are accurately identified through iterations.

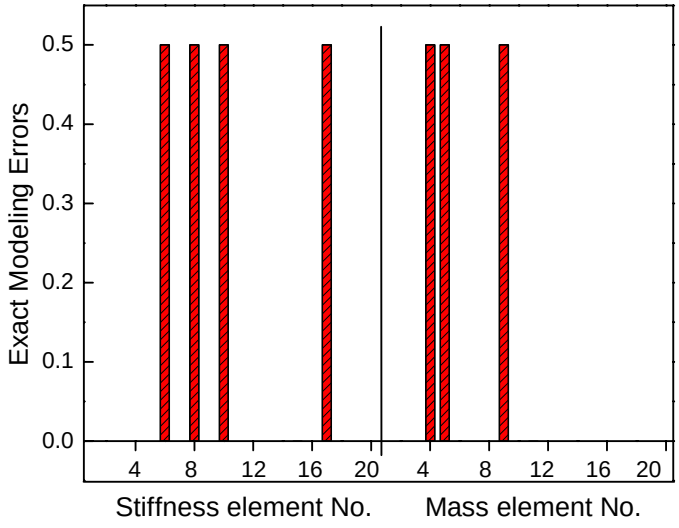

(a) exact modeling errors

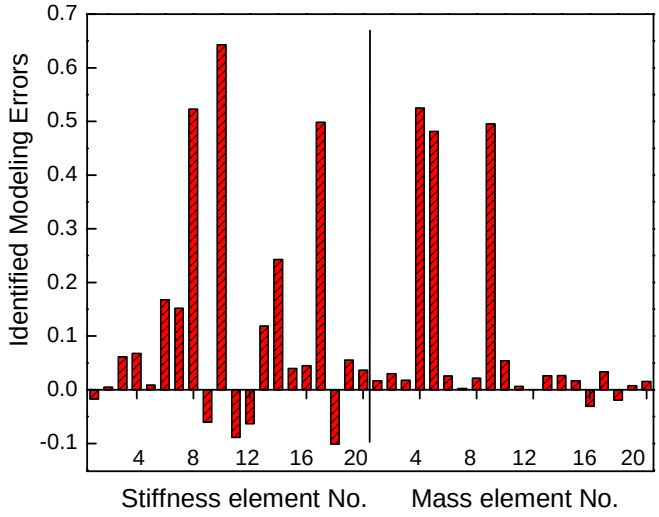

(b) 1st iteration

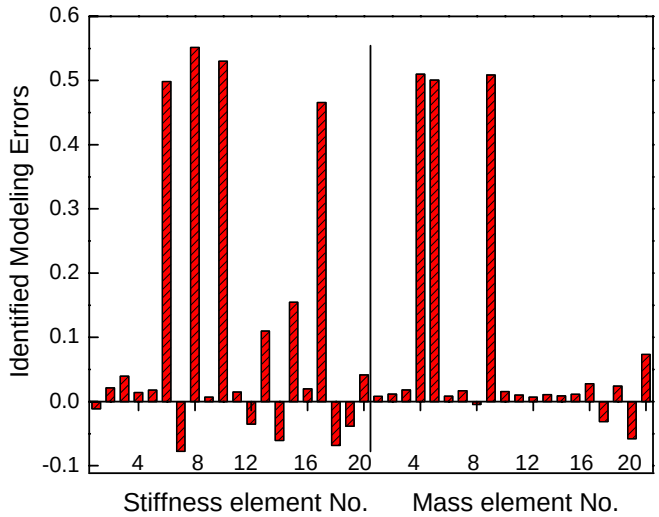

(c) 5th iteration

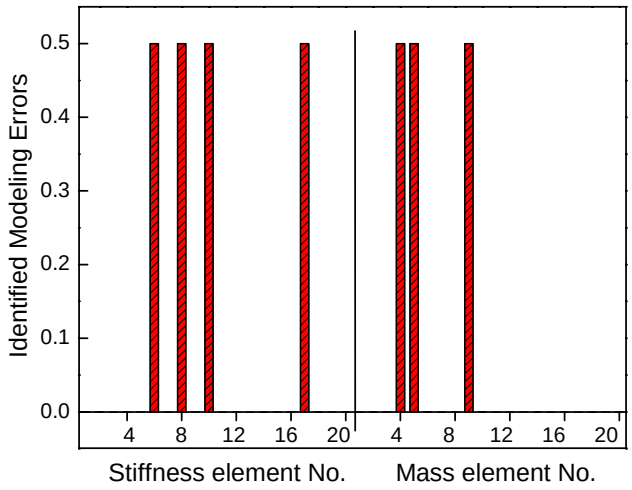

(d) 10th iteration

Fig. 4.13 Iteration results of identified stiffness and mass errors (Case 3)

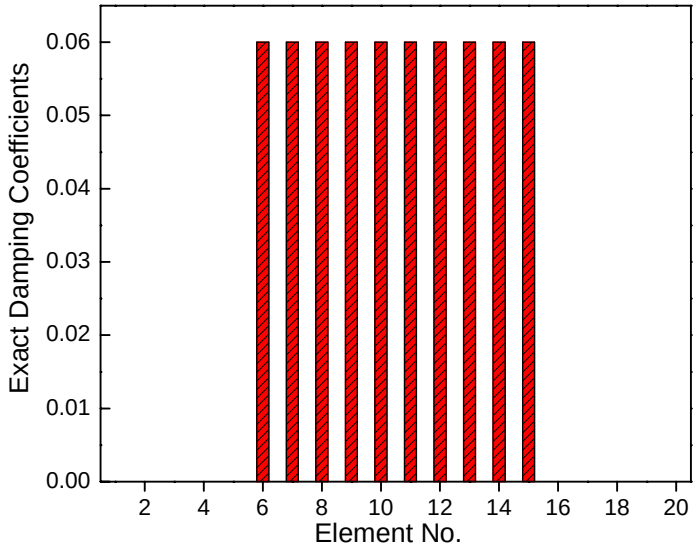

(a) exact damping coefficients

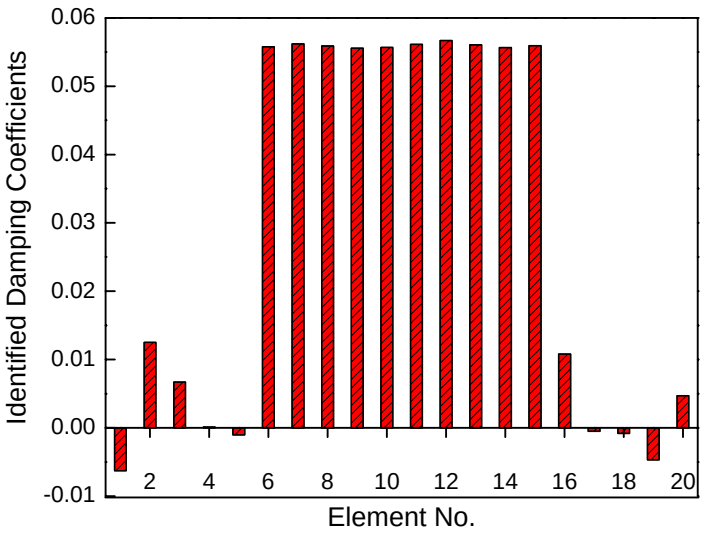

(b) 1st iteration

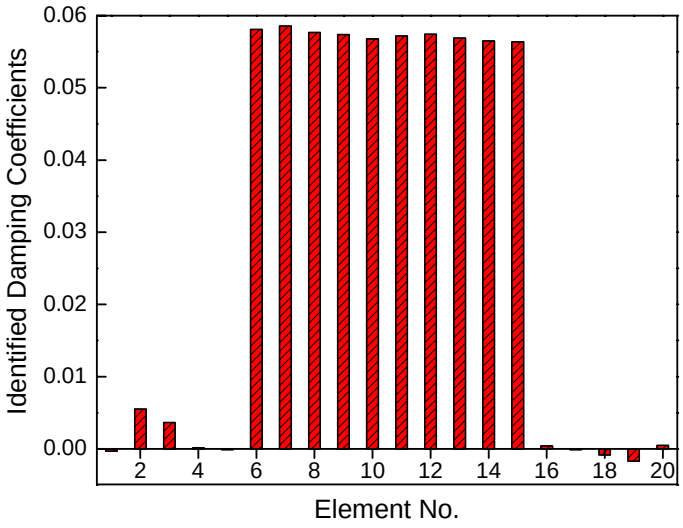

(c) 5th iteration

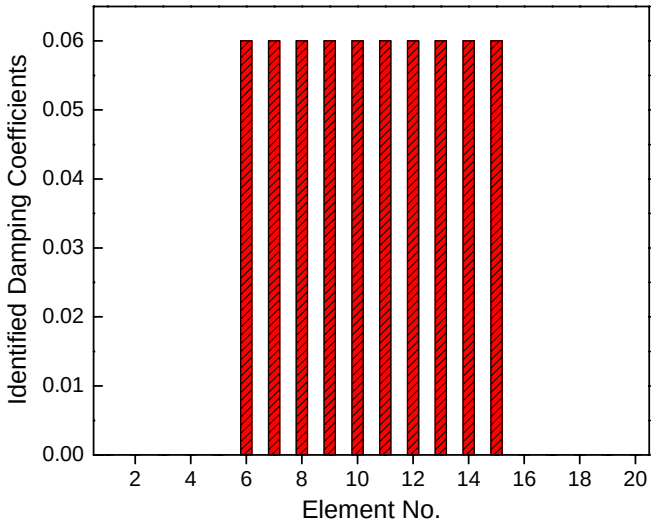

(d) 10th iteration

Fig. 4.14 Iteration results of identified damping coefficients (Case 3)

Case 4 (Measured FRF Data with Noise)

In order to study the effect of measurement noise on the FRF updating process of damped structures, the same GARTEUR structure with structural damping shown in Fig. 4.1 is chosen to be studied. To simulate the 'experimental' model, FE modeling errors and structural damping coefficients listed in Table 4.3 are introduced to the original FE model in this case. To generate noise-contaminated measured data, we assume that 3% random

noise is added to the simulated 'experimental' FRF data. One incomplete column of the receptance matrix of the 'experimental' model is supposed to have been measured at 250 frequency points in a frequency range of 0-500Hz, with excitation being in the *u* direction at node 11. In order to average the effect of measurement noise, in each iteration, FRF data from 40 different frequency points, which are away from resonance and anti-resonance regions, are randomly chosen for updating. To evaluate convergence of the iteration process, a normalized residue value, which is defined as the difference between the 'experimental' FRF and their updated counterparts at all selected frequency points, is calculated after each iteration, as shown in Fig. 4.15. It is observed that the residue value does not change much after 45 iterations, which means the convergent solutions are obtained. The iteration results of modeling errors and damping coefficients are shown in Figs 4.16-4.17 and Fig. 4.18, respectively. Compared with the exact errors introduced, quite accurate results of the modeling errors have been obtained, especially the mass errors. However, the identified results of damping coefficients are not very good. Though all the major locations of damping coefficients are identified, the updated results of damping coefficients are not accurate. Moreover, redundant coefficients also occur at locations where there should be no coefficients. This is because the magnitude of damping coefficients is quit small compared with that of modeling errors and the information of damping coefficients tends to be obliterated by measurement errors with high level of noise. Generally, ill-conditioning of updating problem may occur when measured FRF data contain noise. Therefore, techniques of locating the major modeling errors first and subsequently reducing the number of unknowns should be taken to improve the condition and hence the accuracy of the solution.

During the updating procedure, the first iteration solutions obtained using different sets of frequency points were examined. And only those parameters having large values at the corresponding modeling errors and damping coefficients were selected for next iteration. In this way, localization of major modeling errors and reduction of the number of updating parameters were achieved. The total number of parameters of the structure is 234 since it has 78 elements and each element has three parameters (one mass parameter, one stiffness parameter and one damping parameter). After the localization, only 52 parameters (the exact number of parameters to be updated is 21 as shown in Table 4.3) were considered in the actual updating process. Fig. 4.19 shows some FRF curves of the 'experimental', analytical and updated models. It can be seen that the regenerated FRF data from the updated model overlay well over those of the 'experimental' model at resonance regions and there exist large differences between the two sets of FRF data at anti-resonance regions. It means that the accuracy of the identified damping coefficients has affected the updated model significantly in this case although the modeling errors have been corrected accurately. Therefore, techniques of overcoming measurement noise problem in the model updating procedure need to be further developed and investigated.

Table 4.3 Location of introduced modeling errors and damping coefficients (Case 4)

Element No.	1	2	44	45	46	47	48	49	
Stiffness Error (%)	-50	-50	100	100	100	100	-50	-50	
Element No.	34		66		72			73	
Mass Error (%)	100		100		100			100	
Element No.	1	7	14	21	26	33	40	46	47
Damping Coefficient	0.08	0.08	0.08	0.08	0.08	0.08	0.08	0.08	0.08

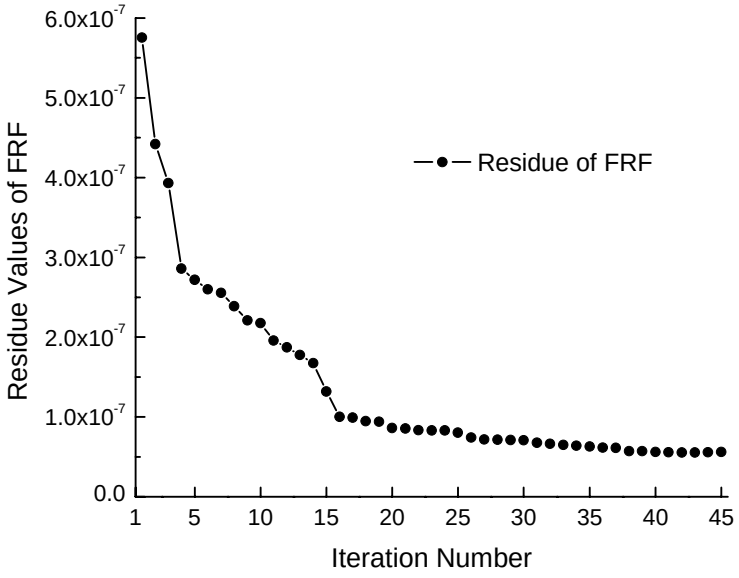

Fig. 4.15 Change of FRF residue values *vs* number of iteration (Case 4)

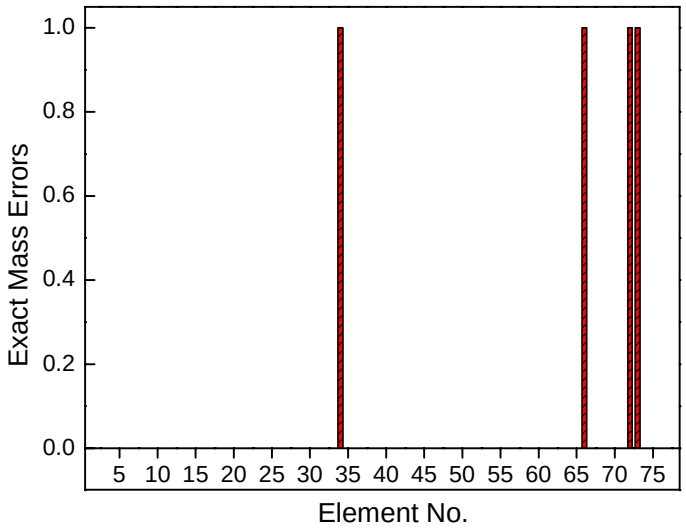

(a) exact mass modeling errors

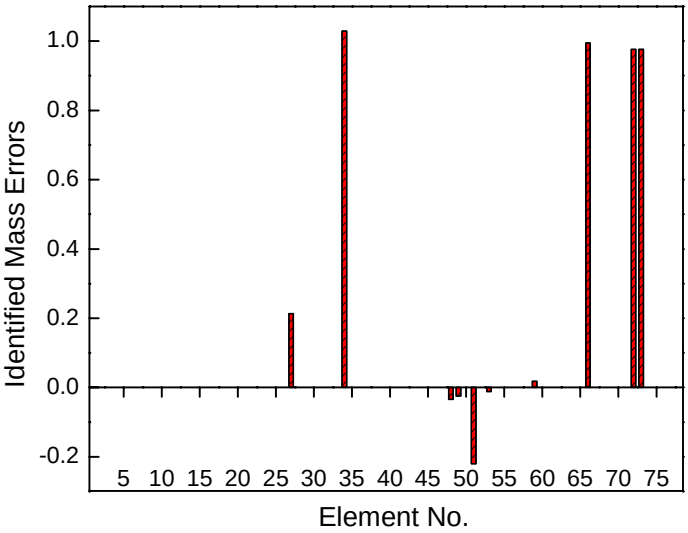

(b) 1st iteration

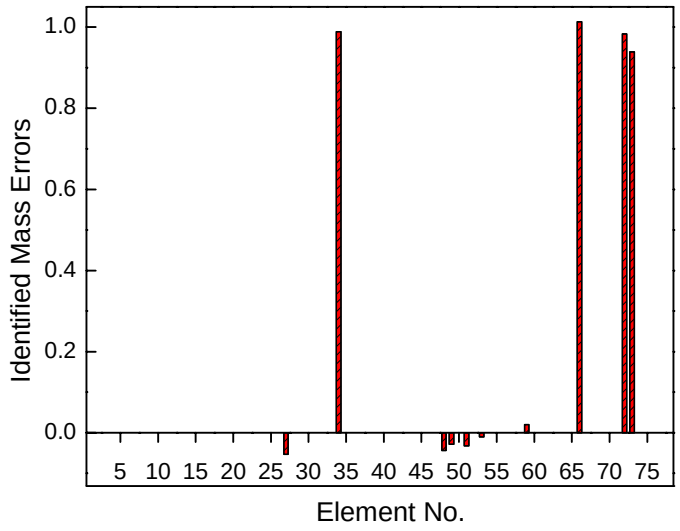

(c) 20th iteration

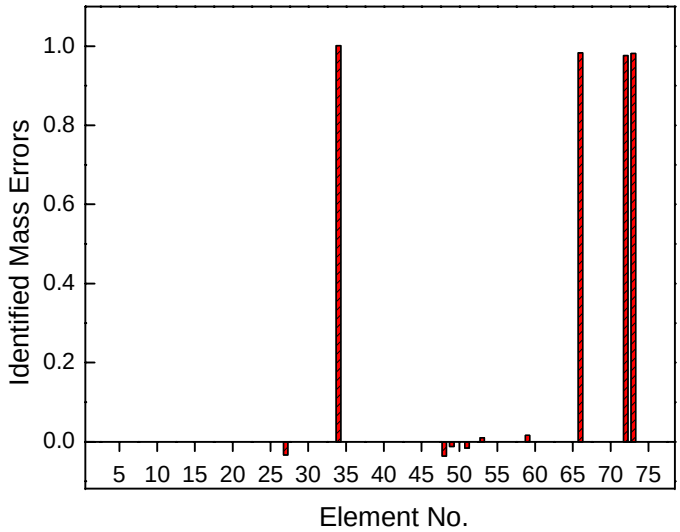

(d) 45th iteration

Fig. 4.16 Iteration results of identified mass modeling errors (Case 4)

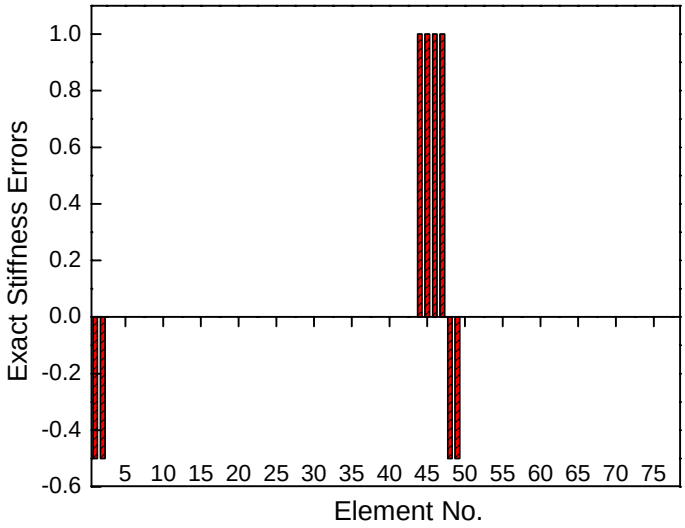

(a) exact stiffness modeling errors

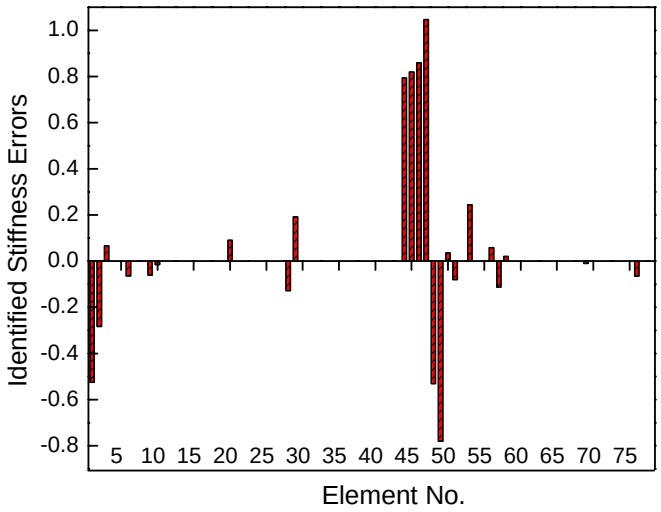

(b) 1st iteration

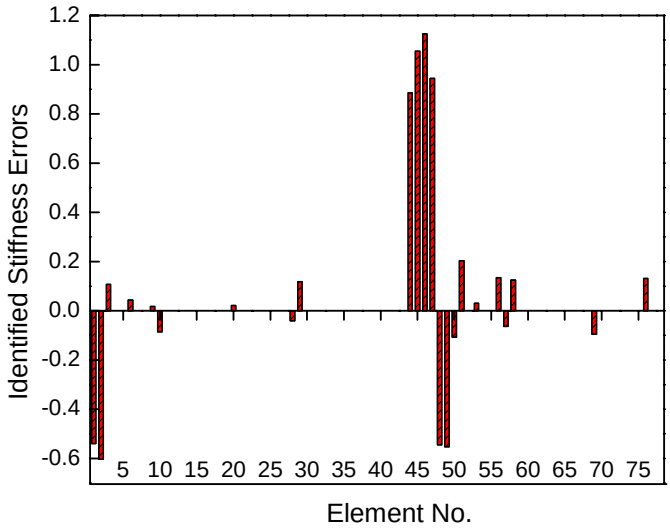

(c) 20th iteration

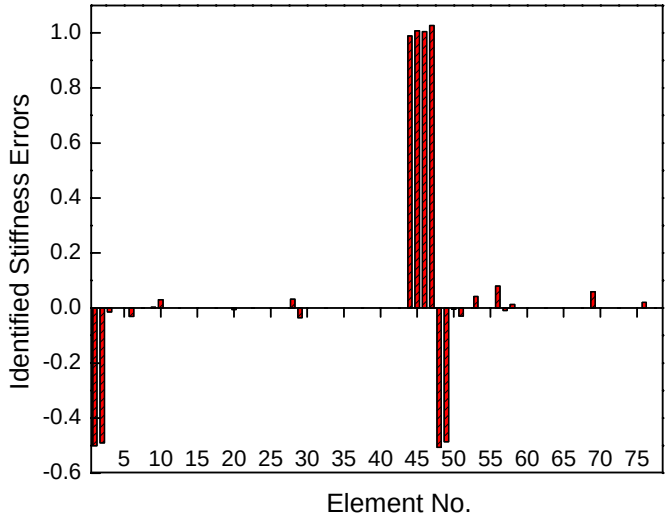

(d) 45th iteration

Fig. 4.17 Iteration results of identified stiffness modeling errors (Case 4)

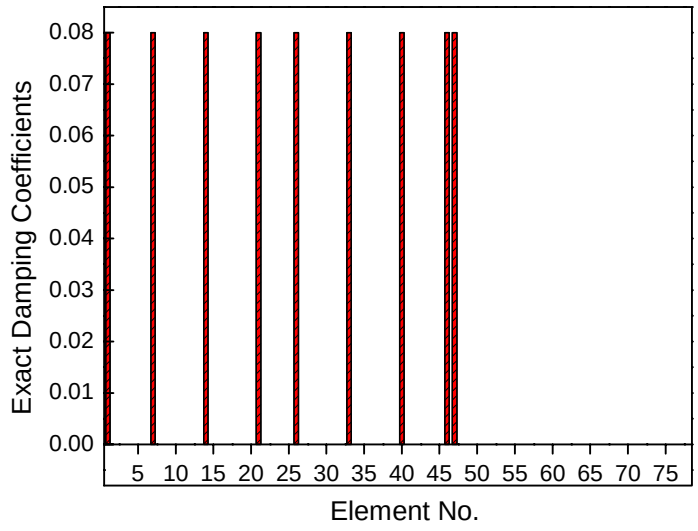

(a) exact damping coefficients

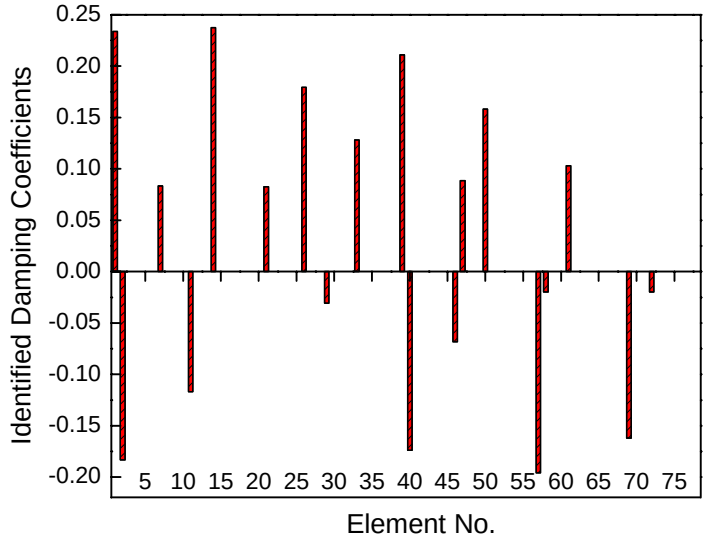

(b) 1st iteration

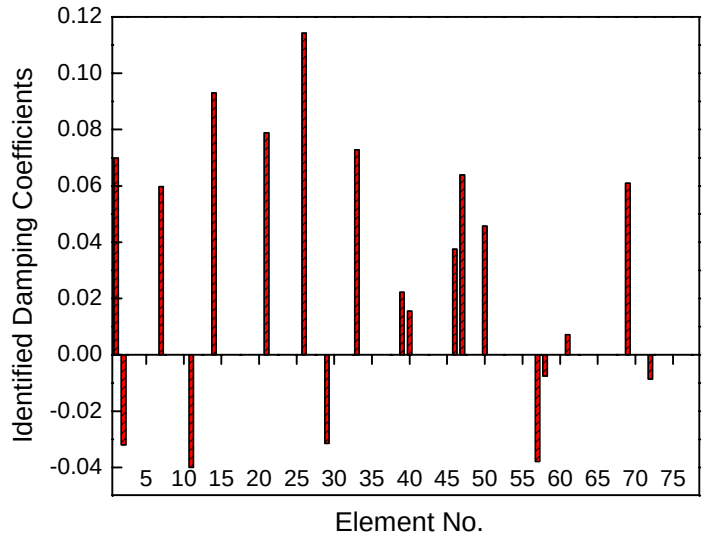

(c) 20th iteration

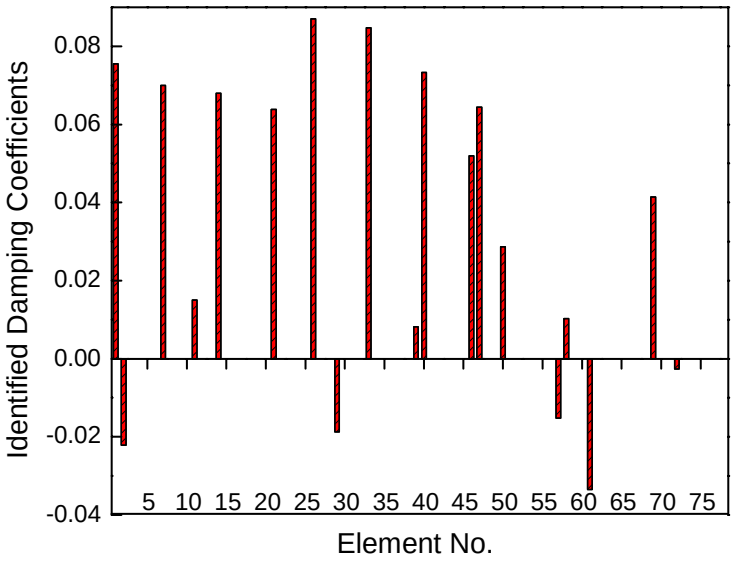

(d) 45th iteration

Fig. 4.18 Iteration results of identified damping coefficients (Case 4)

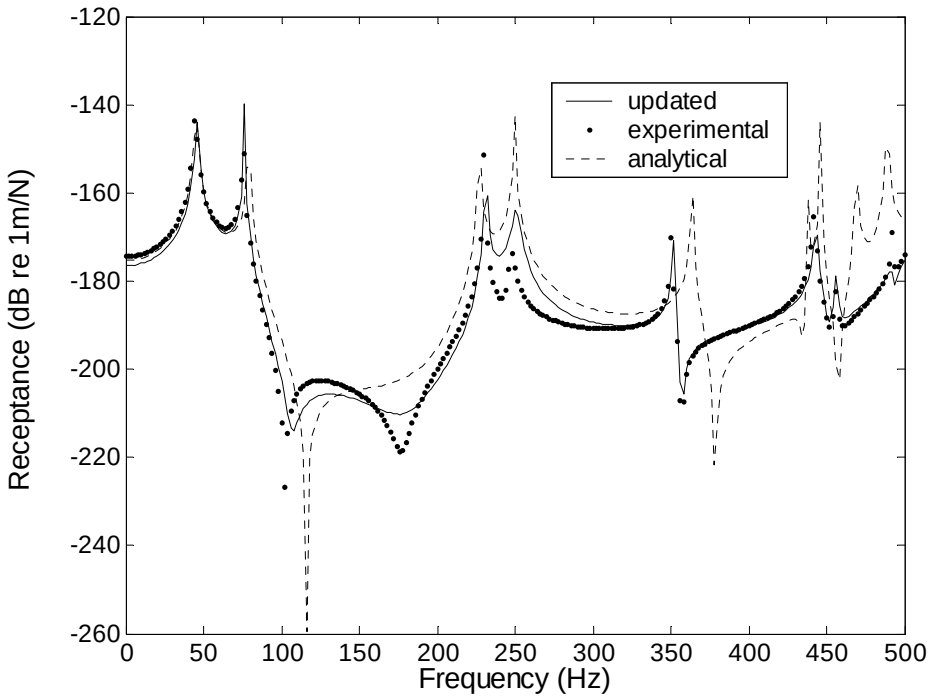

Fig. 4.19 Comparisons of the analytical, the 'experimental' and the updated FRF curves (Case 4)

4.4 Concluding Remarks

In this chapter, existing real FRF based updating method has been further developed and extended for the sake of model updating of generally damped structures. In order to overcome the complexity problem of measured modes, the complex updating formulations using measured FRF data have been successfully established to directly identify damping coefficients and at the same time to correct modeling errors in the cases of proportionally damped and non-proportionally damped structures. To evaluate the applicability of the proposed complex FRF based method, numerical case studies based on a typical and realistic GARTEUR structure with structural damping and a truss structure with viscous damping have been performed. Promising results identified for these cases have proved that this method is feasible and practical when applied to the identification of damping coefficients as well as mass and stiffness modeling errors. The effect of measurement noise in FRF data on the complex updating process has also been studied. The sufficient accuracy of the identified damping coefficients has not been achieved in the case of FRF data contaminated by 3% measurement noise. It indicates that some improvements are required to overcome measurement noise problem during the practical model updating process of complex and generally damped structures for the proposed method. This will be discussed in the following chapter.

Chapter 5

Identification of Damped Structures Using Taguchi Method

5.1 Introduction

The objective of model updating is to improve the analytical FE model using vibration test data. Generally, most model updating methods are shown to be very efficient when using simulated noise-free 'experimental' data in numerical examples. In practical measurement, it is inevitable that experimental data will be contaminated by measurement noise. Noise errors may be either random or systematic. Random errors can be reduced by careful experimental technique, choice of excitation method and by averaging test data. Systematic errors, which are difficult to be removed from test data, are serious problems in model updating. When test data contaminated by noise are employed for model updating, the updated results are usually not as accurate as those obtained from noise-free situation. Therefore, it is vital to improve the noise-resisting abilities of the current updating methods when updating erroneous FE models using measured noise-contaminated data.

To eliminate the effect of noise contamination in model updating, recently a few new hopeful approaches have been proposed, such as neural network method (Levin and Lieven, 1998b) and genetic algorithm method (Friswell *et al.*, 1998). These methods are based on mapping or optimization and are different from those original updating methods based on dynamic equation properties, such as sensitivity methods. Therefore, these methods are less sensitive to measurement noise. Kwon and Lin (2005) applied a novel approach: the

Taguchi method to model updating. Taguchi method (Taguchi, 1986), which has been widely used for robust design and quality engineering in industry, is computationally efficient in searching the main parameters which need to be updated. Moreover, it has the capability of resisting the influence of measurement noises that are contained in the experimental data. In the first stage, Taguchi method has been successfully established to update FE models without considering damping properties of structures. In fact, most of practical structures are generally damped and damping can not be neglected during model updating procedure. Since the Taguchi method has shown its efficiency in model updating of undamped structures, it is believed that it has the potential to be further developed to update generally damped structures. In the following sections, objective functions and the updating formulation using SN Ratio for damped structures will be addressed.

5.2 Formulation of Objective Function

Essentially, Taguchi method is an optimization method for an objective function, which is defined as the difference between experimental and analytical data in model updating. This method is computationally efficient since the main effects of parameters are evaluated using orthogonal arrays with the least number of simulations rather than using stochastic approach. Moreover, the updated results are robust against various noises such as random errors and systematic errors because parameters are updated so that **signal to noise** (SN) ratio is maximized. In addition, the updating process can be more straightforward since it maximizes the SN ratio at each iteration. As reference data for model updating, both FRF data and modal data can be chosen if the appropriate objective functions are determined.

Objective Function Based on Modal Data

In general, model updating refers to updating parameters of existing analytical model such that the difference between analytical and experimental models is minimum. Hence, the updating problem may be formulated as an objective function, which is defined as the difference between analytical and experimental data, to be minimized. Modal data are commonly employed in most updating methods. Hence, the objective function based on modal data can be defined as (Friswell *et al.*, 1998),

$$J_1 = W_\omega J_\omega + W_\phi J_\phi , \tag{5.1}$$

where J_ω and J_ϕ are objective functions related to natural frequencies and mode shapes, respectively. Here, W_ω and W_ϕ are weighting functions for each objective function. These objective functions are defined as, when the first *n* modes are used,

$$J_\omega = \sum_{r=1}^{n} \left(\frac{(\omega_X)_r - (\omega_A)_r}{(\omega_X)_r} \right)^2 , \tag{5.2}$$

$$J_\phi = \sum_{r=1}^{n} \left(\{\phi_X\}_r - \{\phi_A\}_r \right)^T \left(\{\phi_X\}_r - \{\phi_A\}_r \right). \tag{5.3}$$

It should be noted that the measured mode shapes are automatically mass-normalized if proper calibration is done. Therefore, experimental mode shapes can be used directly in equation (5.3). If the measured mode shapes are not mass-normalized, the objective function J_ϕ should employ the form recommended in (Kwon and Lin, 2005).

It is believed that proper weightings of objective function can improve results significantly. Hence, these relative weightings need to be carefully selected. Considering natural

frequencies are measured more accurately than mode shape elements, the weighting on natural frequencies, W_ω, should be higher than the weighting on mode shapes, W_ϕ. However, if the weighting W_ω is set heavy for objective function while the weighting W_ϕ is too low, the information from mode shapes may not be sufficiently reflected in the solution. Due to these facts, W_ω=10 and $W_\phi = 1$ are recommended for numerical simulations (Friswell *et al.*, 1998). It is also known that the number of modes used in objective function will affect the updated results (Kwon and Lin, 2005). Hence, in order to update the parameters concerned, a sufficient number of modes are required to be included in the objective function. And low frequency modes are usually used for the objective function, which are normally more accurate and reliable both in modal testing and finite element analysis.

Objective Function Based on FRF Data

The objective function can also consider measured and analytically predicted FRFs for updating. However, the direct difference of FRFs for objective function may cause bad performance of updating process because the objective function is dominated by the FRFs at the regions of resonant peaks. Hence, balancing the effect of frequency points is needed whether these points are selected from the regions near resonances or anti-resonances. In practical application, the objective function is defined as the difference between the logarithmic magnitude of FRFs (Kwon and Lin, 2005),

$$J_2 = \sum_j \sum_k \left(\frac{\log\left|H_j^X(\omega_k)\right| - \log\left|H_j^A(\omega_k)\right|}{\omega_k} \right)^2, \tag{5.4}$$

where $H_j^X(\omega_k)$ and $H_j^A(\omega_k)$ are experimental and analytical FRFs, respectively and the subscript *j* represents the number of FRFs. Here, to reduce the gain in high frequencies, the differences between FRFs are divided by frequency ω_k since the FRFs at higher frequencies are more likely to be erroneous because of the discretization effect in analytical FE model.

Using measured FRFs as reference data for model updating has an advantage that the errors from modal parameter identification can be eliminated. However, how to select frequency points efficiently should be noted. To update parameters, the objective function should vary monotonously according to the change of parameters. The stable frequency points, which are at non-monotonous FRF regions such as regions close to and at resonances, should be avoided. If a parameter A increases ($A_0<A_1<A_2$), then corresponding FRF should also increase or decrease accordingly at selected frequency points. Therefore, as shown in Fig. 5.1, the frequency points, such as ω_1, which are likely to have non-monotonous characteristics of FRF, are to be avoided.

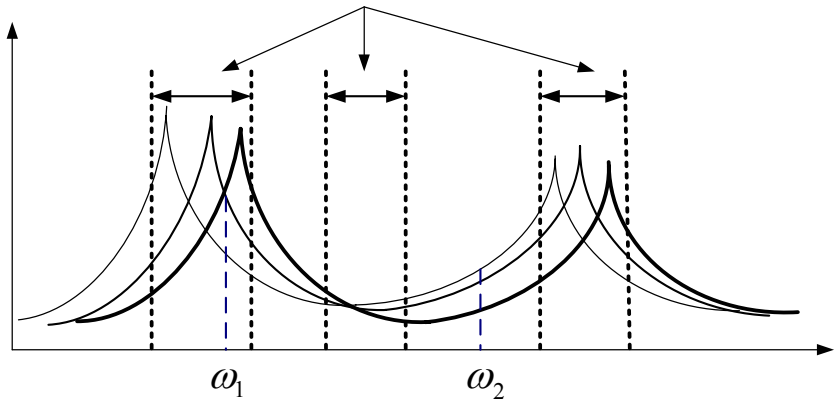

Fig. 5.1 FRFs corresponding to parameter value changes:
—— A_0; —— A_1; ━━ A_2.

Signal to Noise Ratio

As a better alternative form of objective function, the SN ratio was adopted to increase robustness of design parameter against measurement noises in model updating (Kwon and Lin, 2005). According to the Taguchi method, the optimization of objective functions defined in equations (5.1) and (5.4) can be classified as smaller-the-better process. Therefore, the SN ratio is defined as,

$$SN = -10 \log\left(\frac{1}{n} J\right), \tag{5.5}$$

where n is the number of modes or number of frequency points employed. Then, the minimization of the objective function J becomes maximizing the SN ratio, which may achieve considerable noise-resisting capability.

5.3 Orthogonal Array

To investigate the main effects of each parameter on the SN ratio, an orthogonal array (OA) is employed in running simulations. An orthogonal array can reduce the number of simulations efficiently since it searches parameters in such an efficient way that it is not necessary to simulate all possible combination of cases. An OA can be represented by a notation *OA(N,p,s,t)* where N, p, and s represent the number of experiments, parameters, and levels, respectively and t represents the number of columns (Hedayat *et al.*, 1999). In the following, an OA with 3-level factors is employed to optimize parameters since it covers a wider range of parameter variations than those of 2-level factors. Table 5.2 shows the orthogonal array *OA(9,4,3,2)* in which 9 times of simulation is required to evaluate the main effects of up to 4 parameters with 3 levels. Each column of OA in Table 5.2 consists

of '0', '1' and '2', which represent different levels. Parameters are assigned to the columns in OA whereas rows represent the parameter setting method for efficiently screening main effect of each parameter concerned. In case the number of parameters is less than the column number, those columns not assigned are left to be empty. Hence, the orthogonal array with equal or more number of columns than the parameters' number should be chosen. Moreover, a smallest possible orthogonal array is recommended since the number of simulations becomes larger accordingly with the increase of an OA size.

Table 5.1 OA (9,4,3,2) orthogonal array

Run Number	Parameters				SN ratio
	1 (*A*)	2 (*B*)	3 (*C*)	4 (*D*)	
1	0	0	0	0	SN_1
2	0	1	1	2	SN_2
3	0	2	2	1	SN_3
4	1	0	1	1	SN_4
5	1	1	2	0	SN_5
6	1	2	0	2	SN_6
7	2	0	2	2	SN_7
8	2	1	0	1	SN_8
9	2	2	1	0	SN_9

5.4 Formulation of Updating Using SN Ratio

Without loss of generality, a model updating problem with 4 design variables, *A*, *B*, *C* and *D*, is considered to be optimized using Taguchi method. The design variables correspond to parameters of analytical model to be updated. Here*, OA(9,4,3,2)* shown in Table 5.1 is used to explain the following updating process. Each design parameter can be assigned to columns arbitrarily. For convenience, the parameters, *A*, *B*, *C* and *D*, are assigned from the

first column to next columns in sequence. In the orthogonal array, '1' represents the current level of parameters whereas '0' and '2' represent the decreased and increased levels, respectively, by predefining level intervals of each parameter Δ_i, *i*=*A, B, C*, and *D*. The main effect on SN ratio of decreased or increased value of parameters, which are represented by '0' and '2', respectively, are compared with the main effect of current level '1' of parameters. Then the parameters are adjusted according to the evaluated main effect of each parameter in order to maximize SN ratio. This procedure continues iteratively until SN ratio tends to be stable.

In order to study the main effect of each parameter concerned, a total of 9 simulations associated with rows in *OA(9,4,3,2)* should be performed. For instance, considering the first and second rows in *OA(9,4,3,2)*, the corresponding SN ratios are calculated from setting levels of each parameter according to the row vectors of OA as,

$$SN_{\mathbf{1}}^{k} = SN\left(A_{\mathbf{0}}^{k}\ B_{\mathbf{0}}^{k}\ C_{\mathbf{0}}^{k}\ D_{\mathbf{0}}^{k}\right) \text{ and } SN_{\mathbf{2}}^{k} = SN\left(A_{\mathbf{0}}^{k}\ B_{\mathbf{1}}^{k}\ C_{\mathbf{1}}^{k}\ D_{\mathbf{2}}^{k}\right), \tag{5.6}$$

where SN_j^k, *j*=1, 2 are the SN ratios calculated using equation (5.5) and the subscript *j* represents run number of simulations related to rows in OA. Here, the levels '0' and '2' of each parameter, A_i^k, B_i^k, C_i^k, and D_i^k, *i*=0, 2, can be obtained from the current level '1' of parameters, $A_{\mathbf{1}}^k$, $B_{\mathbf{1}}^k$, $C_{\mathbf{1}}^k$, and $D_{\mathbf{1}}^k$, as,

$$A_{\mathbf{0}}^{k} = A_{\mathbf{1}}^{k} - \Delta_A^k,\ B_{\mathbf{0}}^{k} = B_{\mathbf{1}}^{k} - \Delta_B^k,\ C_{\mathbf{0}}^{k} = C_{\mathbf{1}}^{k} - \Delta_C^k,\ D_{\mathbf{0}}^{k} = D_{\mathbf{1}}^{k} - \Delta_D^k,$$

$$A_{\mathbf{2}}^{k} = A_{\mathbf{1}}^{k} + \Delta_A^k,\ B_{\mathbf{2}}^{k} = B_{\mathbf{1}}^{k} + \Delta_B^k,\ C_{\mathbf{2}}^{k} = C_{\mathbf{1}}^{k} + \Delta_C^k \text{ and } D_{\mathbf{2}}^{k} = D_{\mathbf{1}}^{k} + \Delta_D^k. \tag{5.7}$$

Here superscript *k* represents the iteration number accounting for iterative updating process. Similar to $SN_{\mathbf{1}}^k$ and $SN_{\mathbf{2}}^k$, other SN ratios (*j*=3,4,...,9) can also be obtained. Then, the

average SN ratios for levels $A_{\mathbf{0}}^k$, $A_{\mathbf{1}}^k$ and $A_{\mathbf{2}}^k$ of parameter A, $SN\left(A_{\mathbf{0}}^k\right)$, $SN\left(A_{\mathbf{1}}^k\right)$ and $SN\left(A_{\mathbf{2}}^k\right)$ can be calculated from the corresponding columns of OA as,

$$SN\left(A_0^k\right)=\frac{SN_1^k+SN_2^k+SN_3^k}{3},\quad SN\left(A_1^k\right)=\frac{SN_4^k+SN_5^k+SN_6^k}{3}$$

$$\text{and}\quad SN\left(A_2^k\right)=\frac{SN_7^k+SN_8^k+SN_9^k}{3}. \tag{5.8}$$

The average SN ratio $SN\left(B_{\mathbf{0}}^k\right)$, $SN\left(B_{\mathbf{1}}^k\right)$ and $SN\left(B_{\mathbf{2}}^k\right)$ for levels $B_{\mathbf{0}}^k$, $B_{\mathbf{1}}^k$ and $B_{\mathbf{2}}^k$, have a similar form. Then, the main effects of parameter at levels, $A_{\mathbf{0}}^k$, $A_{\mathbf{1}}^k$ and $A_{\mathbf{2}}^k$ are given by $\left(SN\left(A_{\mathbf{0}}^k\right)-SN_{ave}^k\right)$, $\left(SN\left(A_{\mathbf{1}}^k\right)-SN_{ave}^k\right)$ and $\left(SN\left(A_{\mathbf{2}}^k\right)-SN_{ave}^k\right)$, respectively. Here, SN_{ave}^k is defined as,

$$SN_{ave}^k=\frac{\left(SN_1^k+SN_2^k+\cdots+SN_9^k\right)}{9}. \tag{5.9}$$

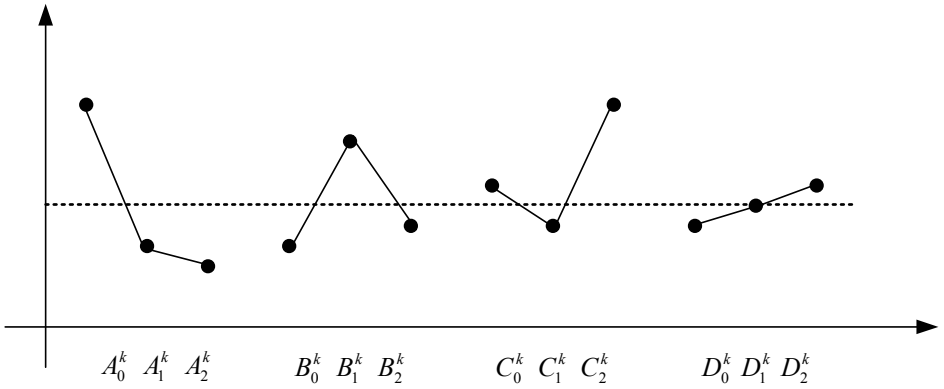

Fig. 5.2 Plots of factor effects: (a) decreasing; (b) level interval adjustment; (c) increasing; (d) ignored.

Similarly, the main effects of parameter at levels, $B_{\mathbf{0}}^k$, $B_{\mathbf{1}}^k$ and $B_{\mathbf{2}}^k$, are given by $\left(SN\left(B_{\mathbf{0}}^k\right)-SN_{ave}^k\right)$, $\left(SN\left(B_{\mathbf{1}}^k\right)-SN_{ave}^k\right)$ and $\left(SN\left(B_{\mathbf{2}}^k\right)-SN_{ave}^k\right)$, respectively. The main effects of other parameters concerned can be obtained in a similar manner. Since orthogonal arrays are perfectly balanced for each parameter, other effects are averaged out in order to calculate the main effect of specific parameters (Park, 1996). As shown in Fig.

5.2, the main effects of each parameter on SN ratio can be effectively visualized in plots of factor effects.

If the main effects are to be evaluated for each parameter at each iteration, analysis of variance (ANOVA) is required to determine the significance of an individual parameter by comparing its variation with the overall variation (Phadke, 1989). The variance of each parameter $V^k(i)$, i= A, B, C and D, is written as,

$$V^k(i) = \left(SN\left(i_{\mathbf{0}}^k\right) - SN_{ave}^k\right)^2 + \left(SN\left(i_{\mathbf{1}}^k\right) - SN_{ave}^k\right)^2 + \left(SN\left(i_{\mathbf{2}}^k\right) - SN_{ave}^k\right)^2. \qquad (5.10)$$

For simplicity, Pareto ANOVA (Park, 1996) is employed to select main parameters for updating and ignore the parameters with slight effect. Only significant parameters, which cumulatively contribute to 95% of total summation variance of each factor, are chosen. For example, as shown in Fig. 5.2, the main effect of parameter *D*, whose variance of main effects is smaller than that of other parameters, is ignored.

In order to show an illustrative example for updating process, the main effects of each parameter are assumed to be represented by the plots of factor effects (Fig. 5.2). Then, the parameters are updated in such a manner that the SN ratio becomes maximum. If the main effect of a parameter decrease or increase according to the parameter change as shown in Fig. 5.2 (a) or (c), then the parameter is adjusted to be decreased or increased at the next step k+1 as,

$$A_1^{k+1} = A_1^k - t\Delta_A^k \text{ and } C_1^{k+1} = C_1^k + t\Delta_C^k, \text{ with } \Delta_A^{k+1} = \Delta_A^k \text{ and } \Delta_C^{k+1} = \Delta_C^k, \qquad (5.11)$$

where t is a constant related to the amount of parameter changes at the next step. In order to check the SN ratio values between levels, the value of t is set to be 0.5. On the other hand, if a parameter approaches to its optimum value, the SN ratio of the parameter becomes maximal at the current level such as B_1^k in Fig. 5.2 (b). Then, the parameter remains the same value as last step and level interval is reduced to half as,

$$B_1^{k+1} = B_1^k \quad \text{and} \quad \Delta_B^{k+1} = \Delta_B^k / 2. \tag{5.12}$$

By reducing the level interval, precise optimum value of parameter can be achieved. In case of small main effect of parameter D, $D_1^{k+1} = D_1^k$ is used instead of increasing the parameter at next step because the main effect of parameter D is ignored due to its small variance. After current level '1' at iteration step k+1 is updated using equations (5.11) and (5.12), other two levels '0' and '2' at step k+1 are calculated using equation (5.7). The same updating process is repeated until optimum values of parameters are obtained when the SN ratio becomes stable.

5.5 A Two-level Scheme for Model Updating

In recent years, some researchers have proposed various methods for FE model updating concerning general structural models in which damping is involved. An efficient way reported is to update FE modeling errors and damping factors in sequence (Lu and Tu, 2004). This kind of updating method concerns updating FE models of lightly damped structures where damping can be neglected when FE modeling errors are updated alone in the first step. Considering the fact that in a lightly damped system, damping has negligible influence on the resonant frequencies of the system, the updating procedure proposed here

is divided into two levels using two different Taguchi updating procedures. In this two-level updating scheme, structural modeling errors and damping coefficients are updated in sequence considering that there is no interaction between these two types of parameters. In the first-level updating, both the experimental and original models are assumed to be free of damping since the structure is lightly damped. Only modeling errors (stiffness and mass parameters in particular) are updated using Taguchi method. Modal data are chosen as reference data for the objective function in this case. Based on the updated modeling errors from the above first-level updating, the second-level updating procedure deals only with damping coefficients. And another objective function based on FRF data, which are complex from experimental structural model, is employed in Taguchi method. Though this two-level updating scheme identify modeling errors and damping coefficients in different levels respectively, this approximate method can obtain the identified results with reasonable accuracy especially damping coefficients even noise-contaminated measured data are used, which will be shown in numerical example later.

5.6 Basic Considerations for the Two-level Updating Scheme

As mentioned in above section, reasonable reference data should be chosen for the objective functions in order to achieve the well identified results. In general, for a lightly damped structure, damping has only negligible influence on the natural frequencies and mode shapes whereas it affects the magnitudes of FRF data at the regions of resonances and anti-resonances largely. Therefore, considering damping is neglected in the first-level updating, we prefer modal data as reference data rather than FRF data in the first-level

updating and choose the objective function which is based on modal data. For the modal data based objective function, W_ω=15 and $W_\phi = 1$ are suggested for numerical simulations in order to highlight the influence of natural frequencies on updated results since mode shapes are more sensitive to damping. It should be noted that the identified modal data of practical structures are always complex due to damping properties. Hence, it is recommended that the absolute values (norm modulus) of complex modal data should be selected for updating modeling errors. It is believed that this approximation will not introduce large errors in the updating procedure. However, in the second-level updating, the reference data and objective function to be chosen should be more sensitive to damping property change since damping coefficients are the target parameters to be identified after model errors have been updated. Hence, FRF data are considered for updating damping coefficients in the second-level updating due to the fact that the experimentally measured FRF data are general complex in practical vibration test and the magnitudes and phases of complex FRF data are more likely to be affected by damping property change. Moreover, it should be noted that the FRF data in the vicinity of resonant and anti-resonant frequencies are heavily influenced by damping properties of structures. Therefore, in order to achieve well identified results, only these complex FRF data at the frequency points around the resonant or anti-resonant regions need to be chosen as reference data for the updating procedure. However, the frequency points which are likely to have non-monotonous characteristics of FRF, should be avoided, as mentioned in section 5.2.2.

The identification of damping in structural systems is extremely important in structural

dynamics since the transient response, transmissibility, decay time or other characteristics of a structural system are dominated by energy dissipation. However, unlike the overall stiffness and mass matrices, the damping matrix is hard to be constructed from the element damping matrix as what we do for stiffness matrix since understanding of damping mechanisms is still quite primitive. In the present study, we focus on the identification of the damping coefficient values under a preselected element damping model. For this purpose, a special element damping model of generally damped systems is employed. For simplicity, it is assumed that the individual element damping matrix has the same form as that of the element stiffness matrix. Since the damping matrix $[D]$ is a linear combination of the element damping matrices, then a p-value formulation of the damping matrix to be identified can be established as,

$$[D] = \sum_{i=1}^{N} [D_k^e] = \sum_{i=1}^{N} p_d^i [K_i^e], \tag{5.13}$$

where $[D_i^e]$ and $[K_i^e]$ are the element damping matrix and element stiffness matrix, respectively and p_d^i is the parameter with respect to the i^{th} element damping matrix. The damping matrix represented by equation (5.13) implies that the overall damping model of the structure is proportional at element level. This is a practical consideration in the identification of damping coefficients of structural systems. Once the damping coefficients are identified using experimental data from vibration test, an updated FE model can be constructed including damping matrix, which will represent the dynamic characteristics of the experimental model more accurately. It is noted that when the values of damping coefficients p_d^i are the same for all the elements, the overall damping model of the structure becomes proportional.

As damping effect on structural parameters is ignored at the first-level updating, additional errors have been introduced due to the loss of damping when modal data are used for updating. Though this two-level updating scheme is deemed to be efficient for identification of parameters, the influence of the additional errors on updated results should be noted. In case the errors result in a significant reduction in the accuracy of the identification (usually it is not the case for lightly damped structures), repeating the two-level scheme twice in the whole updating process are considered together with various FRF data sets in order to compensate for the influence of additional errors. Hence the expected accuracy of the identified results can be achieved for this case. This solution can also be extended to the case that the damping of general structures is slightly heavy.

5.7 Numerical Case Study

Cantilever Beam with Measurement Noise

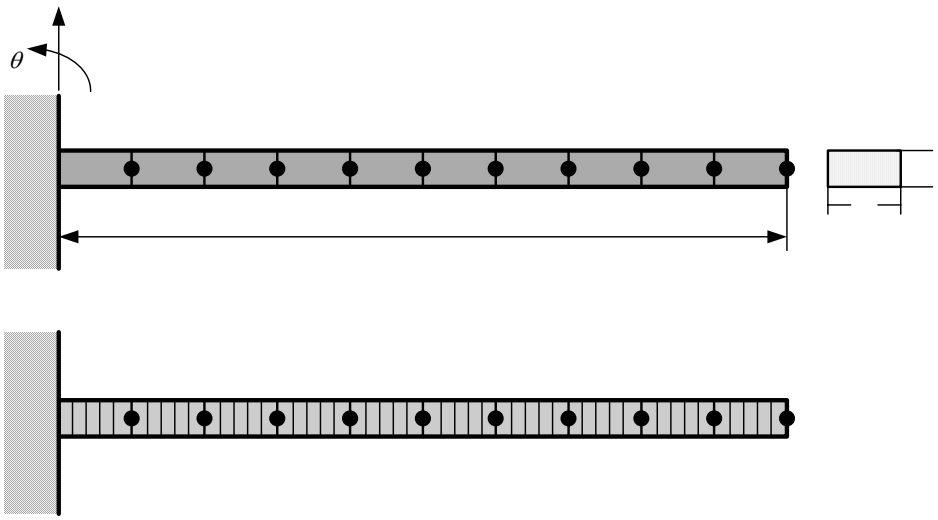

Fig. 5.3 The cantilever beam: (a) analytical model; (b) 'experimental' model (• measurement point).

In order to verify the effectiveness of the proposed two-level scheme when applied to model updating of generally damped structures, the analytical FE model of a cantilever beam shown in Fig. 5.3 (a) is considered. In this case, the FE model of the beam has 20 parameters, which include stiffness parameters and damping coefficients, to be updated. The first 10 non-dimensionalized parameters associated with stiffness, β_i, are defined as the ratios of Young's modulus, $\beta_i = E_i^X / E_i^A$. The other 10 damping coefficients, p_d^i, are selected as given in equation (5.13). In this work, the optimum values of β_i and p_d^i are sought in an iterative way in order to maximize the SN ratio. Therefore, the model updating of the cantilever beam becomes the problem of identifying stiffness parameter errors and damping coefficients in the analytical model. In order to simulate measured data, the 'experimental' model is generated using a refined FE model with 5 times mesh density of the analytical model as shown in Fig. 5.3 (b). This 'experimental' model has stiffness reduction of 50% in the 11^{th}-15^{th} and 16^{th}-20^{th} elements, and 30% in the 31^{st}-35^{th} and 36^{th} -40^{th} elements, respectively. Moreover, the damping matrix of the 'experimental' model is assumed to have the same form as that in equation (5.13). The values of damping coefficients p_d^i are assumed to be 0.05 at and near the joints positions (the 1^{st}-5^{th}, 6^{th}-10^{th} and 11^{th}-15^{th} elements) while those at other positions are all zero. Both complex modal data and FRF data are generated for updating based on the 'experimental' model with damping.

To evaluate the robustness of this updating method, random noise errors in measured data as well as systematic noise errors in the analytical model are considered. For systematic noise errors, parameter error is included such that the density, ρ =7895 kg/m^3, is used for

the analytical model whereas the density of the 'experimental' model is assumed to be ρ =7973.95 kg/m^3 which is 1% higher than that of the analytical model. As discussed before, in the first level updating, modal data from the 'experimental' model are used as reference data for the objective function. Due to the difficulties in the measurement of rotational DOFs in practice, only mode shape data from translational DOFs in the 'experimental' model are adopted during the formulation of the objective function in equation (5.1). Generally, the lower modes of FE model are subject to little discretization errors. Therefore, considering the discretization effect, the first 8 modes are used as reference data for updating the 10 stiffness parameters of the analytical model. In order to demonstrate the robustness of the method against random noise, 1% and 5% random noises are added to natural frequencies and mode shapes of simulated 'experimental' data, respectively. Here, it should be noted that the real absolute values of the 'experimental' complex mode shape vectors are employed during updating process.

To assess the main effect of each stiffness parameter, orthogonal array, $OA(27,13,3,2)$, which requires 27 runs of simulations at each iteration, is employed in optimization. And 10 parameters for updating are assigned to $OA(27,13,3,2)$ in sequential manner and last 3 columns of the array are left to be empty. The initial values of stiffness parameters are set to be $\beta_i^{\mathbf{1}}=1$, $i=1,2,..,10$, with initial level intervals to be $\Delta_{\beta_i}^{\mathbf{1}}=0.2$, $i=1,2,..,10$. Here, the initial level intervals can be chosen from a wide range of values considering practical situation of model updating. For physical consideration, initial level intervals should be set between 0 and 1. If too small initial level intervals are used, the main effect of parameters

may be subject to the effect of noises and convergence tends to be slow. On the other hand, initial level intervals close to 1 should be avoided since the pairing of natural frequencies and mode shapes can be unreliable due to the large variance of parameters. Note that the level intervals are apt to be smaller value because the level intervals are decreased by half using equation (5.12) when the parameters approach to the optimum value. Therefore, after dozens of iteration, the level intervals would be very small and updating process might slow down. However, the problem can be effectively resolved by resetting level intervals, for example, $\Delta_{\beta_i}^{k}$ =0.01, i=1,2..,10, at every 50 iteration (k=50, 100, 150, etc).

As can be seen in Table 5.2, the difference between analytical and 'experimental' modal data, such as natural frequency and mode shape (MAC), has been reduced significantly by updating the parameters of the analytical model. During the updating process, parameter errors in the analytical model are located and corrected as shown in Fig. 5.4. From Fig. 5.4,

Table 5.2 Modal data of the 'experimental', analytical and updated models of the cantilever beam

Mode No.	'Experimental' Frequency (Hz)	Analytical Frequency	Errors (%)	Initial MAC	Updated Frequency	Errors (%)	Updated MAC
1	4.34 + 0.11i	4.95	14.4	0.9995	4.35 + 0.11i	0.32	0.9999
2	28.46 + 0.25i	31.03	9.1	0.9994	28.22 + 0.27i	0.85	0.9999
3	73.21 + 0.80i	86.90	18.7	0.9985	73.63 + 0.84i	0.59	0.9998
4	153.5 + 1.92i	170.41	11.1	0.9958	152.84 + 2.16i	0.46	0.9998
5	250.31 + 2.31i	282.13	12.7	0.9918	251.48 + 2.35i	0.47	0.9992
6	381.12 + 3.14i	422.67	10.9	0.99	381.05 + 3.67i	0.13	0.9992
7	528 + 6.55i	593.03	12.4	0.9833	531.5 + 6.69i	0.66	0.9982
8	685.01 + 6.82i	794.49	16.0	0.9748	698.8 + 7.79i	2.01	0.9962
9	896.08 + 9.28i	1027.3	14.7	0.9674	916.64 + 10.8i	2.30	0.9975
10	1113.3 + 11.68i	1277	14.7	0.9916	1131.2 + 11.8i	1.61	0.9975

it can be observed that compared with the actual errors introduced, the parameter errors have been identified with reasonable accuracy even in presence of both random noises and systematic errors. And then, since the corrected stiffness parameter have been obtained, the corresponding improved analytical model can be constructed with confidence for further identification of damping coefficients in next step.

Fig. 5.5 shows the SN ratio plot of the updating process of stiffness parameters, where SN ratio seems to have reached a maximum value after 200 iterations. However, according to the changed value of the level interval given by equation (5.12), the level interval may become very small after a substantial number of iterations. This small level interval might result in a local minimum solution. However, the possibility of this local minimum solution can be avoided effectively by resetting level interval as shown in SN ratio plot of Fig. 5.5.

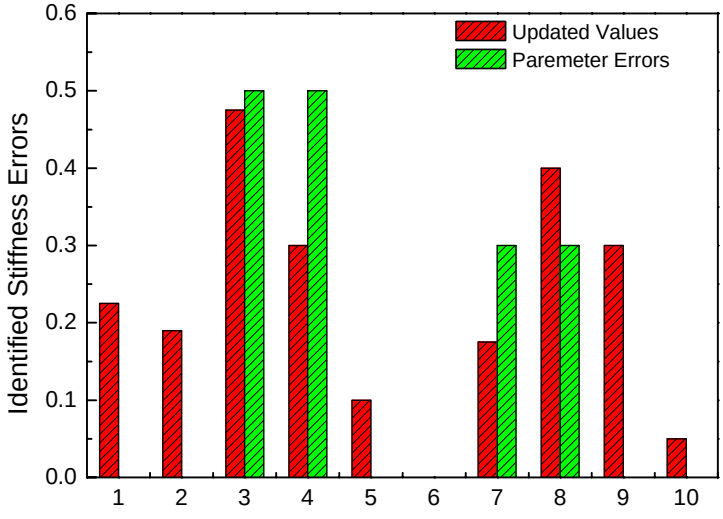

(a) 5th iteration

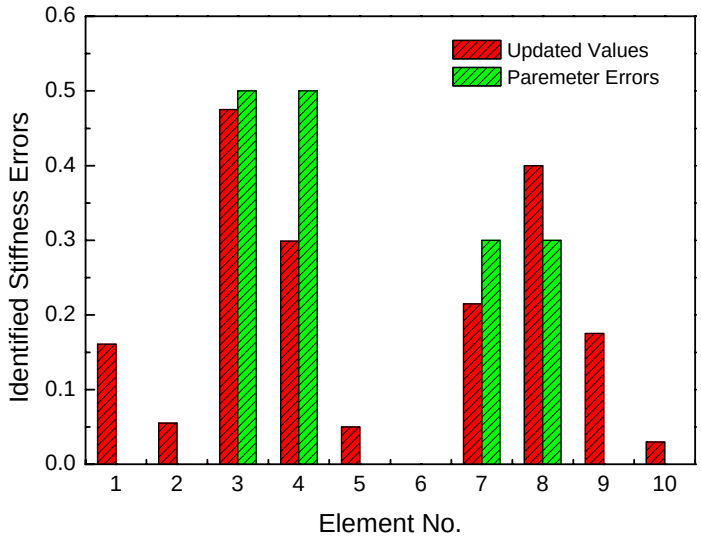

(b) 50th iteration

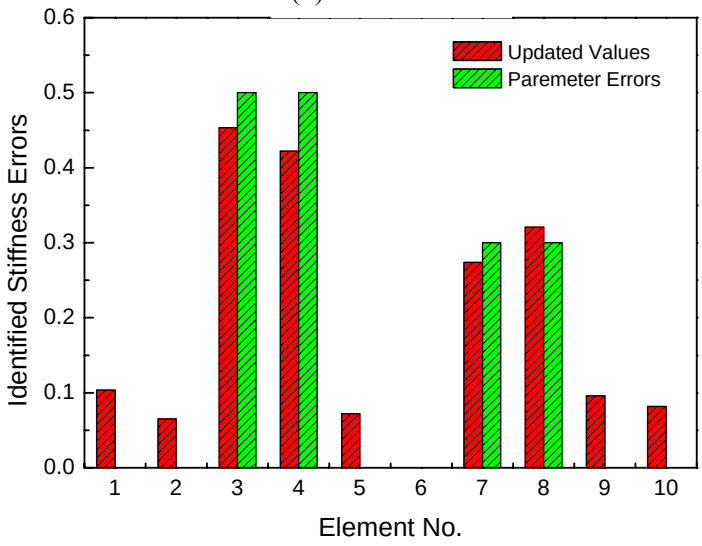

(c) 100th iteration

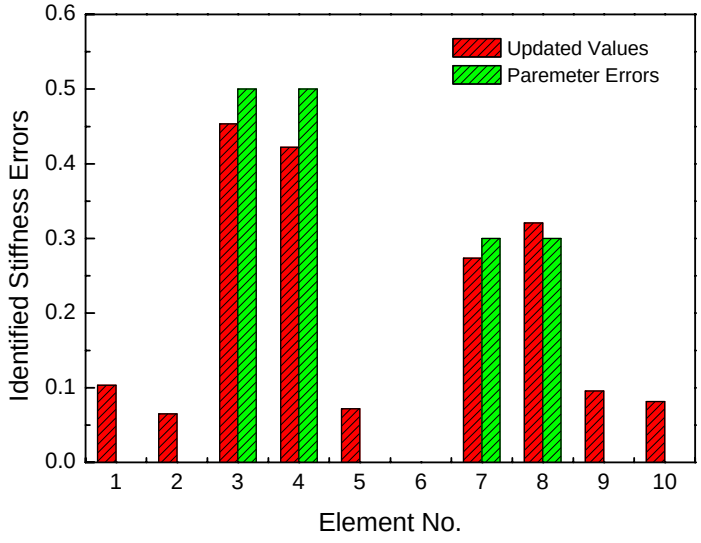

(d) 200th iteration

Fig. 5.4 Iteration results for identification of stiffness parameter errors

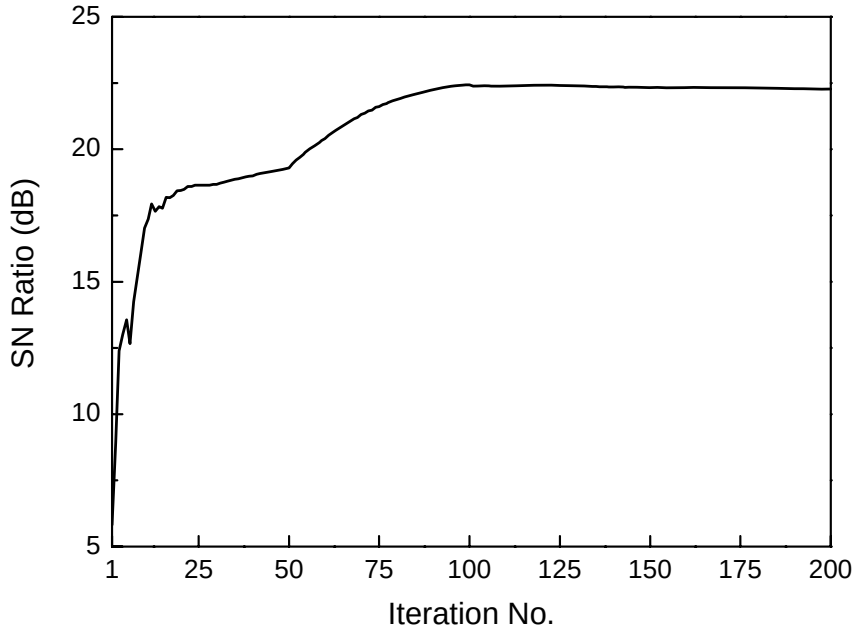

Fig. 5.5 SN ratio plot of updating process of stiffness parameters

Since the stiffness parameters have been well updated using Taguchi method in the first step, now the damping coefficients need to be identified based on the primarily modified model without damping. In the second level updating, the incomplete 'experimental' FRF data are used as reference data for the objective function due to the unavailable rotational DOFs. The five sets of FRF data, which are measured at node 2, 4, 6, 8 and 10 with excitation point at node 10 (free end), are selected from all simulated 'experimental' FRF data. Each 'experimentally' measured FRF, which is contaminated by measurement random noise, is assumed to have the form as,

$$H'_j(\omega_k) = H_j(\omega_k)(1+\sigma), \ (j = 2,4,6,8,10)\,, \tag{5.14}$$

where H'_j indicates contaminated 'experimental' FRFs by noise and subscript j in FRFs represents the measurement point as shown in Fig. 5.3 (b). In order to evaluate the robustness of the Taguchi method against measurement noise, the uniformly distributed random noise σ is assumed to be 5% in this study. The initial values of damping

coefficients in the analytical model are all set to be 0, i.e. p_d^i=0, i=1, 2.., 10. As shown in Fig. 5.6, there are significant differences between the FRFs of the analytical model and the simulated 'experimental' FRF data. These differences are to be corrected by identifying damping coefficients of the updated analytical FE model later. As mentioned earlier, in order to optimally identify damping coefficients, the complex FRFs at 6 specific frequency points (24 Hz, 70 Hz, 180 Hz, 260 Hz, 350 Hz and 520 Hz) are quite carefully selected from simulated 'experimental' data at the frequency points around the resonant or anti-resonant regions such that FRFs at frequency points which fall within non-monotonic regions can be avoided.

Similar to the first level updating, the same orthogonal array is employed to evaluate the main effects of the 10 damping parameters and these parameters are assigned to the orthogonal array in sequential manner. The initial level intervals, $\Delta^1_{p_d^i}$, i=1,2..,10, are set to 0.005, which correspond to 10% of target parameters. Usually, due to the influence of noises on the main effect of parameters and slow convergence, too small initial values of level intervals are kept from being selected. On the other hand, initial level intervals with large values should be avoided because too much deviation of the analytical data from the experimental data may result in non-monotonous characteristics of FRFs at specific frequency points. To avoid a local minimum solution and slow updating process, level interval values are reset to be 0.001 after dozens of iterations.

Since damping information in FRFs has smaller values as compared with stiffness information in FRFs, a longer iteration procedure is needed for the identification of

damping parameters. As shown in Fig. 5.7, the identified results of damping parameters are obtained through 350 iterations. It can be seen that the identified results may not be accurate enough as compared with that of stiffness parameters in terms of location as well as magnitude as seen in Fig. 5.4 (d). Nevertheless, the identified results are close to the exact damping parameters with reasonable accuracy as shown in Fig. 5.7 (d). It can be seen from Fig. 5.6 that the differences between regenerated and 'experimental' FRFs are reduced significantly by maximization of SN ratio. The increased SN ratio means closeness between analytical and 'experimental' data as shown in Fig. 5.8. The identified results would be further improved if more suitable FRFs are used as reference data. However, selecting stable frequencies out of a large number of frequency points may also result in loss of damping information. It should be noted that there still exists a problem how optimum frequency points can be selected, which needs to be investigated further.

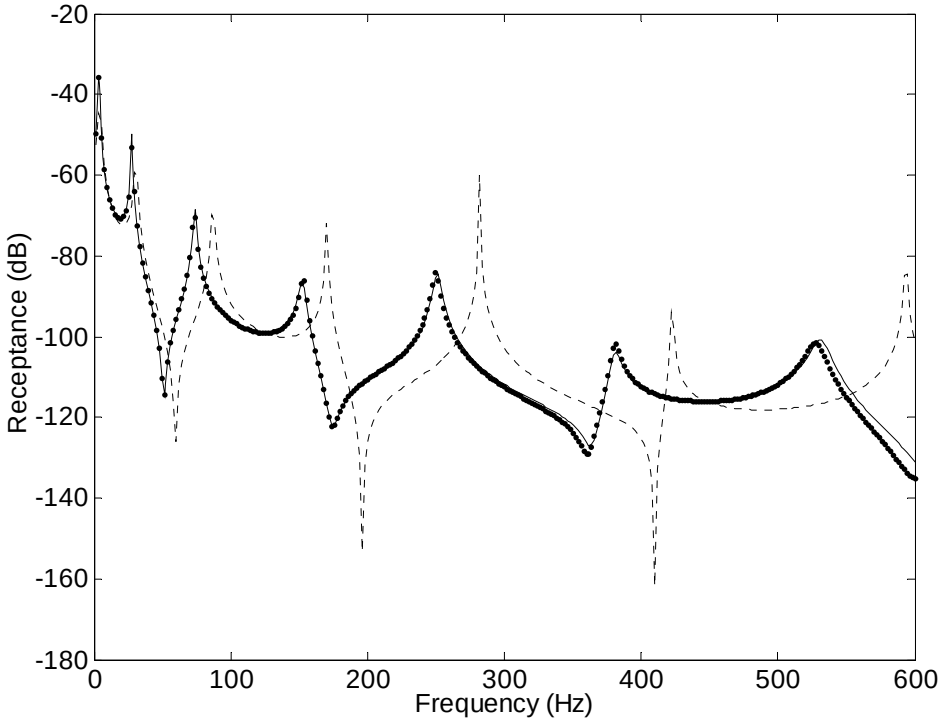

Fig. 5.6 Comparison of the analytical, the 'experimental' and the updated FRF curves ($H_6(\omega)$) (------- analytical, • experimental and —— updated.)

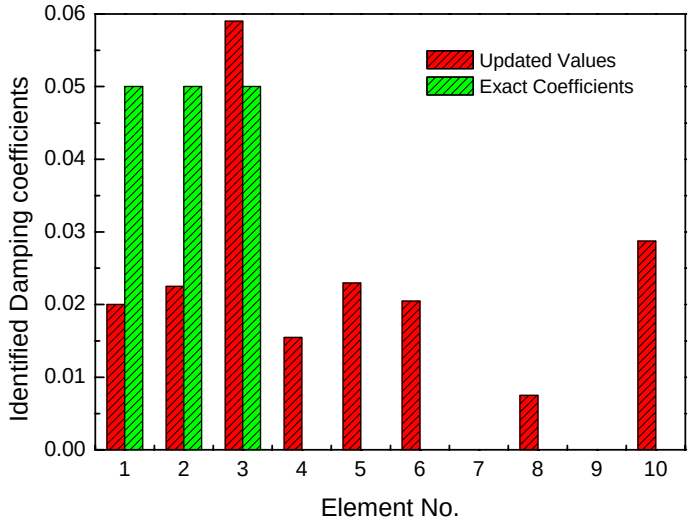

(a) 10th iteration

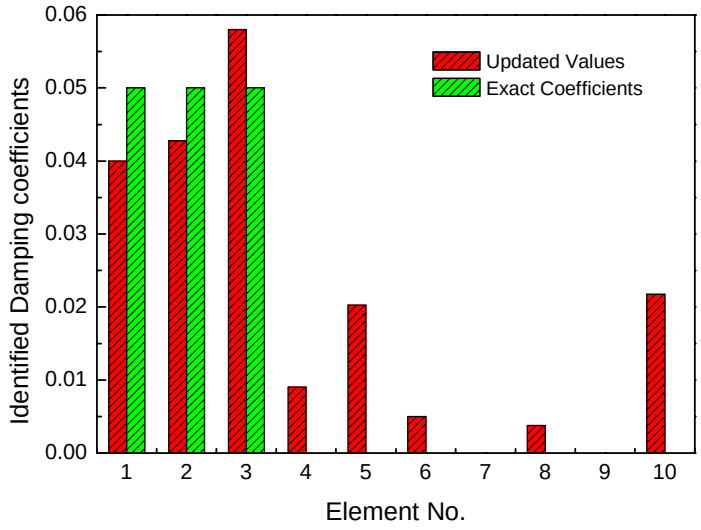

(b) 100th iteration

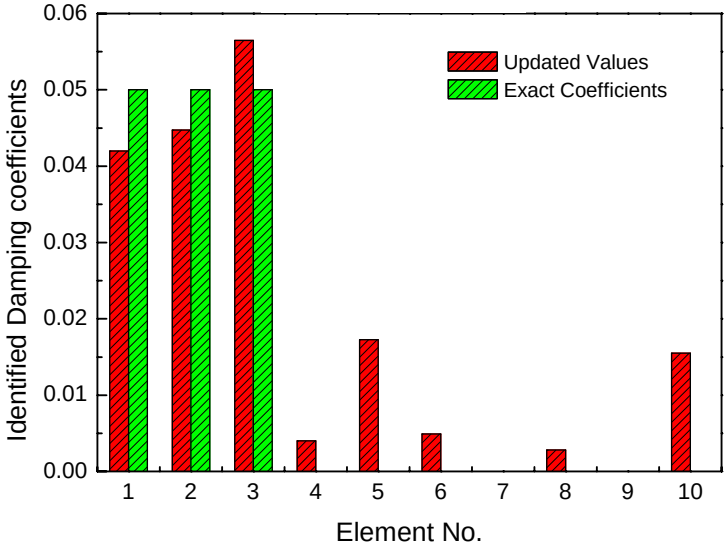

(c) 200th iteration

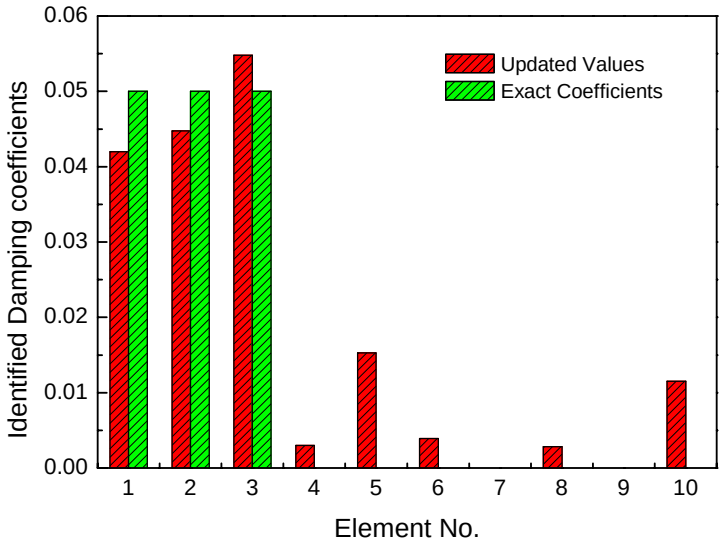

(d) 350th iteration

Fig. 5.7 Iteration results for identification of damping parameters

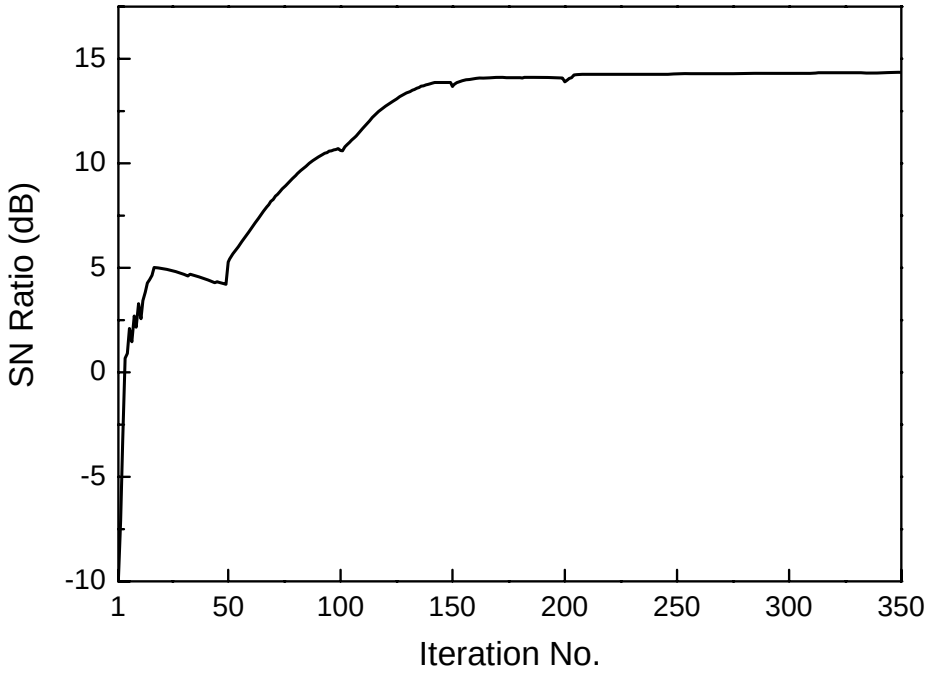

Fig. 5.8 SN ratio plot of updating process of damping parameters

5.8 Summary

In this chapter, Taguchi method has been further applied to the case of FE model updating of damped structures by optimizing the objective function. In order to identify damping

property effectively, a two-level updating scheme of the Taguchi method has been proposed to update stiffness modeling errors and identify damping coefficients respectively in different levels. A numerical example based on a cantilever beam with structural damping demonstrates that Taguchi method is feasible and efficient when applied to identification of damped structures even using noise-contaminated test data. The updated results of stiffness modeling errors and damping coefficients are reasonably accurate and robust against random and systematic noise errors even in case of a high level noise. Moreover, the method can be computationally efficient since the orthogonal array is employed rather than stochastic search. For reference data, modal data and FRF data are used for the different objective functions in the two different levels respectively since modeling errors and damping coefficients are identified sequentially in the two-level updating scheme.

Chapter 6

Model Updating Using Vibration Test Data Under Base Excitation

This chapter presents a new method which employ measured data under base excitation for model updating. Mathematical formulations directly using measured response function data under base excitation to identify modeling errors, have been established. The simulated numerical case studies have been performed to investigate the feasibility of the proposed method. In addition, the effect of measurement noise in response function data on this updating method has also been studied.

6.1 Introduction

Modal testing is widely and successfully used for the determination of vibration properties of structural systems in engineering practice. In many situations of modal testing, in order to simulate operational loads, base motion excitation is involved in simulated operational tests. Due to the size limitation of microsystems, base excitation is also an indispensable technique applied in vibration testing of microsystems. Although base excitation test by itself is a technique of vibration measurement, the measured response functions, which are defined by displacement output and acceleration input, do represent the actual dynamic properties of structural systems just as traditional FRFs do. To date, most of the modal testing techniques developed do not specifically address the identification of modal parameters using this type of test data acquired using base excitation. Beliveau *et al*. (1986) considered the relative motion of a structural system with respect to its base and presented a procedure to obtain modal information directly from the measured frequency response of the acceleration for the case of base excitation. Vigneron and Soucy (1987) proposed a method for modal parameters estimation from driven-base tests based on the relationship

between response function data under base excitation and conventional frequency response functions. Thomas, *et al*. (1989) developed a method which can be used to convert the motion-to-motion FRFs under base excitation test into motion-to-force FRFs using the equation of relative motion. Then, the modified FRF data could be analyzed directly using algorithms of modal parameter estimation. Lee and Chou (1991) presented a formulation to describe response functions under driven-base excitation for continuous structures with both input and output being accelerations. A similar formulation by having displacement as output instead was established by Chen *et al*. (1995). Chou and Wang (2001) derived a mathematical model to characterize frequency response functions between input and output velocities and then modal parameters could be extracted based on the measured response functions in the case of base excitation.

It is believed that in the current state of practice, only a few of the model updating methods are capable of incorporating base excitation test data directly. This may be because most of updating methods developed assume the availability of measured FRF data or modal data which can be acquired relatively easily using most existing modal testing techniques. Mark (1998) presented an updating procedure, in which a large mass was introduced to convert the driving motions (base excitations) into equivalent external excitation forces so that test data under base excitation can be used in FRF based updating methods indirectly. However, some approximation about the applied forces has been made during the modeling procedure. Moreover, the value of the large mass can not be determined accurately, which is usually chosen based on experiences and can affect the accuracy of the updated results. In fact, base excitation test data can be adopted to update FE models directly since the measured response function data naturally represent the vibration properties of structural systems. And model updating using base excitation test data is likely to be more appropriate than

using modal data. This is because modal analysis may introduce additional analysis errors and the obtained modal data are usually incomplete due to the limitation of test techniques.

In the response based model updating method the response function measured under base excitation can be considered as correlation targets directly. In this case, the method of updating would seem particularly similar to the FRF based updating methods since the properties of the response functions measured in case of base excitation test are similar to FRFs obtained from force input. Moreover, an updating method based on test data under base excitations is sometimes more appropriate for updating FE models of both macro/large and micro/small structural systems. This is because a base excitation technique using shakers is usually more preferred in the vibration testing of structures with very small feature size where conventional testing techniques such as attaching an exciting shaker or using an impulse hammer becomes difficult to apply.

In the following sections, a new model updating method will be presented which seeks to update analytical FE models of a group of structures on which only vibration tests under base excitations can be made to measure response functions. Compared with other existing FRF based updating methods, the proposed new method has the advantage that it can be applied to updating erroneous FE models accurately using measured response function data under base excitation directly. In order to demonstrate the practical applicability of the proposed method, extensive numerical simulations have been carried out based on a cantilever beam and a truss structure as well as a typical experimental example.

6.2 Base Excitation

Typically modal testing involves exciting a structural system with either an impact hammer or a shaker. The location and magnitude of the loads are selected such that enough energy can be imparted to the system to excite the modes of interest. In many applications, the information needed from a test is not only for the identification of the modes, but also for the verification of the response to operational loads. For this reason, simulated operational tests are performed, many of which involve the applications of base motion excitations. In this type of test, a test structure is fixed onto a shake table or displacement driven actuators subject to controlled motions. Usually, to evaluate the response to road input, automotive systems are tested based on known road/base excitation inputs. Many aerospace components are also tested in this manner to evaluate their dynamic responses to launch, or flight vibrations. Due to the limitation of input techniques when applied to test structures with small feature size, vibration tests of micro-systems such as hard disk drive are also performed using base excitation test to investigate the dynamic characteristics of these systems.

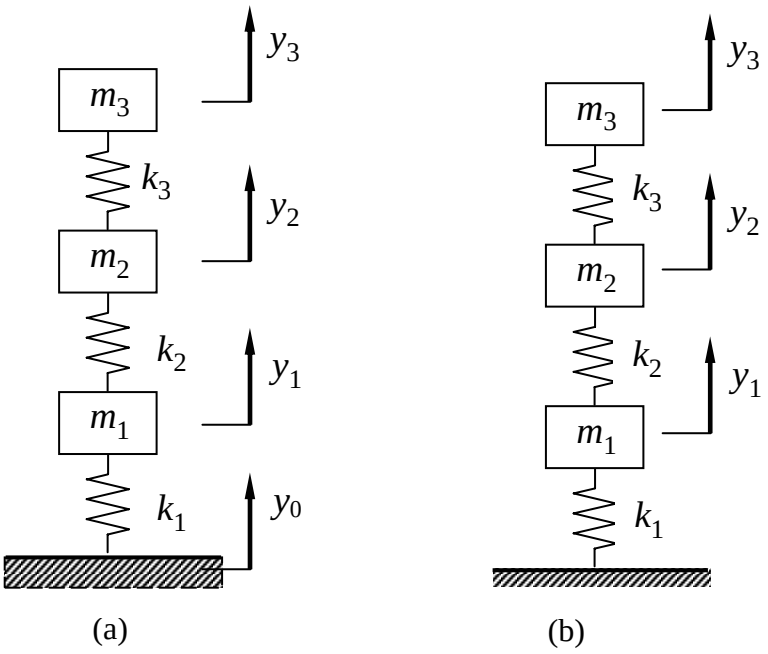

Fig. 6.1 A three DOFs mass-spring system with a (a) moving base (b) fixed base

In engineering practice, base-excitation model is widely used for studying buildings subjected to earthquakes, packaging during transportations, vehicle responses, and even the design of accelerometers. In order to demonstrate the basic concept of base excitation, a simple mass-spring system with three degrees-of-freedom (DOF) shown in Fig. 6.1(a) is considered. Here, all DOFs of the system are relative to ground. Hence the measured responses of the system would also be relative to ground (In the later formulas and examples, if not specifically mentioned, all the responses would be relative to ground). The system is only subjected to a displacement input from the moving base. The governing equations of motion of this mass-spring system with base excitation are written as,

$$\begin{cases} m_3\ddot{y}_3 + k_3(y_3 - y_2) = 0 \\ m_2\ddot{y}_2 + k_2(y_2 - y_1) + k_3(y_2 - y_3) = 0 \\ m_1\ddot{y}_1 + k_1(y_1 - y_0) + k_2(y_1 - y_2) = 0 \end{cases}, \tag{6.1}$$

where y_0 is the displacement input of the base. Assume that the displacement responses are expressed as $y_j = Y_j e^{i\omega t}$ $(j = 1, 2, 3)$ due to a base excitation input $y_0 = Y_0 e^{i\omega t}$. Then (6.1) can be re-written in matrix form in frequency domain as,

$$\left(\begin{bmatrix} k_3 & -k_3 & 0 \\ -k_3 & k_3 + k_2 & -k_2 \\ 0 & -k_2 & k_2 + k_1 \end{bmatrix} - \omega^2 \begin{bmatrix} m_3 & 0 & 0 \\ 0 & m_2 & 0 \\ 0 & 0 & m_1 \end{bmatrix} \right) \begin{Bmatrix} y_3 \\ y_2 \\ y_1 \end{Bmatrix} = \begin{Bmatrix} 0 \\ 0 \\ k_1 y_0 \end{Bmatrix}. \tag{6.2}$$

Now, define new response functions with base excitation input as $H_j \equiv y_j / y_0$ $(j = 1, 2, 3)$, after some manipulation, (6.2) becomes,

$$\left(\begin{bmatrix} k_3 & -k_3 & 0 \\ -k_3 & k_3 + k_2 & -k_2 \\ 0 & -k_2 & k_2 + k_1 \end{bmatrix} - \omega^2 \begin{bmatrix} m_3 & 0 & 0 \\ 0 & m_2 & 0 \\ 0 & 0 & m_1 \end{bmatrix} \right) \begin{Bmatrix} H_3 \\ H_2 \\ H_1 \end{Bmatrix} = \begin{Bmatrix} 0 \\ 0 \\ k_1 \end{Bmatrix}. \tag{6.3}$$

Upon solving (6.3), the response functions of the system with base excitation input can be obtained as,

$$\begin{Bmatrix} H_3 \\ H_2 \\ H_3 \end{Bmatrix} = \left[\begin{bmatrix} k_3 & -k_3 & 0 \\ -k_3 & k_3+k_2 & -k_2 \\ 0 & -k_2 & k_2+k_1 \end{bmatrix} - \omega^2 \begin{bmatrix} m_3 & 0 & 0 \\ 0 & m_2 & 0 \\ 0 & 0 & m_1 \end{bmatrix} \right]^{-1} \begin{Bmatrix} 0 \\ 0 \\ k_1 \end{Bmatrix}. \qquad (6.4)$$

Based on equation (6.4), a typical response function, which is the transfer function between response output y_3 and base excitation input y_0, has been calculated and is shown in Fig. 6.2(a). Compared with conventional FRF of the same mass-spring system fixed to the ground with the input excitation force being applied at coordinate y_1, the curve of the new response function under base excitation has similar shape to that of the conventional FRF, although the actual values of amplitudes of the two curves are different. The frequency locations of the resonance peaks of the two different types of response functions are the same. This means that the natural frequencies of the system measured using base excitation test are the same as those measured using input excitation force. If appropriate modal test and modal analysis techniques are used, modal data such as natural frequency, mode shape and damping ratio can also be obtained from the measured response functions under base excitation.

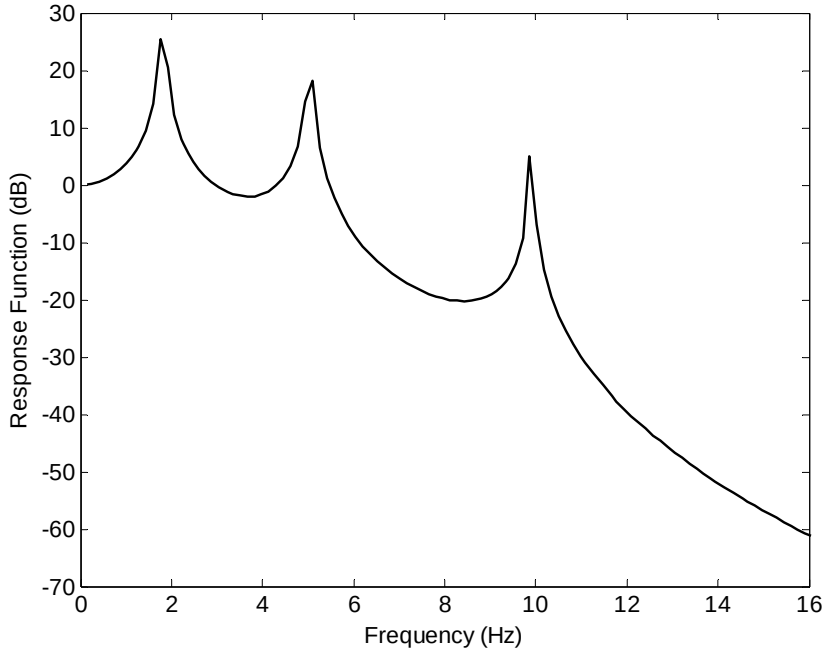

(a) with base excitation

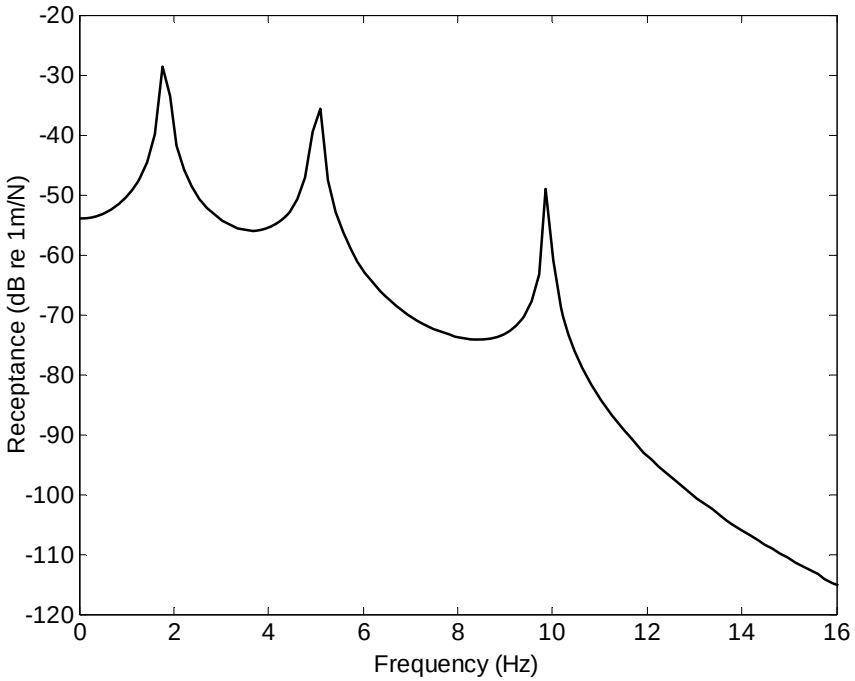

(b) with force excitation

Fig. 6.2 Response functions of a system with moving and fixed bases

6.3 Model Updating Using Vibration Test Data Under Base Excitation

6.3.1 Theory

To demonstrate how a model updating method using vibration test data under base excitation can be developed, the mass-spring system shown in Fig. 6.1(a) with analytical modeling errors is first considered. The equations (6.3) of motion of the experimental model and the analytical model of the system can be written respectively as,

$$([K_X]-\omega^2[M_X])\ \{H_X\} = \{F_X\}, \tag{6.5}$$

$$([K_A]-\omega^2[M_A])\ \{H_A\} = \{F_A\}, \tag{6.6}$$

where $\{H_X\}$ and $\{H_A\}$ are the experimental and analytical response functions under base excitation and, $\{F_A\}=\{0\ \ 0\ \ k_1\}^T$ and $\{F_X\}=\{0\ \ 0\ \ (k_1+\Delta k_1)\}^T$ respectively. Assume that $[K_X]=[K_A]+[\Delta K]$, $[M_X]=[M_A]+[\Delta M]$ and $\{F_X\}=\{F_A\}+\{\Delta F\}$, upon subtracting equation (6.6) from equation (6.5) and rearranging, one has,

$$([\Delta K]-\omega^2[\Delta M])\{H_X\}=-([K_A]-\omega^2[M_A])\{\Delta H\}+\{\Delta F\}. \tag{6.7}$$

A model updating formula can then be developed based on equation (6.7) to identify stiffness and mass modeling errors $[\Delta K]$ and $[\Delta M]$, assuming that $[K_A]$ and $[M_A]$ are given and $\{H_X\}$ has been measured. The formulation of such an updating procedure is presented as follows. Upon substituting the actual parameters of the mass-spring system into equation (6.7), one has,

$$\begin{bmatrix} \Delta k_3-\omega^2\Delta m_3 & -\Delta k_3 & 0 \\ -\Delta k_3 & \Delta k_3+\Delta k_2-\omega^2\Delta m_2 & -\Delta k_2 \\ 0 & -\Delta k_2 & \Delta k_2+\Delta k_1-\omega^2\Delta m_1 \end{bmatrix}\begin{Bmatrix} H_{3X} \\ H_{2X} \\ H_{1X} \end{Bmatrix}=\begin{Bmatrix} 0 \\ 0 \\ \Delta k_1 \end{Bmatrix}$$

$$-\begin{bmatrix} k_{3A}-\omega^2 m_{3A} & -k_{3A} & 0 \\ -k_{3A} & k_{3A}+k_{2A}-\omega^2 m_{2A} & -k_{2A} \\ 0 & -k_{2A} & k_{2A}+k_{1A}-\omega^2 m_{1A} \end{bmatrix}\begin{Bmatrix} H_{3X}-H_{3A} \\ H_{2X}-H_{2A} \\ H_{1X}-H_{1A} \end{Bmatrix}, \tag{6.8}$$

where $\{H_X\}\equiv\{H_{3X}\quad H_{2X}\quad H_{1X}\}^T$ and $\{H_A\}\equiv\{H_{3A}\quad H_{2A}\quad H_{1A}\}^T$. After some further mathematical manipulations, equation (6.8) can be turned into the following,

$$\begin{bmatrix} -\omega^2 H_{3X} & 0 & 0 & H_{3X}-H_{2X} & 0 & 0 \\ 0 & -\omega^2 H_{2X} & 0 & -H_{3X}+H_{2X} & H_{2X}-H_{1X} & 0 \\ 0 & 0 & -\omega^2 H_{1X} & 0 & -H_{2X}+H_{1X} & H_{1X}-1 \end{bmatrix}\begin{Bmatrix} \Delta m_3 \\ \Delta m_2 \\ \Delta m_1 \\ \Delta k_3 \\ \Delta k_2 \\ \Delta k_1 \end{Bmatrix}$$

$$=-\begin{bmatrix} k_{3A}-\omega^2 m_{3A} & -k_{3A} & 0 \\ -k_{3A} & k_{3A}+k_{2A}-\omega^2 m_{2A} & -k_{2A} \\ 0 & -k_{2A} & k_{2A}+k_{1A}-\omega^2 m_{1A} \end{bmatrix}\begin{Bmatrix} H_{3X}-H_{3A} \\ H_{2X}-H_{2A} \\ H_{1X}-H_{1A} \end{Bmatrix}. \tag{6.9}$$

Equation (6.9) is formulated using response functions under base excitation measured at one single frequency point ω. If sufficient number of frequency data points are used, equation (6.9) will become a set of over-determined equations. And general inverse of the coefficient matrix can be used to solve the equation sets for the unknown mass and stiffness

modeling errors. Subsequently, an updated analytical model can be reconstructed after the modeling errors have been identified.

Having established the formulation of the updating method using measured response functions under base excitation for the simple mass-spring system, application of the method to more general case of continuous systems needs to be developed. For a continuous structural system with moving base, the equations of motion of the system in frequency domain can be written as,

$$([K]-\omega^2[M])\{u\}=\{f\}. \tag{6.10}$$

Here, it is assumed that the structural system under consideration is undamped. For simplicity, assume further that the first node in the FE formulation of the structural system is fixed at the base whose motion is specified, then this node will have the same motion as that of the base. Cases other node(s) being fixed to the base can be similarly treated by rearranging the mass and stiffness matrices. Under the base excitation in this case, the only possible external unknown forces applied to the system are applied at the nodes fixed to the base. Suppose that the displacement vector of the fixed node is $\{\hat{u}_0\}$, equation (6.10) can then be written as,

$$([K]-\omega^2[M])\cdot\begin{Bmatrix}\{\hat{u}_0\}\\ \{\hat{u}\}\end{Bmatrix}=\begin{Bmatrix}\{\hat{f}\}\\ \{0\}\end{Bmatrix}, \tag{6.11}$$

where $\{\hat{u}\}$ is the displacement vector corresponding to those unfixed nodes and $\{\hat{f}\}$ is the unknown external force vector applied at the fixed node. Assume that the stiffness and the mass matrices of the structural system can be partitioned into sub-matrices according to the DOFs of the fixed nodes and the DOFs of the unfixed nodes, as,

$$[K]=\begin{bmatrix}[K_{11}] & [K_{12}]\\ [K_{21}] & [K_{22}]\end{bmatrix}, \quad \text{and} \quad [M]=\begin{bmatrix}[M_{11}] & [M_{12}]\\ [M_{21}] & [M_{22}]\end{bmatrix}, \tag{6.12}$$

where subscript *1* corresponds to the DOFs of the fixed node and subscript *2* corresponds the DOFs of the unfixed nodes, respectively. Upon separating $\{\hat{u}_0\}$ and $\{u\}$ in the displacement vector, we can rewrite equation (6.11) as,

$$([K]-\omega^2[M])\begin{Bmatrix}\{0\}\\ \{\hat{u}\}\end{Bmatrix}=\begin{Bmatrix}\{\hat{f}\}\\ \{0\}\end{Bmatrix}-([K]-\omega^2[M])\begin{Bmatrix}\{\hat{u}_0\}\\ \{0\}\end{Bmatrix}. \tag{6.13}$$

Substituting the sub-matrices of [*M*] and [*K*] into equation (6.13), one can obtain the following two equations,

$$([K_{12}]-\omega^2[M_{12}])\{\hat{u}\}=\{f\}-([K_{11}]-\omega^2[M_{11}])\{\hat{u}_0\}, \tag{6.14}$$

$$([K_{22}]-\omega^2[M_{22}])\{\hat{u}\}=-([K_{21}]-\omega^2[M_{21}])\{\hat{u}_0\}. \tag{6.15}$$

Suppose that the fixed node has motion only in one direction as it is usually the case in base excitation where base motion is specified in one specific direction, the displacement vector of this node $\{\hat{u}_0\}$ can be written as $\{\hat{u}_0\}=\{u_0 \quad 0 \quad 0 \quad 0 \quad 0 \quad 0\}^T$ (considering one node has six DOFs). Then, upon dividing both sides by u_0, equations (6.14) and (6.15) become,

$$([K_{12}]-\omega^2[M_{12}])(\{\hat{u}\}/u_0)=(\{\hat{f}\}/u_0)-([K_{11}]-\omega^2[M_{11}])\{e\}, \tag{6.16}$$

$$([K_{22}]-\omega^2[M_{22}])(\{\hat{u}\}/u_0)=-([K_{21}]-\omega^2[M_{21}])\{e\}. \tag{6.17}$$

where $\{e\}\equiv\{1 \quad 0 \quad 0 \quad 0 \quad 0 \quad 0\}^T$. From equation (6.17), we can obtain the response functions of the system under base excitation input as,

$$\{H(\omega)\}\equiv(\{\hat{u}\}/u_0)=-([K_{22}]-\omega^2[M_{22}])^{-1}([K_{21}]-\omega^2[M_{21}])\{e\}. \tag{6.18}$$

Here, it should be noted that the response function is obtained in the case of arbitrary excitation input. No matter what kind of base excitation (sinusoidal excitation or random excitation) is applied, the response function is same since it is the natural property of the mechanical system. Now we have established the relationship between the response functions under base excitation and system matrices. Based on equation (6.18), a model updating method can be developed assuming that the response function data under base

excitation $\{H(\omega)\}$ have been measured. From (6.18), one can have the following for the analytical and experimental models respectively,

$$([K_{22}]_A - \omega^2[M_{22}]_A)\{H\}_A = -([K_{21}]_A - \omega^2[M_{21}]_A)\{e\}, \tag{6.19}$$

$$([K_{22}]_X - \omega^2[M_{22}]_X)\{H\}_X = -([K_{21}]_X - \omega^2[M_{21}]_X)\{e\}. \tag{6.20}$$

Let the sub-matrices of the system matrices and the error matrices be related as,

$$\begin{cases} [K_{22}]_X = [K_{22}]_A + [\Delta K_{22}], & [M_{22}]_X = [M_{22}]_A + [\Delta M_{22}] \\ [K_{21}]_X = [K_{21}]_A + [\Delta K_{21}], & [M_{21}]_X = [M_{21}]_A + [\Delta M_{21}] \end{cases}, \tag{6.21}$$

and the analytical and experimental response functions under base excitation of the system be related as,

$$\{H\}_X = \{H\}_A + \{\Delta H\}, \tag{6.22}$$

where $\{\Delta H\}$ is the response function difference between the analytical and experimental models. Upon substitution of (6.21) and (6.22) into (6.20), one has,

$$\begin{aligned} &[[K_{22}]_A + [\Delta K_{22}] - \omega^2([M_{22}]_A + [\Delta M_{22}])][\{H)_A + \{\Delta H\}] = \\ &\qquad -[[K_{21}]_A + [\Delta K_{21}] - \omega^2([M_{21}]_A + [\Delta M_{21}])]\{e\} \end{aligned}. \tag{6.23}$$

Subtracting (6.19) from (6.23) and rearranging, following equation can be established,

$$\begin{aligned} &[[K_{22}]_A - \omega^2[M_{22}]_A] \cdot \{\Delta H\} + [[\Delta K_{22}] - \omega^2[\Delta M_{22}]]\{H\}_X = \\ &\qquad -[[\Delta K_{21}] - \omega^2[\Delta M_{21}]]\{e\} \end{aligned}. \tag{6.24}$$

After some rearranging, (6.24) becomes,

$$\begin{aligned} &[[\Delta K_{22}] - \omega^2[\Delta M_{22}]]\{H\}_X + [[\Delta K_{21}] - \omega^2[\Delta M_{21}]]\{e\} = \\ &\qquad -[[K_{22}]_A - \omega^2[M_{22}]_A]\{\Delta H\} \end{aligned}. \tag{6.25}$$

Equation (6.25) can be employed to solve for the unknown modeling errors if the experimental response function data and the analytical model are available. However, before this aim can be achieved, some parameterization of modeling errors is needed. To parameterize the modeling errors, it is assumed here in this work without much loss of

generality that the error mass and stiffness matrices can be expressed as linear combinations of element mass and stiffness matrices, respectively,

$$[\Delta M] = \sum_{i=1}^{N} a_i [M^e]_i \quad \text{and} \quad [\Delta K] = \sum_{i=1}^{N} b_i [K^e]_i , \tag{6.26}$$

where $[M^e]_i$ and $[K^e]_i$ are the i^{th} element mass and stiffness matrices respectively, and a_i and b_i are the design parameter changes associated with the i^{th} element. And the $\sum$ sign denotes matrix building and not straight summation. From (6.26), one can also derive the error matrices of sub-matrices as following,

$$\begin{cases} [\Delta M_{22}] = \sum_{i=1}^{N} a_i [M_{22}^e]_i \\ [\Delta M_{21}] = \sum_{i=1}^{N} a_i [M_{21}^e]_i \\ [\Delta K_{22}] = \sum_{i=1}^{N} b_i [K_{22}^e]_i \\ [\Delta K_{21}] = \sum_{i=1}^{N} b_i [K_{21}^e]_i \end{cases}, \tag{6.27}$$

where $[M_{22}^e]_i$ and $[M_{21}^e]_i$ are the sub-matrices of the i^{th} element mass matrix and $[K_{22}^e]_i$ and $[K_{21}^e]_i$ are the sub-matrices of the i^{th} element stiffness matrix which are accordingly expanded and partitioned. Upon substituting equation (6.27) into equation (6.25), one can obtain the following,

$$\begin{aligned} \Big[\sum_{i=1}^{N} b_i [K_{22}^e]_i - \omega^2 \sum_{i=1}^{N} a_i [M_{22}^e]_i \Big] \{H\}_X + \Big[\sum_{i=1}^{N} b_i [K_{21}^e]_i - \omega^2 \sum_{i=1}^{N} a_i [M_{21}^e]_i \Big] \{e\} \\ = -\left[[K_{22}]_A - \omega^2 [M_{22}]_A \right] \{\Delta H\} \end{aligned} . \tag{6.28}$$

Equation (6.28) can be transformed into a set of linear algebraic equations in terms of unknown design parameter changes a_i $(i = 1, 2, \cdots, N)$ and b_i $(i = 1, 2, \cdots, N)$ as,

$$\begin{bmatrix} s_1^a & s_2^a & \cdots & s_N^a & s_1^b & s_2^b & \cdots & s_N^b \end{bmatrix} \begin{Bmatrix} \{a\} \\ \{b\} \end{Bmatrix} = -\left[[K_{22}]_A - \omega^2 [M_{22}]_A \right] \{\Delta H\}, \quad (6.29)$$

where s_i^a, s_i^b, $\{a\}$ and $\{b\}$ are,

$$\begin{cases} s_i^a = -\omega^2 [M_{22}^e]_i \{H\}_X - \omega^2 [M_{21}^e]_i \{e\} \\ s_i^b = [K_{22}^e]_i \{H\}_X + [K_{21}^e]_i \{e\} \\ \{a\} = \begin{pmatrix} a_1 & a_2 & \cdots & a_N \end{pmatrix}^T \\ \{b\} = \begin{pmatrix} b_1 & b_2 & \cdots & b_N \end{pmatrix}^T \end{cases} . \quad (6.30)$$

Equation (6.29) is established based on measured response function data under base excitation at one measurement frequency. In practical vibration test under base excitation, response function data are measured at many different measurement frequencies. When response function data at sufficient number (n) of measurement frequencies are used, equation (6.29) may be turned into a set of over-determined algebraic equations which can be simply written into matrix form as,

$$[S]\{p\} = \{q\}, \quad (6.31)$$

where,

$$[S] = \begin{bmatrix} s_1^a(\omega_1) & s_2^a(\omega_1) & \cdots & s_N^a(\omega_1) & s_1^b(\omega_1) & s_2^b(\omega_1) & \cdots & s_N^b(\omega_1) \\ s_1^a(\omega_2) & s_2^a(\omega_2) & \cdots & s_N^a(\omega_2) & s_1^b(\omega_2) & s_2^b(\omega_2) & \cdots & s_N^b(\omega_2) \\ \vdots & \vdots & \cdots & \vdots & \vdots & \vdots & \cdots & \vdots \\ s_1^a(\omega_n) & s_2^a(\omega_n) & \cdots & s_N^a(\omega_n) & s_1^b(\omega_n) & s_2^b(\omega_n) & \cdots & s_N^b(\omega_n) \end{bmatrix},$$

$$\{p\} = \begin{Bmatrix} \{a\} \\ \{b\} \end{Bmatrix} \quad \text{and} \quad \{q\} = \begin{Bmatrix} -\left[[K_{22}]_A - \omega_1^2 [M_{22}]_A \right] \{\Delta H(\omega_1)\} \\ -\left[[K_{22}]_A - \omega_2^2 [M_{22}]_A \right] \{\Delta H(\omega_2)\} \\ \vdots \\ -\left[[K_{22}]_A - \omega_n^2 [M_{22}]_A \right] \{\Delta H(\omega_n)\} \end{Bmatrix}.$$

Here $[S]$ is a known coefficient matrix which is formed using the given analytical model and the measured response function data under base excitation. Equation (6.31) can be solved for $\{p\}$ using linear least squares methods and then the solution $\{p\}$ is used to reconstruct the updated analytical model together with the original analytical design

parameter. Following above updating procedures, an accurate updated model, which agrees well with the experimental response function data, can be established.

It has to be pointed out that during the development of the new model updating method under base excitation, it has been assumed that only one node is assumed to be fixed to the base where excitation is generated. In practical vibration test under base excitation, however, there might be several nodes specified in an analytical model which are fixed to the base. In the case where multiple nodes are fixed, only the sub-matrices of the system matrices associated with the DOFs of the fixed nodes and unfixed nodes will need to be changed through proper partition. And the vector $\{e\}$ which is associated with the DOFs of the fixed nodes should also be changed accordingly.

6.3.2 Practical Considerations

During the derivation of the formulas of the updating method, displacement response functions are applied while, in practical vibration testing, the measured responses of the system would typically be accelerations and not displacements. Since the displacement response function is defined as $H(\omega) = u_i(\omega)/u_0(\omega)$, ($i$=1,2,...,$n$), where $u_0(\omega)$ and $u_i(\omega)$ are the Fourier transforms of excitation and response time signals respectively, then the acceleration response function would be $I(\omega) = \ddot{u}_i(\omega)/u_0(\omega)$, ($i$=1,2,...,$n$). Similar to the relationship between receptance and accelerance, there would be a certain relationship between these two kinds of response functions. In the general case where an arbitrary excitation is applied and the response is measured, the relationship can be expressed as $H(\omega) = -I(\omega)/\omega^2$, which may be derived from the non-sinusoidal vibration and FRF properties theory in (Ewins, 2000b). Therefore, if the acceleration response function is

measured, the displacement response function would also be available based on the relationship. During the practical updating procedure, $H(\omega) = -I(\omega)/\omega^2$ should be employed to replace displacement response function in the formulas when measured acceleration response function data are available.

Equation (6.31) is obtained using the analytical and measured response function data under base excitation in the case where damping matrix of the experimental model is not considered. In engineering practice, experimentally derived responses function data contain damping information and are always complex in nature. Since the measured response function data of practical structures are complex while this updating method requires real response function data, some kind of numerical pre-treatment of measured complex response function data becomes necessary before the suggested updating method can be performed. Here, the complex-to-real conversion methods, which have been described in chapter 4, can be proposed to extract real response function data from measured complex response function data. It is suggested that the real data, whose frequency points are off resonances, be used for updating. However, these two conversion methods are approximate methods in which the imaginary parts of measured response function data are ignored. Since it is believed that most practical structures are lightly damped, these methods do provide real experimental response function data for model updating without introducing larger errors in the procedure.

There also exist other realization methods, which were presented to produce real normal modes from experimental complex modes, such as Niedbal (1984) and Ibrahim (1983). The first method suggested by Niedbal (1984) involves a complex transformation between complex and real mode shapes. It writes the real mode shape matrix as $\Phi_R = \Phi_C T$, where

Φ_C is the complex mode shape matrix and T is a complex matrix. The complex transformation T is calculated by separating above equation into real and imaginary parts and setting the real part of T equal to identity matrix. Thus the real mode shape matrix can be expressed as $\Phi_R = \mathrm{Re}(\Phi_C) + \mathrm{Im}(\Phi_C)(\mathrm{Re}(\Phi_C)^T\,\mathrm{Re}(\Phi_C))^{-1}\,\mathrm{Re}(\Phi_C)^T\,\mathrm{Im}(\Phi_C)$ since the complex matrix T has been obtained in terms of Φ_C. An alternative technique (Ibrahim, 1983) is to solve the eigenvalue problem of the damped system directly to obtain an estimate of $[M]^{-1}[K]$ which may then be used to compute the normal modes of the system. The first method can be similarly employed here to obtain real response function data from experimental complex response functions.

In practice, it is not realistic to assume that all the coordinates which are specified in the analytical model have been measured since some coordinates are physically inaccessible such as internal DOFs and some others are very difficult to measure such as rotational DOFs. When the measured coordinates are incomplete, direct solution of the updating problem is generally not possible and some approximation has to be introduced. During the calculation of the coefficient matrix $[S(\omega)]$ and the difference vector $\{q(\omega)\}$, those unmeasured elements of the response function vector are replaced by their analytical counterparts. Then, it will lead to the same linear algebraic equations as equation (6.31), which constitute a first order approximation due to the incompleteness of measured coordinates. Again, when measured data at several frequency points are used for the equations, linear least squares methods can be used to solve for $\{p\}$. Of course, the obtained $\{p\}$ in this way is only a first-order approximation and an iteration scheme is required in the process in order to accurately obtain the exact solution. During the iteration process, an objective function to be minimized should be chosen in order to determine whether the

convergent p-values are obtained. Here, the Euclindean norm of p-values, $\|\{p\}\|$ is define as the objective function for convergence criterion. Generally, it is believed that convergence of the p-values is achieved when the value of $\|\{p\}\|$ is less than 10^{-5}.

It should also be noted that convergence of updated parameters in iteration process is an important measure of the success of the updating procedure. Mathematically, the updating formulation in equation (6.31) is based on a particular form of matrix perturbation analysis in the case where the measured coordinates are incomplete. According to matrix perturbation theory, in order to guarantee convergence of the iteration process, some restriction should be made on the extent the difference between the analytical and experimental models. The restriction proposed by Lin and Ewins (1994) may be taken into consideration here. The Euclidean norms of the errors matrices should be of second-order when compared with those of the analytical mass and stiffness matrices themselves, namely,

$$\frac{\|[\Delta M]\|}{\|[M_A]\|} \le \varepsilon, \quad \frac{\|[\Delta K]\|}{\|[K_A]\|} \le \varepsilon, \text{ where } \|D\| = \sqrt{\sum_{i=1}^{n}\sum_{i=1}^{n} d_{ij}^2}. \tag{6.32}$$

Although the value of ε varies for different systems, computational experience shows that for structural dynamic systems, the maximum value of ε may reach 0.3. Since the Euclindean norm is used and modeling errors are generally localized, the relative amplitudes of changes for individual design parameters can easily be more than 100% and still satisfy this requirement, as shown in the numerical case studies below.

6.4 Numerical Case Studies

Case 1 - Cantilever Beam

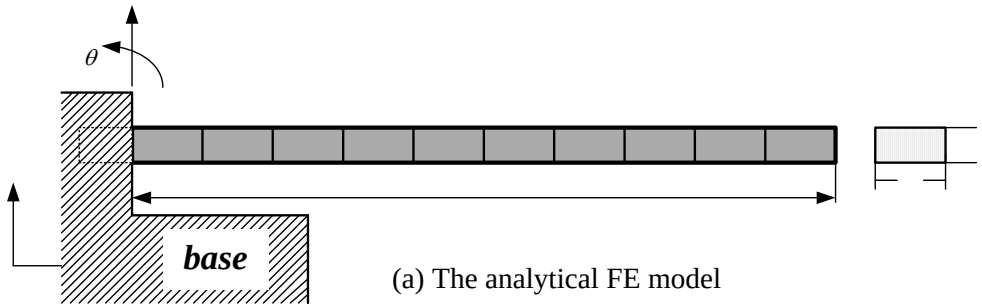

(a) The analytical FE model

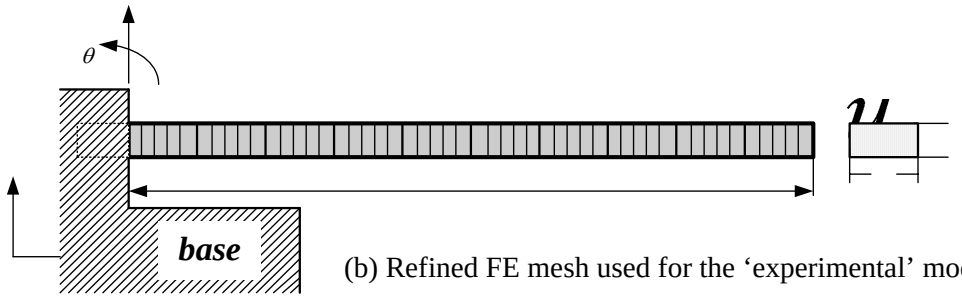

(b) Refined FE mesh used for the 'experimental' model

Fig. 6.3 A cantilever beam attached to a base

In order to demonstrate its practical application, the proposed model updating method using vibration test data under base excitation has been applied to a cantilever beam shown in Fig. 6.3(a). The left end of this cantilever beam is fixed to the base, which has the same displacement as that of base motion in vertical direction. Following parameters are used for this cantilever beam: Young's modulus of elasticity E=2.06e11N/m^2, cross sectional area $A=b\times h$=0.02×0.006m^2; length of the beam L=1.0m; material density ρ=7895.0kg/m^3. The analytical FE model of the beam, which is to be updated, is formulated using 10 bending beam elements as shown in Fig. 6.3(a). In order to simulate the practical structure more realistically, the 'experimental' model in this case is generated using a much refined finite element mesh as shown in Fig. 6.3(b). And this model consists of 50 beam elements, which is five times that of the coarse analytical FE model and may be considered to be close to the practical structure. To generate the 'experimental' response function data, it is assumed that the cross-section areas of the 11th-15th, the 16th-20th, the 21st-25th and the 31st-35th elements are increased by 120% and the second moments of area of the 16th-20th, the 31st-35th, the 36th-40th, and the 41st-45th elements are reduced by 60%, respectively.

In this case, only the translational DOFs of the bending beam are assumed to have been measured since the measured DOFs are usually incomplete in practical vibration test. We suppose that the response function data of the 'experimental' model have been measured over a frequency range covering just the first 6 resonances, with base excitation applied at the fixed node in *u* direction. Based on equation (6.31), the response function data at 10 measurement frequency points are chosen in the measured frequency range to construct the coefficient matrix $[S(\omega)]$ and the difference vector $\{q(\omega)\}$. Since approximation is made during the derivation of the updating formulation of this proposed method due to the incomplete measured DOFs in this case and the refined 'experimental' model is used, iteration process is required during updating. The iteration results for identification of element modeling errors are shown in Fig. 6.4. It can be seen that all the introduced modeling errors are well identified after 9 iterations. The response function curves of the 'experimental', analytical and updated models are shown in Fig. 6.5. From this figure, one can expect that the regenerated response function data from the updated model overlay the 'experimental' ones. There are a few differences between the regenerated and 'experimental' response function data only at the resonant and anti-resonant regions, which is also the phenomenon in the response function data of two incompatible FE models.

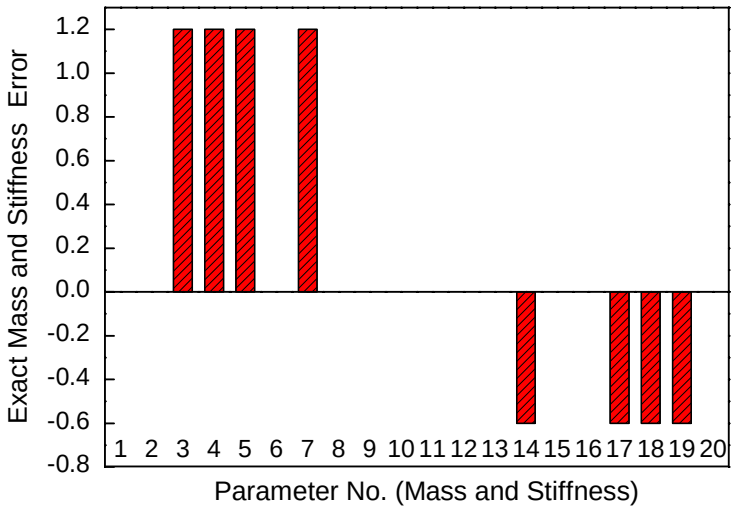

(a) The exact mass and stiffness modeling errors introduced

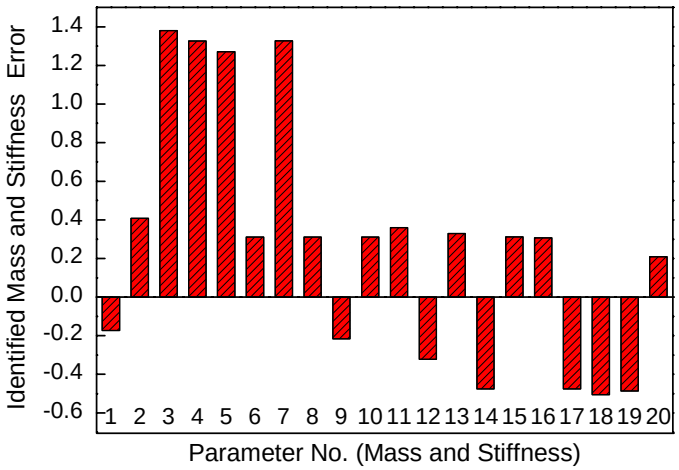

(b) Identified modeling errors of 1st iteration

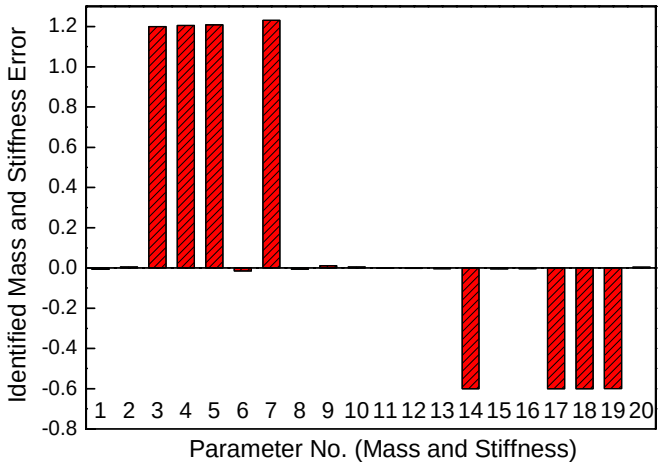

(c) Identified modeling errors of 9th iteration

Fig. 6.4 Comparison of the introduced and identified modeling errors (Case 1)

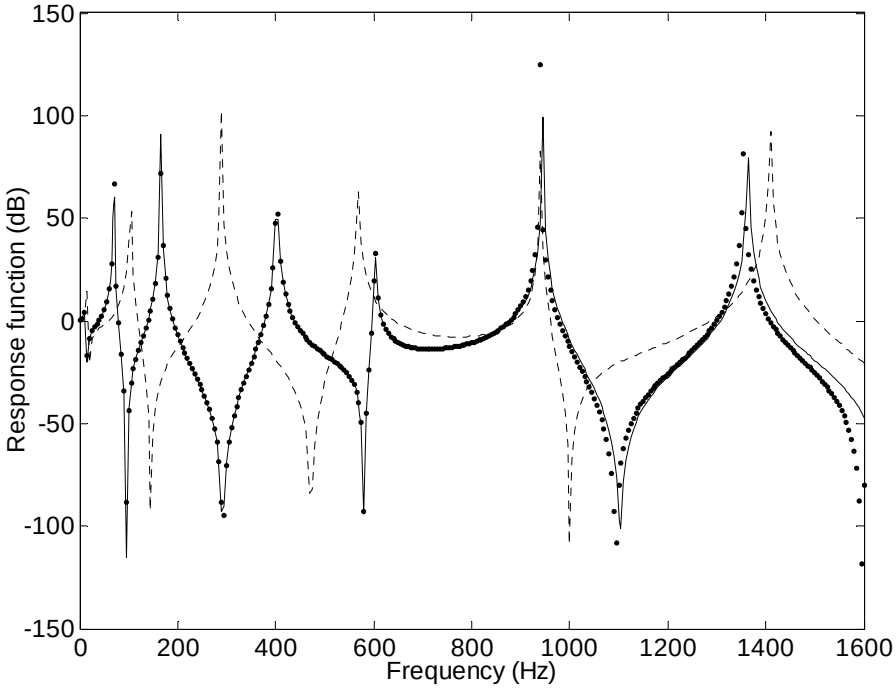

Fig. 6.5 Comparison of the analytical, the 'experimental' and the updated response function curves (Case 1) (—— updated, • experimental, ····· analytical.)

Case 2 - Truss Structure with Complete Coordinates

In this case a simulated example based on a GARTEUR structure, which has been attached to an excitation base, is presented. This complex 2-D structure can be used to assess the practical applicability of various model updating techniques efficiently. As shown in Fig. 6.6, the FE model of this structure is almost same as that has been adopted in Chapter 4.

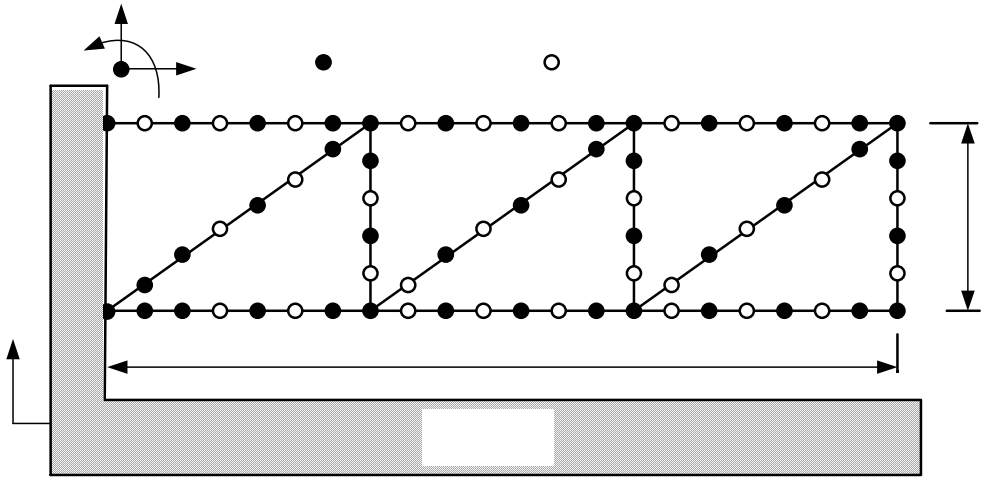

Fig. 6.6 The **GARTEUR** structure with excitation base

The identical material properties and geometric parameters of elements have employed in the FE model. The difference is that this structure has two points fixed to the base. Therefore, the total number of DOFs in the FE model is 222. In order to generate the 'experimental' data, mass and stiffness modeling errors are introduced in the elements of the FE model of the structure by changing the cross-section area *A* and the second moment of area *I* of some of elements respectively as shown in Table 6.1.

Table 6.1 Location of mass and stiffness modeling errors (Case 2)

Element No.	34	66	72	73
A Error (%)	100	100	100	100

Element No.	1	2	28	29	43	44	45	46	47	48	49	50
I Error (%)	-90	-90	100	100	100	100	100	-90	-90	-90	-90	-90

We suppose that the response functions of all DOFs in the 'experimental' model have been measured over a frequency range covering just the first 8 resonances, with base excitation applied at the fixed nodes in the *v* direction. Based on equation (6.31), response function data at 20 frequency points are chosen in the measured frequency range to establish the coefficient matrix $[S(\omega)]$ and the difference vector $\{q(\omega)\}$. The accurate results for the identification of element modeling errors are shown in Fig. 6.7. The comparison of the response function curves of the 'experimental', analytical and updated models are shown in Fig. 6.8, from which it is found that the regenerated response function data from the updated model overlay perfectly with those of the 'experimental' model.

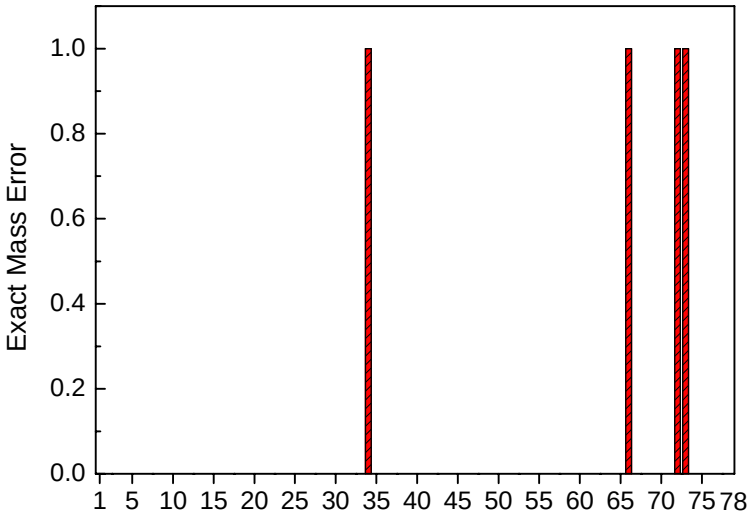

(a) The exact mass modeling errors

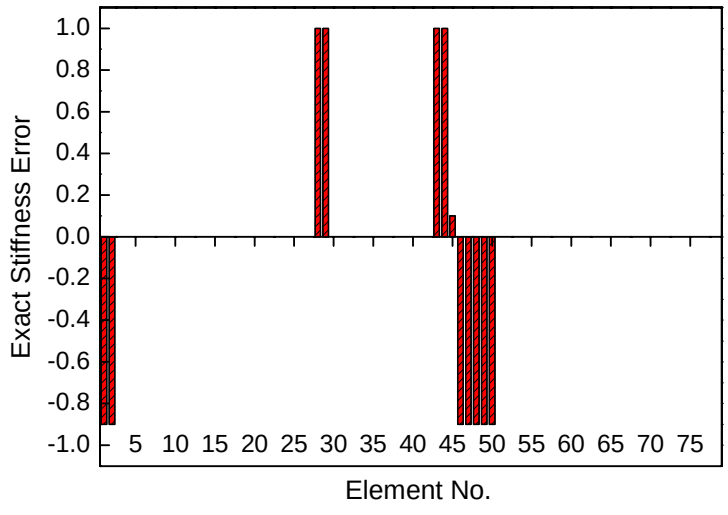

(b) The exact stiffness modeling errors

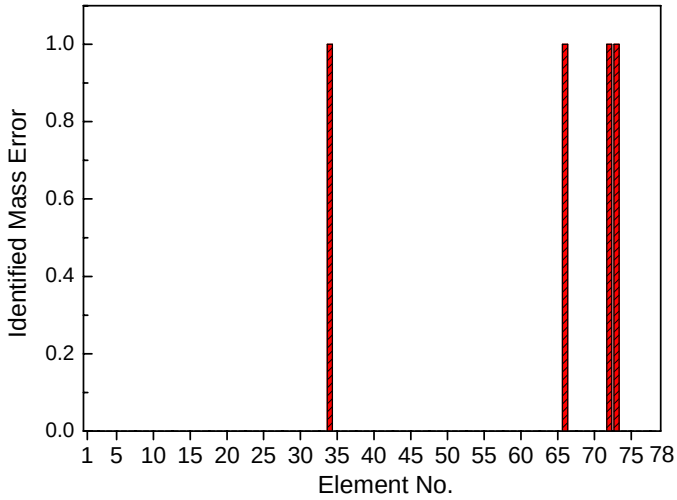

(c) The identified mass modeling errors

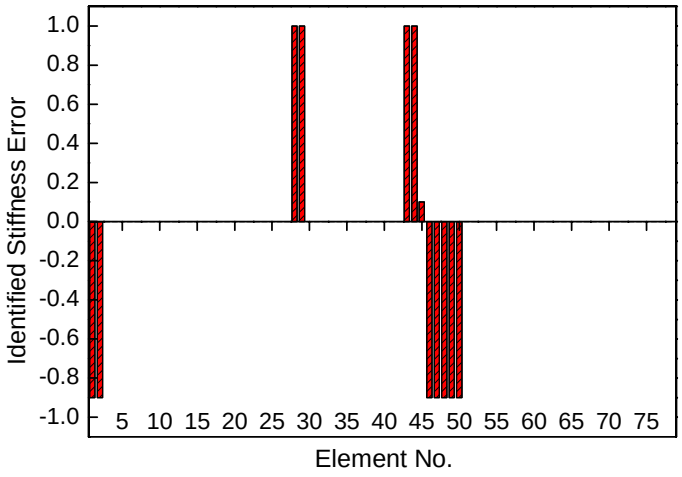

(d) The identified stiffness modeling errors

Fig. 6.7 Comparison of the exact and identified modeling errors (Case 2)

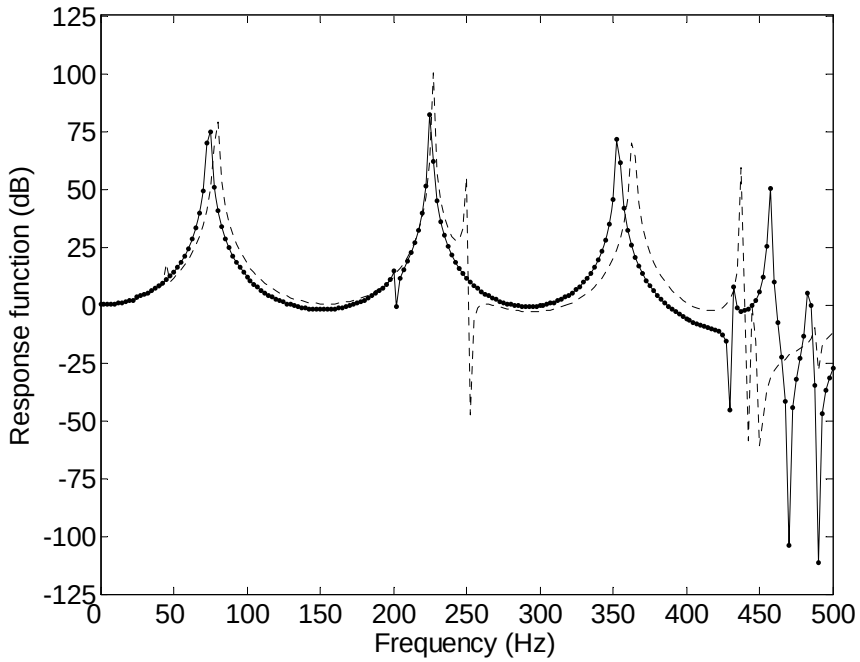

Fig. 6.8 Comparison of the analytical, the 'experimental' and the updated response function curves (Case 2)(——updated, • experimental , -------- analytical.)

Case 3 - Truss Structure with Incomplete Coordinates

In practical vibration test, it is not realistic that all the coordinates which are specified in the analytical FE model have been measured. Therefore, the effect of incompleteness of measured coordinates upon the updating procedure should be assessed rigorously based on a typical structural system. Due to the incomplete measured DOFs, those unmeasured elements of the experimental response function vector are replaced by their analytical counterparts when the coefficient matrix $[S(\omega)]$ and the difference vector $\{q(\omega)\}$ are calculated. Since some approximation has been made during the formulation of the coefficient matrix and the difference vector, iterations are required in the updating process in order to accurately identify the modeling errors.

Table 6.2 Location of mass and stiffness modeling errors (Case 3)

Element No.	34	66	67
A Error (%)	150	150	150

Element No.	7	8	26	27	40	41	47	48	54
I Error (%)	-90	-90	150	150	150	150	20	-90	-90

Table 6.3 The selected elements to be updated and their corresponding parameter number (Case 3)

Parameter No.	1	2	3	4	5	6	7	8	9	10	11	12	13
Element No.	1	2	7	8	14	15	21	22	26	27	33	34	40
Parameter No.	14	15	16	17	18	19	20	21	22	23	24	25	
Element No.	41	47	48	54	55	59	60	66	67	71	72	78	

In this numerical example, the same GARTEUR structure fixed to the base shown in Fig. 6.6 was considered again. And the response function data of the ‘experimental’ model are supposed to be incomplete in the sense that only the translational DOFs (*u* and *v*) of those hatched nodes are measured. In order to simulate the ‘experimental’ data, mass and stiffness modeling errors are introduced in the analytical model of the structure by changing

the cross-section area A and the second moment of area I of some elements as shown in Table 6.2. Since in practical FE modeling of structures, modeling errors generally occur in the modeling of joint elements, localization of modeling errors should be taken into consideration first before the application of the updating method in order to reduce computational time and improve the condition. Therefore, in this case we only choose those elements which are located at joint positions to be updated as shown in Table 6.3. The exact mass and stiffness modeling errors of the selected 25 elements are shown in Fig. 6.9(a). The response function data have been measured over a frequency range covering just the first 8 resonances, with base excitation at the fixed nodes in the v direction. Based on equation (6.31), response function data at 20 frequency points are randomly chosen from the measured frequency range to construct the coefficient matrices $[S(\omega)]$ and the difference vector $\{q(\omega)\}$ in each iteration. After 20 iterations, convergence of the solution $\{p\}$ is obtained. The iteration results for the identification of element modeling errors are shown in Fig. 6.9. Fig. 6.10 shows some of the 'experimental', analytical and regenerated (using the updated model) response function curves. From comparison of the response functions in this figure, it is observed that the agreement between the regenerated and 'experimental' response function data is excellent.

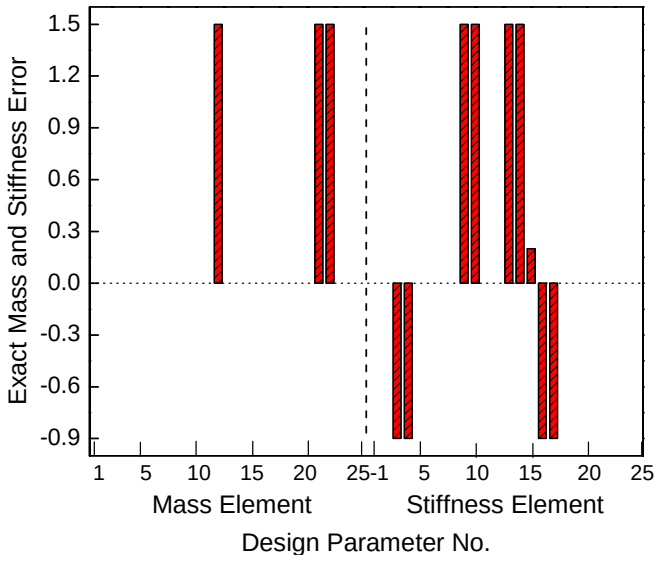

(a) The exact mass and stiffness modeling errors

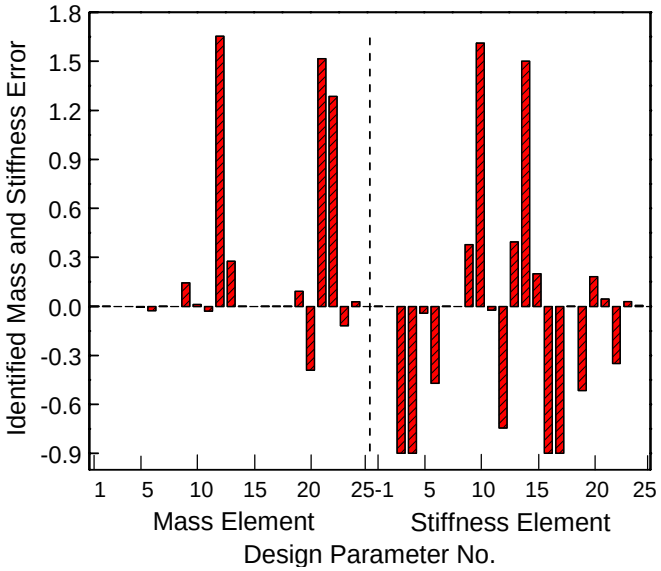

(b) 1st iteration

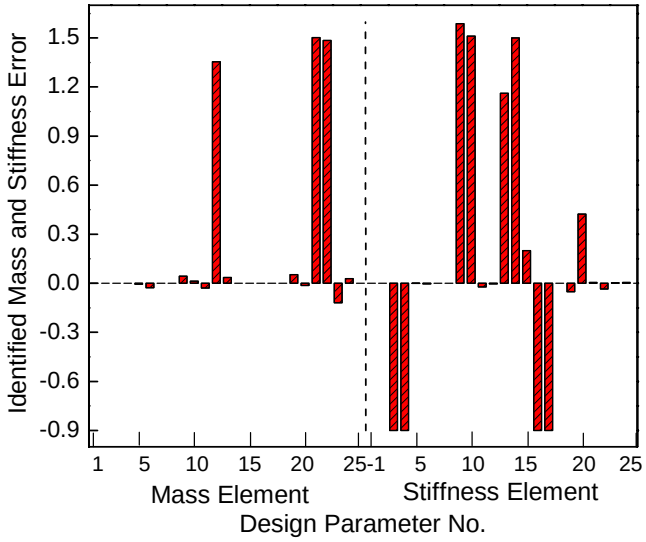

(c) 5tn iteration

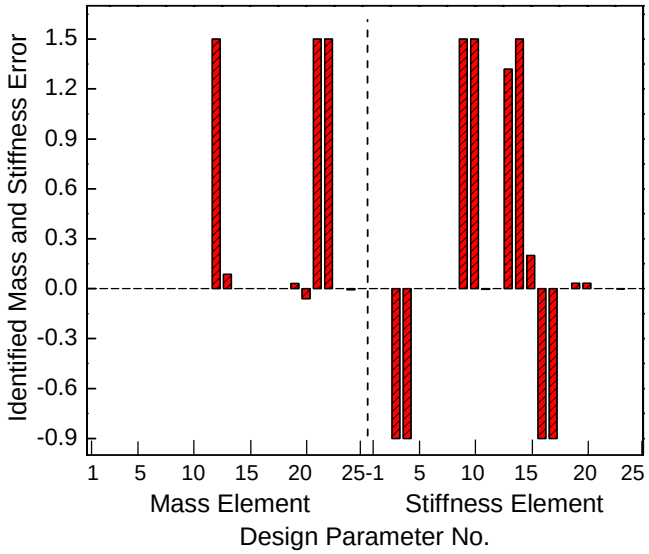

(d) 10th iteration

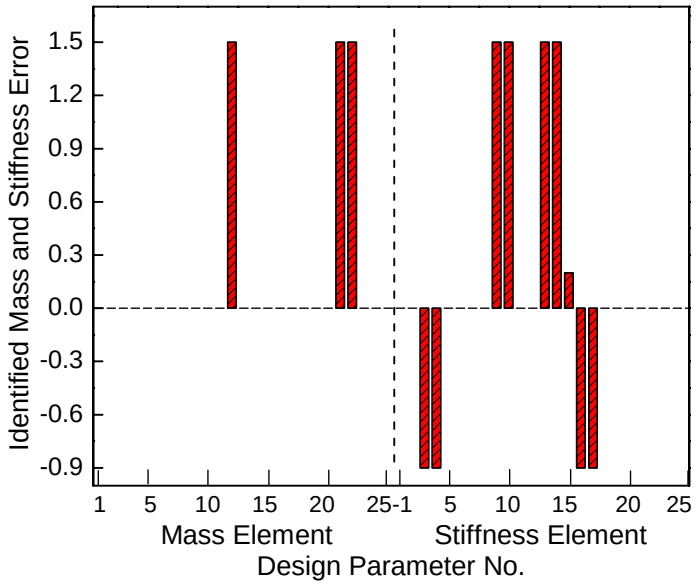

(e) 20th iteration

Fig. 6.9 Comparison of the exact and identified modeling errors (Case 3)

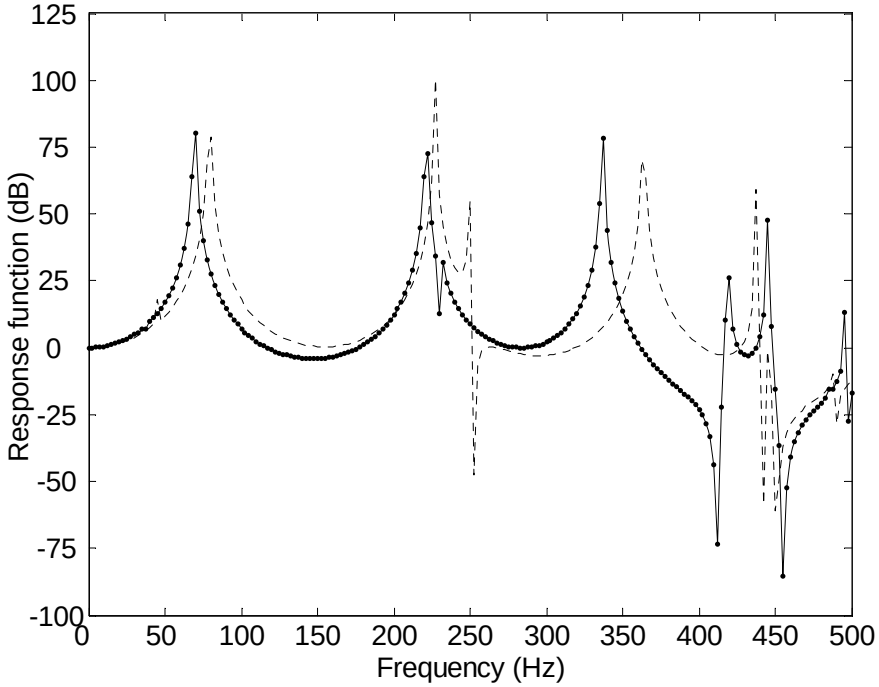

Fig. 6.10 Comparison of the analytical, the 'experimental' and the updated response function curves (Case 3) (—— updated, • experimental , ····· analytical.)

Case 4 - Noise Problem (GARTEUR Structure)

In engineering practice, the measured response data from vibration test are usually contaminated by measurement noise. The influence of measurement noise on the updating procedure described above is inevitable and the identified results of parameters may be

biased. In order to investigate the effect of measurement noise on the updating process, the FE model of the same GARTEUR structure shown in Fig. 6.6 is considered to be updated. Suppose that 3% random noise is added to the simulated measured response function data. To generate the 'experimental' response function data, the modeling errors for this case are introduced in the analytical FE model of the structure as shown in Table 6.4 and Fig. 6.11(a). In this case, localization of element modeling errors is also carried out first before updating in order to improve the condition and the accuracy of the solution. Therefore, only the selected elements as list in Table 6.3, which are located at joint positions, are to be updated. The response function data have been measured over a frequency range covering just the first 8 resonances, with base excitation at the fixed nodes in the *v* direction. Since the noise contaminated and incomplete response function data are employed in calculation of $[S(\omega)]$ and $\{q(\omega)\}$, more iterations in the updating procedure are required for averaging the effect of measurement noise. And, in each iteration, different sets of 40 frequency points are randomly selected from total 250 frequency points to calculate the coefficient matrix. The iteration results of identified element modeling errors are shown in Fig. 6.11, from which it can be seen that convergence of the solution is obtained after 40 iterations. The response function curves of the 'experimental', analytical and updated models are shown in Fig. 6.12. As can be seen, a good agreement between the regenerated response function data from the updated model and those of the 'experimental' model is achieved even in presence of measurement noise.

Table 6.4 Location of mass and stiffness modeling errors (Case 4)

Element No.	34	66	67
A Error (%)	100	100	100

Element No.	7	8	26	27	40	41	47	48	54
I Error (%)	-90	-90	100	100	100	100	20	-90	-90

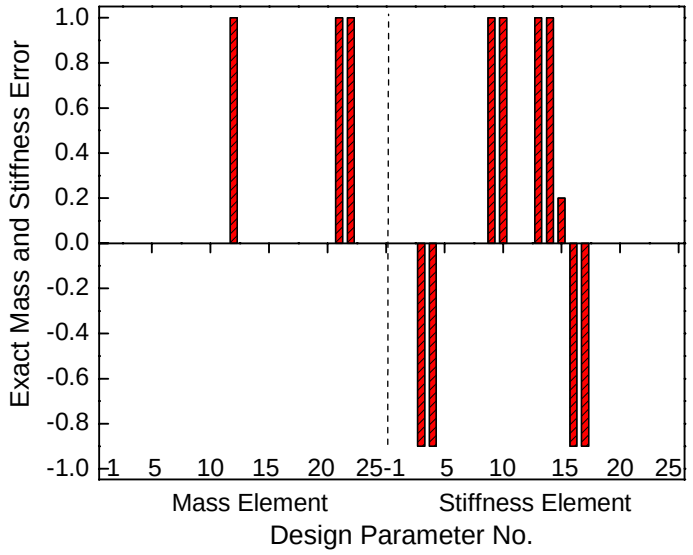

(a) The exact modeling errors

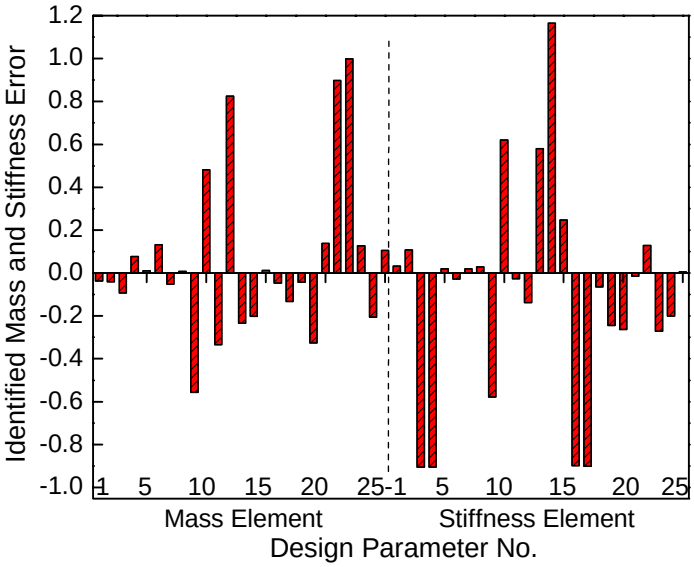

(b) 1st iteration

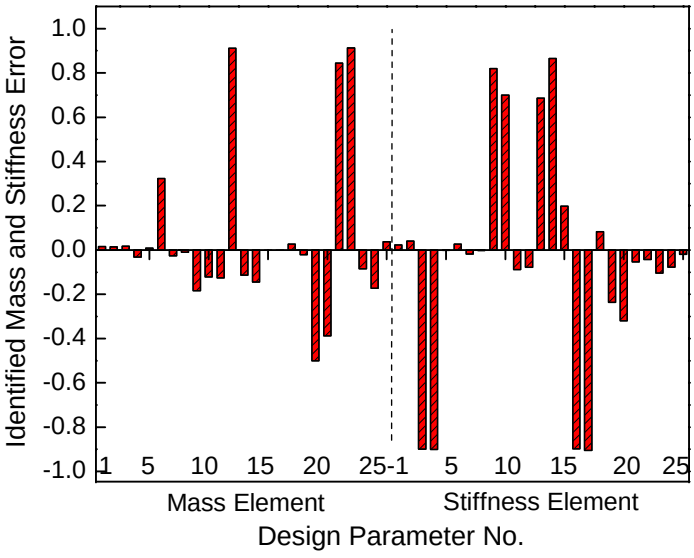

(c) 10th iteration

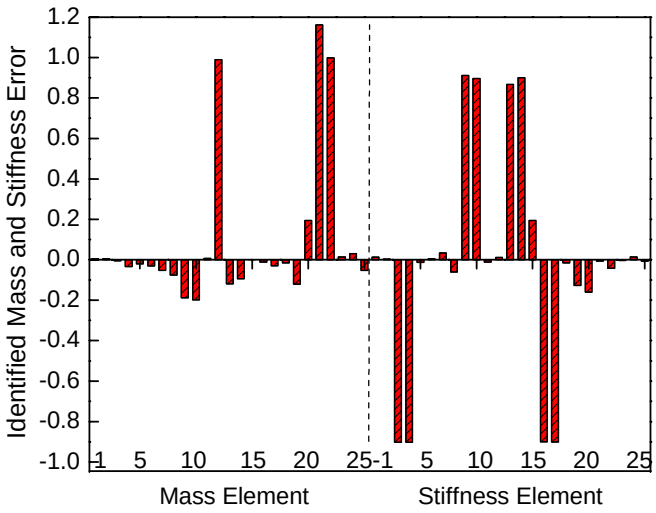

(d) 20th iteration

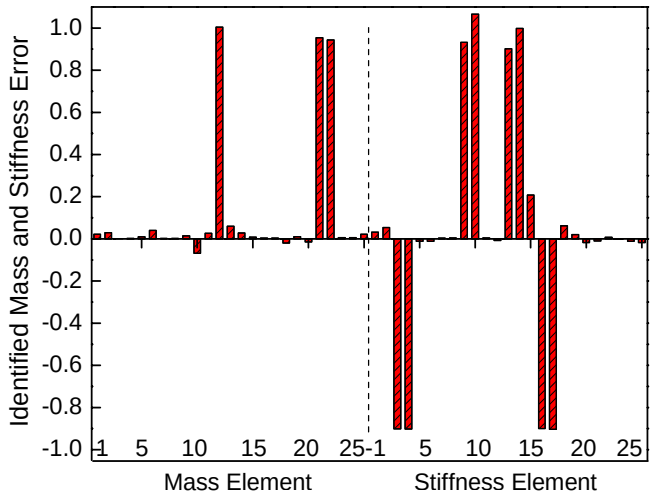

(e) 40th iteration

Fig. 6.11 Iteration results of identified modeling errors (Case 4)

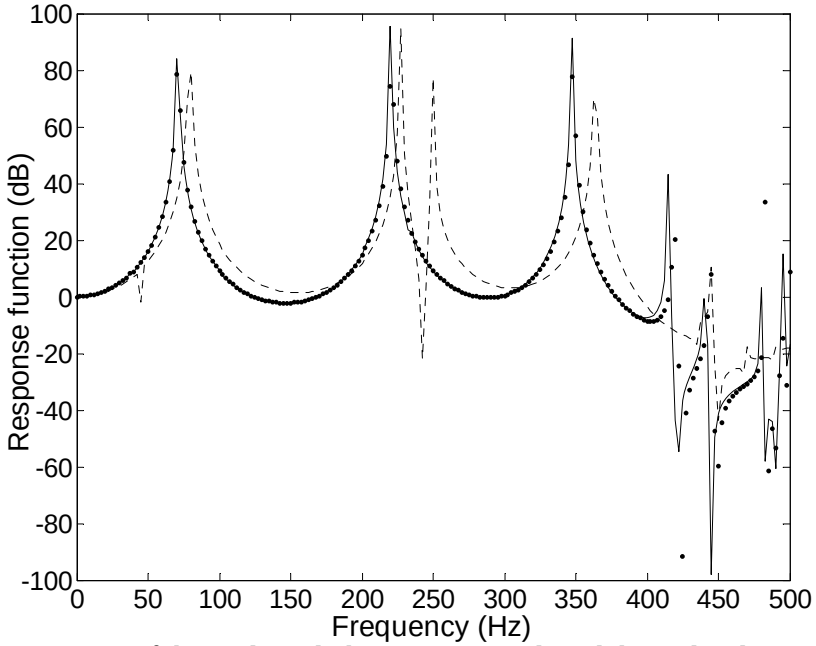

Fig. 6.12 Comparison of the analytical, the 'experimental' and the updated response function curves (Case 4) (—— updated, • experimental , ····· analytical.)

6.5 Experimental Case study

Normally, in vibration test of microsystems, a microsystem attached to a base is excited by base driving motion and response function data under base excitation are measured in order to extract modal parameters or validate the analytical models. To demonstrate the practical application of the proposed method in model updating of microsystems, in this case study, a vibration test of a micro-structure using base excitation is performed to obtain measured response function data for model updating. In the experiment, a mini-cantilever, which may represent a typical micro-structure, is designed and fabricated as the experimental model. As shown in Fig. 6.13, this mini-cantilever is fixed to shake table, which drive it to move in vertical direction. The geometry of the mini-cantilever is un-uniform as show in Fig 6.13, which is deliberately designed for convenience of model updating. The widths of beam cross-section at the 7^{th}-8^{th}, 11^{th}-12^{th} and 15^{th}-16^{th} elements are only half of those of other elements. This means that the experimental model of the mini-cantilever has 50% reduction of mass and stiffness at the 7^{th} -8^{th}, 11^{th}-12^{th} and 15^{th}-16^{th} elements compared with the FE model which is constructed using the uniform width. The parameters used for the mini-cantilever are as follows: Young's modulus of elasticity E=70.3e9N/m^2, cross sectional area $A=b\times h$=0.006×0.001m^2; length of the beam L=0.05m; material density ρ =2700.0kg/m^3. In order to simulate the mini-cantilever realistically and reduce the discretization errors, the analytical FE model of the mini-beam, which is to be updated, is formulated using 20 bending beam elements as shown in Fig. 6.13.

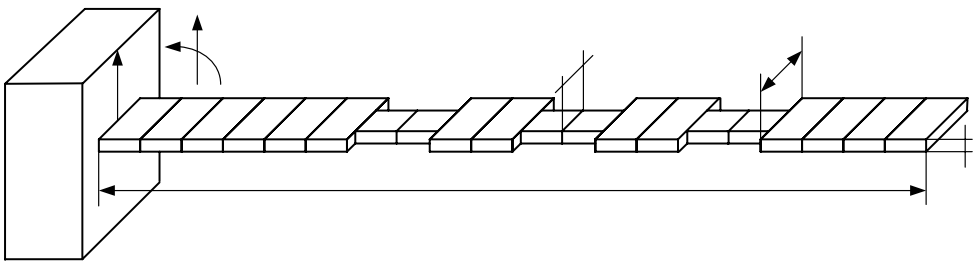

Fig. 6.13 The mini-cantilever with excitation base

The experimental response function data were acquired via base excitation test. The left end of the mini-cantilever is fixed to the baseplate which is connected to the shake table. The sine-sweeping signal generated from the analyzer drove the shake table to move only in vertical direction (*u*-direction). An LDV was employed to measure velocity response data at 20 measurement points on the mini-cantilever and an accelerometer was attached to the baseplate to obtain the input from base motion. The velocity response function data under base excitation were obtained for a frequency range of 10-4000Hz at the measurement points, and only the translational DOFs in the *u*-direction of the mini-cantilever were measured. The measured response function data should be converted to displacement response function data as their analytical counter parts before being used for updating.

In view of light damping exhibited by the structure, the proposed complex-to-real conversion method was adopted by taking the real parts of the measured complex response function as the real response function. The experimental response function data at 80 frequency points were carefully chosen from the measured frequency range with 400 points covering the first 3 resonances to construct the coefficient matrix $[S(\omega)]$ and the difference vector $\{q(\omega)\}$ in equation (6.31). Since approximation is made during the derivation of the updating formulation of this proposed method in the case of incomplete measured DOFs and the experimental response function data were used, iteration process was required during calculation of p-values. In order to reduce the number of parameters to be updated and improve the computational condition, the macro element proposed by Jung (1992) was adopted for model updating. The mass matrix of the i^{th} macro element may have a form as $[M^m]_i = \sum_{j=1}^{2} [M^e]_j, (i = 1,\cdots,10)$, which is a summation of mass matrices of two individual beam elements, and the stiffness matrix of the i^{th} macro element has the similar

form. There are totally ten macro elements in the analytical FE model during updating procedure and hence, the number of the parameters to be identified is 20 including 10 for mass modeling errors and 10 of stiffness modeling errors.

The iteration results for identification of modeling errors are shown in Fig. 6.14. It can be seen that all the FE modeling errors in the 4^{th}, 6^{th} and 8^{th} macro elements are successfully located and well identified after 25 iterations. However, there also occur distinct redundant errors in parameters of the 2^{nd}, 9^{th} and 10^{th} macro elements. This may be due to the effect of measurement noise in the experimental response function data on the identified results. In order to assess convergence of the iteration procedure, the residue values of p-values were calculated in each iteration, which are shown in Fig. 6.15. It can be found that the residue values do not change much more after 25 iterations, which means the convergent resolutions of p-values are obtained. A typical regenerated response function from the updated FE model is plotted in Fig. 6.16 together with the measured and analytical ones. From this figure, it can be observed that good agreement between the regenerated and measured response function is achieved. However, there are still a few differences between the regenerated and measured response function data only at the third resonant region and the second anti-resonant region.

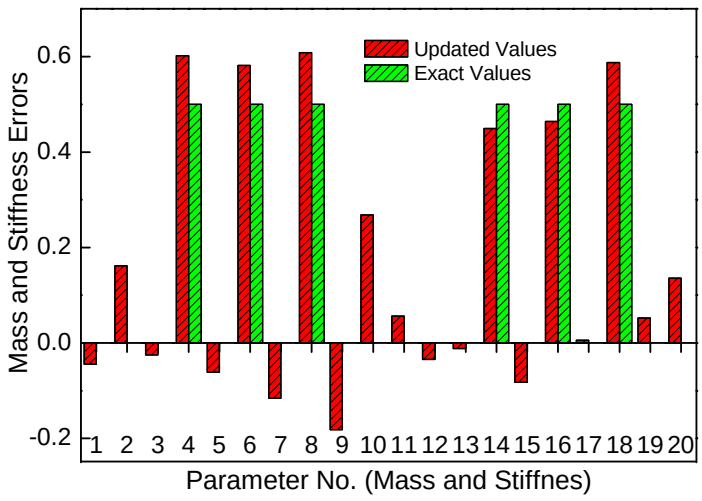

(a) 1^{st} iteration

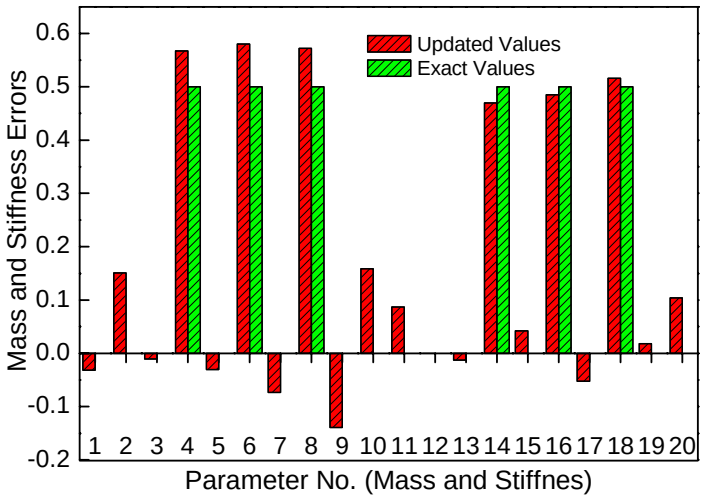

(b) 5th iteration

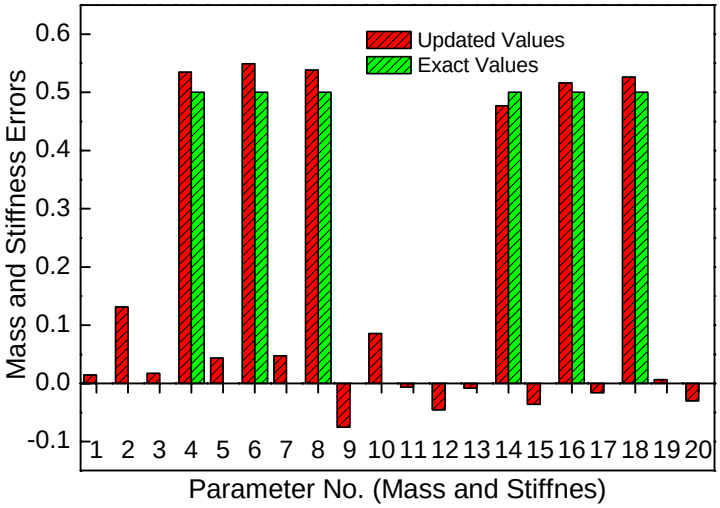

(c) 15th iteration

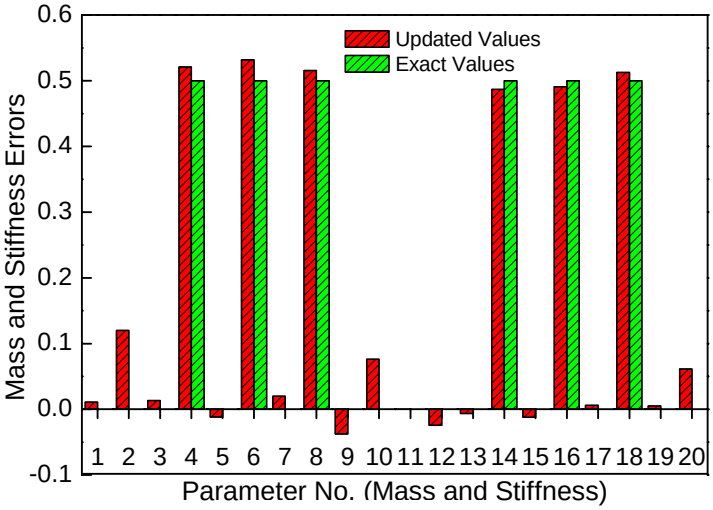

(d) 25th iteration

Fig. 6.14 Iteration results of identified modeling errors (Experimental Case)

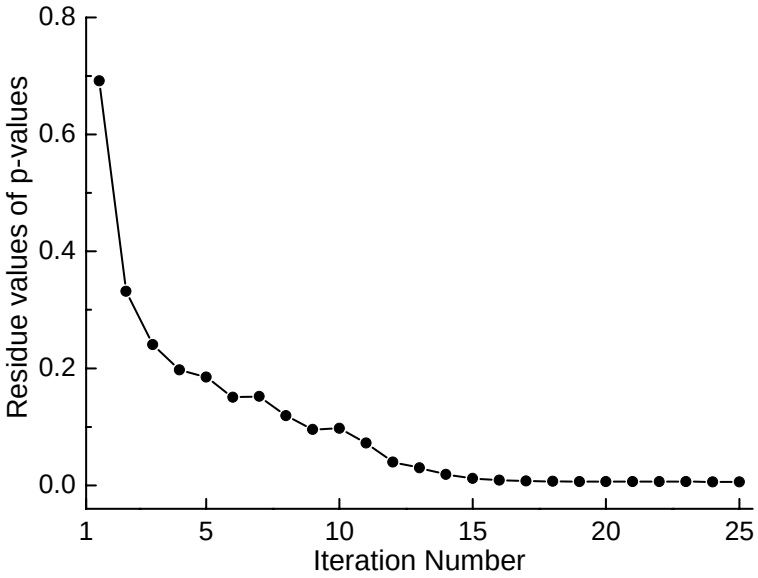

Fig. 6.15 Change of residue values of p-values *vs* number of iterations (Experimental Case)

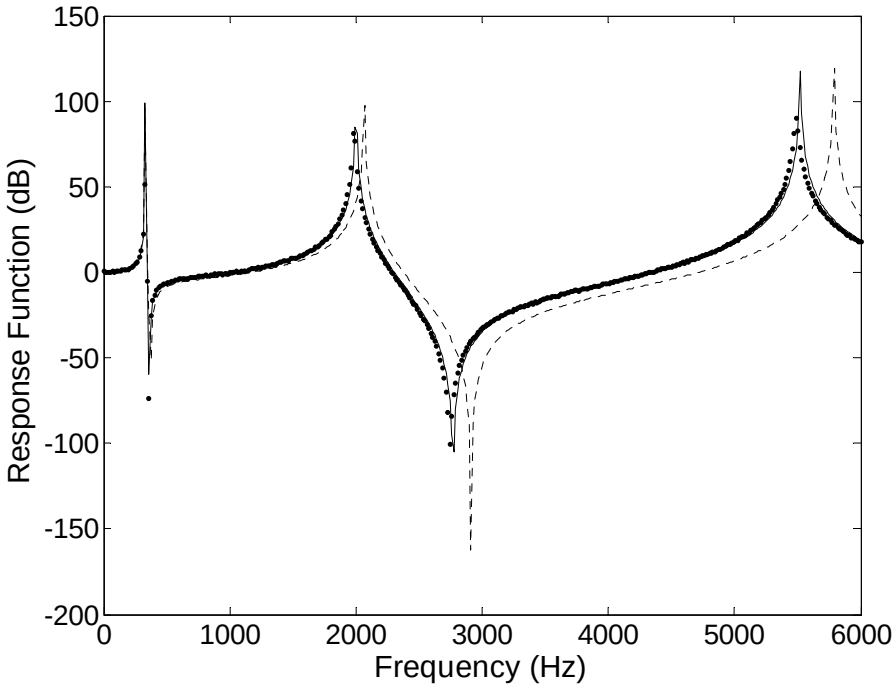

Fig. 6.16 Comparison of the analytical, the measured and the updated response function curves (Experimental Case) (—— updated, • measured, ····· analytical.)

6.6 Conclusion Remark

In many practical cases of vibration test, only response functions under base excitation can be obtained due to difficulties and constraints which prevent conventional FRFs from being

measured accurately. However, analytical models need to be updated/validated using the conventional data. In this chapter, a novel model updating method has been successfully developed which employs response function data measured under base excitation directly. Considering conventional FRF data or the derived modal data are not readily available in the case of base excitation test, mathematical formulations of a model updating method using measured response function data under base excitation directly to identify mass and stiffness modeling errors, have been successfully established. Numerical case studies based on a cantilever beam as well as a more realistic practical GARTEUR structure with complete and incomplete coordinates have been conducted to assess the applicability of the proposed model updating method. The success of these cases has proved the feasibility and practicality of the proposed method when applied to the identification of mass and stiffness modeling errors. Even in the case where measured response function data are contaminated by 3% measurement noise, very promising results have been obtained. The experimental example based on a mini-cantilever under base excitation demonstrated that the method can be adopted in practical application of model updating with confidence since the designed modeling errors were well identified using real experimental response function data. Although in these cases the structural models are relatively simple, the method has shown its potential to be applied to model updating of more complex practical structures, especially microsystems, using base excitation test data.

Chapter 7

Modal Analysis of Head Actuator Assembly

In this chapter modal testing and FE analysis of a microsystem based on an example of head actuator assembly, are conducted. The comparison between the FE model of HAA and the experimental data is performed so that the FE model is validated for the later model updating.

7.1 Introduction

A Head Actuator Assembly in an HDD can be considered as a typical microsystem, whose main mechanical components such as slider and suspension have feature size in micron scale. As a mature tool for understanding vibration behavior of a specific system, modal testing has also been gradually used to identify modal properties of microsystems. A basic experimental setup of modal testing includes excitation mechanism, transducer system, data analyzer and processing system. To achieve good performance of modal testing, the excitation mechanism must be capable of exciting any mode of interest of a microsystem without changing its natural modal property in actual operating conditions. It should have the ability to exert at any selected point in the microsystem and ideally approach a point excitation force. The force distribution should cover a wide band of frequencies especially high frequency range. Therefore, special excitation technique and measurement instrument are required for modal testing of the HAA. The voice coil motor (VCM) has been adopted by Jiang and Miles (1999) as a special exciter to drive the lateral motion of the HAA under actual operating condition. Alternatively, base excitation where the test structure is attached

to a shaker table, can also be employed (Xu, 2002). However, in this excitation method the normal operation condition of the HAA is not preserved since the HAA is removed from HDD.

A commercial HDD (IBM 2.5'' DJSA-210), where an HAA is positioned on the baseplate through the pivot shaft and attached to the cover, is considered in this work. Vibration test of the HAA of that HDD is conducted in order to identify its representative dynamic characteristics. In lateral direction, modal testing of the HAA is carried out using VCM excitation close to the operating conditions without cover and disk. Both VCM and shaker excitation approaches are adopted in vertical direction measurement for the HAA. To characterize vibration response of the HAA, LDV, which is a non-contact and precise measurement technique, is employed to pick up velocities in both lateral and vertical directions. In the case of base excitation, the acceleration input from the base is measured by making use of a traditional accelerometer.

7.2 Vibration Testing of the HAA

Vibration testing is performed on the HAA to investigate its vibration properties. This typical HAA comprises of sets of sliders, suspensions and arms, a pivot, a body portion surrounding the pivot and VCM as shown in Fig. 7.1. Since test is carried out without the cover and the disk, only vibration characteristics of the HAA supported by the baseplate, are measured. The measurement equipment used in this testing includes a LDV, a dynamic signal analyzer (HP3560A) and a data processing and analyzing software (ICATS).

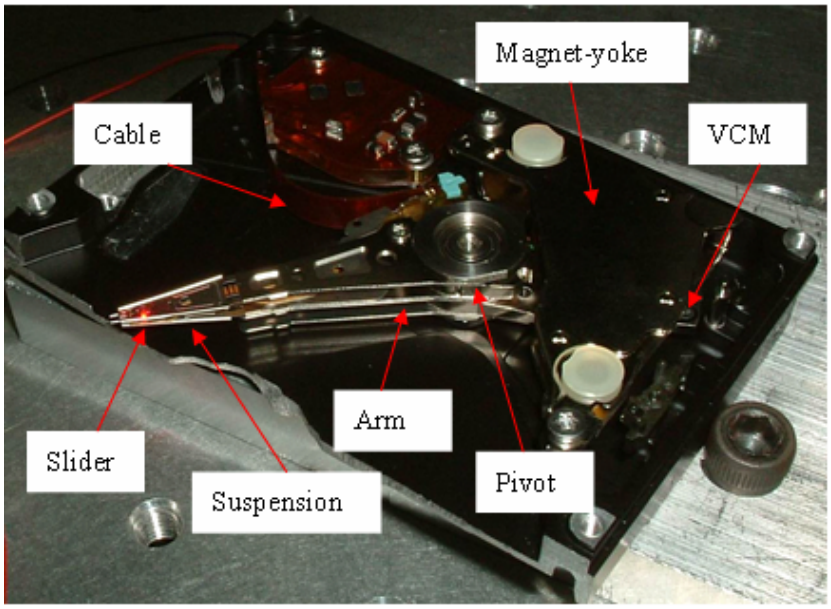

Fig. 7.1 The head actuator assembly of IBM 2.5'' HDD

The experimental studies are conducted in two different cases, respectively. In the first case, the HAA close to the operating condition without cover and disk is excited by VCM current input in the lateral direction. In the second case, the HAA is taken out from the HDD and driven vertically by an electro-magnetic shaker. The measured data are acquired by the analyzer and processed by the software. Then, the dynamic characteristics of the HAA are analyzed combining these two step measurements.

VCM excitation in lateral direction

Fig. 7.2 illustrates the schematic diagram of the experimental set-up in the case of VCM current excitation during vibration test. The head actuator arm is fixed on the pivot which is connected to the baseplate through a screw and the baseplate is attached to the testing table. The top cover is removed from the HDD and the disk is also taken away from the spindle motor since the laser point of LDV will otherwise be blocked by the cover and the disk during measurement. Here, the VCM works as a special exciter to provide a driving force.

An input signal from a waveform generator of the frequency analyzer is fed into the VCM through coil leads. For frequency-domain measurements, a sweeping sine voltage signal is used as input, whose value is set to 2.0 Volt. And an LDV measures velocity response of the HAA under excitation. The signal from the LDV is then connected back to the analyzer. In order to measure the input current to the VCM, a resistor should be connected to the circuit.

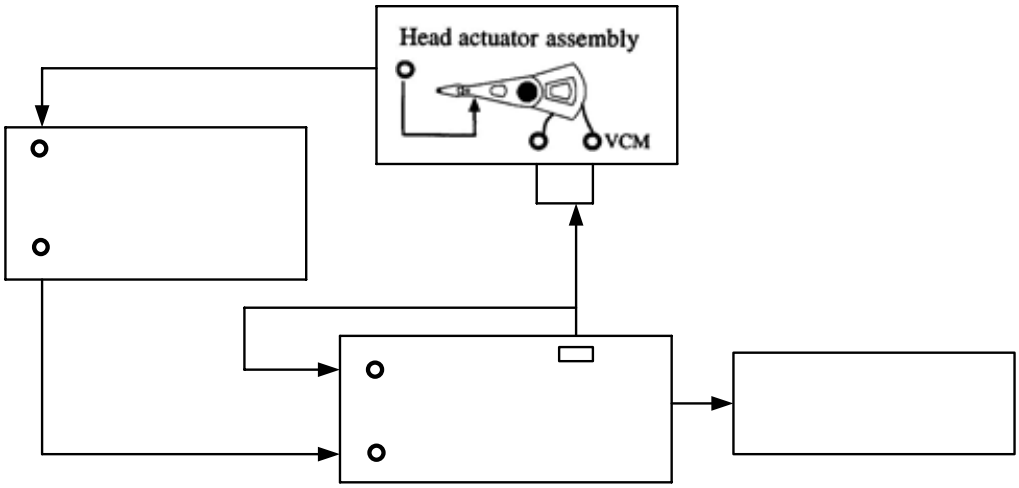

Fig. 7.2 The experimental setup for response measurement of HAA (VCM excitation)

Here, for simplicity, the input voltage fed to the VCM is directly measured since there exists a proportional relationship between the input current and the input voltage. In each measurement, the laser beam of the LDV is positioned at various locations separately such as the side of the slider, the ribbed edge of the suspension, and the side of the arm. During the measurement of the velocity response of the slider, the profile of the slider is covered by a strip of reflective tape where the laser beam can be focused. After the signals are gathered and processed using the frequency analyzer, FRFs are obtained so that modal analysis can be performed using post processing software ICATS. During modal analysis, a curve-fitting method can be applied to obtain natural frequencies, damping ratios and modal constants of the HAA system for each mode. The experimental tests are repeated from the top slider, top

suspension and top arm to the bottom set, respectively.

Response in lateral direction

Fig. 7.3 shows a typical FRF of the top slider, whose velocity response is measured in the lateral direction under VCM excitation. It can be seen that there exist many resonance peaks in the frequency region of interest from 100 Hz to 10000 Hz. These resonances

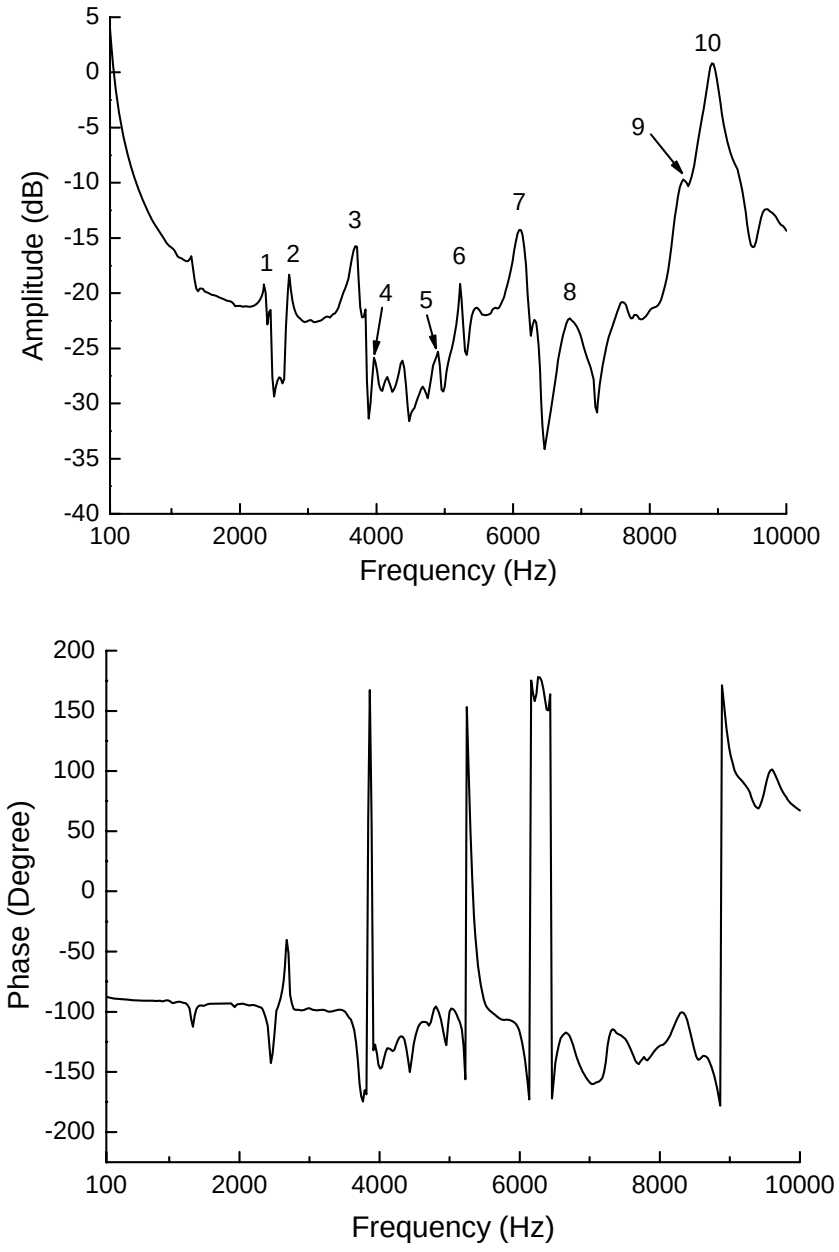

Fig. 7.3 The velocity FRF of the top slider in lateral direction (VCM excitation)

correspond to various vibration modes of the HAA under the operating condition. To obtain modal data of the HAA, modal analysis procedure should be carried out on the measured FRFs in lateral direction and then various vibration modes can be readily identified.

It can be seen from Fig. 7.3 that the most significant resonance is at the frequency 8909 Hz (peak 10), where the slider has experienced a large amount of lateral motion. Since large lateral motion will significantly contribute to track misregistration, it has great interest for investigation of dynamic characteristics of the HAA. There are also other three major peaks at frequencies of 2711 Hz, 3701 Hz and 5246 Hz, respectively. The resonances at these frequencies may contribute to the lateral motion of the HAA greatly although the amplitudes of these are smaller as compared with that at frequency 8909 Hz. It will be shown in later modal analysis that the modes at these four frequencies (including 8909 Hz) are the lateral modes, which affect the lateral motion of the HAA significantly.

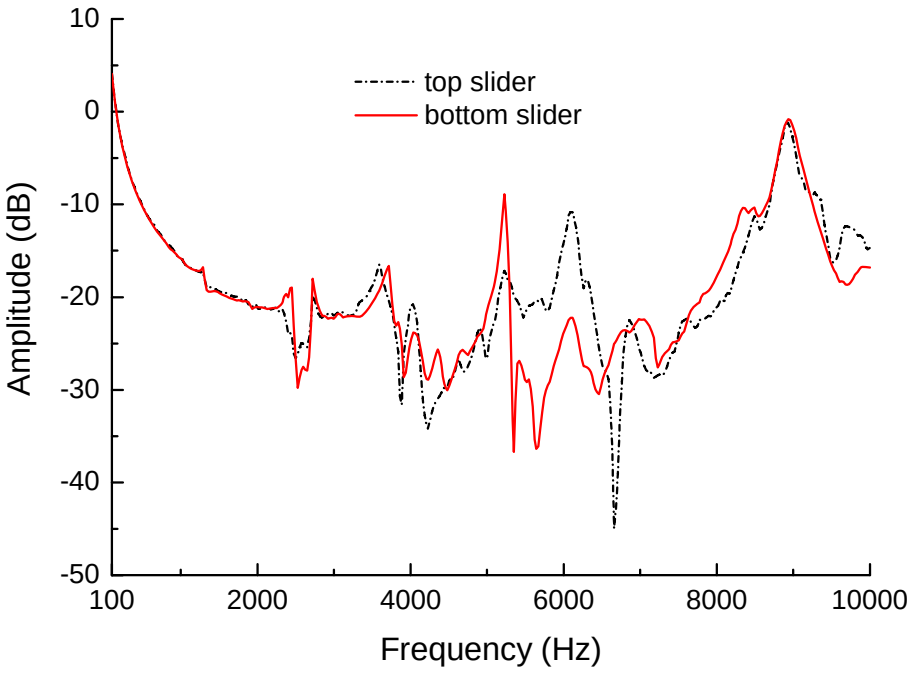

Fig. 7.4 The velocity FRFs of sliders in lateral direction (VCM excitation)

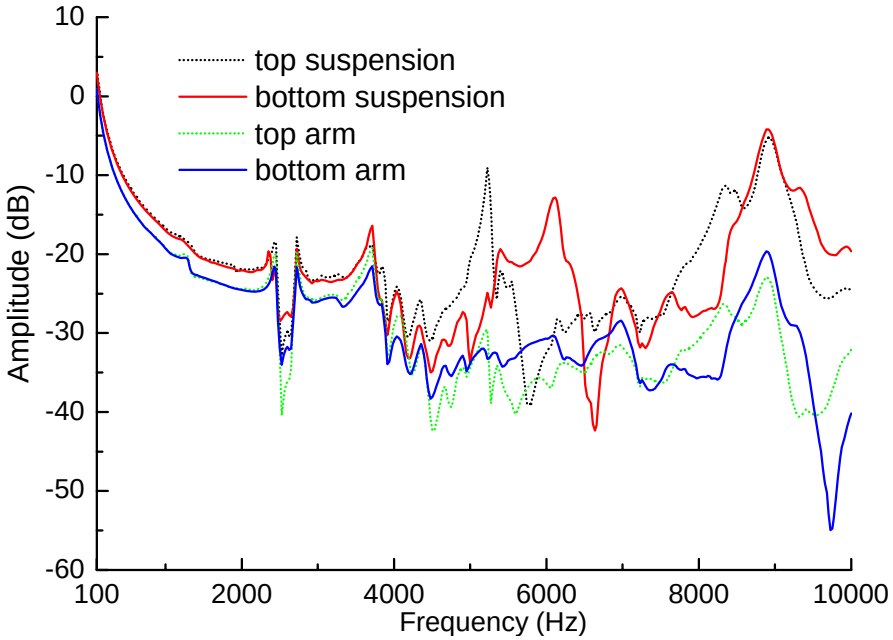

Fig. 7.5 The velocity FRFs of the suspensions and arms in lateral direction (VCM excitation)

The FRFs of the two sliders measured at different locations are presented in Fig. 7.4. Similar to those shown in Fig. 7.3, there are also four corresponding resonance peaks in the FRF curves for slider, at 2711 Hz, 3701 Hz, 5246 Hz and 8909 Hz, respectively. It is observed that the resonance peak at frequency 8909 Hz is always the major resonance. Similar characteristics can be found from the FRF spectra acquired at the measuring points on the suspensions and the arms (Fig. 7.5). It means that the possible mode at frequency 8909 Hz is the major mode, which dominates the lateral motion of the HAA. In fact, that mode is identified as torsion mode subsequently by modal testing and finite element analysis since it displays considerable lateral motions on the sliders and suspensions. It can be seen that if dynamic response of an individual suspension is measured, the torsion mode is one predominant factor contributing to slider's lateral motion.

Modal analysis

In order to extract accurate modal parameters, modal analysis procedure is to be conducted based on various sets of the FRFs measured under VCM excitation. Modal analysis technique involves curve fitting a theoretical expression for an individual FRF to the actual measured data. Before modal analysis, the FRF data recorded in the analyzer are transferred to the software ICATS in terms of complex values. Here, the circle-fit method is selected for analysis, which is based on the fact that at frequencies close to natural frequency, the FRF can often be approximated to that of a single DOF system plus a constant offset term (Ewins, 2000b). This assumption allows the use of the circular nature of a Nyquist plot of the FRF of a single DOF system by curve fitting a circle to just a few measured data points. This process can be repeated again for each of the resonances individually until the whole FRF curve has been analyzed. One typical circle-fit analysis of the FRF data is presented in Fig. 7.6. After the analysis of parameters identification, natural frequency and damping ratio of each mode can be obtained as well as mode shape. Both the identified natural frequencies and structural damping ratios are listed in Table 7.1.

Table 7.1 The identified natural frequencies and damping ratios of the modes in lateral direction (VCM excitation)

Peak No.	Natural Frequency (Hz)	Structural damping (%)
1	2446	3.88
2	2711	3.35
3	3701	3.19
4	3954	2.38
5	4934	1.69
6	5246	1.54
7	6126	2.90
8	6804	5.61
9	8482	2.19
10	8909	2.21

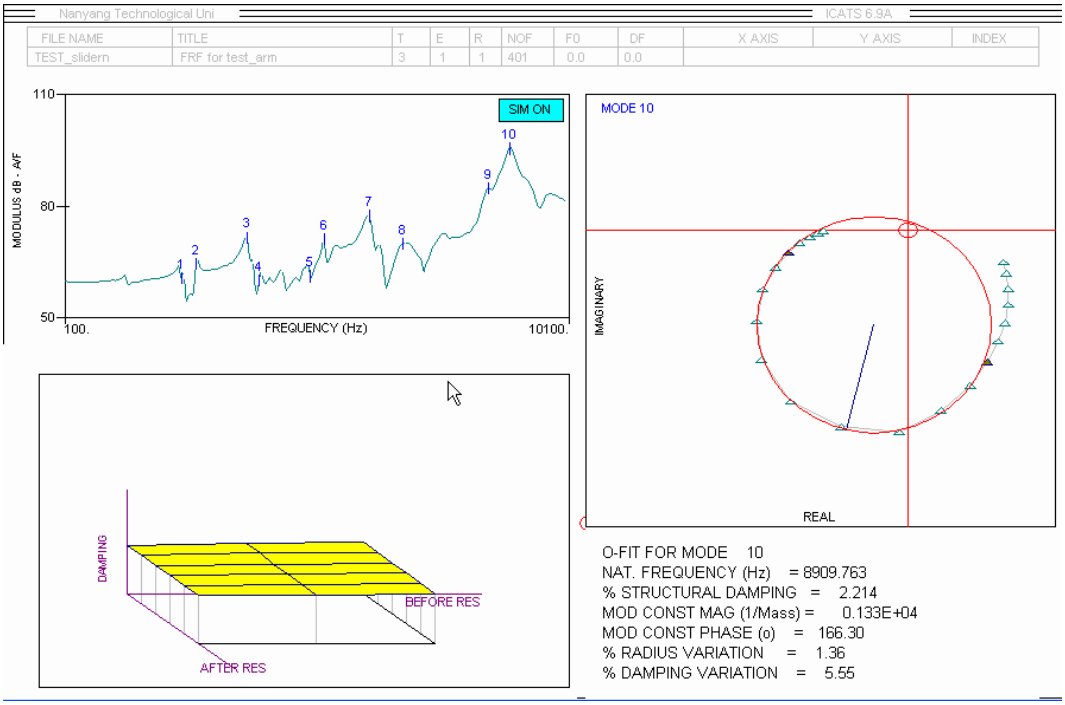

Fig. 7.6 Circle-fit modal analysis of the FRF of slider for mode 10

Response in vertical direction

The lateral vibration of the HAA is of major concern in the dynamic analysis due to its contribution to track-seeking error of the HAA under operation. However, the motion in vertical direction is of interest in analyzing its effect on flying height of the R/W head. The vertical responses of the HAA near operating condition are taken into consideration here. Since the cover and the disk have been removed and the internal HAA structure is exposed, vertical velocity response can be readily measured by LDV in the case of VCM excitation. The laser beam is focused on various positions of the top surface of the arm and suspension during measurement, respectively. Measurements on the slider and VCM surfaces are not taken due to the difficulty in conducting them.

A typical FRF of the top suspension measured in vertical direction is shown in Fig. 7.7. It can be observed that there are more resonance peaks in the frequency region of interest than

in the case of lateral direction measurement. Some of the resonances correspond to the various modes of the HAA tested in lateral direction such as peak c, d, f, etc, which are listed in Table 7.2. Others can be characterized as new modes, which occur when vertical direction measurement is conducted. However, the values of these peaks are usually much smaller than those of the corresponding peaks in lateral measurement since the vibration level in vertical direction is low as compared with that in lateral direction in the case of VCM excitation. Other FRFs measured at the suspension and the arm tips are shown in Fig. 7.8. Compared with the FRFs of the suspensions in lateral direction, these FRFs have no significant resonances in the frequency range of interest, which means that the suspension and arm do not experience large vertical motions under VCM excitation. Most resonances occur because of the coupling between the lateral motion and vertical motion of the HAA. Hence, the dynamic characteristics of the HAA in vertical direction are not as distinct as those in lateral direction but these are able to provide additional information for identification of modal data in lateral direction, especially mode shapes, which are of interest and deserve further investigation.

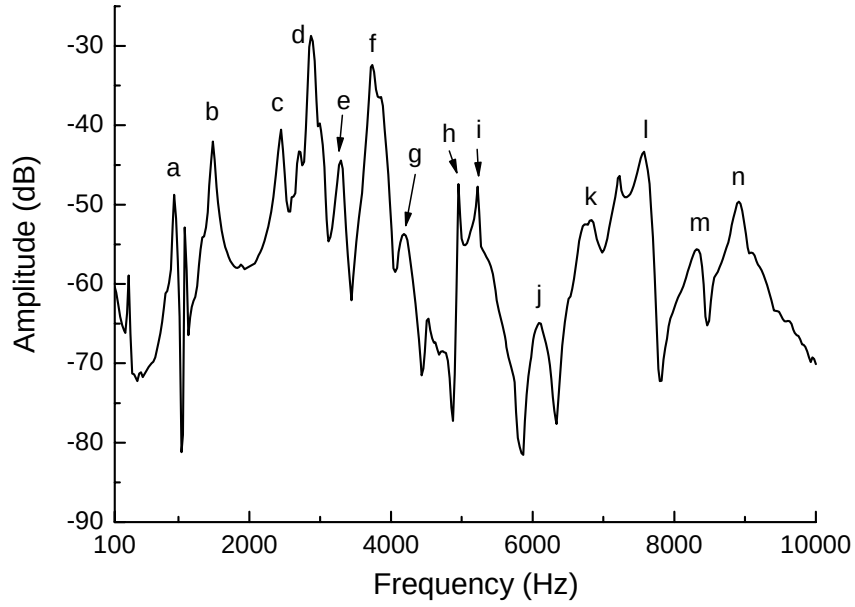

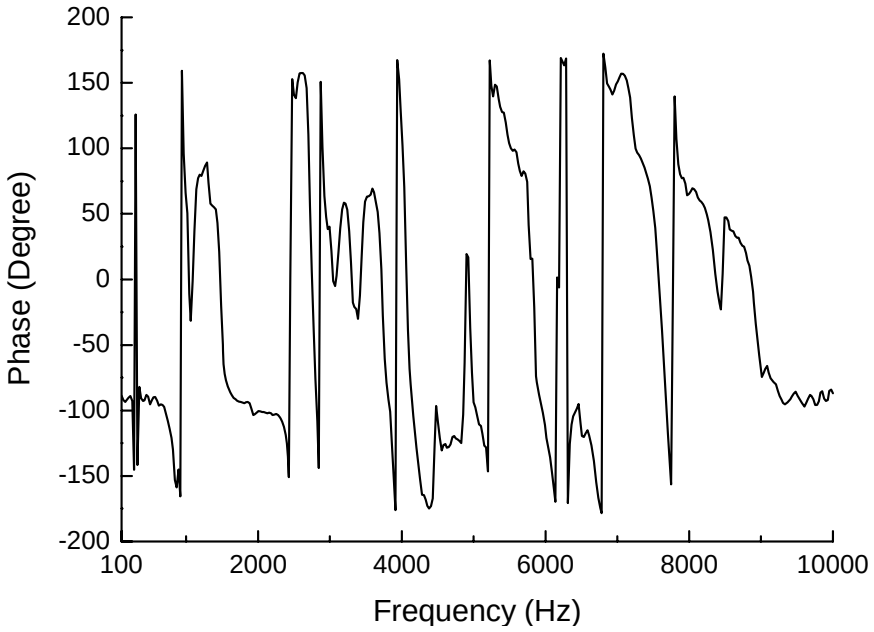

Fig. 7.7 The FRF of suspension in vertical direction (VCM excitation)

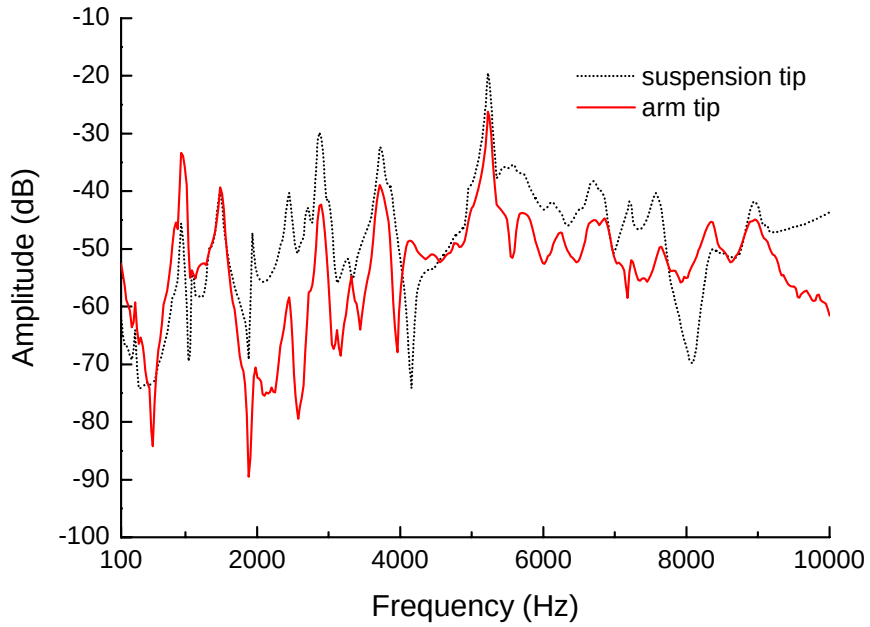

Fig. 7.8 The FRFs of suspension and arm in vertical direction (VCM excitation)

Modal analysis of the measured FRFs in vertical direction is performed and modal parameters of each mode are extracted, which are listed in Table 7.2. Comparing this table with Table 7.1, it can be found that modal data of some modes are highly close to those identified from the lateral measurement. After a large number of FRFs are measured at

sufficient number of points located at the surface of the HAA structure, modal constants of each mode can be identified and various mode shapes can be plotted after modal analysis.

Table 7.2 The identified modal data of the modes in vertical direction (VCM excitation)

Peak No.		Natural frequency (Hz)	Structural damping (%)	Mode shape
a		953	4.84	arm 1st bending
b		1479	4.81	arm bending coupled with coil 1st bending
c	1	2449	3.68	suspension and arm torsion coupled QR lateral mode
d	2	2867	2.13	suspension 1st bending coupled with arm light bending mode
e		3301	2.28	suspension bending and arm bending
f	3	3733	2.01	suspension 2nd bending coupled with arm light bending mode
g		4215	4.65	suspension and arm 1st torsion mode
h	5	4957	1.31	light torsion of suspension coupled with arm bending
i	6	5213	1.51	lateral sway mode coupled torsion mode of the suspension and arm
j	7	6126	2.64	suspension and arm 2nd torsion mode
k		7196	1.90	suspension and arm bending mode
l		7589	1.65	suspension and arm bending mode with QR longitudinal motion
m	9	8354	2.30	light torsion of suspension and arm
n	10	8916	2.09	torsion of suspension and arm

Base excitation in vertical direction

In the case of base excitation, the head actuator arm is taken out of the HDD, attached to a shaker, and then driven in vertical direction. The experimental facilities used in this test are the same as those in the previous test. The difference is that an accelerometer, a shaker and a power amplifier are involved. Fig. 7.9 illustrates the schematic diagram of the system setup for base excitation measurement. The HAA structure under test is mounted on a rigid platform which is conjunct to the shaker so that the base is subject to only translational

excitation in one specific direction. The accelerometer is attached to the connection part between the HAA and the platform in order to measure the base acceleration input. The LDV is employed to measure the velocity response of the HAA under base excitation. A sine sweeping signal generated from the analyzer drives the shaker table to move only in vertical direction after it is amplified through the power amplifier. Then, excitation and response signals are picked up and fed into the analyzer and subsequently various FRFs in the case of base excitation are obtained and plotted after processing.

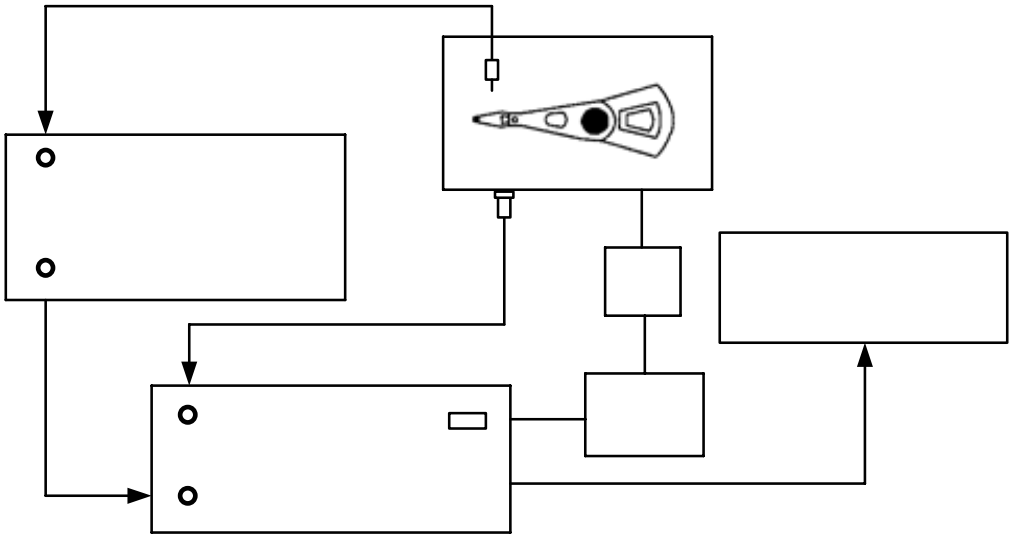

Fig. 7.9 The experimental setup for measuring the response of HAA (shaker excitation)

A typical FRF measured at the top suspension tip is shown in Fig. 7.10. It can be seen that there also exist some resonance peaks in the frequency range of interest, whose values are much higher than those of the corresponding peaks in vertical direction measurement by VCM excitation. This is because base excitation is more capable of exciting vibration modes in vertical direction compared with VCM excitation. After modal analysis, the natural frequencies and structural damping factors are identified and listed in Table 7.3. From both Fig. 7.10 and Fig. 7.3, it is observed that the mode (peak V) at 5214 Hz (peak 6

at 5246 Hz in lateral direction) exhibits peaks in vertical and lateral directions, respectively. It is identified as a torsion mode. From the comparison of Fig. 7.10 and Fig. 7.7, it is found that peak I, peak II and peak III at 1015 Hz, 2868 Hz and 3703 Hz correspond to peak **a** at 953 Hz, peak **d** at 2867 Hz and peak **f** at 3733 Hz in vertical direction measurement under VCM excitation, respectively. The modes at these frequencies are identified as bending

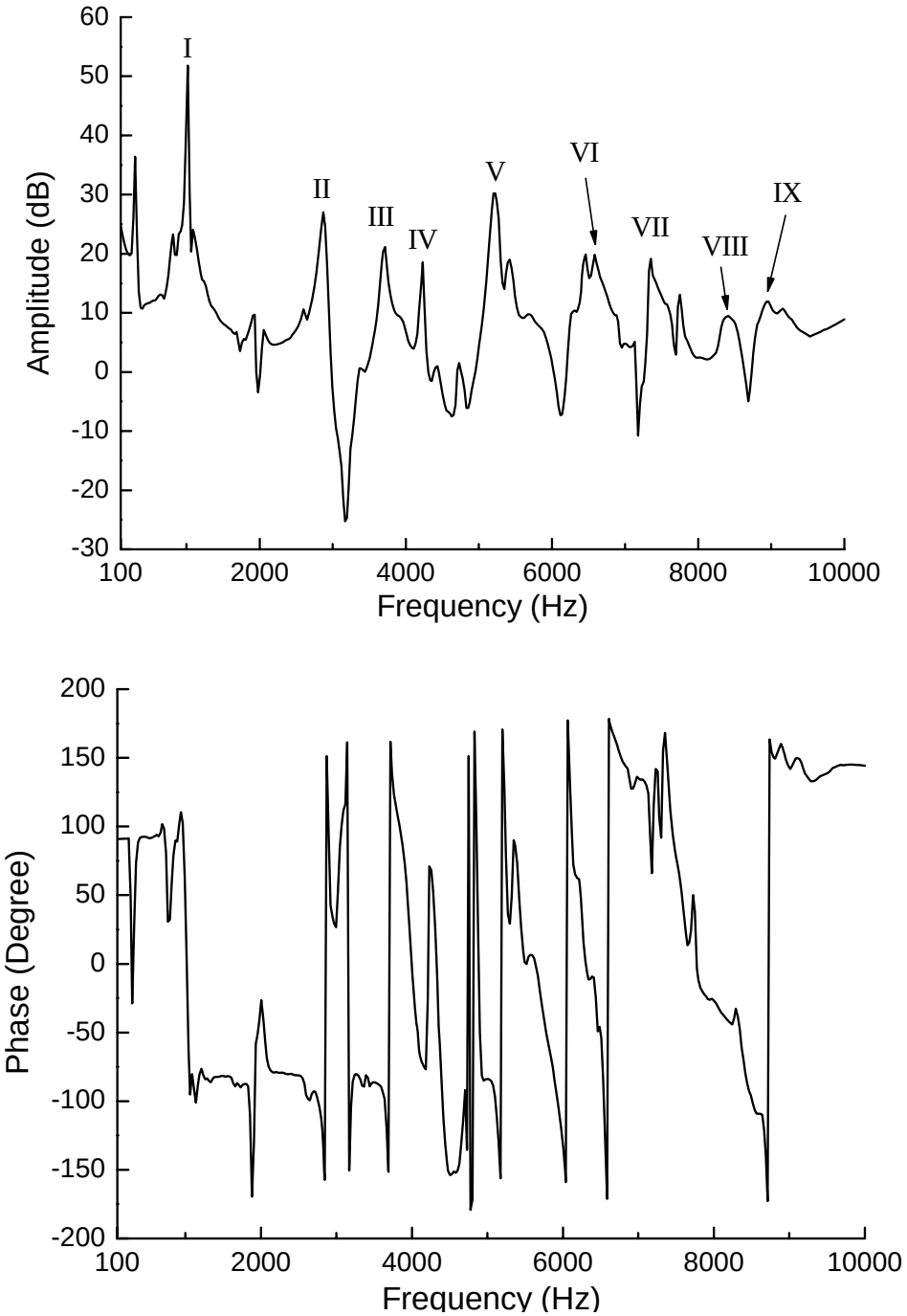

Fig. 7.10 The velocity FRF of suspension in vertical direction (base excitation)

modes. However, compared with the identified results in Table 7.2, some modes have not been identified since base excitation has no capability to excite most modes of interest due to its one dimension driven motion. Hence, it is evident that VCM excitation is more suitable for identification of the interested lateral modes of the HAA than base excitation.

Table 7.3 The identified natural frequencies and damping factors of the modes in vertical direction (base excitation)

Peak No.	Natural Frequency (Hz)	Structural damping (%)
I	1015	4.70
II	2868	1.54
III	3703	1.66
IV	4210	1.61
V	5214	1.23
VI	6564	1.42
VII	7387	2.10
VIII	8469	1.62
IX	8946	0.68

Fig. 7.11 shows other mobility FRFs measured at the suspension and arm under vertical base excitation. Compared with the FRFs by VCM excitation in vertical direction, these FRFs have a significant resonance at peak I, whose amplitudes are very high, especially in the low frequency range. It means that the suspension and the arm have experienced a large vertical motion at frequency 1015 Hz in the case of base excitation. Most resonances occur due to vertical bending or torsion motion of the HAA. Moreover, the figure indicates that the suspension has stronger vertical vibrations in the frequency range of interest than the arm since the suspension is more flexible. It should be mentioned that since the actual boundary condition of the HAA under base excitation is slightly different from that in the case of VCM excitation, vibration measurement using base excitation may only provide

additional information to the determination of modes in vertical direction.

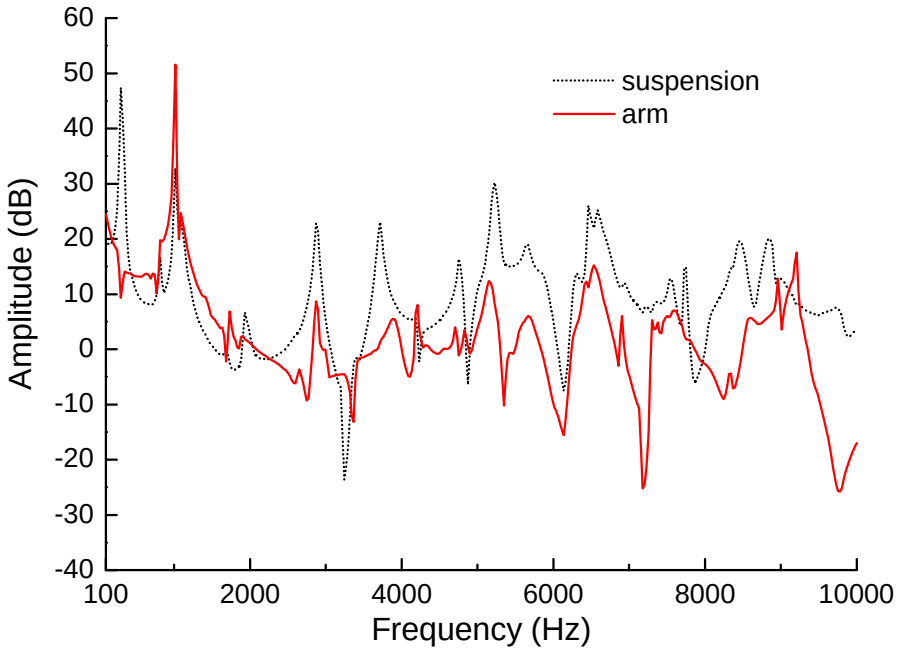

Fig. 7.11 The FRFs of arm and suspension in vertical direction (base excitation)

7.3 Mode Shape Measurement

In general, after all FRFs have been measured at a series of pre-defined measurement points of a structure, modal parameters are extracted using modal analysis and then mode shapes can be presented based on identified modal constants with the help of modal analysis software. It is clear from previous discussions that VCM as a special exciter is more suitable for vibration testing of the HAA close to operating conditions. In this section, the measured mode shapes of the HAA under VCM excitation are addressed.

To obtain various mode shapes, the same HAA as depicted in Fig. 7.1 is tested again. In the experiment, the HAA is placed on the baseplate with the pivot firmly attached by a side screw. An advanced vibration testing facility, PSV-300 system (LDV), is employed to

characterize dynamic responses of the HAA. This system consists of scanning head, vibrometer controller and data management system as shown in Fig. 7.12. The vibration velocity measured by LDV is passed onto the controller.

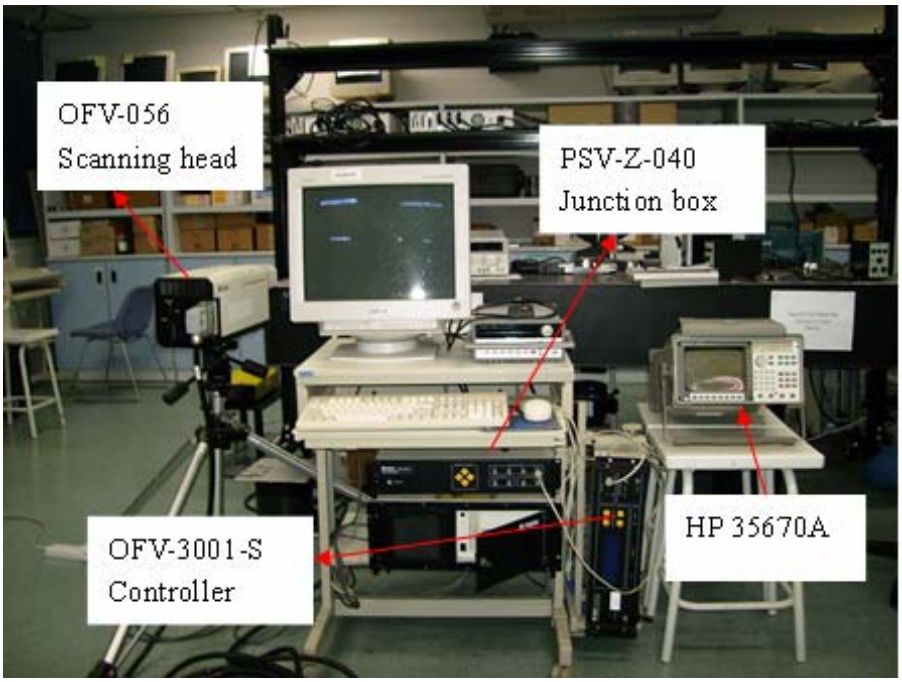

Fig. 7.12 LDV (PSV-300 system) used in the experiment

A data acquisition software integrated in PSV-3000 system is used to provide the platform to collect excitation and response signals. An advanced 'scan module' in the system software is adopted for setting up the test such as defining measurement points on the surface of test structure and their corresponding coordinates (i.e. *x*, *y* or *z*). In vibration test, a periodic chirp (pseudo random) signal from the waveform generator is applied to the VCM for current input excitation, which is predominately in lateral direction. The velocity responses are measured either in lateral or vertical direction. Meanwhile, the excitation voltage signal is read by the data acquisition software and then the FRFs, which have a form of velocity over current, are obtained after the data are processed.

When all FRFs are acquired at the defined points, they are exported to the post processing modal analysis software together with the measurement points and their corresponding coordinates. The software will build the geometry model of the structure under testing, link it with the measuring points and read or store the FRF data at each defined point. Most modal analysis functions can be executed such as curve fitting, mode sorting, mode shape reconstruction and animation.

Mode shape in lateral direction

In order to obtain mode shapes in lateral direction, a total of 52 measurement points at the profile of the HAA are defined. After the FRFs at the defined points are measured and transferred to the system, modal analysis is carried out to identify modal parameters. The identified modal constants at all the defined points are plotted using the software according to the geometry positions of the measured points. Thus, the mode shape of each mode can be presented visually and some typical mode shapes are shown in Fig. 7.13. Here, only the results for the major modes of concern are presented such as torsion mode and lateral bending mode since these modes contribute to lateral motions of the HAA significantly.

The lateral translation modes and suspension torsion modes shown in Fig. 7.13 correspond to peak 1, 3, 7 and 10 in the FRF curve shown in Fig. 7.3, respectively. Fig. 7.13(a) shows a side view of the structure of the HAA with measurement points. In Figs. 7.13(b)-7.13(e), the lines represent the deformed sketch of the structure in lateral direction. The offset of the sketch line from the original position represents mode constants at the measured points.

From Fig. 7.13(b), it can be seen that in the lateral bending mode, the entire HAA has a translational motion in lateral direction (top view). In this case, the measured mode shape agrees well with the one predicted by Xu (2000). Fig. 7.13(c) shows that there are significant offsets from the lateral motion among various suspensions. It indicates a rotation about the longitudinal axis which has been identified as a torsion mode. This mode occurs due to coupling between the predominated rotation and the translational motion.

It can be found from Fig 7.5 that there are two resonance peaks at 5246 Hz and 8909 Hz respectively corresponding to the responses of the slider and the suspension. They are identified as the various suspension torsion modes with the aid of measurement results in the vertical direction. From Fig. 7.13(d) and 7.13(e), it is observed that the two suspensions bend in the lateral direction while the arms remain unchanged. For the first torsion mode shown in Fig. 7.13(d), the two suspensions bend out-phase while second shown in Fig. 7.13(e) the suspensions bend in-phase. The suspensions exhibit considerably large lateral amplitudes and this indicates that these two modes will contribute to the off-track error significantly.

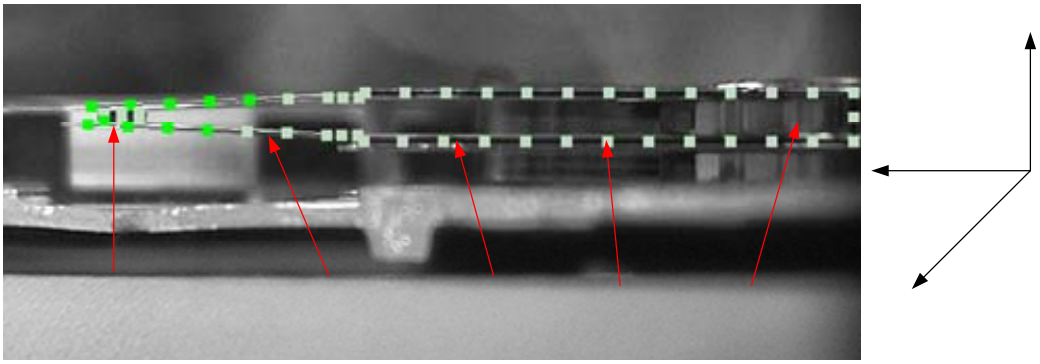

(a)

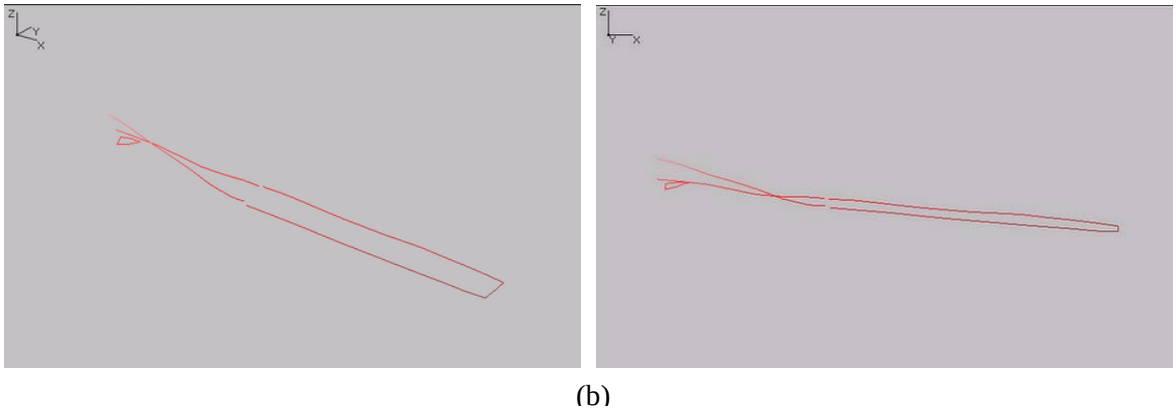

(b)

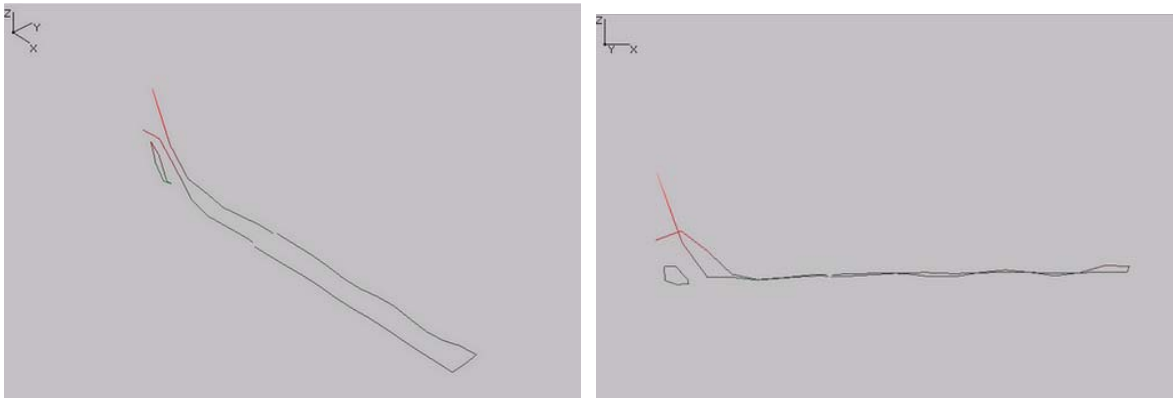

(c)

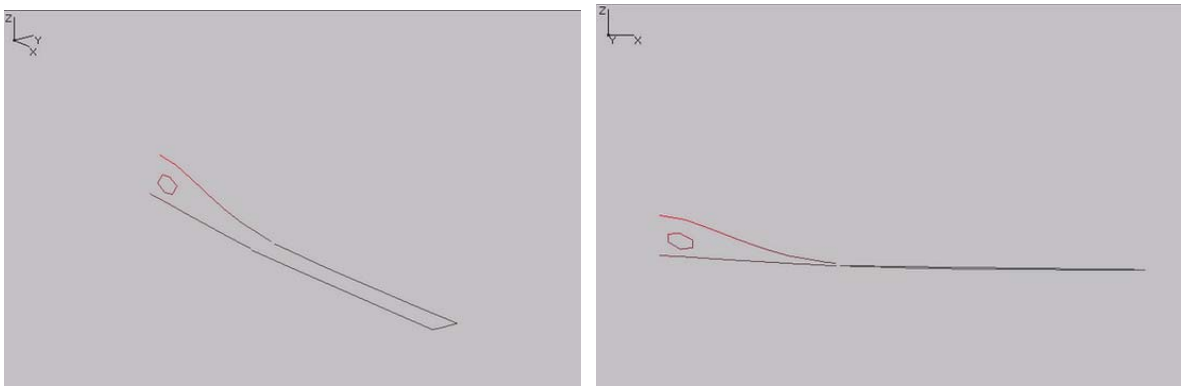

(d)

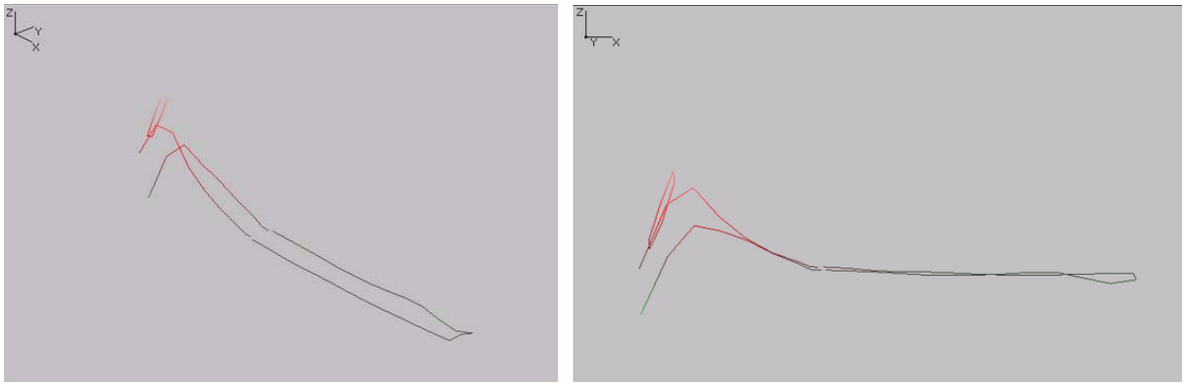

(e)

Fig. 7.13 The mode shapes in lateral direction: (a) side view; (b) lateral bending mode; (c) lateral translation (d) out-phase suspension torsion (e) in-phase suspension torsion

Mode shape in vertical direction

When measurement of the vertical response is implemented, the laser beam of the LDV is focused on the top surfaces of the suspension and the arm with 78 pre-defined measurement points. The same measurement and modal analysis processed are followed. Base on the analyzed results, Table 7.2 summarizes the modal parameters of the arm and the suspension modes that are successfully processed by the analysis software. Fig. 7.14 shows the animated mode shapes of the suspension and the arm, where the curved lines represent the deformation behavior of the HAA and both side view and skewed view are presented.

Mode **a** at 953 Hz is the top arm first bending mode, where the arm bends lightly like a cantilever, causing the bending of the suspension. If the arm were perfectly rigid, the dynamics of the individual suspensions would be uncoupled, and each suspension would vibrate independently of other suspensions. However, with a flexible arm, it is obvious that the motions of the suspensions will interact each other and with that of the arm.

The arm bending motion in the vertical direction can also be observed in the following mode: mode **b** (1479 Hz) and mode **e** (3301 Hz). The end of the arm attached to the body is observed in vibration due to the motion of the VCM or the body. However, the mode shapes of these modes could not be completely reconstructed without full measurement on the body or VCM during modal testing. Nevertheless it is evident that these modes are all related to the coil or body motion. These modes would have been verified if the corresponding mode shapes predicted from the finite element model in Table 7.4 are

available as we will discuss later in this chapter.

For mode **c**, the torsional motion can be observed from either the arm or the suspension at frequency 2449 Hz coupled with light lateral bending of the suspension and the arm. Mode **d** at 2867 Hz and mode **f** at 3733 Hz are the first and second suspension bending modes respectively, where the top arm remains relatively motionless. For mode **f** there exists a motion due to the coupling of the two sliders.

The two familiar the suspension and arm torsion modes occur at 4215 Hz (mode **g)** and at 6126 Hz (mode **j)**, respectively. These modes are the first and second torsion modes of the suspension and arm, respectively. Mode **h** at 4957 Hz is observed as light torsion of the suspension coupled with arm bending. For the torsion mode **i** at 5213 Hz, the coupled torsion of the suspension and arm is observed while the arm torsion is relatively small.

For mode **k** at 7196 Hz, the suspension and arm bending mode occurs, which is the second bending mode. The bending motions of the suspension and arm for mode **l** at 7589 Hz are coupled by the QR longitudinal motion. The suspension torsion and arm torsion modes are observed for mode **m** at 8354 Hz and for mode **n** at 8916 Hz, respectively. The former is a light torsion mode in which suspension torsion causes a relatively light torsion of the arm while for the latter torsion mode, it can be observed that one side of the suspension rises while its opposite side drops with respect to the longitudinal axis. Meanwhile, the arm has relatively strong torsion compared with that of the former torsion mode.

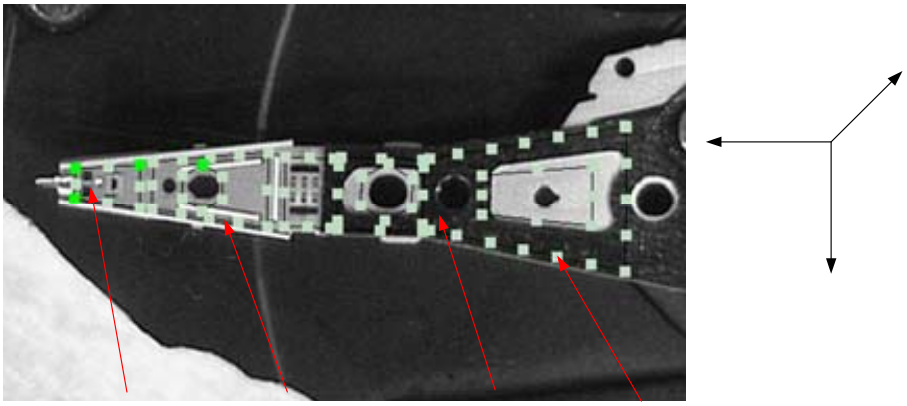

(a)

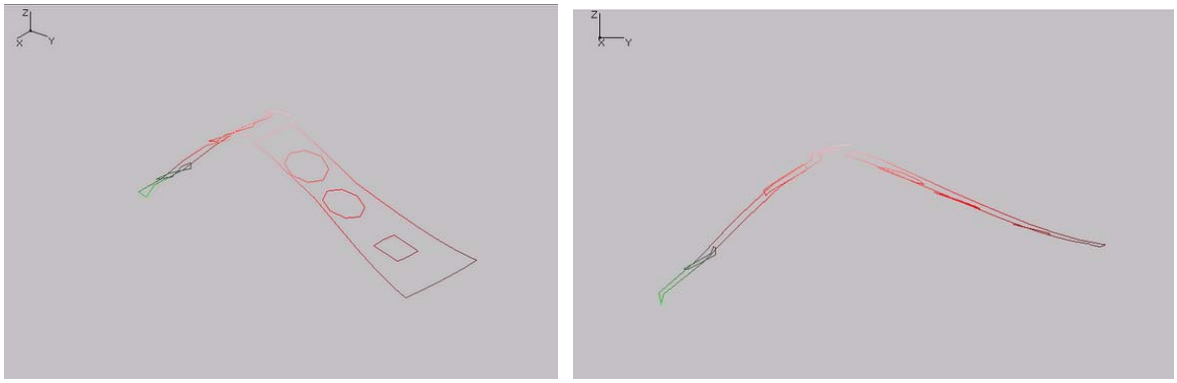

(b) arm 1st bending at 953 Hz

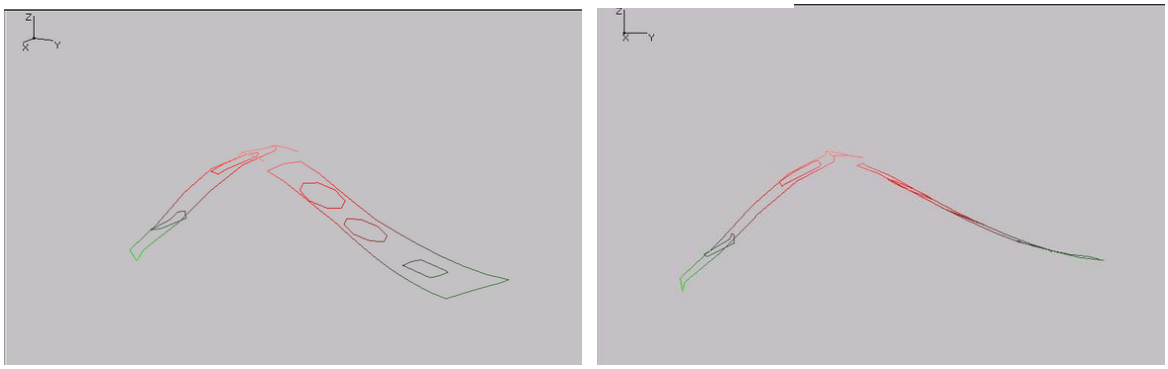

(c) suspension and arm bending coupled with coil 1st bending at 1479

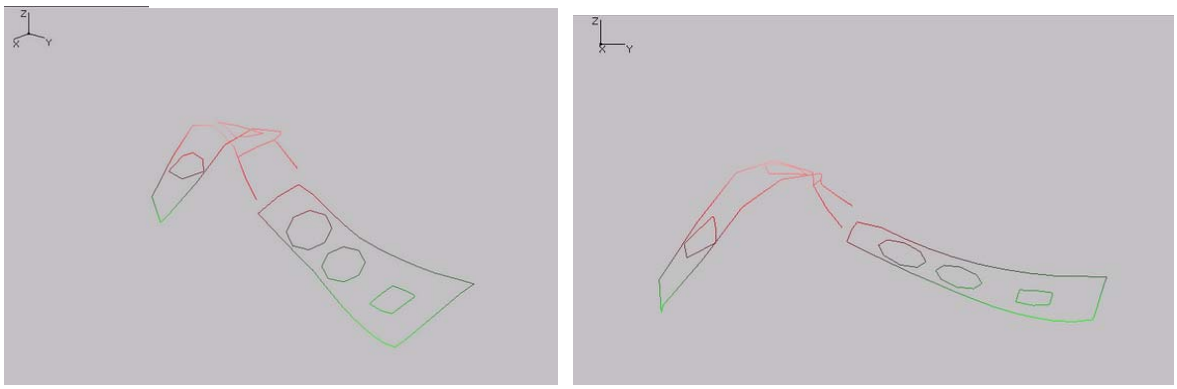

(d) suspension and arm torsion coupled with light lateral bending at 2449 Hz

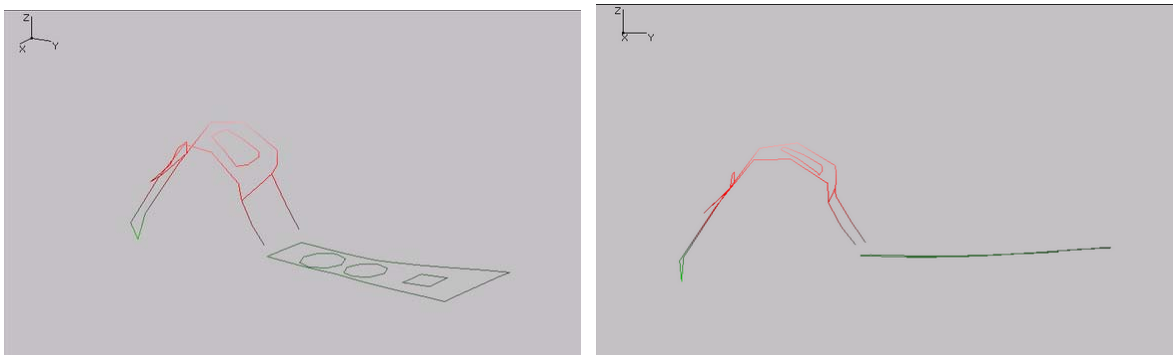

(e) suspension 1st bending with arm light bending mode at 2867 Hz

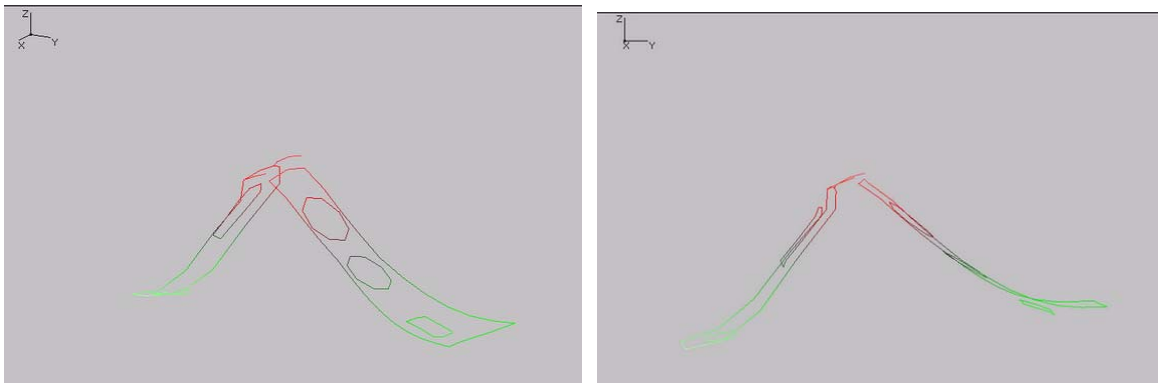

(f) suspension bending and arm bending at 3301 Hz

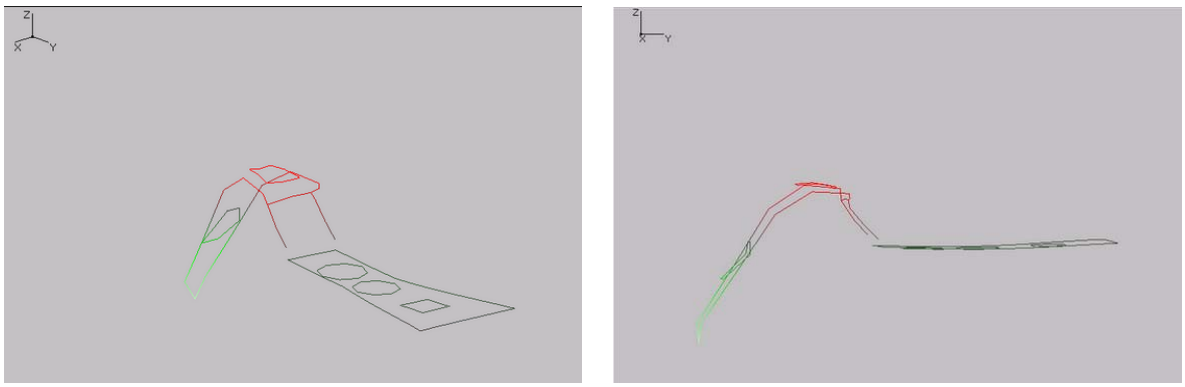

(g) suspension 2nd bending coupled with arm light bending mode at 3733 Hz

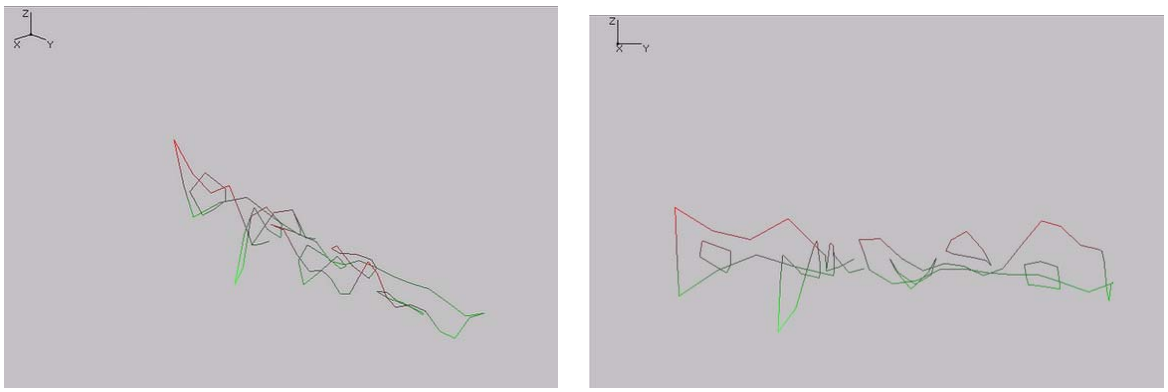

(h) suspension and arm 1st torsion mode at 4215 Hz

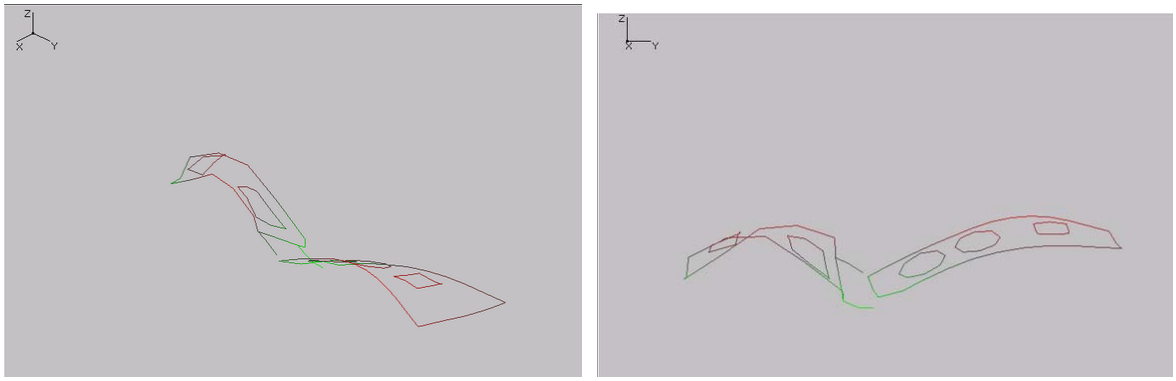

(i) light torsion of suspension coupled with arm bending at 4956 Hz

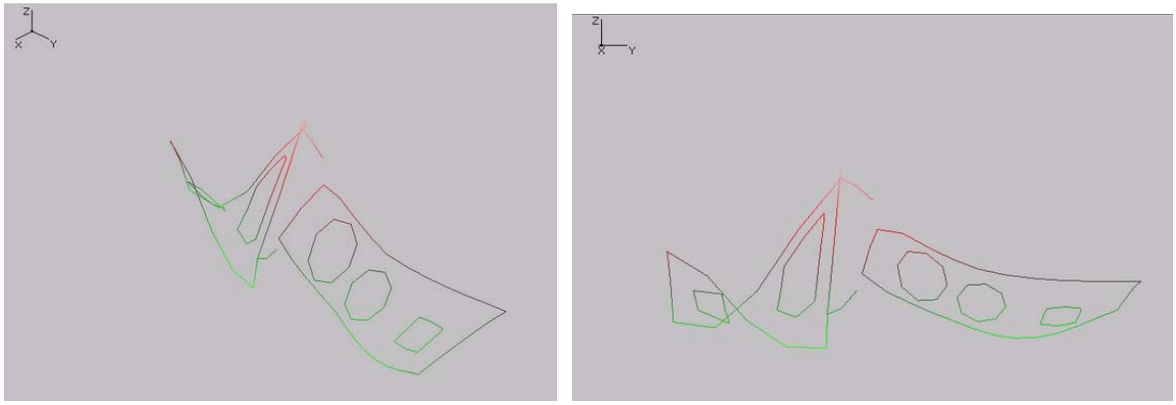

(j) torsion mode of the suspension and light torsion of the arm at 5213 Hz

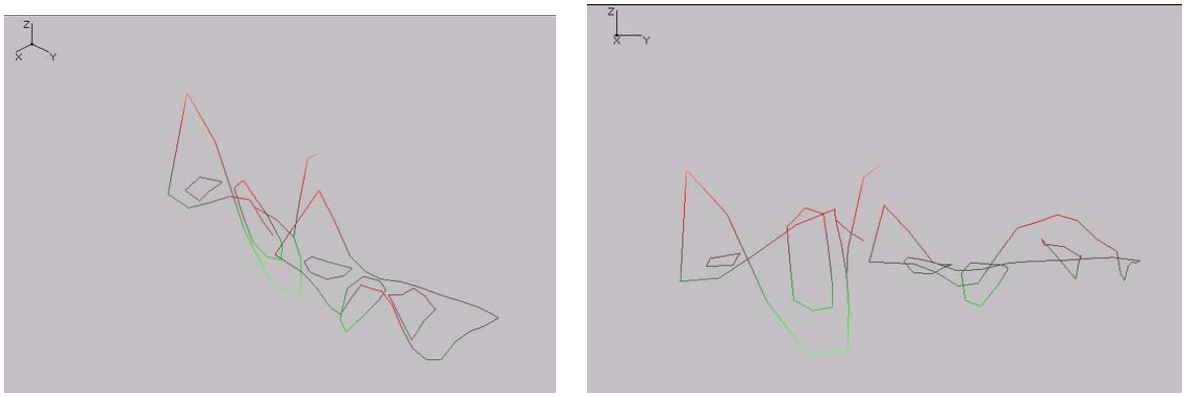

(k) suspension and arm 2nd torsion mode at 6126 Hz

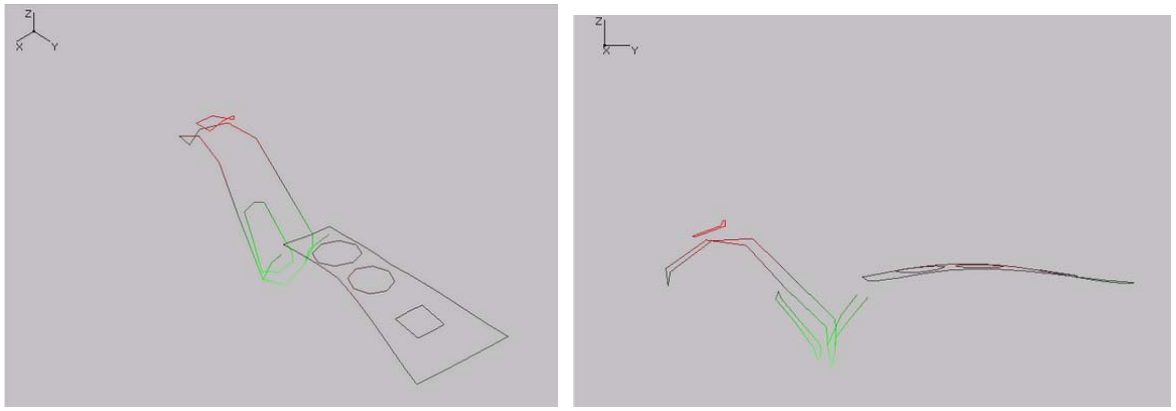

(l) light bending mode of suspension and arm at 7196 Hz

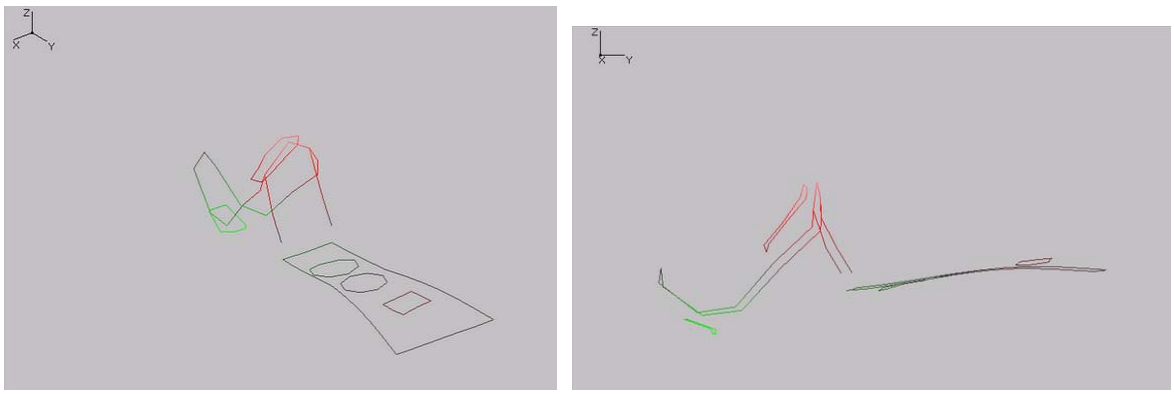

(m) light suspension bending and arm bending mode at 7589 Hz with QR longitudinal

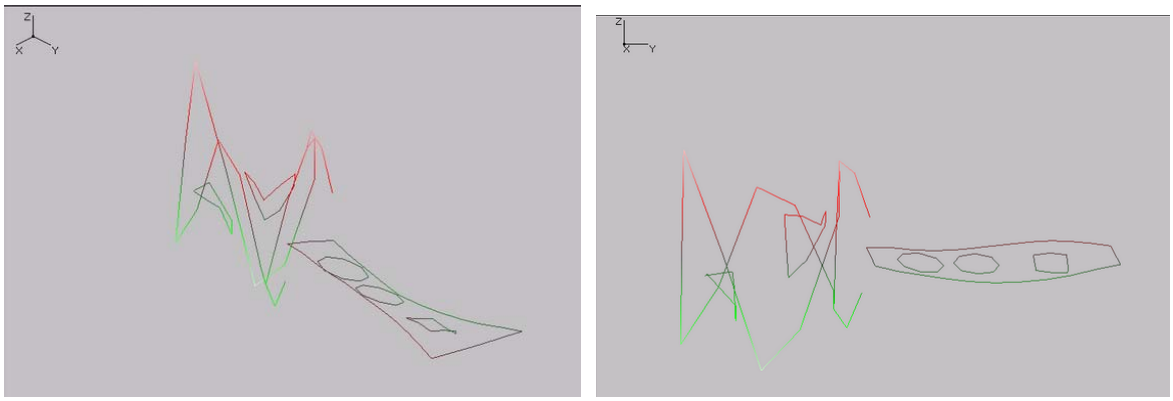

(n) light torsion of suspension and arm at 8354 Hz

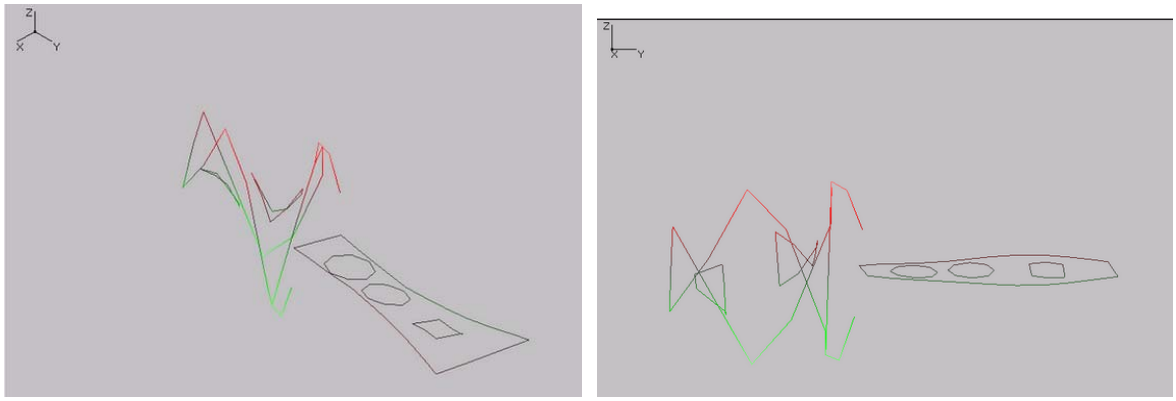

(o) torsion of suspension and light bending of arm at 8916 Hz

Fig. 7.14 The mode shapes of the HAA in vertical direction

7.4 Finite Element Analysis of Head Actuator Assembly

In this section, a finite element model of the HAA is developed and then modal analysis of the HAA are carried out. The analytical modes and FRFs are predicted under different test conditions using FEM and the corresponding identified results are presented.

7.4.1 Finite Element Modeling

A full and accurate mathematical model of the HAA is hard to be achieved using experimental measurements alone due to its structural complexity. Therefore, analytical FEM, which is a powerful numerical method with wide engineering application, is required to model the structure of the HAA in sufficient detail. The main components of the HAA include two sliders, two suspensions, two flexures, three arms, one pivot and one VCM. The details of the pivot include shaft, sleeve and ball bearing. An FE model of the head actuator is created using commercial finite element software, ANSYS, in order to study its dynamic characteristics close to the operating conditions without cover and disk. In the FE model, 4-node shell elements (SHELL63) are used for the suspension. 3-D 8-node solid elements with rotations (SOLID45) are used for the solids such as the sliders and arms. 3-D spring-damper elements (COMBIN14) are employed to simulate the pivot ball bearings. The whole model consists of 13842 elements and 17091 nodes, respectively. The detailed FE model of the HAA is shown in Fig. 7.15. The parameters of general material properties in this FE model are listed in Table 7.4.

For simplicity of modeling, in the FE model, the sliders are attached to the suspensions directly through coupled nodes by neglecting the gimbals, and the suspensions are attached to the flexures through coupled nodes. In addition, the flexures and the arms are also connected together through coupled nodes. The suspensions are modeled by actual geometry with an initial angle, which can apply preload to the sliders. In practice, the VCM

is made of coil and composite, and its exact material properties and internal structure are unknown. In the FE model, the VCM is considered as a structure with uniform mass since this simplification of VCM has no effect on the dynamic analysis of the HAA.

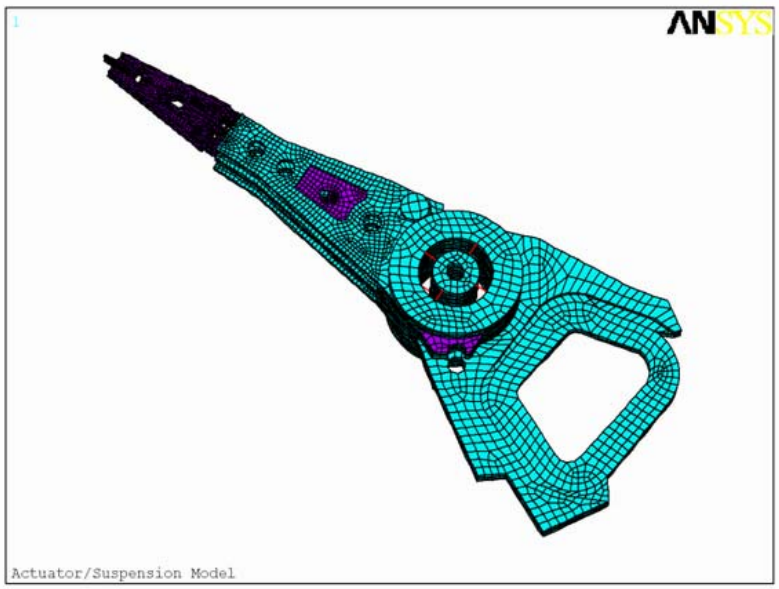

Fig. 7.15 The finite element model of the HAA

In the actual geometry model, the head actuator is supported by the pivot shaft through two ball bearings, so its quasi-rigid body motion has six DOFs. This means that the head actuator can not only rotate about the pivot shaft axis (*z* direction) but also rotate about the lateral direction (*y* direction) and longitude direction (*x* direction) and translate in *x*, *y* and *z* coordinate directions. It should be noted that it is impossible to model the realistic pivot ball bearing accurately since it is a highly nonlinear component. As a result the ball bearings here are modeled by eight linear 3-D spring-damper elements. The more detailed description and formulation of the pivot ball bearing is presented by Xu (2002). For the boundary conditions in this model, the actuator is clamped at the bottom of the bearing shaft since there is no cover, and the two sliders are coupled together since they contact tightly due to the pre-load after the disk is removed.

Table 7.4 The parameters of materials used in the FE model

Name Component	Material	Young's Modulus(pa)	Density (kg/m^3)	Poisson Ratio	Thickness (mm)
Arm	Stainless steel	1.93e11	8030	0.30	
Suspension	Stainless steel	1.93e11	8030	0.30	0.061
Flexure	Stainless steel	1.93e11	8030	0.30	0.020
Slider	Al2O3-TLC	4.12e12	4250	0.27	
VCM		0.758e11	6000	0.343	
Bond-layer		0.02e11	1000	0.3	
Pivot Stiffness	Stainless steel	5.184e11	8030		

7.4.2 Modal Analysis of the HAA

To fully evaluate dynamics of the HAA, FE modal analysis, which has been successfully used to study the dynamics of HDD assemblies, is performed. In an assembly, usually the flexibilities of the components such as suspension, arm, and pivot bearing will affect the bandwidth of the servo control to a large extent, so the analysis here mainly focuses on the dynamic characteristics of the whole actuator assembly. Since the dynamic characteristics of the system are dominated by low frequency modes, in modal analysis of the HAA using FEM, the natural modes with frequency range of 0-10000Hz are extracted. After finite element modal analysis, the first 18 natural frequencies and their corresponding mode shapes are obtained, which are listed in Table 7.5. Fig. 7.16 has presented these main mode shapes, most of which are observed to coincide with the measured mode shapes in section 7.3. In each diagram of the mode shapes shown in Fig. 7.16, the blue-color lines represent the deformed shape of the actuator and the dark dash lines indicate the undeformed edges. As can be found in Table 7.5, the HAA has many strong modes in vertical and lateral directions, such as

Table 7.5 The calculated natural modes of the HAA using FEM

Mode No.	Natural Frequency(Hz)	Mode Shape		
		Suspension	Arm	VCM
1	51.3	Rigid rotation mode		
2	950.9	Bending of 1st arm		
3	1449.9	Bending of 1st suspension and arm		
4	1534.4		Bending of 3rd arm	
5	2358.7	Light lateral bending of suspensions and arms		Lateral bending
6	2810.7	Bending of 2nd suspension	Light bending of 2nd arm	
7	3198.1	Bending of 2nd suspension and arm		
8	3637.3	Torsion of 1st suspension		
9	4161.6			VCM torsion
10	5324.4	Torsion of 2nd suspension	Light torsion of 1st arm	
11	6089.4	Torsion of 1st suspension and arm		
12	6479.3	Torsion of suspensions and bending of arms coupling with lateral QR motion		
13	7148.1	Light bending of 1st suspension and arm and bending of 3rd arm		
14	7500.1	Light bending of suspensions and arms coupling with longitudinal QR motion		VCM bending
15	7906.4	Torsion of 1st suspension and arm		
16	8336.3	Light torsion of 1st suspension and arm		
17	8616.5	Light torsion of 2nd suspension and light bending of 1st arm		
18	8961.2	Torsion of 1st suspension and arm coupling with bending of 1st arm		

suspension bending and torsion, arm bending and torsion, QR motion, coupling motion of suspension and arm, and so on. Most of these modes will lead to large contribution to the FRFs of the HAA in lateral and vertical directions, which will be demonstrated later.

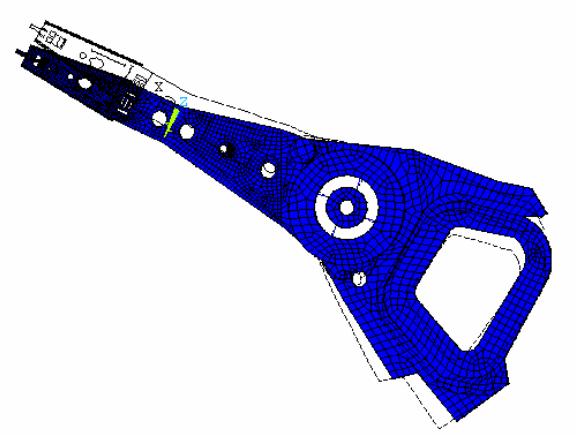

(a) Rigid rotation mode at 51 Hz

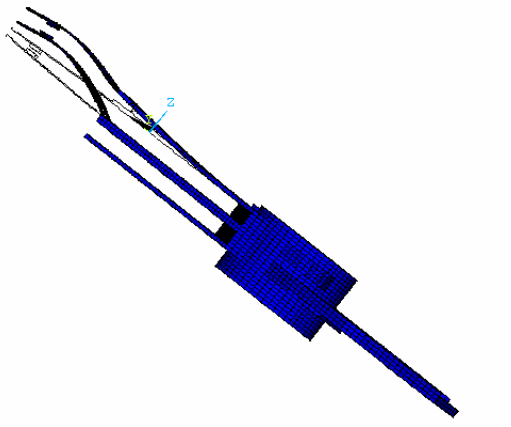

(b) Bending of 1st arm at 951 Hz

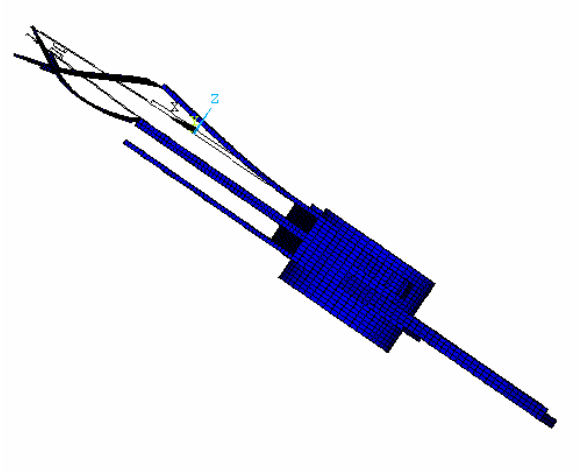

(c) Bending of 1st suspension and arm at 1450 Hz

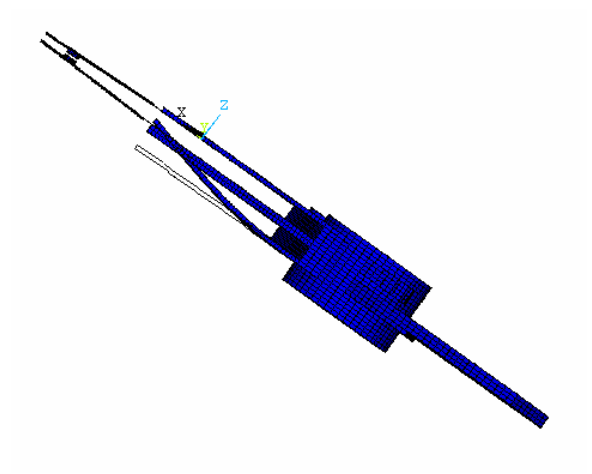

(d) Bending of 3rd arm at 1534 Hz

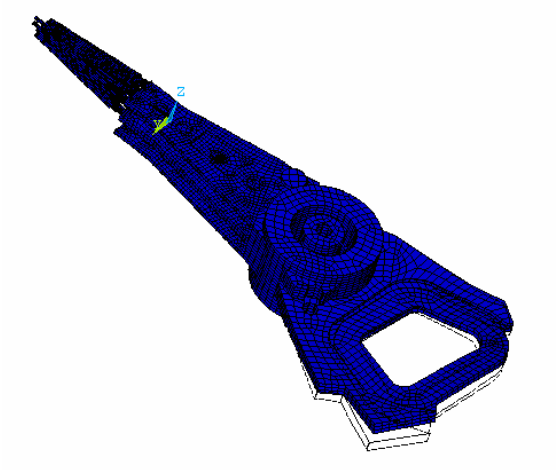

(e) VCM lateral bending and light lateral bending of suspension and arm at 2359 HZ

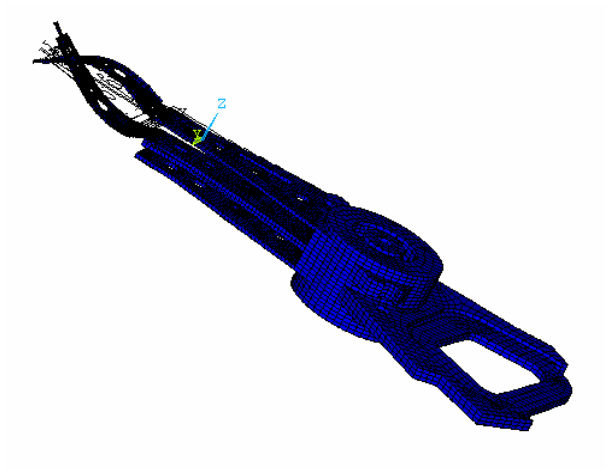

(f) Bending of 2nd suspension with light bending of 2nd arm at 2811 Hz

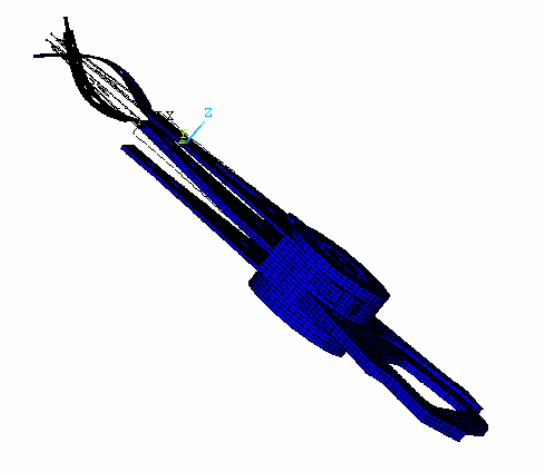

(g) Torsion of 2nd suspension and arm at 3198 Hz

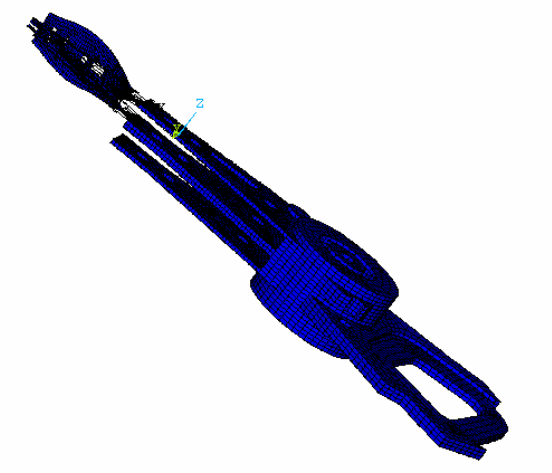

(h) Torsion of 1st suspension at 3637 Hz

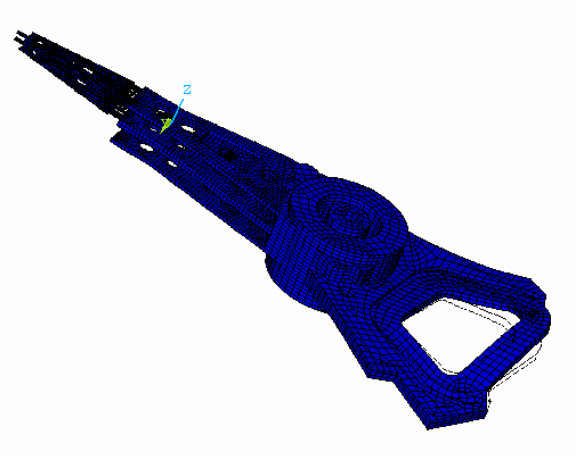

(i) VCM torsion at 4162 Hz

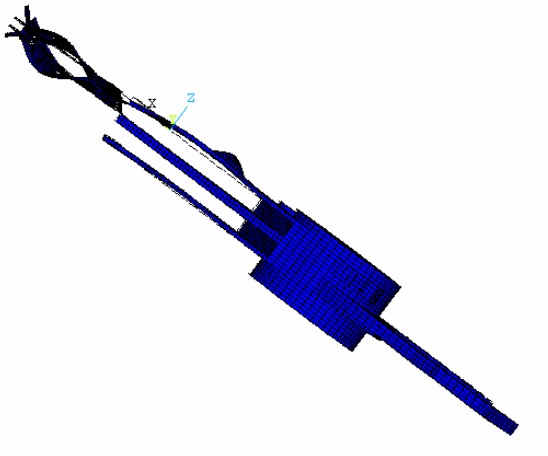

(j) Torsion of 2nu suspension and light torsion of 1st arm at 5324 Hz

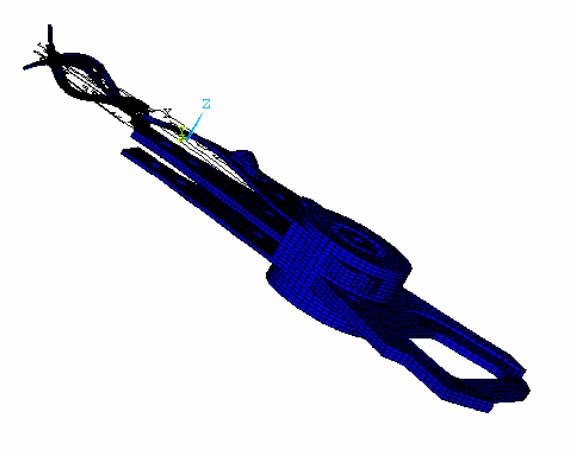

(k) Torsion of 1st suspension and arm at 6089 Hz

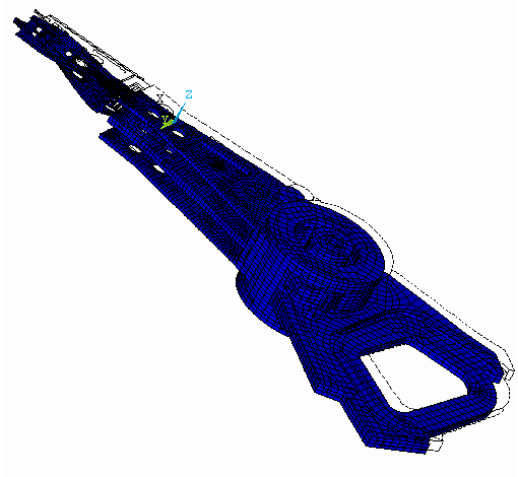

(l) Torsion of suspensions and bending of arms with QR lateral motion at 6479 Hz

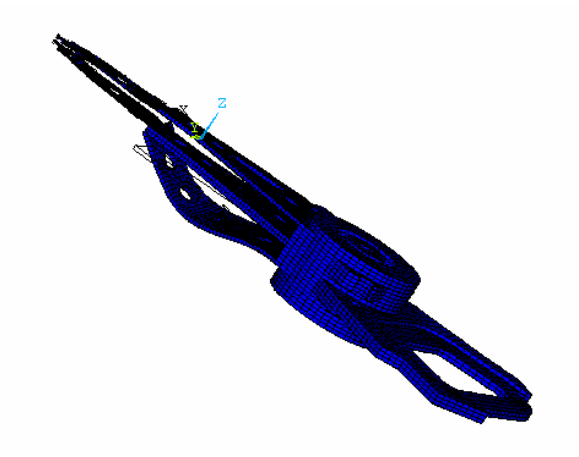

(m) Bending of 3rd arm and light bending of 1st suspension and arm at 7148 Hz

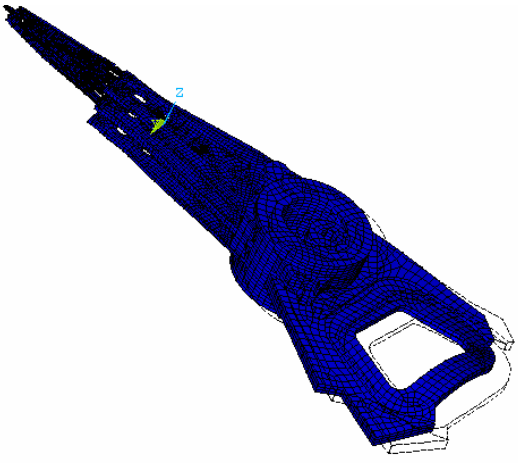

(n) Light bending of suspensions and arms and VCM bending with QR longitudinal motion at 7500 Hz

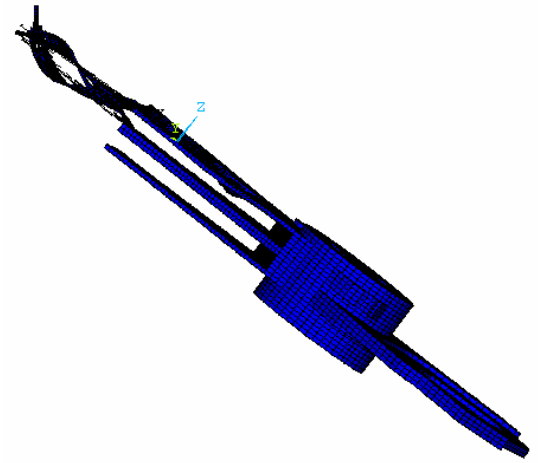

(o) Torsion of 1st suspension and arm at 7907 Hz

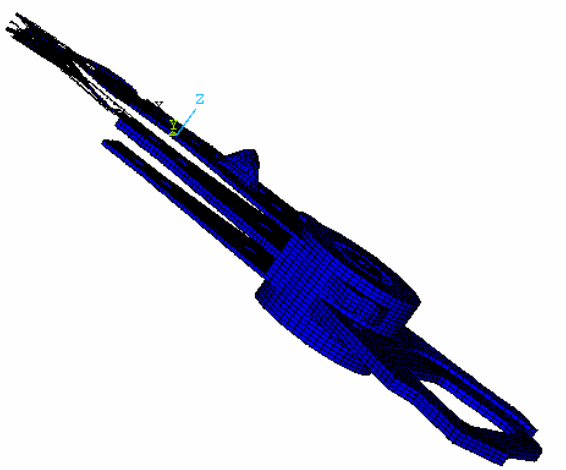

(p) Light torsion of 1st suspension and light bending of 1st arm at 8337 Hz

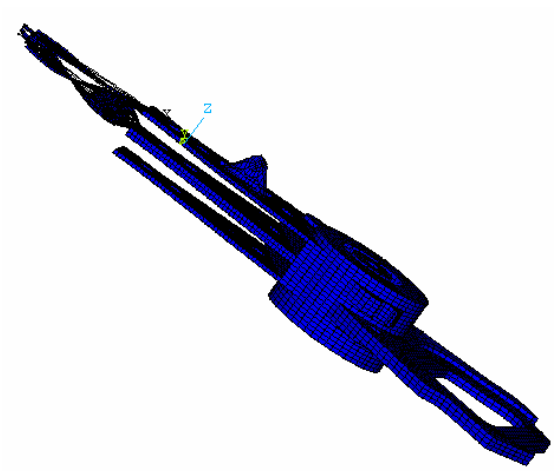

(q) Light torsion of 2nd suspension and light bending of 1st arm at 8617 Hz

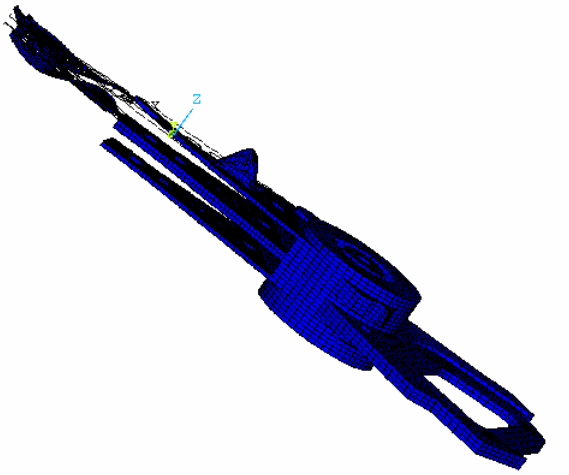

(r) Torsion of 1st suspension and arm with bending of 1st arm at 8961 Hz

Fig. 7.16 The calculated mode shapes of the HAA using FEM

Modes Related to Suspension, Arm and VCM

Among the low frequency modes, the first suspension bending mode is observed at 951Hz in Fig. 7.16(b), which is coupled with the bending mode of the first arm. The first bending mode of the first arm with resonant frequency at 1450 Hz is shown in Fig. 7.16(c), where the first suspension is found to bend in accordance with the motion dictated by the arm, and a relatively small motion on the VCM is observed due to the arm bending mode. Fig. 7.16(f)

shows the bending mode of the second suspension companied by the light bending of the second arm at 2811 Hz, which induces the bending of the first suspension due to the coupling of the sliders. As shown in Fig. 7.16(g), there exists a similar bending mode of the second suspension and arm at 3198 Hz, where the bending of the first suspension is also found. The light lateral bending of the suspensions and the arms at 2359 Hz is found in Fig. 7.16(e), which is one of the major modes in the lateral motion.

The torsion mode of the first suspension at 3637 Hz is illustrated in Fig. 7.16(h), in which the suspension is twisting along its centerline and causing a small amount of in-plane (lateral) motion. The similar phenomenon is observed at the torsion mode of the second suspension coupling of the light torsion of the first arm with resonant frequency at 5324 Hz shown in Fig. 7.16(j). As shown in Fig. 7.16(o), the torsion mode of the first suspension is predicted at 7907 Hz, which brings out the light torsion of the first arm. There is another torsion mode of the suspensions (Fig. 7.16 (k)), which shows the torsion of the first suspension and arm at 6089 Hz.

The light torsion of the first suspension is predicted at 8337 Hz in Fig. 7.16(p), in which the light bending of the first arm is also observed. It is likely that this torsion mode corresponds to an obvious torsion mode of the suspension and arm in the same frequency range in modal testing. Another light torsion of the second suspension at 8617 Hz is shown in Fig. 7.16(q) coupling with the light bending of the first arm. Fig. 7.16(r) shows the significant torsion mode of the suspensions at 8961 Hz, where the first arm is bending and twisting in

order to accommodate the motion. This torsion mode is caused by the out-plane twist deformation of the first suspension, which induces the twist of the second suspension due to coupling. It is obvious that this mode would contribute to a slider lateral motion significantly.

There are four predicted modes, which are related to the VCM. Fig. 7.16(e) shows the VCM lateral bending coupled with the light lateral bending of the suspensions and the arms at 2359 Hz, which is called butterfly mode (Xu, 2000). The torsion mode of the VCM is observed at 4162 Hz (Fig. 7.16(i)), in which one side of the coil is seen to rise, while the opposite end drops in a 180^o out of phase motion. The first bending mode of the VCM (Fig. 7.16(n)) is observed to be coupled with the QR longitudinal motion at 7500 Hz, where the light bending of the suspensions and arms are also be found.

There are another two modes predicted within the frequency range, which are not as important as those described above, such as the first bending mode of the third arm at 1534 Hz (Fig. 7.16(d)) and the second bending mode of the third arm at 7148 Hz (Fig. 7.16 (m)). Generally, these modes are not of interest in this work since they would not have a significant effect on the motion of sliders in lateral or vertical direction.

Quasi-Rigid Body Modes

There exist three Quasi-Rigid (QR) body modes and their corresponding mode shapes have been shown in Fig. 7.16(a), Fig. 7.16(l) and Fig. 7.16(n), respectively. The QR lateral

rotational mode is observed at 51 Hz, where the entire HAA seems to be undergoing a rotating motion along vertical axis. The QR lateral translational mode is predicted at 6479 Hz, whose mode shape shows all components except the bearing shaft are undergoing an in-phase lateral motion. The motion is coupling with the suspension torsion and the arm bending. At frequency 7500 Hz, the QR longitudinal mode is seen to have a coupled motion with the light bending of the suspensions and arms and the VCM bending. In fact, all these QR modes result from elastic connection of the ball bearings in the pivot.

As can be seen from above description of the predicted natural modes, the HAA has many strong modes in vertical direction as well as some lighter modes in lateral direction. Generally, most of the modes in vertical direction will be experienced in the predicted FRFs by the HAA when the vertical excitation is applied. However, in the case that the HAA is excited laterally, not all the modes such as suspension bending, arm bending, and so on, will lead to large contribution to the FRFs in lateral direction. As the head actuator is driven by electromagnetic force in lateral direction close to the operating condition, only the lateral translation and the longitudinal rotation of the actuator assembly are excited. At the same time, some coupling motions in lateral and vertical directions are also involved in.

7.4.3 Frequency Response Functions of FE Model

To forecast vibration behaviors of the HAA, FRFs, which simulate head actuator's responses in case of practical excitation, need to be calculated using FEM. As mentioned in section 7.2, there are two types of FRFs obtained during test according to various excitation mechanisms.

One is the FRF between VCM current input and response output of the actuator and the other is the FRF between base excitation input and response output of the actuator. Usually, the first type of FRF has significance in vibration test and the prediction of the slider's response close to the operating condition using finite element analysis has great importance.

Predicted FRFs under VCM excitation

In the case of VCM current excitation, the input forces are generated due to the interactions between the current in the straight legs of the coil and the magnetic field, and are perpendicular to the straight leg sections. Such forces can be decomposed into radial and circumferential components, and since the radial force has little contribution to the lateral displacement output of the slider, in the FE model only the circumferential force is used as input. The harmonic forces varying in the frequency range of 600-10000Hz, which are employed to simulate the circumferential force, are exerted to the legs of the coil as described in Fig. 7.17. Using harmonic analysis function provided by FEA, the displacement responses

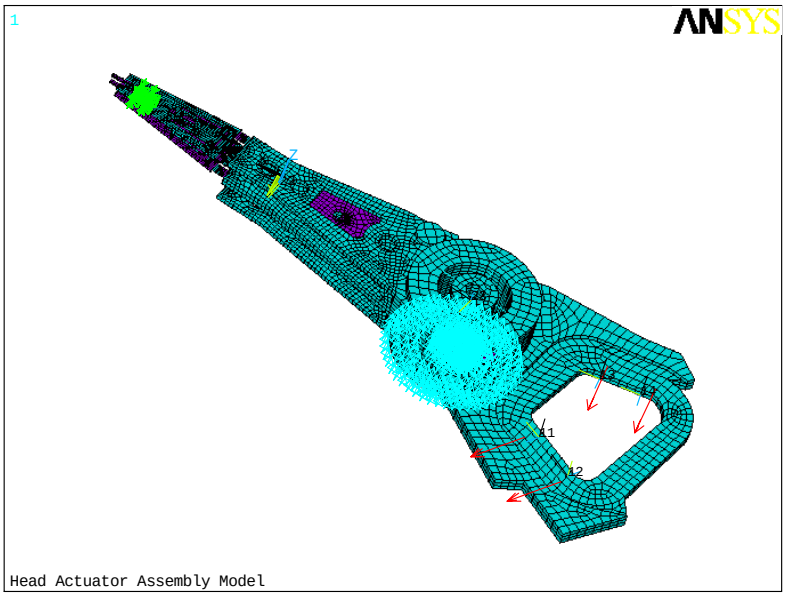

Fig. 7.17 The simulated lateral excitation forces due to current input

of the entire model versus frequency are simulated and obtained. Then, the FRFs between input force and slider response in lateral and vertical directions are calculated and presented, respectively. Meanwhile, the FRFs at other locations of the HAA, such as suspensions and arms under VCM excitation are obtained as well.

Some typical predicted receptance FRFs in lateral direction are displayed from Fig. 7.18 to Fig. 7.24. As can be observed in Fig. 7.18, there are a few apparent resonance peaks in the FRF curves of the sliders, which indicates the sliders will experience only a few significant motions in the lateral direction. These resonances appear due to the fact that various modes of the HAA such as torsion, lateral bending and QR lateral modes are excited by VCM input. The most significant resonance is at frequency 6479 Hz, where the sliders undergo a large amount of motion companied with a phase-shift of 180˚ due to the lateral QR mode. Other four major peaks are also observed at frequency points of 3069 Hz, 3637 Hz, 7907 Hz and 8617 Hz, respectively. From the previous numerical modal analysis results, it has been shown that the modes at these four frequencies are bending and torsion modes of the suspension and the arm respectively, which would contribute to the motion of the HAA in lateral direction. Although the resonance amplitudes at these frequencies are much smaller than that at frequency 6479 Hz, the resonances do affect the lateral motion of the sliders greatly. Similar characteristics can also be observed from the FRFs of the suspensions and the arms (Fig. 7.19), respectively. The resonance peak at frequency 6479 Hz is always extremely distinct, which means that the QR mode at this frequency is the major lateral mode and dominates the lateral motion of the HAA. The resonances at frequencies of 3069

Hz and 3637 Hz are not so distinct in the FRF curves of the suspensions. Moreover, these resonances are almost not observed from the FRFs of the arms since the modes at these two frequencies are torsion modes of the suspensions.

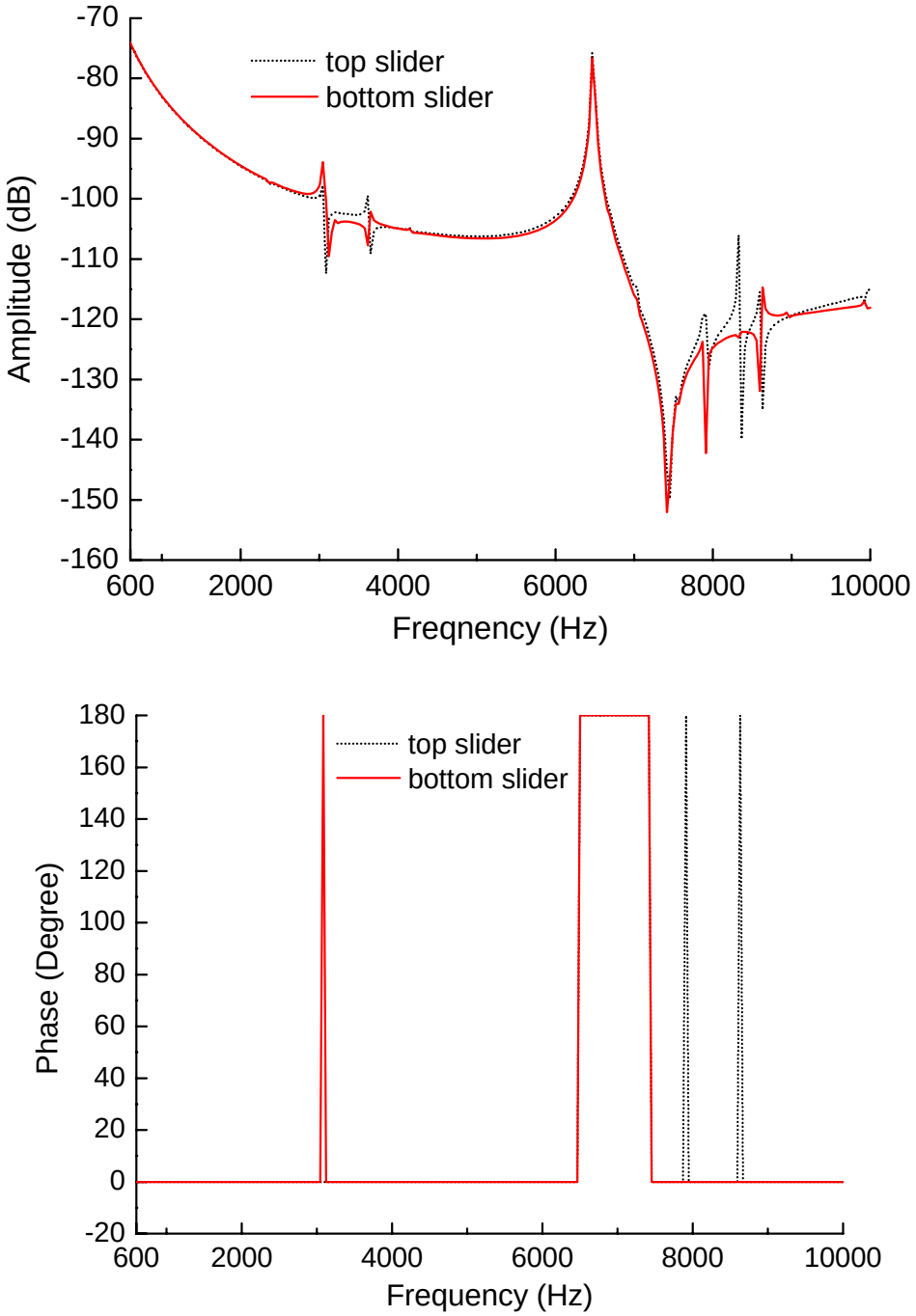

Fig. 7.18 The predicted receptances of the sliders in lateral direction (VCM excitation)

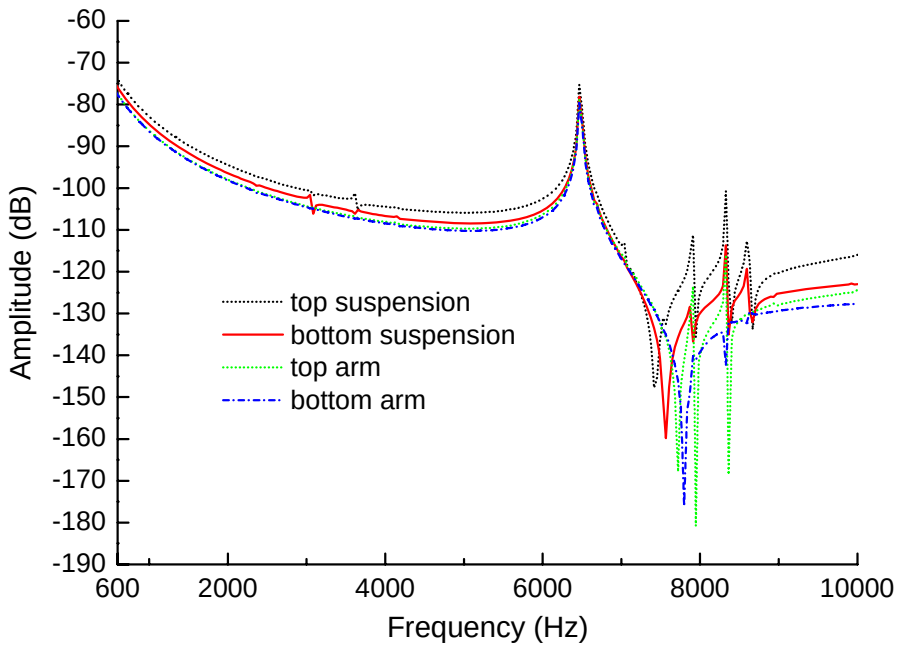

Fig. 7.19 The predicted receptances of the suspensions and arms in lateral direction

The vibration of the HAA in vertical direction is another concern in dynamic response predication using FEM due to its effect on the slider's flying height. The typical predicted FRFs of the slider, the suspension and the arm in vertical direction under VCM excitation are illustrated in Fig. 7.20. As can be observed, more resonance peaks exist in the frequency range from 600 to 10000 Hz than those exhibited in the predicated FRFs in lateral direction. These peaks, which correspond to various predicted modes in vertical direction shown in Table 7.5, occur due to the light vertical motion coupled by the lateral motion. In general, the amplitude values at these resonance peaks are smaller than those at the corresponding peaks of the FRFs in lateral direction as vibration level in vertical direction is much lower under lateral excitation by VCM input. It means that the sliders will not experience large vertical motions in the case of VCM excitation. The figure also shows comparison of the FRFs of the slider, the suspension and the arm, from which it can be observed that the

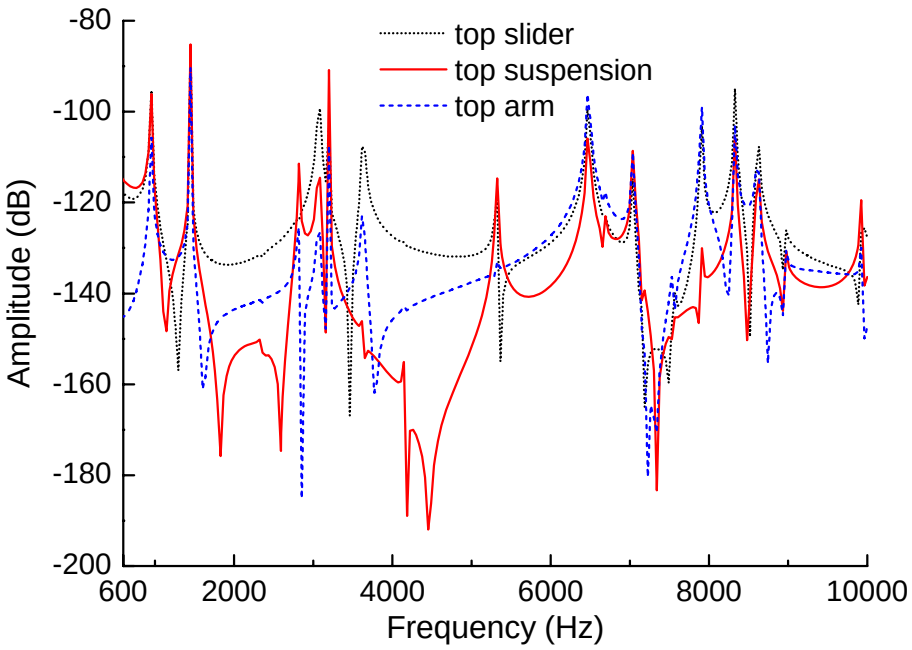

Fig. 7.20 The predicted receptances of the slider, suspension and arm in vertical direction (VCM excitation)

amplitudes of FRFs of the slider, the suspension and the arm decrease in sequence, respectively. It is also found that the slider and the suspension share most resonance peaks since these resonances are induced by the vertical torsion and the bending modes of the suspensions. As can be seen, the dynamic characteristics of the HAA in vertical direction are not as complicated as those in lateral direction since most modes of the HAA are bending and torsion modes of the suspensions and the arms in vertical direction.

Predicted FRFs under Base Excitation

Base excitation testing is a vital way to investigate dynamic characteristics of the HAA although its test condition slightly differs from the practical operating condition of the HAA. Similarly, dynamic responses of the HAA under base excitation can be efficiently predicted by using FEM. In this case, to simulate base excitation, harmonic displacements with the frequency range of 600-10000 Hz were applied to the bottom surface of the pivot in the FE

model and only the displacement input in vertical direction is allowed. After harmonic analysis using FEA, the vertical displacement responses of the entire model are obtained. The FRFs between displacement input and response output are calculated subsequently and the predicted sliders' FRFs in the case of base excitation are presented as well as those of the suspensions and the arms.

A typical predicted FRF of the top slider is shown in Fig. 7.21, from which it is observed that some resonance peaks exist in the frequency range of interest. The predicted FRFs show that the sliders will experience significant vibration at these resonance peaks and the values of these peaks are rather high compared with those of the peaks in the vertical FRF under VCM excitation. This agrees well with what has been observed in the experimental results since vertical modes are more likely to be excited by base excitation in vertical direction. Considering the predicted mode shapes in Fig. 7.16, it can be indicated that almost all peaks appear due to the vertical motion caused by either torsion modes or bending modes. Fig. 7.21 also shows other FRFs of the suspension and the arm predicted in vertical direction under base excitation. Compared with the similar vertical FRFs under VCM excitation, these FRFs have considerable distinct resonance peaks with high amplitude values in low frequency range. It seems that the slider, the suspension and the arm will experience strong vertical motions at frequencies 1450 Hz and 3069 Hz in the case of base excitation. From Fig. 7.21, it is also observed that the stronger vibration in vertical direction will occur at the slider and the suspension rather than at the arm in the frequency range of interest. This can be illustrated from the predicted mode shapes in Fig. 7.16 that

the suspension is more likely to be excited to high level vibration than the arm due to its flexibility.

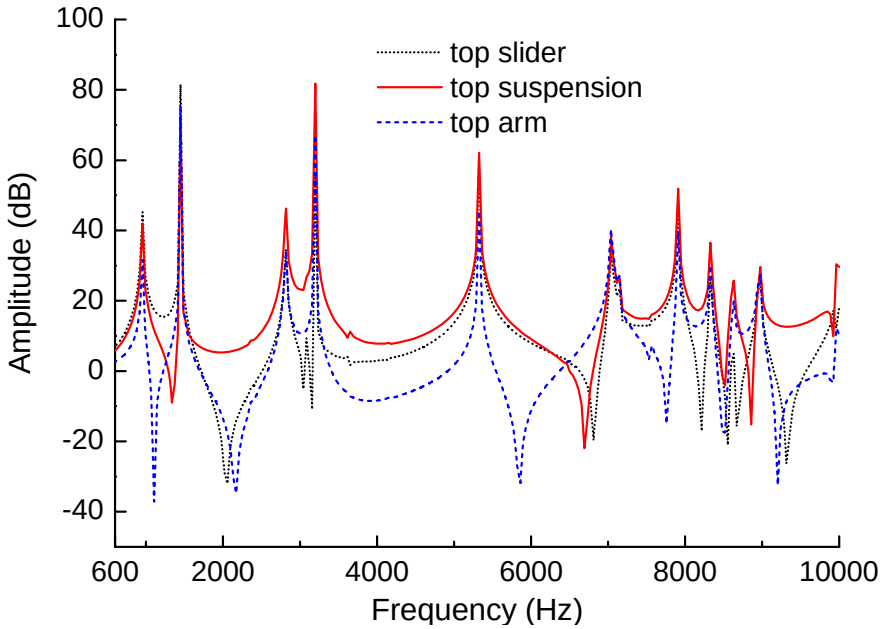

Fig. 7.21 The predicted receptance FRFs of the slider, suspension and arm in vertical direction (base excitation)

7.5 Model Correlation of the HAA

Although analytical modal data and FRFs can be employed to describe the dynamic behaviors of the HAA, the accuracy of the numerical prediction depends on the extent how the mathematical model of the HAA approaches the actual model. Hence, the correlation between the experimental and analytical models is required in order to verify or validate the analytical FE model for further analysis. Based on the work of vibration test and numerical prediction, comparison of the experimental and analytical results of the HAA are carried out to provide sufficient data acquirement for subsequent model updating which can achieve an accurate FE model of the HAA.

Natural frequency and mode shape are the primary modal parameters, which are frequently

chosen for comparison of the experimental and analytical results of a mechanical system. Table 7.6 lists the experimental and analytical natural frequencies and mode shapes of the

Table 7.6 The measured and predicted natural modes of the HAA

Mode No.	Natural Frequency (Hz)			Mode Shape Description
	Modal Testing	FEM	Error	
1	953	950.9	0.2%	Bending of 1st arm
2	1479	1449.9	1.96%	Bending of 1st arm and suspension
3	unmeasurable	1534.4	~	Bending of 3rd arm
4	2449	2358.7	3.69%	Light lateral bending of suspensions and arms and lateral VCM bending
5	2867	2810.7	1.96%	Bending of 2nd suspension and light bending of 2nd arm
6	3301	3189.1	3.39%	Bending of 2nd suspension and arm
7	3733	3637.3	2.56%	Bending of 1st suspension (Torsion of 1st suspension by FEM)
8	unmeasurable	4161.6	~	VCM torsion
9	4215	~	~	suspension and arm 1st torsion mode
10	4956	~	~	Light torsion of suspension coupled with arm bending
11	5213	5324.4	2.14%	Torsion of 2nd suspension and Light torsion of 1st arm
12	6126	6089.4	0.6%	Torsion of 1st suspension and arm
13	unaccounted-for	6479.3	~	Torsion of suspensions and bending of arms coupling with lateral QR motion
14	7196	7148.1	2%	Light bending of 1st suspension and arm and bending of 3rd arm
15	7589	7500.1	0.67%	Light bending of suspensions and arms and VCM bending coupling with longitudinal QR motion
16	unaccounted-for	7906.4	~	Torsion of 1st suspension and arm
17	8354	8336.3	0.21%	Light torsion of 1st suspension and arm
18	unaccounted-for	8616.5	~	Light torsion of 2nd suspension and light bending of 1st arm
19	8916	8961.2	0.51%	Torsion of 1st suspension and arm with bending of 1st arm

HAA obtained from modal testing and FEA, respectively. From the compared results, it can be observed that most analytical natural frequencies have good agreements with experimental ones. Even the biggest percentage error between the analytical and experimental natural frequencies is around 4%, which is consistent with the results of others' research work. However, the compared results for mode shape are not so good as

those for natural frequency. First, more natural modes of the HAA are obtained by FEA than by modal testing. This is due to some limitations of experimental measurement techniques. Second, although most measured mode shapes are identical to predicted ones, there are still a few disagreements between the analytical and experimental mode shapes at certain modes such as the modes at 2449 Hz and 3733 Hz. This may be because the boundary conditions applied to the FE model are a little different from those in the practical test.

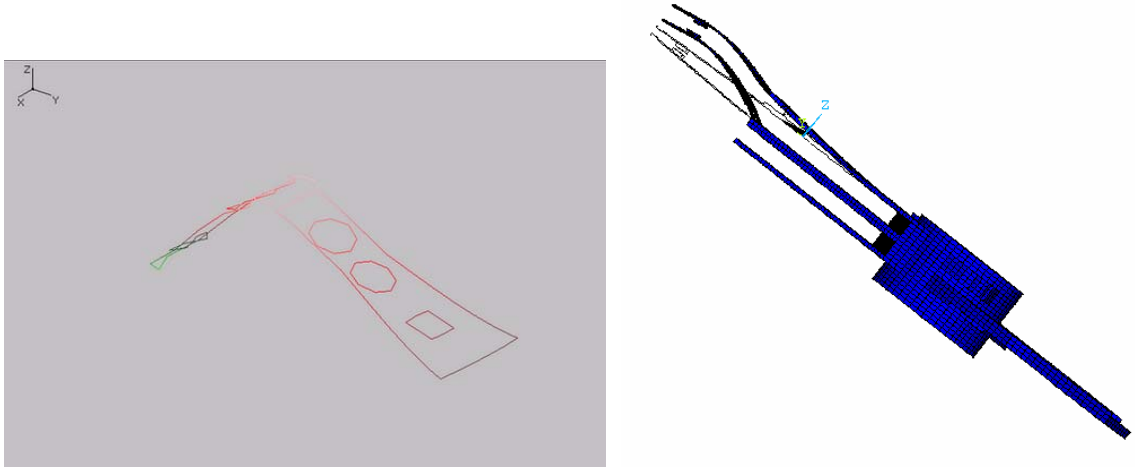

(a) Bending of 1st arm at 953 Hz

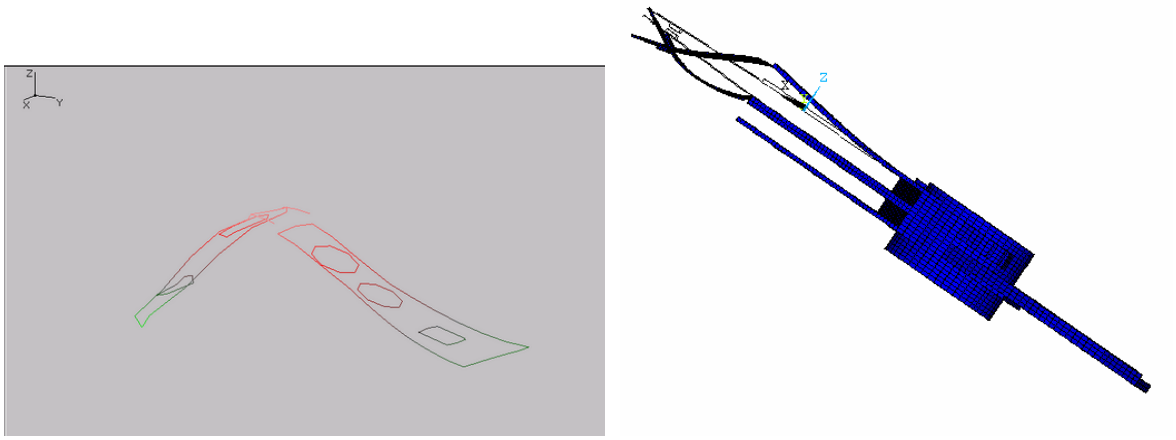

(b) Bending of 1st suspension and arm at 1479 Hz

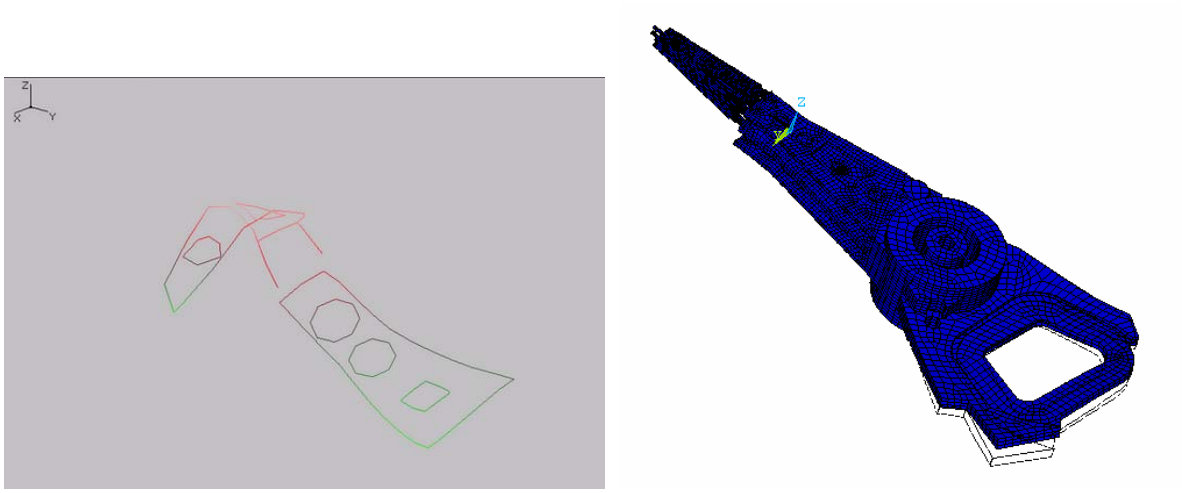

(c) Light lateral bending of 1st suspension and arm at 2449 Hz (coupled by light torsion)

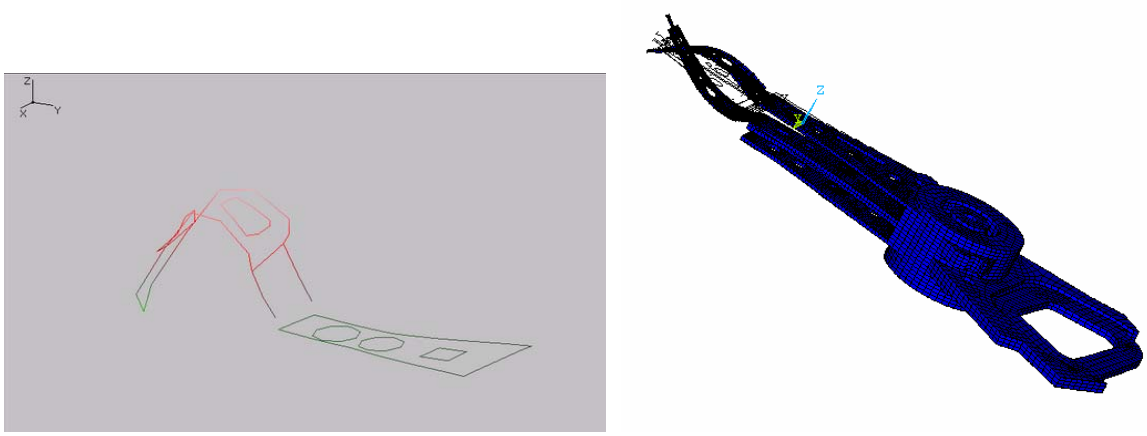

(d) Bending of 2nd suspension with light bending of 2nd arm at 2867 Hz
(causing bending of 1st Suspension)

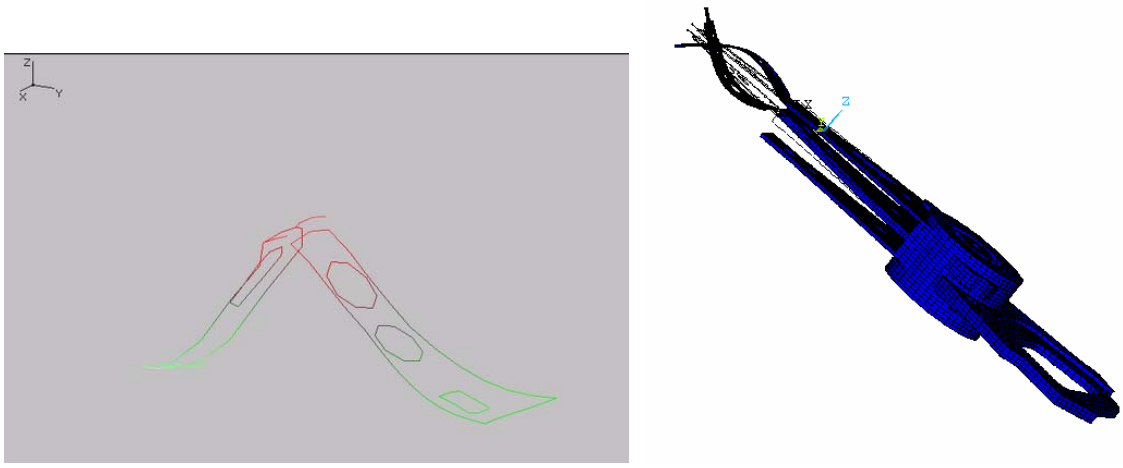

(e) Bending of 2nd suspension and arm at 3301 Hz (causing bending of 1st suspension)

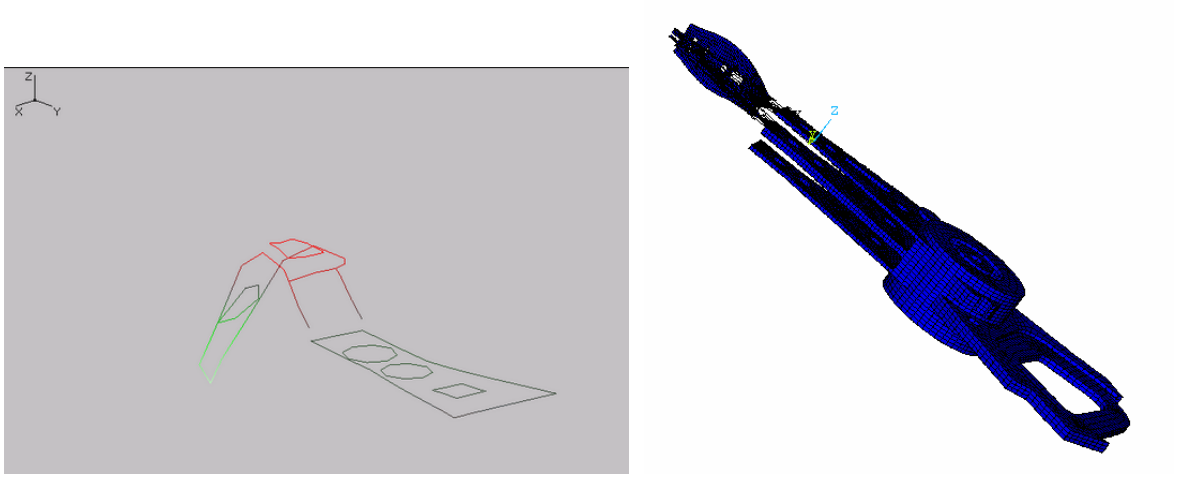

(f) Bending of 1st suspension at 3733 Hz (Torsion of 1st suspension by FEM)

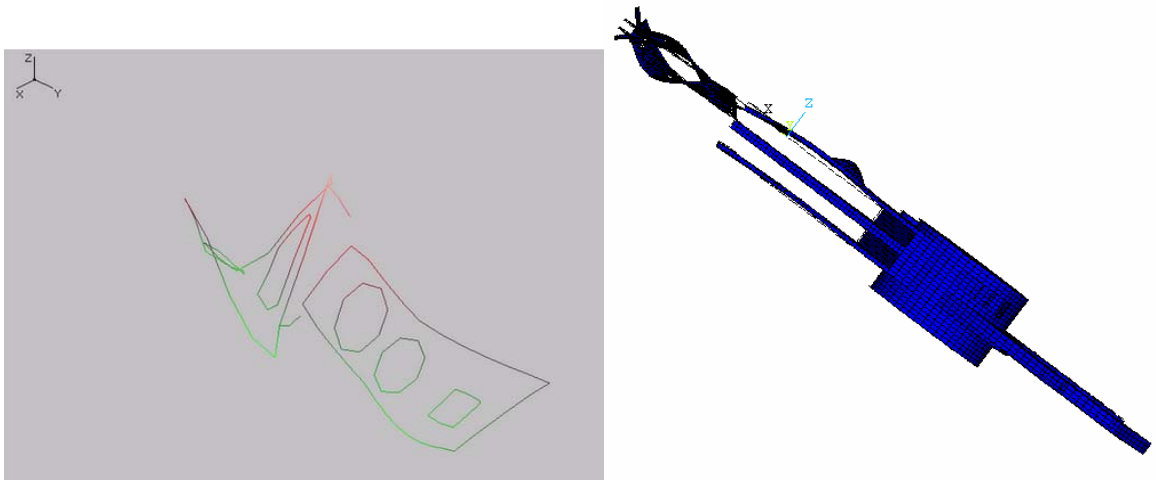

(g) Torsion of 2nd suspension and light torsion of 1st suspension and arm at 5213 Hz

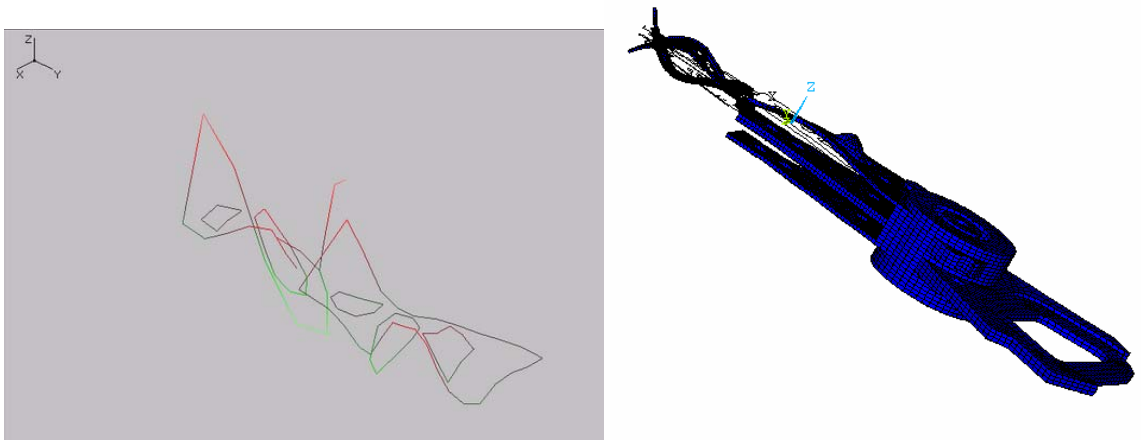

(h) Torsion of 1st suspension and arm at 6126 Hz

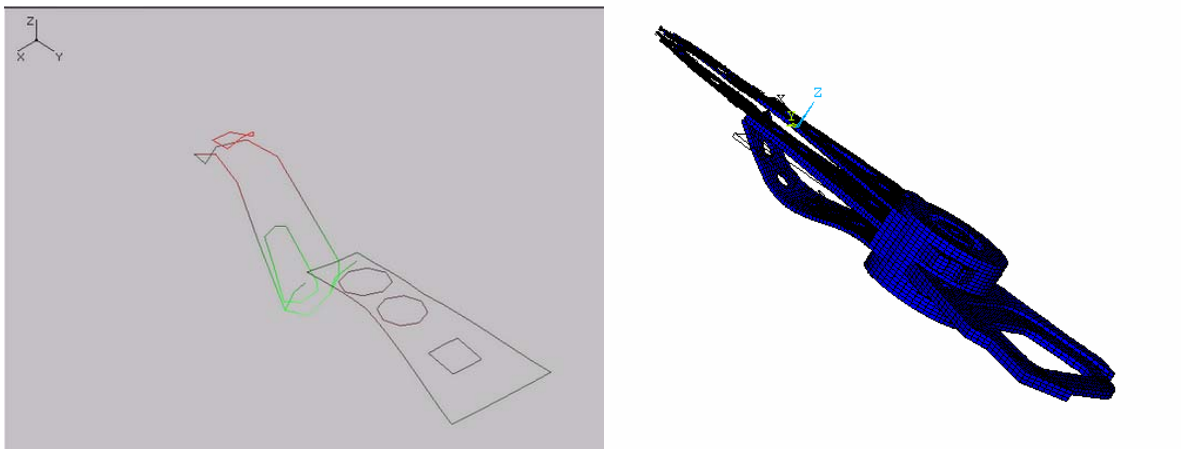

(i) Light bending of 1st suspension and arm at 7196 Hz (with bending of 3rd arm)

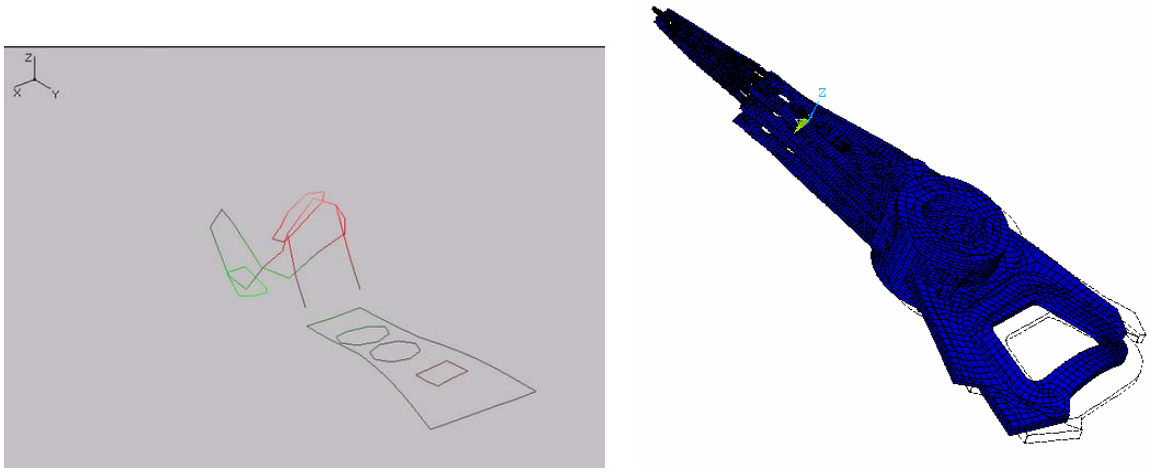

(j) Light bending of suspension and arm at 7589 Hz (with longitudinal QR mode)

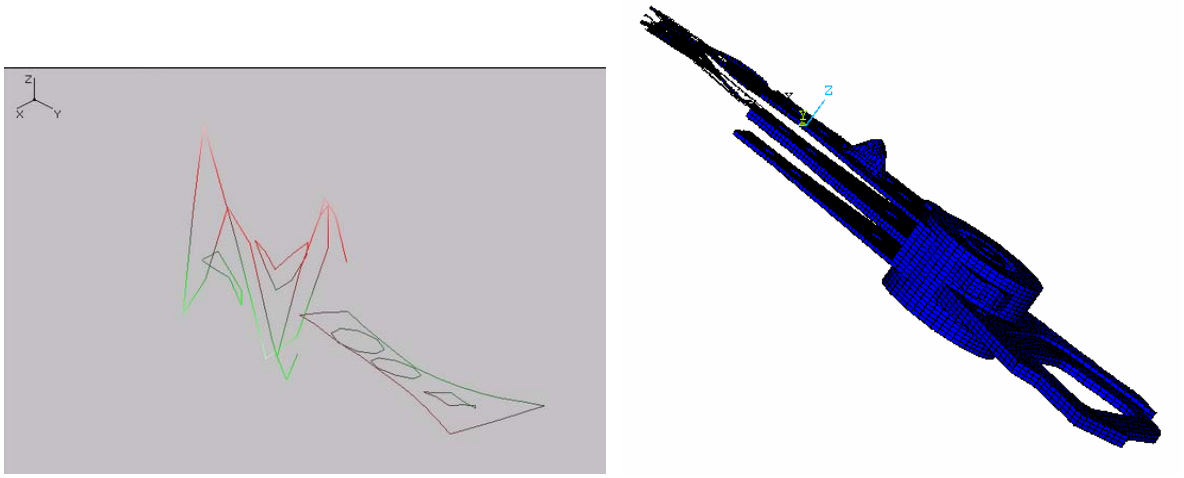

(k) Light torsion of 1st suspension and light bending of 1st arm at 8354 Hz

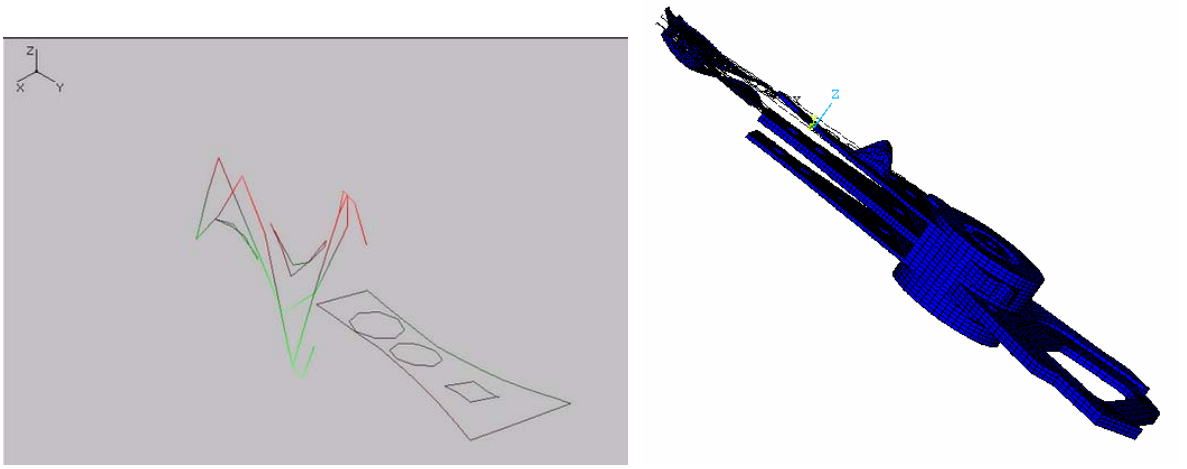

(l) Torsion of 1st suspension and arm coupling with bending of 1st arm at 8916 Hz

Fig. 7.22 The pairs of the matched experimental and analytical mode shapes

As is shown in Fig. 7.22, the left column is the measured mode shapes of the HAA, where the curved lines represent vibration deformation of the HAA. The right column shows the schematic figures corresponding to the deformations simulated by FEM. It should be noted that measurement is done close to the operating conditions, in which the HAA is mounted on the baseplate through a screw. In the FE model, the bottom portion of the pivot shaft is fitted with the boundary conditions to simulate test condition. It is found from experimental measurement and analytical prediction that the HAA has many torsion modes, which lead to contribution of the lateral motions, while only one light lateral bending is indicated. Moreover, the experimental and analytical results show that the HAA has coincident vertical bending and torsion modes, which dominate the vertical motions of the suspensions and the arms. Further, a few modes, which are involved in the motion of the suspensions, such as bending of 1st suspension in Fig. 7.22(e) and torsion of 2nd suspension in Fig. 7.22(g), have shown to be affected by coupling of the sliders significantly.

In order to quantify comparison for modal data, modal assurance criterion (MAC) in equation (2.2) is employed to correlate experimental and analytical mode shapes. Two sets of mode shapes from measured and predicted modes respectively are adopted to construct a MAC matrix, which is formed of individual MAC values. The MAC values of mode shape pairs evaluate the correlation between these modes. Table 7.7 shows the MAC matrix, which is calculated by using the matched mode shape sets of the HAA in Table 7.6. As can be seen, the values of diagonal MAC are very high and close to 100% except that a few of them have the values ranging from 70% to 80%. Most of other MAC elements, which are located at off-diagonal in the matrix, are found to have the values far away from 100%. Hence, the two sets of the mode shapes from modal testing and analytical prediction are considered to be highly correlated. Based on the MAC matrix along with the comparison results from Table 7.6 and Fig. 7.22, it is concluded that the good correlation between the experimental and analytical modal models has been achieved for model validation.

Table 7.7 Tabular of Modal Assurance Criterion Matrix (%)

Ana. mode no.	Experimental mode number											
	1	*2*	*4*	*5*	*6*	*7*	*11*	*12*	*14*	*15*	*17*	*19*
1	**92.9**	3.1	1.5	0.1	4.7	0	1.9	0.2	0	0	1.9	0
2	1.1	**87.1**	2.3	0	0	0.1	0.8	0	0	32.4	0	0.1
4	0.6	1.3	**95.5**	14.3	0	0	23.5	0	0.1	0	0	0
5	0.1	0.1	3.1	**94.2**	5.6	0	0	0	0.2	0.1	4.3	0
6	0	0.1	13.6	1.7	**77.4**	13.5	0	3.6	0	1.7	0	0
7	0.2	0.5	0.6	0.4	7.2	**93.2**	6.7	0	0	0	0	0.2
11	0.4	0	0	0	12.1	8.7	**87.3**	10.1	0	2.3	0.4	0.9
12	0	0	0	39.5	0	0.3	11.7	**79.3**	9.3	0.1	0	0
14	0.3	1.7	0	0	0.2	0.1	1.1	5.7	**86.3**	11.1	0.8	0.1
15	0	0	0.1	0.1	0	0	0	0.7	14.6	**70.1**	2.3	16.4
17	0.2	0.1	0	0	0	4.3	0	0.1	0.7	4.2	**84.4**	7.4
19	0	0.1	0	0	27.2	0	0	0	7.4	1.2	21.7	**90.8**

To compare the experimental and analytical models of a structural system, frequency response function, which describes dynamic response model of a system, is also usually chosen as an object for comparison. Fig. 7.23 shows the comparison of the measured and predicted FRFs at various locations in the HAA in the case of VCM excitation and base excitation, respectively. As can be seen, the FRF curves have different shapes and amplitudes while resonance peaks occur at the almost same frequency locations. This is because the measured and predicted FRFs under VCM excitation have different inputs. One uses current as input and the other uses simulated force as input. Another reason is that the locations of the frequency responses obtained by measurement and prediction are not entirely matched due to the difficulty of positioning the laser point to a specified location in test. It cannot be expected to obtain highly similar FRF curves since the actual measurement environment differs from that in the numerical simulation. The measured lateral FRFs of the HAA show more resonance peaks than those in the predicted ones since the lateral motions may also be caused by some vertical modes due to the coupling motion of the sliders in test condition.

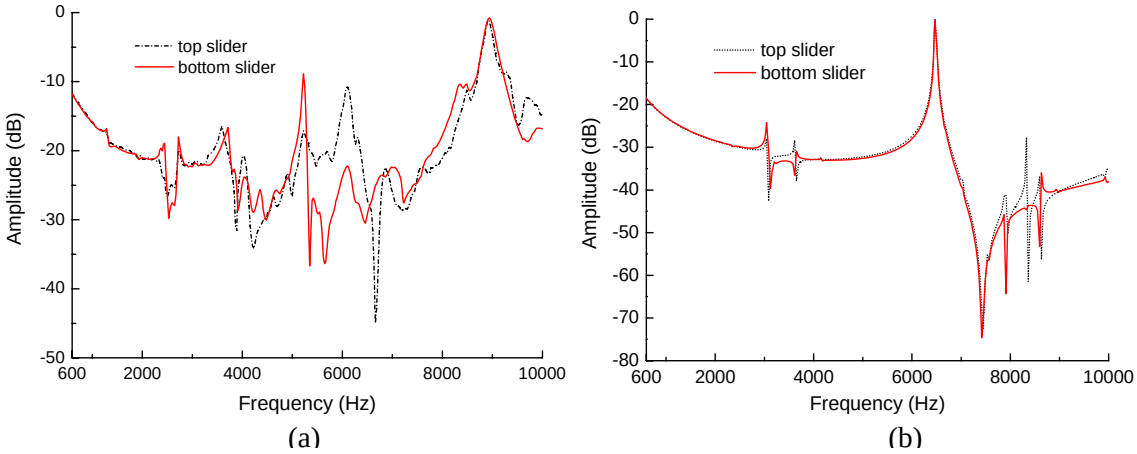

The lateral FRFs of sliders (VCM excitation): (a) measured (b) predicted

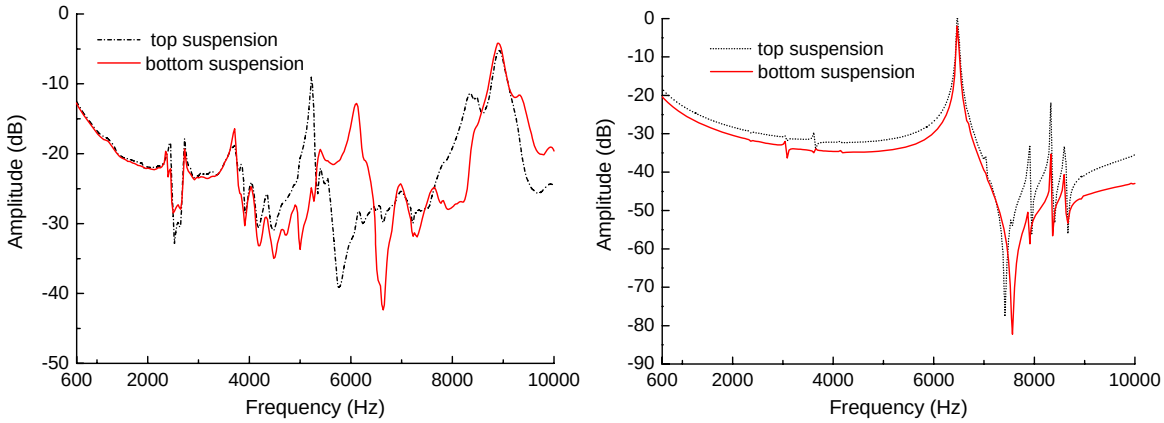

(a) (b)

The lateral FRFs of suspensions (VCM excitation): (a) measured (b) predicted

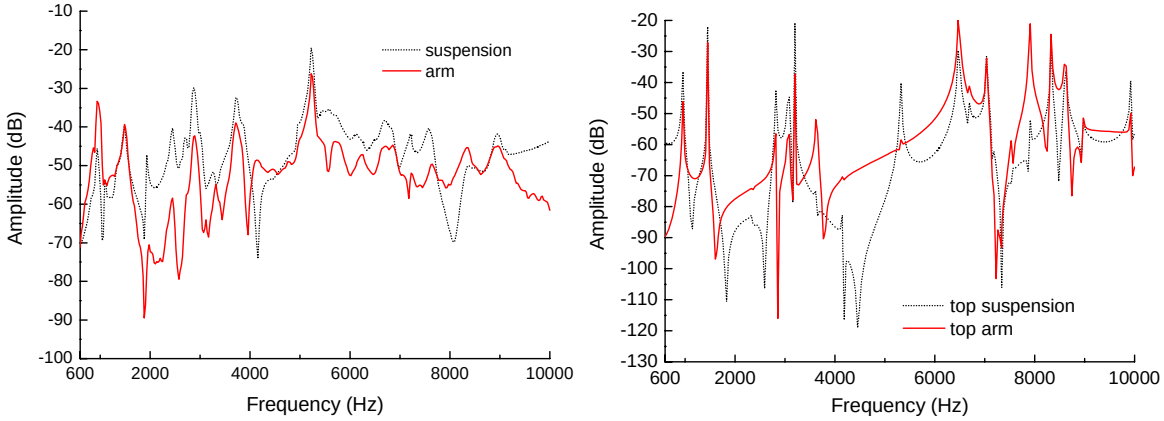

(a) (b)

The vertical FRFs (VCM excitation): (a) measured (b) predicted

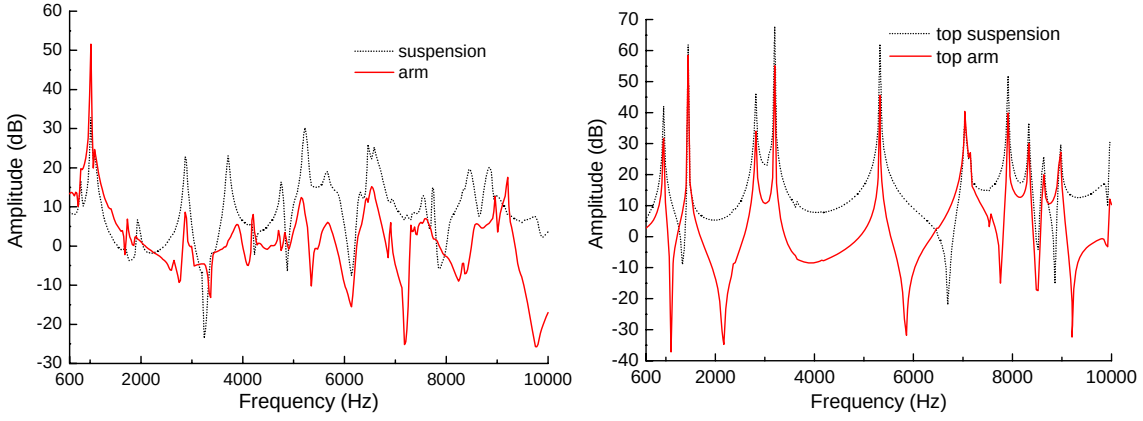

(a) (b)

The vertical FRFs (base excitation): (a) measured (b) predicted

Fig. 7.23 The comparison of the experimental and analytical mobility FRFs

From the predicted FRFs shown above, it can be found that the HAA will experience

significant lateral motion at frequency 6479 Hz in the case of VCM excitation while that is not the case for the measured FRFs. This may be due to the fact that there is a lateral QR mode predicted at that frequency point, which dominates the lateral motion of the HAA, while measurement has not obtained it. In fact, QR modes are significantly affected by the stiffness of the ball bearing in the pivot. In the FE model, the ball bearings are simulated using spring-damper elements and their stiffness values are determined based on the test results of an isolated pivot. Due to the nonlinearity of the ball bearings, spring-damper element may not accurately describe the actual dynamic behavior of the pivot under vibration. Therefore, the stiffness of the ball bearing is the key parameter, which needs to be considered when the model updating procedure of the HAA is performed. It is also observed that the typical experimental FRFs have smaller amplitudes in resonant frequency ranges than the analytical ones. This is because the damping properties of the HAA have been exhibited when the structure is vibrating while it is totally neglected in the FE model for the simplicity of analysis. Hence, damping is another crucial factor, which cannot be ignored during the model updating procedure.

7.6 Summary

Characterization of dynamic behaviors of a microsystem, based on modal testing and finite element modal analysis of the HAA, is presented in this chapter. The FRFs were measured in the case of VCM and base excitation and the modal analysis procedure was performed. It is evident that the vibration responses of the HAA are various since lots of modes and coupling motions are involved in the oscillatory motion. Under test, some significant lateral modes are

shown to be pure lateral bending or torsion modes accounting for track seeking errors. In vertical vibration, many strong bending modes and torsion modes exhibit in the frequency range of interest. For simulation, the full analytical FE model of the HAA was established and the modes in lateral and vertical directions were predicted using FEA as well as the analytical FRFs with different inputs.

Based on modal testing and FEA of the HAA, the input experimental and analytical data are collected and prepared for subsequent model updating. In order to validate the FE model, the analytical modes and the predicted FRFs were generally compared and correlated with the measured ones. It has been found that the experimental and analytical modal data agree well though a few modes cannot be properly matched. Furthermore, some discrepancies exist between the measured and predicted FRFs in terms of amplitude and shape. It is concluded that the FE model of the HAA cannot be fully validated by vibration test data though this FE model is believed to be not far from the actual one. Consequently, the proposed updating methods can be applied to this model to demonstrate how the practical updating procedure of a typical microsystem can be achieved.

Chapter 8

Conclusions and Recommendations

8.1 Conclusions

The rapid development of microsystems poses a grand challenge for modeling and testing of microsystems. In order to achieve an accurate and reliable mathematical model, original FE models of microsystems need to be modified by incorporating experimental information. However, the particularity of vibration testing techniques for micrsoystems brings out the difficulty in the traditional model updating methods. Most techniques can only measure natural frequencies of microstructures while mode shapes and conventional FRFs are usually not obtained since the measurement of excitation force is hardly achieved. Therefore, the appropriate experimental data of microstructures cannot be provided for model updating by most testing techniques since most traditional updating methods are based on modal data and FRF data. On the other hand, the characterization of damped microsystems presents an issue in FEM simulation. Because damping force, to which microstructures are subjected, is more notable in dynamic equation of micro-scale than that in macrostructures and it affects microsystems' performance significantly. The damping models in microstructures are so complicated that they are hard to be described accurately only by means of analytical methods especially for air damping. Hence, the identification of damped microstructures using vibration test data is required in modeling of microsystems.

Focusing on the updating techniques and their unsolved issues when applied to model updating of microsystems, this dissertation has presented a complex formulation of the FRF method and a new method using base excitation test data directly for updating. The conclusions of the research drawn in this dissertation are listed below.

The major issues in vibration test of microsystems are the particular excitation and measurement techniques and various damping mechanisms. They require the model updating methods to be able to match experimental data from damped structural models of microsystems. A critical review and discussion shows that most of the updating methods are still far from being mature and there have yet to be robust approaches that can be successfully applied to model updating of microsystems. The typical vibration testing techniques for microsystems were discussed. It has been observed that LDV technology combined with base excitation is a promising vibration test technique for model updating of microstructures. Because it has the capability to obtain response functions under base excitation, which are the most appropriate experimental data for most updating methods. In addition, air damping is shown to be dominant in microdynamics of microsystems and hard to be characterized by analytical methods alone. The updating techniques should be able to not only modify FE models of microstructures but also identify their damping.

The relationship between viscous and structural damping models in a damped system has been studied in detail. For a proportionally damped system, an exact relationship exists between structural and viscous damping models, which is described as $\eta_r = 2\xi_r$. The identified damping matrix is not proportional though the equivalent mode shapes remain real. In the case of non-proportional damping, the equivalent mode shapes are almost the same as their counterparts of the original system except differing by a complex scaling factor. Numerical examples have efficiently demonstrated that the error in estimating modal parameters induced by wrongly interpreting damping model is quite small. Furthermore, a physically meaningful equivalent damping matrix exists in the case of the system with distributed damping, while it is not the case if damping is localized. Therefore, the

appropriate selection of damping model is critical in the latter case. Experimental example based on a simple vibration test has verified the validity of the relationship between the two damping models for practical damped structural systems.

The real FRF based updating method has been further developed and extended to the case of model updating of generally damped structures. The complex FRF updating formulations to directly identify damping coefficients and update modeling errors simultaneously, have been established for the cases of proportionally damped and non-proportionally damped structures, respectively. Simulated numerical case studies based on practical structures with various damping have been carried out to assess the applicability of the proposed complex FRF based updating method. The success of these cases has proved the feasibility and practicality of the method when applied to identifying damping coefficients, as well as mass and stiffness modeling errors. The impact of noise-contaminated FRF data on the updated results has also been evaluated for the complex updating process. It is observed that sufficient accuracy of identified damping coefficients is not obtained for the case where measured FRF data contain high level of measurement noise.

A two-level updating scheme based on Taguchi method has been proposed for model updating of damped structures, where modeling errors and damping coefficients are identified respectively in different levels. A numerical example based on a cantilever beam with structural damping verifies the feasibility and efficiency of the proposed technique when applied to updating of generally damped structures even using noise-contaminated test data. The identified results of stiffness errors and damping coefficients are reasonably accurate and robust against various noises including random and systematic errors even in

the case of a high level of uncertainty. Modal data and FRF data can be used for the different objective functions in the two levels of the updating scheme respectively.

A novel method has been developed for model updating using base excitation test data directly since conventional FRFs or derived modal data are not readily available in base excitation test. The mathematical updating formulations, where response function data measured under base excitation are employed directly to identify modeling errors, have been established. Simulated numerical examples based on a cantilever and a practical GARTEUR structure have been carried out to evaluate the applicability of the method. The successful cases have proved the feasibility and practicality of the proposed method in the case of identification of mass and stiffness modeling errors. Very promising results can be obtained even for the case of the measured response function data contaminated by high level measurement noise. Experimental example based on a mini-cantilever under base excitation demonstrates that this method can be applied to FE model updating of practical microstructures using base excitation test data with confidence.

To characterize dynamic properties of a microsystem, modal testing and finite element analysis based on the example of HAA have been carried out, respectively. The measurement of FRFs and the modal analysis procedure have been conducted. The various FRFs of the HAA close to operating condition have been measured in the case of VCM and base excitation. Under testing, the HAA possesses certain significant modes in lateral direction, which are pure lateral bending or torsion modes in contributions to the lateral responses. Many strong bending and torsion modes are also exhibited clearly in vertical vibration. A full FE model of the HAA has been established and the analytical modal data have been predicted

by FEA as well as the FRFs with various input. It is obvious that the predicted modes and FRFs are more sophisticated than the measured ones.

To validate the FE model of the HAA for later possible model updating, the analytically predicted modes and FRFs have been compared and correlated with the experimentally measured ones. The comparison indicates that the experimental and analytical modal data agree well though a few modes cannot be accounted. However, there is no such a good agreement for the case of the FRFs and some differences in terms of amplitudes and shapes exist between the measured and predicted FRFs. Hence, it is concluded that the validation of the FE model of the HAA has not be perfectly achieved by vibration test data while this model approaches the actual structural model. The proposed updating methods can be subsequently applied to updating this model to show a practical updating procedure of a microsystem.

8.2 Contributions

Based on the research work undertaken for model updating of microsystems, the main achievements delivered by this dissertation are summarized as follows.

The modal identification procedure, where arbitrary selection of a damping model for a damped system, such as viscous damping is interpreted as structural one or vice versa, is involved, has been investigated. The relationships between structural and viscous damping models have been presented for the cases of proportionally and non-proportionally damped systems and it is demonstrated by numerical simulations and an experimental example.

The complex updating formulation of the FRF method for generally damped structures have been successfully established to directly identify damping coefficients and simultaneously update mass and stiffness modeling errors. The applicability of the proposed method has been demonstrated based on simulated numerical examples. The effect of measurement noise in FRF data on the complex updating process has been investigated and it is shown that the accuracy of identified damping coefficients will be affected notably in case of high level of measurement noise.

The two-level Taguchi updating scheme has been proposed to identify stiffness modeling errors and damping coefficients respectively in different levels. This technique has been approved to be efficient and have high noise-resistance when applied to updating damped structural models even using highly noise-contaminated test data.

The novel method directly using response function data measured under base excitation for model updating has been developed successfully. The applicability of the proposed method has been demonstrated by various numerical and experimental case studies. The noise-resistance ability of the methods has been evaluated for the case of quite noisy test data. The experimental example shows the practical application of this method to FE model updating of microstructures using base excitation test data.

Modal testing and finite element analysis of the microsystem, HAA, have been performed to comprehensively characterize its dynamic properties such as modes and FRFs, respectively. To validate the analytical FE model of the HAA for later model updating, the analytically predicted data have been compared and correlated with experimentally measured ones. Based on the comparison, one conclusion is drawn that the FE model has not been efficiently

validated by vibration test data. The proposed updating methods can be applied to updating the FE model of the microsystem subsequently.

8.3 Recommendations

Extensive investigation work on model updating of microsystems has been performed in this thesis. To improve the performance of the updating techniques developed in this work and convert this technology into practical design tool in model updating, some further development that may be of interest in this field has also been suggested. The following topics are the potential areas of research which are most likely to prove to be promising.

In order to identify damped structures using the FRF based method, an appropriate damping model needs to be introduced into FE model. In the present study, individual damping element in FE model is proportional to the corresponding stiffness elements with appropriate coefficients. In next step, the general form of proportional damping in equation (4.13) will be employed in damping element level during the construction of global damping matrix. This may be a more general and reasonable expression of damping element. Then, the complex FRF sensitivity with respect to damping coefficients can be calculated for updating to determine the appropriate coefficients. Of course, numerical and experimental examples should be carried out to rigorously evaluate the effectiveness of this damping matrix for model updating of structures with various damping, such as viscous damping, structural damping or others. Moreover, it is believed that damping at the joint positions of structures is more significant than that at other locations. Therefore, the effective localization technique needs to be developed for the case of damped structural models. This technique should include the complex FRF sensitivity with respect to damping coefficient since the complexity of FRFs is naturally related to general non-proportional

damping. In addition, the parameterization of damping with respect to macro element may be considered to reduce the number of damping coefficients significantly since most practical structures have localized damping at joint positions. Thus, the adverse effect of noisy measurement data on the identified damping coefficients can be weakened for the propose method.

For the novel updating method using base excitation test data, the non-uniqueness of design parameters may occur in updating procedure as it usually behaves in other FRF based methods. The possible mechanism which leads to the non-unique solution should be explored. In order to avoid non-unique solution, the correlation technique, which uses Modal Assurance Criterion in equation (2.2) to efficiently correlate the experimental and the updated modal data, will be employed to examine the exact updated parameter. Then, the set of correction factors for modeling errors, which achieves the updated model with the highest values of MAC, can be assumed the unique solution for model updating. For further application to general structures, the updating method using base excitation test data needs to consider identifying damping while updating stiffness and mass modeling errors. Hence, the sensitivity of response functions with respect to damping coefficients should be formulated. The mathematical formulas for updating modeling errors and damping coefficients are to be established for the case of general damping. Various numerical cases should be performed to assess the effectiveness of the method for damped structure case.

In this study only a few experimental examples have been undertaken to demonstrate the applicability of the proposed updating methods because of the limited period of time. It is necessary for these methods to be more rigorously tested using actual application examples. Vibration tests for various cases are required to be designed and performed deliberately

such as optimization of measurement and excitation locations, typical structural models with various damping and various boundary conditions for test structures. Due to time limitation and shortage of fund, practical application to model updating of microsystems just starts its first step in this work. Modal testing of the typical microsystem, the HAA, needs to be conducted strictly to collect ample and high quality test data. The valid FE model with appropriate mesh size, which predicts quite similar dynamic properties to the structural model in the frequency range of interest, should be established. Subsequently, a FE model updating procedure based on the FE model and experimental data should be thoroughly performed using the proposed methods.

References

Adhikari S. and Woodhouse J., 2001, Identification of damping: Part 1, viscous damping, *Journal of Sound and Vibration*, 243(1), pp. 43-61

Ahmadian H., Mottershead J. E. and Friswell M. I., 1998, Regularisation methods for finite element model updating, *Mechanical Systems and Signal Processing*, 12(1), pp. 47-64.

Aritegui J. L. and Geers T. L., 2000, Shock Analysis of a Disk Drive Assembly, *J. Info. Storage Proc. Syst*, Vol. 2, pp. 25-31.

Attala Mauro J., 1996, Model Updating Using Neural Networks, Ph.D. Dissertation, Virginia Polytechnic Institute and State University.

Attala Mauro J., 1998, On Model Updating Using Neural Networks, *Mechanical Systems and Signal Processing*, 12(1), pp. 135-161.

Balmés E., 1997, New Results on the Identification of Normal Modes from Experimental Complex Modes, *Mechanical Systems and Signal Processing*, Vol. 11(2), pp. 229-243.

Bao M. H., H. Yang, Yin H. and Sun Y. C., 2002, Energy transfer model for squeeze-film air damping in low vacuum, *Journal of Micromechanics and Microengineering*, 12, pp. 341-346.

Baruch M., 1982, Optimal correction of mass and stiffness matrices using measured modes, *AIAA Journal*, 20(11), pp. 1623-1626.

Beliveau J. G., Vigneronc F. G., Soucy Y. and Draisey S., 1986, Modal parameter estimation from base excitation, *Journal of Sound and Vibration*, Vol. 107, pp. 435-49.

Berger H., Barthe L. and Ohayon R., 1990, Parametric updating of a finite element model from experimental modal characteristics, *Mechanical Systems and Signal Processing*, 4(3), pp. 233-242.

Berman A. and Nagy E. J., 1983, Improvement of a large analytical model using test data, *AIAA Journal*, 21(8), pp. 1168-1173.

Blech J. J., 1983, On isothermal squeeze films, *J. Lubr. Technol A*, 105, pp. 615-620.

Caesar B., 1986, Update and identification of dynamic mathematical models, *4th IMAC*, pp. 394-401.

Caesar B., 1987, Updating system matrices using modal testing data, *5th IMAC*, pp. 453-459.

Caughey T. K., 1960, Classical normal modes in damped linear dynamic systems, *Journal of Applied Mechanics*, 27, pp. 269-271.

Caughey T.K., O'Kelly M.E.J., 1965, Classical normal modes in damped linear dynamic systems, Transactions of ASME, *Journal of Applied Mechanics*, 32, pp. 583–588.

Chang C. C. C., Chang T. Y. P., Xu Y. G. and To W. M., 2002, Selection of training samples for model updating using neural networks, *Journal of Sound and Vibration*, 249(5), pp. 867-883.

Chen G. and Ewins D. J., 2001, Verification of FE models for model updating, *19th International Modal Analysis Conference*, pp. 385-391.

Chen, J. S., Su, C. P. and Chou, Y. F., 1995, Modal Analysis for Miniature Structures, *Proceedings of the International Modal Analysis Conference*, pp. 969-975.

Chen Kun-Nan, Gau Wei-Hsin, Hu Yuh-Chung, 2006, Identification of material and geometrical parameters for microstructures by dynamic finite element model updating, *Microsystem technologies*, 12, pp. 736-745.

Chen S.Y., Ju M.S., Tsuei Y.G., 1996, Extraction of normal modes for highly coupled incomplete systems with general damping, *Mechanical Systems and Signal Processing*, 10, pp. 93-106.

Cho Y. H., Pisano A. P. and Howe R. T., 1994, Viscous damping model for laterally oscillating microstructures, *Journal of Microelectromechanical Systems*, 3, pp. 81-87.

Chou Y. F., Wang L. C., 2001, On the modal testing of microstructures: its theoretical approach and experimental setup, *Journal of Vibration and Acoustics*, 123, pp. 104-109.

Christian R. G., 1966, The theory of oscillating-vane vacuum gauges, *Vacuum*, 16, pp. 175-

8.

David I. G. Jone, 2001, Handbook of viscoelastic vibration damping, John Wiley & Sons, LTD.

Davis C. Q., Freeman D. M., 1998, Using a light microscope to measure motions with nanometer accuracy, *Optic. Eng.*, 37, pp. 1299-1304.

Deborah F. Pilkey, 1998, Computation of a damping matrix for finite element model updating, Ph.D. Dissertation, Virginia Polytechnic Institute and State University.

Ewins, D. J., 2000a, Adjustment or updating of models, *Sadhaba-Academy proceeding in Engineering Sciences*, Vol. 25, Part 3, pp. 235-245.

Ewins, D. J., 2000b, Modal Testing: Theory, Practice and Application, Second Edition, Research Studies Press.

Ewins, D. J. and M. Imregun, 1988, On the reliability of computational dynamic response prediction capabilities (DYNAS), *Society of Enviromental Engineering Journal*, 56 (1).

Fotsch D. and Ewins D.J., Application of MAC in the Frequency Domain, *18th IMAC*. pp. 1225-1231.

Frees G. M., and Miu D. K., 1990, Experiment and numerical analysis of read/write head suspension dynamics for high-performance floppy drive systems, *Journal of Vibration and Acoustics*, 112, pp. 26-32.

Friswell, M. I., Inman, D. J., and Pilkey, D.F., 1998, Direct Updating of Damping and Stiffness Matrices, *AIAA Journal*, Vol. 36, No. 3, pp. 491-493.

Friswell M. I. and Mottershead J. E., 1995, Finite element model updating in Structural Dynamics, Kluwer Academic Publishers.

Friswell M. I. and Penny J. E. T., 1992, Assessing model quality in parameter updating procedures, *10th IMAC*, pp. 188-194.

Friswell M. I., Penny J. E. T. and Garvey S. D., 1998, A combined genetic and eigensensitivity algorithm for the location of damage in structures, *Computers and Structures*, 69, 547-556.

Fritzen C. P. and Zhu S., 1991, Updating of finite element models by means of measured information, *Computers and Structures*, 40(2), 475-486.

Furlong, C., Kok, R., and Ferguson, C. F., 2005, Dynamic analysis and characterization of MEMS accelerometers by computational and opto-electromechanical methodologies, *Proceedings of the 43rd Annual IEEE International Reliability Physics Symposium*, pp. 325-329.

Guyan R. J., 1965, Reduction of stiffness and mass matrices, *AIAA Journal*, 3(2), pp. 380.

Hedayat A. S., Sloane N. J. A, and Stufken J., 1999, Orthogonal Arrays-Theory and Applications. Springer-Verlag.

Heylen W., 1987, Optimisation of model matrices of mechanical structures using experimental modal data, Ph.D. Dissertation, Mechanical Engineering Department, K. U. Leuven.

Heylen W. and Avitabile P., 1998, Correlation considerations – Part 5 (Degree of Freedom Correlation techniques), *16th IMAC*, pp. 207-214.

Hughes, T. J. R., 1987, The Finite Element Method. Prentice - Hall.

Ibrahim, S.R., 1983, Computation of normal modes from identified complex modes, *AIAA Journal,* Vol. 21, no. 3, pp. 446-451.

Imregun M. and Visser W. J., 1991, A review of model updating techniques, *Shock and Vibration Digest*, 23(1), pp. 9-20.

Imregun M., Visser W. J. and Ewins D. J., 1995a, Finite element model updating using frequency response function data-I. Theory and initial investigation, *Mechanical systems and signal processing*, 9(2), pp. 187-202.

Imregun M., Sanliturk K. Y. and Ewins D. J., 1995b, Finite element model updating using frequency response function data-II. Case study on a medium-size finite element model, *Mechanical systems and signal processing*, 9(2), pp. 203-213.

Jiang, L. X. and Miles, R.N., 1999, A passive damper for the vibration modes of the Head Actuator in Hard Disk Drive, *Journal of sound and vibration*, Vol. 220, pp. 683-694.

Jung H., 1990, Sensitivity analysis using macro elements, *15th International Modal Analysis Seminar*, K.U. Leuven.

Jung H., 1992, Structural dynamic model updating using eigensensitivity analysis, Ph.D. Thesis, Department of Mechanical Engineering, Imperial College, London, U.K..

Jung H. and Ewins D. J., 1991, Compatibility of measured and predicted vibration modes in model improvement studies, *AIAA Journal*, 29(5), pp. 798-803.

Jung H. and Ewins D. J., 1992, Error sensitivity of the inverse eigensensitivity method for model updating, *10th IMAC*, pp. 992-998.

Kasai T. and Link M., 2002, Identification of non-proportional modal damping matrix and real normal modes, *Mechanical systems and signal processing*, 16(6), pp. 921-934.

Kidder R. L., 1973, Reduction of structural frequency equations, *AIAA Journal*, 11(6), pp. 892.

Kwon K. S. and Lin R. M., 2004, Frequency selection method for FRF-based model updating, *Journal of Sound and Vibration*, 278, pp. 285-306.

Kwon K. S. and Lin R. M., 2005, Robust finite element model updating using Taguchi method, *Journal of Sound and Vibration*, 280, pp. 77-99.

Lallement G. and Piranda J., 1990, Localization methods for parameter updating of finite element models in elastodynamics, *8th IMAC*, pp. 579-585.

Lallement G. and Zhang Q., 1988, Inverse sensitivity based on the eigensolutions: Analysis of some difficulties encountered in the problem of parametric, *13th International Modal Analysis Seminar*, K.U. Leuven, pp. 1-16.

Lawrence E. M., Speller K. E., Yu D. L., 2003, MEMS characterization using laser Doppler vibrometry, Reliability, Testing, and Characterization of MEMS/MOEMS II, *Proceedings of SPIE*, 4980, pp. 51-62.

Lee, J. C., and Chou, Y. F., 1991, Driven-Base Modal Parameter Estimation for Continuous Structures, *Proc. of 9th International Modal Analysis Conference*, pp. 789-796.

Levin R. I. and Lieven N. A. J., 1998a, Dynamic Finite Element Model Updating Using Simulated Annealing and Genetic Algorithms, *Mechanical Systems and Signal Processing*, 12(1), pp. 91-120.

Levin R. I. and Lieven N. A. J., 1998b, Dynamic Finite Element Model Updating Using Neural Networks, *Journal of Sound and Vibration*, 210(5), pp. 593-607.

Li B. Q., Wu H. Y., Zhu C. C. and Liu J. H., 1999, The theoretical analysis on damping characteristics of resonant microbeam in vacuum, *Sensors and Actuators A 77*, pp. 191-194.

Li G. and Hughes H., 2000, Review of viscosity damping in micro-machined structures, *Proc. SPIE 4176*, pp. 30-46.

Lieven N. A. J. and Ewins D. J., 1990a, Error location and updating finite element models using singular value decomposition, *8th IMAC*, pp. 768-773.

Lieven N. A. J. and Ewins D. J., 1990b, Expansion of modal data for correlation, *8th IMAC*, pp. 605-609.

Lieven N. A. J. and Ewins D. J., 1992, Effect of incompleteness and noise on error matrix calculations, *10th IMAC*, pp. 1406-1413.

Lifshitz R. and Roukes M. L., 2000, Thermodynamic damping in micro- and nanomechanical systems, *Phys. Rev. B 61*, pp. 5600-5609.

Lin C. and Ibrahim S. R., 1984, The use of complex versus normal modes in structural model improvement, *Proceeding of the 2nd IMAC*, pp. 415-424.

Lin R. M., Identification of the dynamic characteristics of nonlinear structures, 1990, Ph.D Thesis, Imperial College of Science, Technology and Medicine, London, U.K..

Lin R. M. and Ewins D. J., 1990, Model updating using FRF data, *15th International Modal Analysis Seminar*, K.U. Leuven, pp. 141-163.

Lin R. M. and Ewins D. J., 1994, Analytical model improvement using Frequency Response Functions, *Mechanical Systems and Signal Processing*, 8(4), 437-458.

Lin R. M., Lim M. K. and Du H., 1995, Improved inverse eigensensitivity method for structural analytical model updating, *Journal of Vibration and Acoustics*, 117(2), pp. 192-198.

Lin R. M. and Lim M. K, 1997, Relationship between improved inverse eigensensitivity and FRF sensitivity methods for analytical model updating, *Journal of Vibration and Acoustics*, 119, pp. 354-362.

Lin R.M., Wang W.J., 2006, Review: Structural dynamics of microsystems—current state of research and future directions, *Mechanical Systems and Signal Processing*, Vol. 20, Issue 5, pp. 1015-1043.

Link M., Weiland M. and Barragan J. M., 1987, Direct physical matrix identification as compared to phase resonance testing: assessment based on practical application, *5th IMAC*, pp. 804-811.

Link Ryan J. and Zimmerman David, 2007, An approach for model updating of a multiphysics MEMS micromirror, *Journal of Dynamic Systems, Measurement, and Control*, Vol. 129, pp. 357-366.

Lord Rayleigh, 1897, Theory of sound (two volumes). New York: Dover Publications, 1945 re-issue, second edition.

Lu Y. and Tu Z. G., 2004, A two-level neural network approach for dynamic FE model updating including damping, *Journal of Sound and Vibration*, 275(3-5), pp. 931-952.

Maia, N.M.M., Silva, J.M.M., He J., Lieven, N.A.J., Lin, R.M., Skingle, G.W., To W.M. and Urgueira, A. P. V., 1997, Theoretical and experimental modal analysis, Taunton, Somerset, England: Research Studies Press; New York: Wiley.

Mark Donley, 1998, Correlation of FE models to base excitation tests, *Proceedings of the 16th International Modal Analysis Conference*, pp. 959-964.

Marwala T. and Hunt H. E. M., 1998, Fault Identification Using Finite Element Models and Neural Networks, *Mechanical Systems and Signal Processing*, 12(1), pp. 475-490.

M'Closkey, Robert T., Gibson, Steve, and Hui, Jason, 2000, Modal parameter identification of a MEMS Gyroscope, *Proceedings of the American Control Conference*, Vol. 3, pp.

1699-1704.

Minas C. and Inman D. J., 1988, Correcting finite element models with measured modal results using eigenstructure assignment methods, *6th IMAC*, pp. 583-587.

Minas C. and Inman D. J., 1990, Matching finite element models to modal data, *Journal of vibration and acoustics*, 112(1), pp. 84-92.

Mottershead J. E. and Friswell M. I., 1993, Model updating in Structural Dynamics: A survey, *Journal of sound and vibration*, 167(2), pp. 347-375.

Nash M., 1990, An approach to the reconciliation of finite element modal test studies, *8th IMAC*, pp. 187-194.

Natke H. G., 1989, Updating computational models in the frequency domain based on measured data: a survey, *Probabilistic Engineering Mechanics*, 3(1), pp. 28-35.

Natke H. G., 1991, Error localization within spatially finite-dimensional models, *Computational Mechanics*, 8, pp. 153-160.

Nayfeh A. H., Younis M. I., 2004, A new approach to the modeling and simulation of flexible microstructures under the effect of squeeze-film damping, *Journal of Microemechanics and Microengineering*, 14, pp.170-181.

Niedbal N., 1984, Analytical determination of real normal modes from measured complex responses, *Proceedings of the 25th Structures*, *Structural dynamics and Materials conference*, pp. 292-295.

Nobari A. S., Robb D. A. and Ewins D. J., 1992, A new modal-based method for structural dynamic model updating and joint identification, *10th IMAC*, pp. 741-750.

O'Callahan J. C., 1989, A procedure for an improved reduced system (IRS) model, *7th IMAC*, pp. 17-21.

O'Callahan J.C. and Chou C.M., 1988, Localization of model errors in optimized mass and stiffness matrices using modal test data, *6th IMAC*, pp. 49-55.

O'Callahan J. C., Liew I. W., Avitabile P. and Madden R., 1986, An efficient method of determining rotational degrees of freedom from analytical and experimental modal data, *4th IMAC*, pp. 50-58.

Ojalvo I. U., 1987, Efficient computation of mode shape derivatives for large dynamic systems, *AIAA Journal*, 25(10), pp.1386-1390.

Ojalvo I. U., Ting T., Pilon D. and Twomey W., 1989, Practical suggestions for modifying math models to correlate with actual modal test results, *7th IMAC*, pp. 347-354.

Ozdoganlar O. B., Hansche B. D., and Carne T. G., 2003, Experimental modal analysis for Microsystems, *Proc. of 21st International Modal Analysis Conference*.

Park S. H., 1996, Robust Design and analysis for Quality engineering. Chapman & Hall.

Pascual R., Golinval J.C. and Razeto M., 1997, A frequency domain correlation technique for model correlation and updating, *15th IMAC*, pp. 587-592.

Paz M., 1984, Dynamic condensation, *AIAA Journal*, 22(5), pp. 724-727.

Pilkey Deborah F., 1998, Computation of a damping matrix for finite element model updating, Ph.D. Dissertation, Virginia Polytechnic Institute and State University.

Piranda J. and Lallement G. and Cogan S., 1991, Parametric correction of finite element models by minimization of an output residual: improvement of the sensitivity method, *9th IMAC*, pp. 363-368.

Phadke M. S., 1989, Quality Engineering using Robust Design. Prentice Hall.

Rad S. Z., 1997, Methods for updating numerical models in structural dynamics, Ph.D. Thesis, Department of Mechanical Engineering, Imperial College, U.K.

Reix C., Tombini C., Gerard A., Strobbe J. and Dasotte E., 1996, Updating the damping matrix using frequency response data, *Proceedings of the 14th IMAC*, pp. 585-590.

Rembe C., Kant R., Muller R. S., 2001, Optical measurement methods to study dynamic behavior in MEMS, *Proceedings of SPIE*, 4400, pp. 127-137.

Rembe C., Tibken B., Hofer E. P., 2001, Analysis of the Dynamics in microactuators using

high-speed cine photomicrography, *IEEE Journal of Microelectromechanical Systems*, 10, pp. 137-145.

Santos J. M. C. and Arruda J. R. F., 1990, Finite element model updating using frequency response functions and component mode synthesis, *8th IMAC*, pp. 1195-1201.

Sestieri A. and Ambrogio W. D., 1989, Why be modal? How to avoid the use of modes in the modification of vibrating systems, *International Journal of analytical and Experimental Modal analysis*, 4(1), pp. 25-30.

Sharp R. S. and Brooks P. C., 1988, Sensitivities of frequency response functions of linear dynamic systems to variations in design parameter values, *Journal of Sound and Vibration*, 126, pp. 167-172.

Shulz M. J. and Inman D. J., 1994, Model updating using constrained eigenstructure assignment, *Journal of sound and vibration*, 178(1), pp. 113-130.

Sidhu J. and Ewins D.J., 1984, Correlation of finite element and modal testing studies of a practical structure, *2th IMAC*, pp. 756-762.

Swei S. M., Gao P., Lin R. M., 2001, A dynamic analysis for the suspension structure in hard disk drives using piezofilm actuators, *Smart Materials and Structures*, 10, pp. 409-413.

Taguchi G., 1986, Introduction to Quality engineering. Asian Productivity Organization.

Tang W. C., 1990, Electrostatic comb drive for resonant sensor, PhD dissertation, Univ. California, Berkeley, CA.

Thomas G. Carne, David R. Martinez and Arlo R. Nord, 1989, A comparison of fixed-base and driven-base modal testing of an electronics package, *Proc. the 7th International Modal Analysis Conference*, 30, pp. 672-679.

Tilmans H. A. C., Elwenspoek M. and Fluitman J. H. J., 1992, Micro resonant force gauges, *Sensors and Actuators* A 30, pp. 35-53.

Veijola T., Kuisma H., Lahdenperä J. and Ryhänen T., 1995, Equivalent-circuit model of the squeezed gas film in a silicon accelerometer, *Sensors and Actuators* A 48, pp. 239-248.

Vigneron, F. R., Souc, Y., 1987, Driven-base tests for modal parameter estimation, *AIAA*

Journal, vol.25 no.1, pp. 152-160.

Visser W. J. and Imregun M., 1991, A technique to update finite element models using frequency response data, *9th IMAC*, pp. 462-468.

Wang J. H., 1988, Mechanical parameters identification with special consideration of noise effect, *Journal of Sound and Vibration*, 125, pp. 151-167.

Wang K., Yu Y., Wong A.-C., and Nguyen C. T.-C., 1999, VHF free-free beam high-Q micromechanical resonators, *Technical Digest, 12th International IEEE Micro Electro Mechanical Systems Conference*, pp. 453-458.

Wei F. S., 1989, Structural dynamic model modification using vibration test data, *7th IMAC*, pp. 562-567.

Wilson C. J., Bogy D. B., 1996, An experimental modal analysis technique for miniature structures, *Journal of Vibration and Acoustics*, 118, pp. 1-9.

Woodhouse J., 1998, Linear damping models for structural vibration, *Journal of Sound and Vibration*, 215(3), pp. 547-569.

Xu L. M., 2002, Development of vibration modeling, testing and control techniques for Hard Disk Drives, Ph.D. thesis, Nanyang Technological University.

Zbigniew Osiński, 1998, Damping of vibrations, A. A. Balkema, Publisher.

Zhang Q. and Lallement G., 1987, Dominant error localization in a finite element model of a mechanical structure, *Mechanical Systems and Signal Processing*, 1(2), pp. 141-149.

Zienkiewicz O. C., 1971, The Finite Element Method in Engineering Science, McGraw Hill.

Zimmerman D. C. and Widengren M., 1990, Correcting finite element models using a symmetric eigenstructure assignment technique, *AIAA Journal*, 28(9), pp. 1670-1676.

Zhang P., Tang X., Shan B., Brandon J. and Kwan A., 1998, Analytical and experimental modal analysis for operational validation and calibration of a miniature silicon sensor, *Journal of Sound and Vibration*, 214, pp. 903-913.

Zhang X. and Tang W. C., 1995, Viscous air damping in laterally driven microresonators,

Sensors and Actuators A 7, pp. 415-430.

Zook J. D., Burns D. W., Guckel H., Sniegowski J. J., Engelstad R. L. and Feng Z., 1992, Characteristics of polysilicon resonant microbeams, *Sensors and Actuators* A 35, pp. 51-59.

Appendix

The papers that have been published and submitted as follows:

R. M. Lin and J. Zhu, 2006, Model updating of damped structures using FRF data, *Mechanical systems and signal processing*, Volume 20, Issue 8, pp. 2200-2218.

R. M. Lin and J. Zhu, 2007, Finite element model updating using vibration test data under base excitation, *Journal of Sound and Vibration*, Volume 303, Issues 3-5, pp. 596-613.

R. M. Lin and J. Zhu, On the Relationship between Viscous and Hysteretic Damping Models, *Journal of Sound and Vibration* (submitted).